TRANSPORTATION RESEARCH
RECORD

No. 1384

Pavement Design, Management, and Performance

Strength and Deformation Characteristics of Pavement Structures

A peer-reviewed publication of the Transportation Research Board

TRANSPORTATION RESEARCH BOARD
NATIONAL RESEARCH COUNCIL

NATIONAL ACADEMY PRESS
WASHINGTON, D.C. 1993

Transportation Research Record 1384
Price: $25.00

Subscriber Category
IIB pavement design, management, and performance

TRB Publications Staff
Director of Reports and Editorial Services: Nancy A. Ackerman
Senior Editor: Naomi C. Kassabian
Associate Editor: Alison G. Tobias
Assistant Editors: Luanne Crayton, Norman Solomon, Susan E. G. Brown
Graphics Specialist: Terri Wayne
Office Manager: Phyllis D. Barber
Senior Production Assistant: Betty L. Hawkins

Printed in the United States of America

Library of Congress Cataloging-in-Publication Data
National Research Council. Transportation Research Board.

Strength and deformation characteristics of pavement structures / Transportation Research Board. National Research Council.
p. cm.—(Transportation research record, ISSN 0361-1981 ; no. 1384)
ISBN 0-309-05454-0
1. Pavements—Performance. 2. Pavements—Testing. 3. Pavements—Design and construction. I. National Research Council (U.S.). Transportation Research Board. II. Series: Transportation research record; 1384.
TE7.H5 no. 1384
[TE251.5]
388 s—dc20
[625.8] 93-23100
CIP

Sponsorship of Transportation Research Record 1384

GROUP 2—DESIGN AND CONSTRUCTION OF TRANSPORTATION FACILITIES
Chairman: Charles T. Edson, Greenman Pederson

Pavement Management Section
Chairman: Joe P. Mahoney, University of Washington

Committee on Strength and Deformation Characteristics of Pavement Sections
Chairman: Albert J. Bush III, USAE Waterways Experiment Station
Gilbert Y. Baladi, Richard D. Barksdale, Robert C. Briggs, Stephen F. Brown, George R. Cochran, Ronald J. Cominsky, Billy G. Connor, Mark P. Gardner, John P. Hallin, Dennis R. Hiltunen, Lynne H. Irwin, Starr D. Kohn, Robert L. Lytton, Michael S. Mamlouk, Soheil Nazarian, Rasmus S. Nordal, Gonzalo Rada, J. Brent Rauhut, Byron E. Ruth, Larry Scofield, Tom Scullion, Stephen B. Seeds, R. N. Stubstad, Marshall R. Thompson, Per Ullidtz, Jacob Uzan, Thomas D. White, Haiping Zhou

Daniel W. Dearasaugh, Jr., Transportation Research Board staff

The organizational units, officers, and members are as of December 31, 1992.

Transportation Research Record 1384

Contents

Foreword v

System Identification Method for Backcalculating Pavement Layer Properties 1
Fuming Wang and Robert L. Lytton

Some Observations About Backcalculation and Use of a Stiff Layer Condition 8
Joe P. Mahoney, Brian C. Winters, Newton C. Jackson, and Linda M. Pierce

Modified Newton Algorithm for Backcalculation of Pavement Layer Properties 15
Ronald S. Harichandran, Tariq Mahmood, A. Robert Raab, and Gilbert Y. Baladi

New Scenario for Backcalculation of Layer Moduli of Flexible Pavements 23
A. Samy Noureldin

Stiffness of Asphalt Concrete Surface Layer from Stress Wave Measurements 29
Marwan F. Aouad, Kenneth H. Stokoe II, and Robert C. Briggs

Rutting Rate Analyses of the AASHO Road Test Flexible Pavements 36
Marshall R. Thompson and David Nauman

Heavy-Duty Asphalt Pavements in Pennsylvania: Evaluation for Rutting 49
Prithvi S. Kandhal, Stephen A. Cross, and E. Ray Brown

Use of LPC Wheel-Tracking Rutting Tester To Select Asphalt Pavements Resistant to Rutting 59
Yves Brosseaud, Jean-Luc Delorme, and René Hiernaux

Sensitivity of Strategic Highway Research Program A-003A Testing Equipment to Mix Design Parameters for Permanent Deformation and Fatigue 69
Jorge B. Sousa, Akhtarhusein Tayebali, John Harvey, Philip Hendricks, and Carl L. Monismith

Nonlinear Elastic Viscous with Damage Model To Predict Permanent Deformation of Asphalt Concrete Mixes 80
Jorge Sousa, Shmuel L. Weissman, Jerome L. Sackman, and Carl L. Monismith

Mathematical Model of Pavement Performance Under Moving Wheel Load 94
Per Ullidtz

Foreword

The Committee on Strength and Deformation Characteristics of Pavement Sections sponsored three sessions at the 1993 Annual Meeting of the Transportation Research Board. The first five papers in this Record were presented in the session titled Characterization of Pavement Layer Properties. Wang and Lytton introduce a method for backcalculation of pavement layer properties based on the system identification scheme. A stiff layer is an important factor in the backcalculation process, and Mahoney et al. report that a saturated soil condition or water table can result in a stiff layer condition. Harichandran et al. present a robust and efficient algorithm for the backcalculation of pavement layer moduli, which has been implemented in a new backcalculation program named MICHBACK. Noureldin describes a new scenario for backcalculation focusing on the radial distance and deflection of a point on the pavement surface that deflects exactly the same amount as the top of the subgrade beneath the loading center. Aouad et al. discuss various aspects of the spectral analysis of surface waves method to evaluate the stiffness of the asphalt surface layer and lower pavement layers.

These are followed by five papers that were presented at the session titled Rutting. Thompson and Nauman follow up on some of the accomplishments under NCHRP Project 1-26, Calibrated Mechanistic Structural Analysis Procedures for Pavements, by analyzing selected AASHO Road Test data with a proposed pavement surface rutting model. Kandhal et al. evaluate rutting on 34 sections of heavily traveled pavements in Pennsylvania by identifying pavement properties related to rutting and developing a rutting model from the data. Brosseaud et al. describe a study of rutting in asphalt pavements using the LPC wheel-tracking rutting tester in Nantes, France. Sousa, Tayebali et al. discuss Strategic Highway Research Program testing equipment and its sensitivity to mix design parameters. Sousa, Weissman et al. discuss prediction of rutting using a nonlinear elastic viscous damage model.

The final paper in this Record was presented in the session titled Vehicle-Pavement Interaction. Ullidtz studied the interaction of the vehicle and pavement through the use of the Mathematical Model of Pavement Performance, a sophisticated computer model of a defined section of pavement.

System Identification Method for Backcalculating Pavement Layer Properties

FUMING WANG AND ROBERT L. LYTTON

In recent years pavement structural evaluation has relied increasingly on determining material properties by nondestructive deflection testing and backcalculation procedures. The technique used to achieve a convergence of the measured and predicted deflection basins plays an important role in all backcalculation approaches. An iterative method based on the system identification (SID) scheme is developed, and the SID program is used in conjunction with a multilayer elastic model (BISAR program) to backcalculate pavement layer properties. Numerical examples indicate that (*a*) the moduli backcalculated by the suggested SID method compare well with the results from MODULUS, which is a data base backcalculation program, and other developed iterative backcalculation programs; (*b*) the SID is a quickly converging procedure, and the influence of seed values, for a relatively wide range, on the derived results is negligible; and (*c*) it is able to backcalculate pavement layer thicknesses in addition to layer moduli.

Nondestructive testing (NDT) has become an integral part of pavement structural evaluation in recent years. Of many static, vibration, impulse, and vehicular NDT devices, the falling weight deflectometer (FWD) has been most widely used for pavement evaluation (*1*). By dropping a mass from a predetermined height onto a base plate resting on the pavement surface, the FWD can provide variable and large impulse loadings to the pavement, which to some degree simulate actual truck traffic. Pavement deflection is measured through a series of velocity transducers at various distances from the base plate, and the data can be used to backcalculate the in situ pavement properties, such as layer moduli. This information can in turn be used in pavement structural analysis to determine the bearing capacity, estimate the remaining life, and calculate an overlay requirement over a desired design life.

FWD DATA REDUCTION AND BACKCALCULATION METHODS

The analysis of the FWD test data is an inverse process. Instead of predicting the pavement response, the deflection is measured and the pavement properties are backcalculated.

F. Wang, Materials, Pavements and Construction Division, Texas Transportation Institute, Texas A&M University, College Station, Tex. 77843. Current affiliation: CAE Center, Zhengzhou Institute of Technology, Zhengzhou, Henan 450002, People's Republic of China. R. L. Lytton, Civil Engineering Department, Texas A&M University System, College Station, Tex. 77843.

A variety of different methods and computer programs have been developed for backcalculation of layer moduli from FWD test results. Examples include the MODCOMP program developed by Irwin (*2*), the "___ DEF" series of programs described by Bush (*3*), and the MODULUS program developed by Uzan et al. (*4*). The MODCOMP program uses the CHEVRON program for deflection calculations and is notable for its extensive controls on the seed moduli and the range of acceptable moduli. The two programs reported by Bush include the CHEVDEF and BISDEF programs, in which the deflection calculations are performed by the CHEVRON (*5*) and BISAR (*6*) programs, respectively, and the gradient search technique is used. MODULUS is a data base backcalculation program that departs from the usual microcomputer program pattern. Before the actual backcalculation process, MODULUS computes a series of normalized deflection basins using the BISAR program with layer moduli that cover the range of anticipated values in the field. The deflection basins are stored in a data base for subsequent comparison with measured deflection basins. The pattern search algorithm developed by Hooke and Jeeves (*7*) and the three-point Lagrange interpolation technique (*8*) are used to find the layer moduli that minimize the error between measured and computed basins. By replacing the direct computation of deflections with the interpolation scheme, MODULUS is distinctly faster than other iterative backcalculation programs for production cases in which a large number of deflection basins in the same pavement geometry are to be evaluated. When pavement configuration changes, however, the time-consuming task of generating the deflection data base must be repeated.

Most current backcalculation procedures seek only to determine layer moduli and require the thickness of each pavement layer to be specified. The subgrade is assumed to be infinitely thick, or a rigid layer is placed at an arbitrary depth. As reported by other researchers, pavement deflections are sensitive to layer thicknesses. Even modest errors in assumed layer thicknesses can lead to large errors in backcalculated layer moduli (*9*), and the existence of a rigid layer or bedrock underlying the subgrade has a profound effect on the analysis of deflection data (*10*). The subgrade modulus may be significantly overpredicted if a semi-infinite subgrade is falsely assumed when actual bedrock exists at a shallow depth, or it may be underpredicted if a shallow rigid layer is arbitrarily introduced when deep bedrock exists.

Pavement thicknesses can be accurately measured through coring, boring, ground-penetrating radar, or seismic tests. However, pavements cover such a large area that it is impractical to use these techniques to determine the layer thick-

nesses at every point tested with deflection devices. Thus advanced backcalculation procedures are clearly needed to determine the layer thickness, especially the subgrade thickness, as well as moduli from the measured deflection information. In this paper an iterative procedure based on the system identification scheme is presented. It may be considered as an alternative approach to the subject.

SYSTEM IDENTIFICATION METHOD

General Procedure

The objective of the system identification process is to estimate the system characteristics using only input and output data from the system to be identified (*11*). The simplest and intellectually most satisfying method for representing the behavior of a physical process is to model it with a mathematical representation. The model/process is identified when the error between the model and the real process is minimized in some sense; otherwise, the model must be modified until the desired level of agreement is achieved.

There are three general strategies for error minimization in system identification procedures: forward approach, inverse approach, and generalized approach. In the forward approach, the model and the system to be identified are given the same known input, and the output error between the two is minimized. In the inverse approach, the outputs of the model and the system are identical, and their input error is minimized. The generalized approach is a combination of the forward and inverse approaches. In all cases, the minimization of the error between the model and the real process can be conducted with a model parameter adjustment.

The forward approach is not as complicated as the inverse or generalized approaches because, by using a forward model, it is easier to compute the output and to generate the parameter adjustment algorithm. A system identification scheme using the forward approach and parameter adjustment algorithm is shown in Figure 1.

The procedure shown in Figure 1 is exactly analogous to what is being done in backcalculating the moduli of pavements (*12,13*). However, the system identification procedure can also be applied to determine properties of pavement structures in addition to layer moduli, even including the thickness of the layer as one of the unknown parameters.

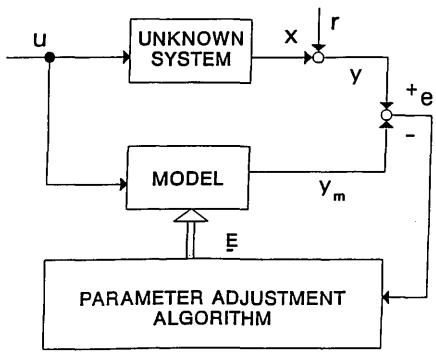

FIGURE 1 System identification (forward approach).

Parameter Adjustment Algorithm

The system identification method requires the accurately measured output data of the unknown system, a suitable model to represent the behavior of the system, and an efficient parameter adjustment algorithm that converges accurately and rapidly. If the data and the model are reliable, the success of system identification studies directly relies on the efficiency of the parameter adjustment algorithm.

An algorithm can be developed for adjusting model parameters on the basis of the Taylor series expansion. Let the mathematical model of some process be defined by n parameters:

$$f = f(p_1, p_2, \ldots, p_n; x, t) \tag{1}$$

where x and t are independent spatial and temporal variables. If any function $f_k(p_1, p_2, \ldots, p_n; x_k, t_k)$ is expanded using a Taylor series and only first-order terms are kept, it can be shown that

$$f_k(p + \Delta p) = f_k(p) + \nabla f_k \cdot \Delta p \tag{2}$$

where the parameters have all been collected into a vector

$$p = [p_1, p_2, \ldots, p_n]^T$$

If we equate $f_k(p + \Delta p)$ with the actual output of the system and $f_k(p)$ with the output of the model for the most recent set of parameters p, the error between the two outputs becomes

$$\begin{aligned} e_k &= f_k(p + \Delta p) - f_k(p) \\ &= \nabla f_k \cdot \Delta p \\ &= \frac{\partial f_k}{\partial p_1}\Delta p_1 + \frac{\partial f_k}{\partial p_2}\Delta p_2 + \cdots + \frac{\partial f_k}{\partial p_n}\Delta p_n \end{aligned} \tag{3}$$

Note that e_k represents the difference between the actual system output and the model output when the independent variables take on values x_k and t_k.

If the error is evaluated at m values ($m \geq n$) of the independent variables, m equations may be written:

$$\left.\begin{aligned} e_1 &= \frac{\partial f_1}{\partial p_1}\Delta p_1 + \frac{\partial f_1}{\partial p_2}\Delta p_2 + \cdots + \frac{\partial f_1}{\partial p_n}\Delta p_n \\ e_2 &= \frac{\partial f_2}{\partial p_1}\Delta p_1 + \frac{\partial f_2}{\partial p_2}\Delta p_2 + \cdots + \frac{\partial f_2}{\partial p_n}\Delta p_n \\ &\vdots \\ e_m &= \frac{\partial f_m}{\partial p_1}\Delta p_1 + \frac{\partial f_m}{\partial p_2}\Delta p_2 + \cdots + \frac{\partial f_m}{\partial p_n}\Delta p_n \end{aligned}\right\} \tag{4}$$

Equation 4 can be conveniently nondimensionalized by dividing both sides by f_k. Furthermore, if we define matrices r,

F, and α as

$$r = [r_1\ r_2\ \ldots\ r_m]^T$$

$$r_k = \frac{e_k}{f_k} \qquad k = 1, 2, \ldots, m$$

$$F = [F_{ki}]$$

$$F_{ki} = \frac{\partial f_k}{\partial p_i} \cdot \frac{p_i}{f_k} \qquad k = 1, 2, \ldots, m \qquad i = 1, 2, \ldots, n$$

$$\alpha = [\alpha_1\ \alpha_2\ \ldots\ \alpha_n]^T$$

$$\alpha_i = \frac{\Delta p_i}{p_i} \qquad i = 1, 2, \ldots, n$$

respectively, Equation 4 may be rewritten as

$$r = F\alpha \tag{5}$$

or

$$F^T r = F^T F\alpha \tag{6}$$

The vector r is completely determined from the outputs of the model and the real system. The matrix F is usually called the sensitivity matrix, because its element F_{ki} reflects the sensitivity of the output f_k to the parameter p_i, and it can be generated numerically if the analytical solution is not available. The technique used for generating the sensitivity matrix F and when it should be updated will be discussed later in this section.

The unknown vector α reflects the relative changes of the parameters. If the sensitivity matrix F or the system of equations is well behaved, it can be obtained by using a generalized inverse procedure to solve Equation 5 (*14,15*). However, there might be column degeneracies in the sensitivity matrix F. This condition may be encountered when two or more parameters have similar effects, or any parameter has a negligible effect, on the behavior of the model f. In these cases Equation 5 may be ill conditioned from the mathematical point of view, and the singular value decomposition (SVD) technique (*16*) is one of the alternative approaches to give a stable solution. SVD diagnoses the sensitivity matrix by calculating its condition number, which is defined as the ratio of the largest of the singular values to the smallest of the singular values. F is singular if its condition number is infinite, but the more common situation is that some of the singular values are very small but nonzero, thus F is ill conditioned. Then SVD gives a solution by zeroing the small singular values, which corresponds to deleting some linear combinations of the set of equations. The SVD solution is very often better (in the sense of the residual $|F\alpha - r|$ being smaller) than LU decomposition solution or Gaussian elimination solution. However, the SVD user has to exercise some discretion in deciding at what threshold to zero the small singular values. In this study the iteration method developed by Han (*17*) is used to solve Equation 6. Han's method not only gives the exact solution if Equation 6 is well posed but also gives a stable solution if Equation 6 is ill posed without deleting any equations.

As soon as α is obtained, a new set of parameters is determined as

$$P^{k+1} = P^k(1 + \alpha) \tag{7}$$

The iteration process is continued until the desired convergence is reached. In this paper the convergence criterion is set to 0.5 percent for α (i.e., the iterative procedure must be repeated until all parameter changes are not more than 0.5 percent).

The sensitivity matrix F in Equation 6 is generated using a multilayer elastic model (BISAR program). The derivatives $\frac{\partial f_k}{\partial p_i}$, where f_k ($k = 1, 2, \ldots, m$) represent the pavement deflections at the sensor locations of FWD and p_i ($i = 1, 2, \ldots, n$) the pavement layer property parameters, are computed as the forward-derived differences. Thus the sensitivity matrix F can be generated by $n + 1$ runs of BISAR.

The sensitivity matrix may be used for more than one iteration. If the parameters have been changed "much," however, it has to be regenerated because it only takes account of the first-order Taylor series and the problem is highly nonlinear, which means that the sensitivity values depend on the parameter values. Otherwise the iteration procedure might not converge, or, more often, it may converge very slowly. In this study the sensitivity matrix is updated when one of the following conditions is encountered:

1. One or more parameters have been increased by more than 100 percent during the past iterations;
2. One or more parameters have been decreased more than 50 percent during the past iterations; or
3. The sensitivity matrix has been used for three iterations, but the 0.5 convergence criterion has not been achieved.

BACKCALCULATION OF LAYER MODULI

On the basis of the procedure described above, the SID microcomputer program has been developed. In this section the program is evaluated by comparing the backcalculated moduli with the results from MODULUS and other developed programs.

Comparison with MODULUS

An actual deflection basin is analyzed using the SID backcalculation program, and the results are compared with those from MODULUS. Deflection data were obtained using the FWD (Dynatest Model 8000) on Section 8 at the Texas A&M Research Annex (*18*). Section 8 consisted of 12.7-cm (5-in.) AC, 30.48-cm (12-in.) crushed limestone base, and 30.48-cm (12-in.) cement-stabilized subbase (very stiff layer) over clay subgrade. The FWD geophones were located at 0, 30.48, 60.96, 91.44, 121.92, 152.4, and 182.88 cm (0, 12, 24, 36, 48, 60, and 72 in.) from the center of the load plate, which had a radius of 15 cm (5.91 in.).

By using the BISAR program to generate the deflection data base and assuming a 635-cm (250-in.) depth from pave-

ment surface to bedrock, the moduli backcalculated by MODULUS for AC layer, base, subbase, and subgrade are E_1 = 140 740 kg/cm² (2,000 ksi), E_2 = 3519 kg/cm² (50 ksi), E_3 = 265 366 kg/cm² (3,771 ksi), and E_4 = 915 kg/cm² (13 ksi).

The SID backcalculation program is used to reduce the same data for Section 8. As do other iterative approaches, the SID requires seed moduli values. Three sets of seed moduli are selected to evaluate the effects of seed parameters on derived results.

First, the seed modulus values are assumed to be E_1 = 105 555 kg/cm² (1500 ksi), E_2 = 4222 kg/cm² (60 ksi), E_3 = 140 740 kg/cm² (2,000 ksi), and E_4 = 704 kg/cm² (10 ksi), which are relatively close to the results given by MODULUS. The 0.5 convergence criterion for α is reached after five iterations, and the sensitivity matrix is regenerated after three iterations.

Next, the seed moduli are changed to E_1 = 70 370 kg/cm² (1,000 ksi), E_2 = 7037 kg/cm² (100 ksi), E_3 = 70 370 kg/cm² (1,000 ksi), and E_4 = 2111 kg/cm² (30 ksi). For this set of seed moduli, only three iterations are needed, but the sensitivity matrix is regenerated after one iteration.

Last, to verify the robustness of the SID approach, the seed moduli are assumed to be significantly different from the previous values: E_1 = 351 851 kg/cm² (5,000 ksi), E_2 = 35 185 kg/cm² (500 ksi), E_3 = 351 851 kg/cm² (5,000 ksi), and E_4 = 3519 kg/cm² (50 ksi).

With these moduli the predicted deflections are approximately four times less than the FWD data, which indicates that very poor seed parameters have been entered. In practice, another set of starting values should be selected in this case. The SID procedure still converges, however. The sensitivity matrix is updated four times, and altogether eight iterations are performed.

The results for the preceding three cases are summarized in Table 1, and the converging process for each case is shown in Figures 2, 3, and 4, respectively. The results backcalculated by the SID program agree very well with those by MODULUS,

TABLE 1 Backcalculated Moduli for Different Seed Values

MODULI (kg/cm²)	E_1 (140740*)	E_2 (3519*)	E_3 (265366*)	E_4 (915*)
"Seed"	105555	4222	140740	704
Backcalculated	150451	3504	262128	906
"Seed"	70370	7037	70370	2111
Backcalculated	150451	3502	262269	906
"Seed"	351851	35185	351851	3519
Backcalculated	151437	3478	265507	906

1 kg/cm² = 14.21 psi

* moduli backcalculated by MODULUS (18).

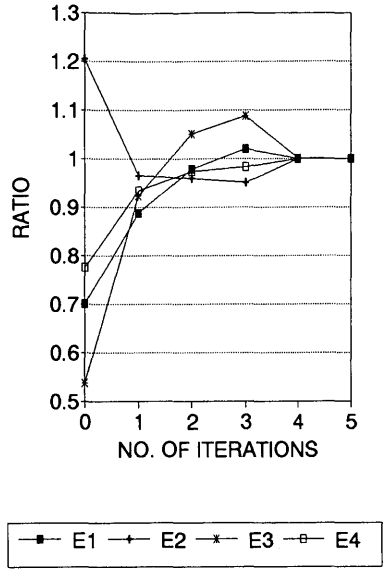

FIGURE 2 Converging process (first set of seed moduli).

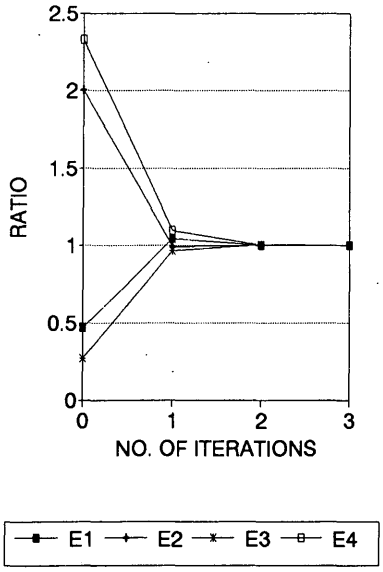

FIGURE 3 Converging process (second set of seed moduli).

and the seed values have a negligible influence on the converged results, although they certainly affect the required number of iterations.

Comparison with Other Iterative Backcalculation Approaches

The SID program is compared with five other iterative backcalculation programs. Pavement data and deflection test data for the comparison are obtained from a real pavement (*19*). The backcalculated moduli from the various programs are

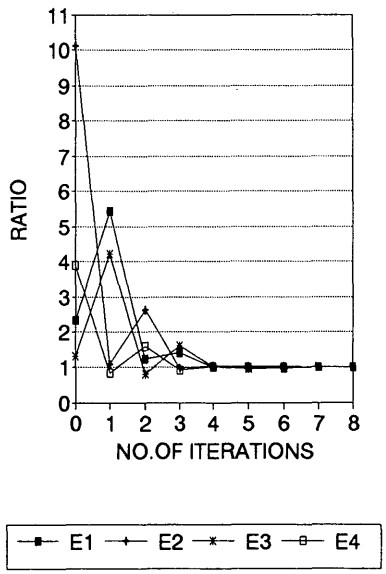

FIGURE 4 Converging process (third set of seed moduli).

TABLE 2 Summary of Backcalculated Moduli (kg/cm²)

Test Site	Program	AC Surface	Aggregate Base	Subgrade
	BISDEF	13652	1776	809
	BOUSDEF	11470	1809	788
1	CHEVDEF	12371	1738	851
	ELSDEF	14074	1661	823
	MODCOMP2	11456	2350	739
	SID(BISAR)	15474	1527	809
	BISDEF	12223	1084	739
	BOUSDEF	11097	1070	697
2	CHEVDEF	10605	1168	739
	ELSDEF	12244	1070	732
	MODCOMP2	9254	1907	654
	SID(BISAR)	11498	1217	704

1 kg/cm² = 14.21 psi

given in Table 2. The results from SID are close to those from the other programs.

BACKCALCULATION OF LAYER MODULI AND LAYER THICKNESSES

By considering the layer thicknesses as unknown parameters, the SID program can be used to backcalculate the layer thicknesses as well as layer moduli. This ability is illustrated by using hypothetical three-layer pavement structures and the real FWD data for Section 8.

Backcalculation of Hypothetical Pavement Layer Moduli and Thicknesses

The SID program is evaluated by comparing the backcalculated layer moduli and thicknesses with hypothesized theoretical values. The comparison is done by assuming three pavement sections with different thicknesses and moduli. Surface deflections of the assumed pavement section are calculated using the BISAR program and are used to backcalculate the layer thicknesses as well as the layer moduli.

The theoretical values and the backcalculated results for the three pavement sections are presented in Table 3. The SID program always converges toward the correct modulus and thickness for all layers.

Application Using Actual Deflection Data

The SID program is applied to determine the subgrade thickness of Section 8 from the FWD data given in Table 1. Since increasing the number of unknown parameters requires more data points to ensure the system overdeterminism, and because of the likelihood of large measurement errors in real data, backcalculating more than four parameters is not recommended without performing the dynamic analysis of FWD data. Therefore the process is divided into two steps:

1. The four layer moduli are backcalculated by assuming the subgrade to be of infinite thickness. The results are compared with those backcalculated previously by introducing a 635-cm (250-in.) depth from surface to bedrock. The subbase and subgrade moduli are much more sensitive to the subgrade thickness than the AC and base moduli. Thus the backcal-

TABLE 3 Summary of Backcalculated Layer Moduli and Layer Thicknesses

	MODULI (kg/cm²)			THICKNESSES (cm)		
	E_1	E_2	E_3	h_1	h_2	h_3
"Seed"	35185	2111	1407	25.4	25.4	635.0
Backcalculated	42222	2815	1759	30.5	30.5	762.0
Theoretical	42222	2815	1759	30.5	30.5	762.0
"Seed"	35185	2111	1407	25.4	25.4	635.0
Backcalculated	70370	4221	2815	38.1	30.5	889.0
Theoretical	70370	4222	2815	38.1	30.5	889.0
"Seed"	35185	2111	1407	25.4	25.4	635.0
Backcalculated	70370	1055	704	15.2	38.1	457.2
Theoretical	70370	1056	704	15.2	38.1	457.2

1 cm = 0.3937 in.

1 kg/cm² = 14.21 psi

TABLE 4 Summary of Backcalculated Results for Section 8

Subgrade Thickness (cm)	Program	Backcalculated Moduli (kg/cm^2)			
		E_1	E_2	E_3	E_4
Infinite (Assumed)	MODULUS	140740	4081	91833	1970
	SID(BISAR)	145736	3941	101051	1900
561 (Assumed)	MODULUS	140740	3519	265365	915
	SID(BISAR)	150451	3519	262128	915
1082 (Backcalculated)	SID(BISAR)	145736	3941	151858	1407

1 cm =0.3937 in

1 kg/cm^2 =14.21 psi

culated AC and base moduli are fixed as known parameters, and the derived subbase and subgrade moduli are taken as the seed values for the next backcalculation step.

2. The subbase and subgrade moduli together with the subgrade thickness are backcalculated. The seed subgrade thickness is selected as 762 cm (300 in.), and a 1082-cm (426-in.) thickness is derived.

The backcalculated results for Section 8, based on three different subgrade thicknesses, are summarized in Table 4. The subgrade thickness significantly affects the backcalculated subbase and subgrade moduli. The subgrade modulus assuming an infinite thickness is approximately twice the value backcalculated assuming a subgrade thickness of 561 cm (221 in.). The backcalculated subgrade modulus with the backcalculated subgrade thickness of 1082 cm (426 in.) from the SID program is in between.

This example clearly illustrates one substantial problem in most current backcalculation procedures. If the subgrade is assumed to be infinitely thick, or a depth to bedrock is arbitrarily selected, the backcalculated subgrade modulus from these two assumptions may be quite different. Since the stiffness of the supporting subgrade is a basic parameter in pavement structural analysis, over- or underprediction of subgrade modulus may lead to under- or overconservative results in pavement evaluation and overlay design.

The SID procedure can be considered as an alternative approach for backcalculating pavement layer moduli and at the same time estimating the subgrade thickness from the FWD data. By using the relatively simple multilayer elastic model to represent the complex behavior of pavement structures, this estimation gives a more consistent prediction in the sense of "equivalent subgrade thickness." The derived layer moduli based on such an equivalent subgrade thickness should be more reliable than that from an analysis based on the assumption of infinite subgrade thickness or the selection of an arbitrary subgrade thickness.

SUMMARY

This paper describes a backcalculation method based on the system identification scheme. The SID program is used with the multilayer elastic model (BISAR program) to backcalculate pavement layer properties. Backcalculated moduli are compared with those from other developed programs, and good agreement is observed. The ability to backcalculate pavement layer thicknesses is illustrated by using hypothetical pavement sections and real FWD data.

The backcalculated results for Section 8 indicate clearly that the subgrade thickness should be carefully determined for the pavement under analysis. The backcalculated subgrade modulus assuming infinite thickness may be twice that obtained from an analysis in which the depth to bedrock is arbitrarily selected, such as 610 cm (20 ft). The SID program promises to give more reliable results by considering the subgrade thickness as one of the unknown parameters to be identified.

The SID method is a very powerful and versatile analysis tool and can be applied to a variety of backcalculations. As has been successfully accomplished at Texas A&M University, the parameters of the creep compliance of the AC layer can be backcalculated from FWD data using the SID program and the dynamic multilayer viscoelastic model UTFWIBM (*20*) or SCALPOT (*21*), and the fracture properties of asphalt concrete materials can also be backcalculated from fatigue test data using the SID program and the microcrack model MICROCR (*22*).

ACKNOWLEDGMENTS

The research described herein was sponsored in part by the Strategic Highway Research Program and by the Excellent Young Teacher Foundation of the State Education Committee of China. The authors are pleased to acknowledge their support.

REFERENCES

1. R. E. Smith and R. L. Lytton. *Synthesis Study of Nondestructive Testing Devices for Use in Overlay Thickness Design of Flexible Pavements*. FHWA/RD-83/097. FHWA, U.S. Department of Transportation, 1984.
2. L. H. Irwin. *User's Guide to MODCOMPS, Version 2.1*. Report 83-8. Local Roads Program, Cornell University, Ithaca, N.Y., 1983.
3. A. J. Bush III. *Nondestructive Testing for Light Aircraft Pavements, Phase II: Development of the Nondestructive Evaluation Methodology*. Report FAA-RD-80-9-II. Federal Aviation Administration, Washington, D.C., 1980.
4. J. Uzan, R. L. Lytton, and F. P. Germann. General Procedure for Backcalculating Layer Moduli. Presented at First International Symposium on Nondestructive Testing of Pavements and Backcalculation of Moduli, American Society for Testing and Materials, Baltimore, Md., June 29–30, 1988.
5. J. Michelow. *Analysis of Stresses and Displacements in an N-Layered Elastic System Under a Load Uniformly Distributed on a Circular Area*. CHEVRON Computer Program, California Research Corporation, 1963.
6. D. L. Dejong, M. G. F. Peutz, and A. R. Korswagen. *Computer Program BISAR*. Koninklijkel/Shell-Laboratorium, Amsterdam, the Netherlands, 1973.
7. A. R. Letto. *A Computer Program for Function Optimization Using Pattern Search and Gradient Summation Techniques*. Master's thesis. Texas A&M University, College Station, 1968.
8. A. Ralston and P. Rabinowitz. *A First Course in Numerical Analysis*. McGraw-Hill, New York, 1978.
9. N. Sivaneswaran, S. L. Kramer, and J. P. Mahoney. Advance Backcalculation Using a Nonlinear Least Squares Optimization

Technique. In *Transportation Research Record 1293,* TRB, National Research Council, Washington, D.C., 1991, pp. 93–102.
10. W. Uddin, A. H. Meyer, and W. R. Hudson. Rigid Bottom Considerations for Nondestructive Evaluation of Pavements. In *Transportation Research Record 1070,* TRB, National Research Council, Washington, D.C., 1986, pp. 21–29.
11. H. G. Natke. *Identification of Vibrating Structures.* Springer-Verlag, New York, 1982.
12. R. L. Lytton. Backcalculation of Pavement Layer Properties. In *Nondestructive Testing of Pavements and Backcalculation of Moduli.* STP 1026. ASTM, Philadelphia, Pa., 1988, pp. 7–38.
13. T. Y. Hou. Evaluation of Layered Material Properties from Measured Surface Deflections. Ph. D. dissertation. University of Utah, Salt Lake City, 1977.
14. N. Stubbs. A General Theory of Non-Destructive Damage Detection in Structures in Leipholz. *Proc., Second International Symposium on Structural Control,* Martinus Nijhoff, Dordrecht, the Netherlands, 1987, pp. 694–713.
15. V. S. Torpunuri. *A Methodology To Identify Material Properties in Layered Viscoelastic Half Spaces.* Master's thesis. Texas A&M University, College Station, 1990.
16. W. H. Press, B. P. Flannery, S. A. Teukolsky, and W. T. Vetterling. *Numerical Recipes. The Art in Scientific Computing.* Cambridge University Press, 1989.
17. T. M. Han. A Numerical Solution for the Initial Value Problem of Rigid Differential Equation. *Science Sinaca,* 1976.
18. T. Scullion, J. Uzan, J. I. Yazdani, and P. Chan. *Field Evaluation of the Multi-Depth Deflectometers.* Research Report 1123-2. Texas Transportation Institute, The Texas A&M University System, College Station, 1988.
19. H. Zhou, R. G. Hicks, and C. A. Bell. BOUSDEF: A Backcalculation Program for Determining Moduli of a Pavement Structure. In *Transportation Research Record 1260,* TRB, National Research Council, Washington, D.C., 1990, pp. 166–179.
20. J. Roesset. *Computer Program UTFWIBM.* The University of Texas at Austin, Austin, 1987.
21. A. H. Magnuson, R. L. Lytton, and R. C. Briggs. Comparison of Computer Predictions and Field Data for Dynamic Analysis of Falling Weight Deflectometer Data. In *Transportation Research Record 1293,* TRB, National Research Council, Washington, D.C., 1991, pp. 61–71.
22. *Performance Models and Validation of Test Results.* SHRP Final Report A-005. Texas Transportation Institute, The Texas A&M University System, College Station, 1993.

Some Observations About Backcalculation and Use of a Stiff Layer Condition

JOE P. MAHONEY, BRIAN C. WINTERS, NEWTON C. JACKSON, AND LINDA M. PIERCE

For the last several years, advances in estimating layer elastic moduli by the use of pavement surface deflections and backcalculation computer programs have been rapid. As the available computer programs have continued to evolve, so too has the understanding of the input and output of such software. The stiff layer [its location (depth) and stiffness] is, of course, just one of the many important considerations in performing backcalculation of deflection data. Both the traditional and some of the more recent observations pertaining to the various mechanisms that can result in a stiff layer condition, and the effect on layer moduli in backcalculation, are reviewed. Recent project work in the state of Washington reveals that a saturated soil condition or water table can result in a stiff layer condition. Empirical evidence is offered suggesting that saturated soil conditions (or water table) should be considered when evaluating the results of current backcalculation processes.

It is often necessary to include a stiff layer with a semi-infinite depth to achieve reasonable backcalculation results. Traditionally, such layers were believed to be needed either because of a rock layer or stress sensitive materials (*1*,*2*). Recent project work in the state of Washington reveals that a saturated soil condition or water table can cause the same requirement.

The problem of routinely performing backcalculation without recognizing the effects of a stiff layer condition will be illustrated by using a SHRP/LTPP GPS site located in Florida (Figure 1). As is so often the case, no information is available that would suggest a stiff layer condition is apparent; however, results given in Table 1 suggest that inclusion of a stiff layer at a depth of about 6.4 m (21 ft) results in more interesting moduli. This illustrative exercise does not prove anything; however, it is common to observe the inverted moduli seen in Table 1 for the base and subgrade when a stiff layer condition is not used.

Naturally, this raises questions about how to locate the depth of such stiff layers and how stiff they should be. These two questions concerning depth and stiffness (modulus of elasticity, actually) of the stiff layer will be the primary focus of this paper. First, we should further examine the various causes of a stiff layer condition.

LOAD AND GEOSTATIC STRESSES

The need for stiff layers within the subgrade domain can certainly be due to rock layers or extremely stiff soils such as some glacial tills. However, there may be other conditions, not so immediately apparent, which warrant the use of a stiff layer within the subgrade. First, we should look at some typical stresses in the subgrade due to an applied load and geostatic conditions.

Another LTPP section (GPS 6A, located in Kentucky) will be used to illustrate this (Figure 2). The boring log did suggest a potential stiff layer at a depth of about 5 m (16.5 ft). By use of the ELSYM5 computer program, the vertical and horizontal stresses were estimated under a 40-kN (9,000-lb) load with a 0.69-MPa (100-psi) contact pressure. Two moduli conditions for the Kentucky LTPP section were used as indicated in Table 2.

The geostatic stresses are caused by the weight of the soil. Vertical geostatic stress, σ_v, can be straightforwardly calculated as follows [after Lambe and Whitman (*3*)]:

$$\sigma_v = (z)(\gamma) \quad (1)$$

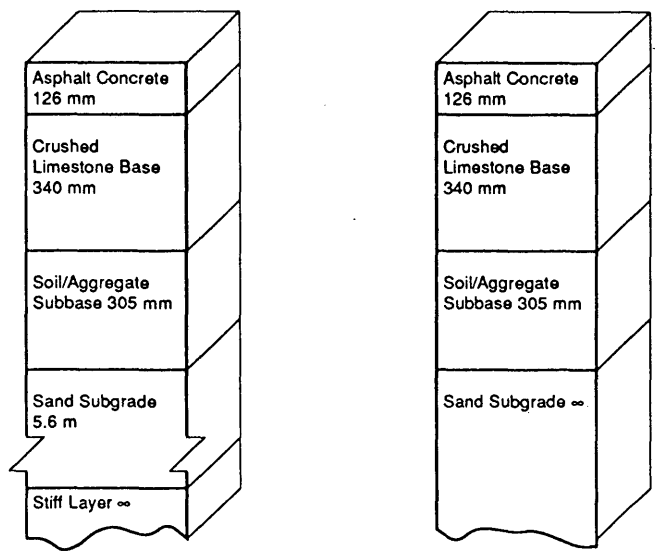

1 mm = 0.039 in.
1 m = 3.28 ft.

FIGURE 1 SHRP/LTPP GPS-1 pavement section, Florida.

J. P. Mahoney and B. C. Winters, University of Washington, 121 More Hall, FX-10, Seattle, Wash. 98195. N. C. Jackson and L. M. Pierce, Washington State Department of Transportation, P.O. Box 47365, Olympia, Wash. 98504-7365.

TABLE 1 Load and Deflection Data and Backcalculated Layer Moduli—SHRP/LTPP GPS-1 Pavement Section, Florida

Load = 75.9 kN		
0 mm	–	382.2 μm
203 mm	–	301.5 μm
305 mm	–	257.0 μm
457 mm	–	201.2 μm
610 mm	–	161.5 μm
914 mm	–	105.2 μm
1,524 mm	–	52.3 μm

Layer	Backcalculated Moduli, MPa	
	Case 1 (with stiff layer)	Case 2 (without stiff layer)
AC (21°C)	10,474	13,900
Base	396	216
Combined Subbase/Subgrade	177	239
Stiff Layer @ 6.4 m	*6,895	NA

*Pre-set (fixed) modulus

1 N = 0.225 lbf
1 mm = 0.039 in
1 km = 0.039 mils
1 kPa = 0.145 psi
1 m = 3.28 ft

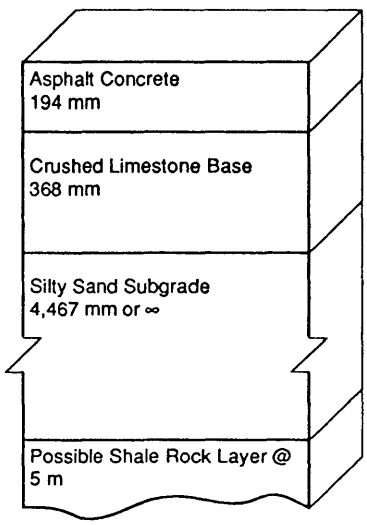

1 mm = 0.039 in.
1 m = 3.28 ft.

FIGURE 2 SHRP/LTPP GPS-6A pavement section, Kentucky.

TABLE 2 Moduli Cases Used for Kentucky LTPP GPS-6A Pavement Section

Layer	Thickness	Moduli, MPa	
		Case 1	Case 2
AC	194 mm	6895	6895
Base	368 mm	345	621
Subgrade	Case 2 Only 4.5 m	276	207
Stiff Layer	Case 2 Only @ 5.0 m	NA	6895

1 kPa = 0.145 psi
1 mm = 0.39 in
1 m = 3.28 ft

where

σ_v = vertical stress,
z = depth, and
γ = total unit weight of the soil.

Horizontal geostatic stress, σ_h, is related to the vertical geostatic stress by the coefficient of lateral stress, which is designated K:

$$K = \frac{\sigma_h}{\sigma_v} \tag{2}$$

$K \approx 0.5$ for normally consolidated sedimentary soils but can approach 3 for heavily preloaded soils (overconsolidated). When $K < 1$, $\sigma_v = \sigma_1$ and $\sigma_h = \sigma_3$. When $K > 1$, $\sigma_h = \sigma_1$ and $\sigma_v = \sigma_3$.

The load and geostatic stresses are separately summarized in Table 3. The geostatic stresses tend to be dominant and become fairly large at depths as shallow as 3.0 m (10 ft). Since the geostatic stresses are static, one might discount σ_v; however, σ_h is analogous to σ_3 as used in most triaxial tests for unstabilized pavement materials [such as AASHTO T-274 (*4*)]. Depending on depth and K, σ_h is fairly large as shallow as 1.5 to 3.0 m (60 to 120 in.). The implication is that such stresses combined with stress-sensitive subgrades can result in a high stiffness condition at depth.

This example concerning load and geostatic stresses only illustrates one reason a stiff layer condition is needed for backcalculation of layer moduli. The next question to address is how deep such layers might be, or more specifically, how the depth to a stiff layer can be estimated.

ESTIMATION OF STIFF LAYER DEPTH

Recent literature provides at least two approaches for estimating the depth to stiff layer (*5*,*6*). Use of either procedure would assume more specific stiff layer indications (say, from a boring log) are not available, which seems to be common. The approach used by Rohde and Scullion (*5*) will be summarized below. There are three reasons for this selection: (*a*) initial verification of the validity of the approach is documented, (*b*) the approach is used in MODULUS 4.0, a backcalculation program widely used in the United States, and (*c*) the approach was adopted for use in the EVERCALC program, results from which will be presented subsequently.

Basic Assumptions and Description

A fundamental assumption is that the measured pavement surface deflection is a result of deformation of the various materials in the applied stress zone; therefore, the measured surface deflection at any distance from the load plate is the direct result of the deflection below a specific depth in the pavement structure (which is determined by the stress zone). This is to say that only the portion of the pavement structure that is stressed contributes to the measured surface deflections. Further, no surface deflection will occur beyond the offset (measured from the load plate) that corresponds to the intercept of the applied stress zone and the stiff layer (the

TABLE 3 Calculated Stresses for Various Depths Beneath the Load—LTPP Kentucky Pavement Section

Load Stress Only

Depth, m	Load Stresses, kPa							
	Case 1				Case 2			
	σ_z	σ_x or σ_y	θ	σ_d	σ_z	σ_x or σ_y	θ	σ_d
1.5	6.2	0.7	7.6	5.5	5.5	0.7	6.9	4.8
3.0	2.1	~0	2.1	2.1	2.8	0.7	4.2	2.1
5.0	1.4	~0	1.4	1.4	2.1	0.7	3.4	1.4
6.1	0.7	~0	0.7	0.7	1.4	~0	1.4	1.4
12.2	~0	~0	~0	~0	~0	~0	~0	~0
25.4	~0	~0	~0	~0	~0	~0	~0	~0

Geostatic Stress Only

Depth, m	Geostatic Stresses, kPa						
	σ_v	σ_h (K = 0.5)	σ_h (K = 3)	K = 0.5		K = 3	
				θ	σ_d	θ	σ_d
1.5	24	12	72	49	12	121	48
3.0	48	23	143	94	24	238	95
5.0	79	40	238	159	39	396	159
6.1	96	48	288	192	48	479	192
12.2	192	96	575	383	96	958	383
25.4	399	199	1196	797	199	1993	797

1 kPa = 0.145 psi
1 m = 3.28 ft

stiff layer modulus being 100 times larger than the subgrade modulus). Thus, the method for estimating the depth to stiff layer assumes that the depth at which zero deflection occurs (presumably due to a stiff layer) is related to the offset at which a zero surface deflection occurs. This is shown in Figure 3, where the surface deflection D_c is zero.

An estimate of the depth at which zero deflection occurs can be obtained from a plot of measured surface deflections and the inverse of the corresponding offsets ($1/r$). This is shown in Figure 4. The middle portion of the plot is linear with either end curved due to nonlinearities associated with the upper layers and the subgrade. The zero surface deflection is estimated by extending the linear portion of the D versus $1/r$ plot to D = 0, the $1/r$ intercept being designated as r_0. Because of various pavement section–specific factors, the depth to stiff layer cannot be directly estimated from r_0—additional factors must be considered. To do this, regression equations were developed on the basis of BISAR computer program–generated data for various levels of the following factors: load = 40 kN (9,000 lb), moduli ratios (E_1/E_{sg}, E_2/E_{sg}, and E_{stiff}/

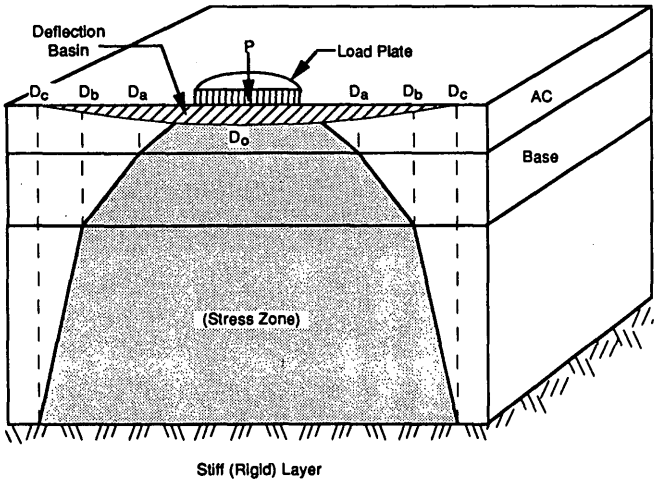

FIGURE 3 Zero deflection due to a stiff layer.

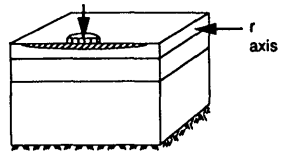

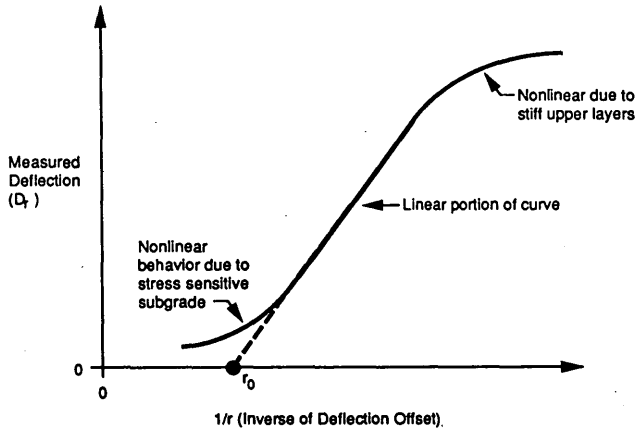

FIGURE 4 Plot of inverse of deflection offset versus measured deflection.

E_{sg}), and layer thicknesses (surface layer, base layer, and depth to stiff layer measured from the pavement surface).

Four separate regression equations were reported by Rohde and Scullion (*5*) for various levels of AC layer thickness. The dependent variable is $1/B$ (where B is the depth to the top of the stiff layer measured from the pavement surface), and the independent variables are r_0 (which is the $1/r$ intercept as shown in Figure 4) and various deflection basin parameters. The equations are as follows: For AC less than 50 mm (2 in.) thick,

$$\frac{1}{B} = 0.0362 - 0.3242(r_0) + 10.2717(r_0^2) - 23.6609(r_0^3) - 0.0037(\text{BCI}) \quad (3)$$

For AC 50 to 100 mm (2 to 4 in.) thick,

$$\frac{1}{B} = 0.0065 + 0.1652(r_0) + 5.4290(r_0^2) - 11.0026(r_0^3) + 0.0004(\text{BDI}) \quad (4)$$

For AC 100 to 150 mm (4 to 6 in.) thick,

$$\frac{1}{B} = 0.0413 + 0.9929(r_0) - 0.0012(\text{SCI}) + 0.0063(\text{BDI}) - 0.0778(\text{BCI}) \quad (5)$$

For AC greater than 150 mm (6 in.) thick,

$$\frac{1}{B} = 0.0409 + 0.5669(r_0) + 3.0137(r_0^2) + 0.0033(\text{BDI}) - 0.0665\log(\text{BCI}) \quad (6)$$

where

r_0 = $1/r$ intercept (extrapolation of the steepest section of the D versus $1/r$ plot) in units of ft^{-1};
SCI = $D_0 - D_{305\ mm}$ ($D_0 - D_{12\ in.}$), surface curvature index;
BDI = $D_{305\ mm} - D_{610\ mm}$ ($D_{12\ in.} - D_{24\ in.}$), base damage index;
BCI = $D_{610\ mm} - D_{914\ mm}$ ($D_{24\ in.} - D_{36\ in.}$), base curvature index; and
D_i = surface deflections (mils) normalized to a 40-kN (9,000-lb) load at an offset i.

Confirmation of Stiff Layer Depths

Data provided to the authors by B. Mårtensson of RST Sweden AB during 1992 provided the initial confirmation of the Rohde and Scullion (*5*) stiff layer calculation (other than reported by Rohde and Scullion). The results provided by Mårtensson are shown in Figure 5. The road (Route Z-675) is located in south-central Sweden. The field-measured depths were obtained by use of borings and a mechanical hammer. The hammer was used to drive a drill to "refusal" [similar to the standard penetration test (SPT)]. Thus, the measured depths could be bedrock, a large stone, or hard till (glacially deposited material); however, this is an area where rock is commonly encountered at relatively shallow depths. Furthermore, the field-measured depths were obtained independently of the FWD deflection data (time difference of several years).

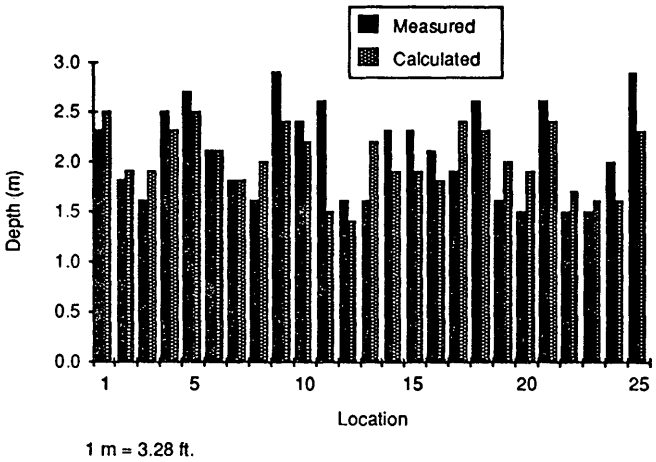

FIGURE 5 Plot of measured and calculated depths to stiff layer for Road Z-675 (Sweden).

The FWD deflections were obtained with a KUAB 50 with deflection sensor locations of 0, 200, 300, 450, 600, 900, and 1200 mm (0, 7.9, 11.8, 17.7, 23.6, 35.4, and 47.2 in.) from the center of the load plate. The equations by Rohde and Scullion (*5*) were used to calculate the depth to stiff layer. Since the process requires a 40-kN (9,000-lb) load and 305-mm (1-ft) deflection sensor spacings, the measured deflections were adjusted linearly according to the ratio of the actual load to a 40-kN (9,000-lb) load.

This initial confirmation resulted in the addition of the Rohde and Scullion (*5*) equations to the program EVERCALC, which is the backcalculation software used by WSDOT (*7*). This program, along with data from two pavements located in Washington State, will be used to illustrate that the depth to stiff layer and the stiff layer modulus are both important in obtaining reasonable layer moduli from the backcalculation process. Furthermore, the stiff layer condition appears, at least in some cases, to be strongly influenced by saturated soil conditions (or the water table).

PAVEMENT SECTIONS AND RESULTS

Two pavement sections will be used to illustrate two basic points: (*a*) that the Rohde and Scullion equations appear to estimate the depth to stiff layer for a wider variety of conditions than initially expected and (*b*) that the stiff layer can be "triggered" by saturated soil conditions. The two pavement sections will be separately described, along with the associated results. One section is located at the PACCAR Technical center [about 100 km (60 mi) north of Seattle, Washington] and the other on a state highway (SR-525) located about 25 km (15 mi.) north of Seattle.

PACCAR Technical Center Pavement Section

This test pavement is being used in a joint study between PACCAR, WSDOT, Caltrans, The University of Washington, and the University of California at Berkeley. The flexible pavement is surfaced with 137 mm (5.4 in.) of dense-graded AC (WSDOT Class B) over a 300-mm (13.0-in.) crushed stone base over a sandy clay subgrade. The water table was measured at a depth of 1.7 m (66 in.).

During October 1991, a Dynatest 8000 FWD was used to obtain deflection measurements at 61 separate locations (129 drops). The applied load varied from 21.7 to 63.4 kN (4,874 to 14,527 lb). During testing, the measured average middepth temperature of the AC layer was 20°C (68°F). By use of EVERCALC 3.3, the layer moduli were estimated for various conditions using the previously mentioned layer thicknesses (surface and base) and Poisson's ratios of 0.35 (AC) and 0.40 (base).

Initially, the stiff layer was fixed with a modulus of 6895 MPa (1,000 ksi), and the depth to stiff layer algorithm estimated the top of the stiff layer to be between 1.5 and 1.8 m (60 and 70 in.), which was extremely close to the measured depth of water table. There are no known rock or other major layer transitions within several feet of the surface at this site. As a result, only 31 of the 130 deflection basins resulted in an RMS error convergence of 2.5 percent or less (2.5 percent was used as an acceptable upper limit). Thus, it was decided to try various moduli values for the stiff layer ranging from a low of 69 MPa (10 ksi) to a high of 6895 MPa (1,000 ksi). The resulting layer moduli are given in Table 4 and associated RMS statistics in Table 5.

The results suggest that the stiff layer was "triggered" by the saturated conditions below the water table and, for this condition, a stiff layer modulus of about 276 MPa (40 ksi) is more appropriate than, say, 6895 MPa (1,000 ksi). This observation is based on the RMS and the layer moduli values. For example, the AC modulus of 3885 MPa (563 ksi) corresponds to an expected value of about 4140 MPa (600 ksi) on the basis of laboratory tests for WSDOT Class B mixes—a rather close agreement. The base modulus of 103 MPa (15 ksi) might be a bit low, but the subgrade modulus of 69 MPa (10 ksi) appears to be reasonable.

The effect of using various stiff layer stiffnesses can be illustrated by use of a basic parameter used in mechanistic-empirical pavement design (new or rehabilitation). This parameter is the horizontal tensile strain at the bottom of the AC layer. These strains were calculated for various FWD load levels, backcalculated layer moduli, and three stiff layer modulus conditions with the results shown in Figure 6. Clearly, the estimated strain levels are significantly influenced by the stiff layer modulus condition.

SR-525 Pavement Section

The field data for this pavement section consisted of FWD (Dynatest 8000) deflection basins and boring logs at Mileposts 1.70 and 2.45. This information was obtained from WSDOT production data associated with the normal pavement design process. The FWD testing was done on April 15, 1992, with a measured middepth AC temperature of 7°C (45°F). The condition of the AC layer was variable with various amounts

TABLE 4 Sensitivity of Layer Moduli as a Function of the Stiff Layer Modulus—PACCAR Test Section

	E_{stiff}						
Pavement Layers	69 MPa	173 MPa	276 MPa	345 MPa	518 MPa	690 MPa	6900 MPa
Asphalt Concrete (MPa)*	6100	5713	3885	3284	2795	2539	1960
Crushed Stone Base* (MPa)	17	29	104	138	186	207	290
Fine-grained Subgrade (MPa)*	9908	297	69	59	48	48	37

*Calculated from runs with a RMS% <=2.5%.

1 kPa = 0.145 psi

TABLE 5 Sensitivity of RMS Values as a Function of the Stiff Layer Modulus—PACCAR Test Section

	E_{stiff}						
RMS (%)	69 MPa	173 MPa	276 MPa	345 MPa	518 MPa	690 MPa	6900 MPa
Mean*	3.0	1.4	1.3	1.7	2.3	2.6	3.8
Standard Deviation*	0.7	0.8	0.9	1.0	1.2	1.3	1.6
Minimum*	1.4	0.4	0.2	0.2	0.6	0.8	1.4
Maximum*	5.6	5.2	6.9	7.5	8.2	8.5	9.4
Total Runs with RMS% <=2.5*	22	113	120	118	80	77	31

*Calculated for 129 deflection basins.

1 kPa = 0.145 psi

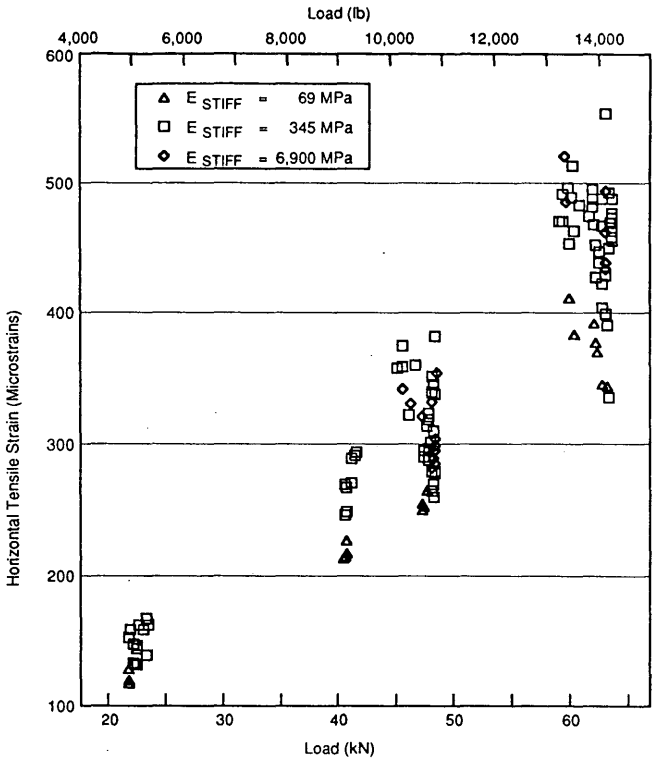

1 kPa = 0.145 psi

FIGURE 6 Calculated horizontal tensile strain versus FWD load for the PACCAR test section.

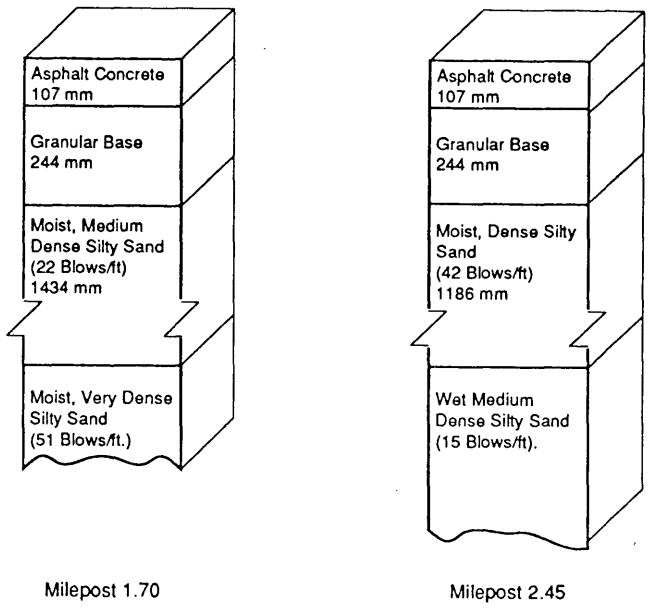

1 mm = 0.039 in.

FIGURE 7 Cross section for SR-525 pavement sections, MP 1.70 and 2.45.

of fatigue and longitudinal cracking, patching, and minor rutting. The boring logs (summaries of which are shown as Figure 7) indicated no specific water table, but moist/wet conditions were encountered at about 0.9 m (3 ft) (MP 1.70) and 0.6 m (2 ft) (MP 2.45).

The stiff layer algorithm in EVERCALC estimated a stiff layer condition at a depth of 1.8 m (5.9 ft) for MP 1.70. This depth coincides with a transition point from a medium dense sand (22 blows per foot measured by SPT) to a very dense sand (51 blows per foot). The calculated stiff layer for MP 2.45 was 1.5 m (5.0 ft), which coincides with a transition from a moist, dense sand (42 blows per foot) to a wet, medium dense sand (15 blows per foot).

The backcalculated layer moduli, stiff layer moduli, and associated RMS values are given in Tables 6 and 7 for MP 1.70 and 2.45, respectively. The results for MP 1.70 appear to best match the lower stiff layer modulus [345 MPa (50 ksi)]. An AC modulus of about 10 350 MPa (1,500 ksi) would be expected on the basis of uncracked laboratory test conditions. The backcalculated AC modulus is within this range. A visual inspection of the AC condition showed no cracking or rutting at this milepost. The base and subgrade moduli are reasonable, with a low RMS level (1.0 percent average based on four deflection basins). The MP 2.45 section is different. The AC layer exhibited fatigue cracking and rutting, resulting in lower AC moduli. Overall, the lower stiff layer stiffness is preferred; however, the average RMS values (again, based on four deflection basins) are all rather high at this milepost.

TABLE 6 Sensitivity of Layer Moduli as a Function of Stiff Layer Modulus—SR-525 Pavement Section, MP 1.70

Pavement Layers	E_{stiff}	
	345 MPa	6900 MPa
Asphalt Concrete (MPa)*	12177	3472
Crushed Stone Base (MPa)*	232	750
Subgrade (MPa)*	89	52
RMS(%)*	1.0	2.7

*Average of all runs

1 kPa = 0.145 psi

TABLE 7 Sensitivity of Layer Moduli as a Function of Stiff Layer Modulus—SR-525 Pavement Section, MP 2.45

Pavement Layers	E_{stiff}	
	345 MPa	6900 MPa
Asphalt Concrete (MPa)*	2611	1616
Crushed Stone Base (MPa)*	190	280
Subgrade (MPa)*	27	21
RMS(%)*	3.7	5.4

*Average of all runs

1 kPa = 0.145 psi

Only 345 MPa (50 ksi) and 6895 MPa (1,000 ksi) were used as stiff layer moduli for this pavement section. Whereas 345 MPa (50 ksi) provides much better results than 6895 MPa (1,000 ksi), 345 MPa (50 ksi) may not be the optimal value for the stiff layer modulus. Consistent with the intent of this paper, these two moduli values were selected only to dem-

onstrate the potential importance of the influence of saturated soil conditions.

SUMMARY AND CONCLUSIONS

Summary

The goal of this paper was to illustrate and support several basic points:

1. The stiff layer is important,
2. The Rohde and Scullion (*5*) algorithm provides a reasonable estimate of the depth to the stiff layer, and
3. The stiffness of the stiff layer appears to be influenced by saturated soil conditions as well as by the more obvious factors (such as rock and stress sensitivity of the subgrade soils).

These points are offered for the reader's consideration. The authors have proved nothing. They have presented some hopefully interesting empirical evidence.

Conclusions

The backcalculation process is a complicated but powerful tool, which will continue to evolve. Much that we now believe we know about the process is based on empirical evidence. This paper shows that the stiff layer is important in the backcalculation process and that saturated soil conditions (or water table) should be considered in so far as we currently do backcalculation with linear elastic theory. Whereas intuitively this concept seems logical, it is absent in current literature. Thus boring logs and evidence of saturated soil conditions may be more important in production work than generally used today. Furthermore, the issue of identifying such conditions appears to diminish below depths of about 3 m (10 ft).

Continued research on potential inputs to backcalculation (such as boring logs) and new procedures (such as finite element analysis) can only contribute to our improved understanding of the backcalculation process.

REFERENCES

1. A. J. Bush. *Nondestructive Testing for Light Aircraft Pavements, Phase II.* Report FAA-RD-80-9-11. U.S. Department of Transportation, 1980.
2. W. Uddin, A. H. Meyer, and W. R. Hudson. Rigid Bottom Considerations for Nondestructive Evaluation of Pavements. In *Transportation Research Record 1070*, TRB, National Research Council, Washington, D.C., 1986.
3. T. W. Lambe, and R. W. Whitman. *Soil Mechanics*. John Wiley and Sons, New York, 1969.
4. *Resilient Modulus of Subgrade Soils*. AASHTO Materials, Part II, 14th edition. American Association of State Highway and Transportation Officials, Washington, D.C., 1986.
5. G. T. Rohde and T. Scullion. *MODULUS 4.0: Expansion and Validation of the MODULUS Backcalculation System*. Research Report 1123-3. Texas Transportation Institute, Texas A&M University System, College Station, 1990.
6. A. S. M. Hossain and J. P. Zaniewski. Detection and Determination of Depth of Rigid Bottom in Backcalculation of Layer Moduli from Falling Weight Deflectometer Data. In *Transportation Research Record 1293*, TRB, National Research Council, Washington, D.C., 1991.
7. J. Mahoney, D. Newcomb, N. Jackson, L. Pierce, and B. Mårtensson. *Pavement NDT Data Applications*. Course notes. Washington State Transportation Center, Seattle, Jan. 1992.

Modified Newton Algorithm for Backcalculation of Pavement Layer Properties

RONALD S. HARICHANDRAN, TARIQ MAHMOOD, A. ROBERT RAAB, AND GILBERT Y. BALADI

An efficient algorithm for the backcalculation of pavement layer moduli from measured surface deflections is presented. The algorithm is an iterative one and can use any mechanistic analysis program for forward calculations (presently an extended precision CHEVRON program is used for this purpose). Most mechanistic-based backcalculation methods attempt to find the layer moduli that minimize the weighted sum of the relative or absolute errors between measured and predicted surface deflections. Using a search technique to achieve such a minimization sometimes requires hundreds of calls to a mechanistic analysis program, and some programs try to speed this up by using a previously created data base. The algorithm presented here is different in that it uses a modified Newton method to obtain the least-squares solution of an overdetermined set of equations. This gives the proposed algorithm a robustness that some other approaches appear to lack. For example, the predicted moduli are not too sensitive to the initially assumed seed moduli or the location of the stiff layers (e.g., CRAM section, composite pavements, shallow or deep bedrock, etc.). Further, a set of auxiliary equations that are totally independent of those used in the modified Newton method and that relate surface deflections to the compressions in each pavement layer are used to improve the speed of convergence. The algorithm is also extended to improve incorrectly specified layer thicknesses. The algorithm is being implemented in a new backcalculation program named MICHBACK.

The backcalculation of layer properties from surface deflection measurements is of considerable importance for the accurate evaluation and design of overlays and the management of existing pavements. Most existing methods predict only elastic layer moduli, but often the layer thicknesses are known only approximately and may also need revision.

There are three general classes of backcalculation methods:

1. Iterative methods that repeatedly adjust the layer moduli and call a mechanistic analysis program until a suitable match of the deflection basin is obtained [e.g., CHEVDEF/BISDEF/ELSDEF series (*1*), EVERCALC (*2*)],
2. Methods that match the measured deflection basin with a data base of deflection basins computed in advance for a variety of layer moduli [e.g., MODULUS (*3*)], and
3. Methods that use statistical regression equations [e.g., LOADRATE (*4*)].

R. S. Harichandran, T. Mahmood, and G. Y. Baladi, Department of Civil and Environmental Engineering, Michigan State University, East Lansing, Mich. 48824-1226. A. R. Raab, Strategic Highway Research Program, 818 Connecticut Avenue, N.W., Washington, D.C. 20006.

Iterative methods are usually slow since they require numerous calls to a mechanistic analysis program, and sometimes the results are sensitive to the initial seed moduli. Methods that use a data base are fast, but the data base of deflection basins corersponding to the range of expected layer properties must be established before backcalculation is performed, and the results are usually sensitive to the seed moduli. Methods that are statistical regression equations are very fast but usually do not have acceptable accuracy.

Almost all existing iterative methods estimate the layer moduli by minimizing an objective function that is the weighted sum of squares of the differences between calculated and measured surface deflections (*3*), that is,

$$\text{minimize } f = \sum_{j=1}^{m} \alpha_j [w_j - \hat{w}_j]^2 \quad (1)$$

where

w_j = measured deflection at Sensor j,
$\hat{w}_j$ = calculated deflection at Sensor j, and
α_j = weighting factor for Sensor j.

Often, the weighted sum of squares of the relative differences between calculated and measured deflections is minimized by choosing each weight in Equation 1 to be inversely proportional to the measured surface deflections. One of the problems with this approach is that the multidimensional surface represented by the objective function may have many local minima, and as a result the minimum to which a numerical procedure converges may depend on the initial seed moduli supplied by the analyst. Another problem is that convergence can be very slow because numerous calls to a mechanistic analysis program (i.e., forward calculations) are required by most numerical minimization techniques to revise the moduli after each iteration. An efficient and general minimization method (Levenberg-Marquardt algorithm) has been implemented in EVERCALC that makes it converge quickly with only a modest number of calls to the mechanistic analysis program (original CHEVRON). The "_____DEF" series of programs also makes only a modest number of calls to a mechanistic analysis program by using empirically determined rules to revise the layer moduli after each iteration, but the results of these programs are sensitive to the initial seed moduli. The EVERCALC program has also been used to suc-

cessfully estimate the asphalt layer thickness in flexible pavements from theoretical deflection basins (*2*).

IMPROVED INITIAL ESTIMATE OF SUBGRADE MODULUS

It is well known that the deflections measured by the sensors far from the applied load are affected mostly by the deeper pavement layers, and some programs initially estimate the subgrade modulus by using only the furthest sensor. This approach is prone to error, especially if the furthest sensor measurement is inaccurate. Recognizing that the subgrade contributes strongly to the deflection at all sensors, a technique is developed for substantially improving the subgrade modulus using a single call to a mechanistic analysis program.

Consider a pavement with n layers for which m surface deflections are measured ($m \geq n$). Let the vector $\{\hat{w}_j\}$ contain the m deflections computed at the top of the jth layer using current estimates of the layer moduli ($\hat{E}_j$). The vertical compression under the sensors in the jth layer is $\{\hat{w}_j\} - \{\hat{w}_{j+1}\}$. For the last layer we take $\{\hat{w}_{n+1}\} = \{0\}$. The vertical compression in any layer represents the accumulated vertical strain, which is inversely proportional to the layer modulus (i.e., proportional to $\hat{e}_j = 1/\hat{E}_j$). Let the compressions in each layer scaled by the layer modulus be

$$\{a_j\} = \hat{E}_j(\{\hat{w}_j\} - \{\hat{w}_{j+1}\}) \tag{2}$$

and the collection of all such vectors be the $n \times m$ matrix

$$[A] = [\{a_1\}\ \{a_2\} \ldots \{a_m\}] \tag{3}$$

The sum of the compressions in each layer must sum to the total surface deflection, that is,

$$\sum_{j=1}^{n} (\{\hat{w}_j\} - \{\hat{w}_{j+1}\}) = \{\hat{w}_1\} \tag{4}$$

or, equivalently,

$$[A]\{\hat{e}\} = \{\hat{w}_1\} \tag{5}$$

The following iterative method can be obtained from Equation 5:

$$[A]^i\{\hat{e}\}^{i+1} = \{w\} \tag{6}$$

where $[A]^i$ is computed using the current moduli estimates $\{\hat{E}\}^i$ and $\{w\}$ are the measured surface deflections. The formulation of this iterative process was first suggested by A. R. Raab (unpublished data). The overdetermined system of equations (n equations in m unknowns) is solved using the method of least squares to obtain the revised inverse moduli $\{\hat{e}\}^{i+1}$. It may appear that Equation 6 can be used iteratively to improve the estimates of all the layer moduli, but unfortunately the iteration is very sensitive and rather unstable for estimating all the unknown layer moduli. Often the upper layer moduli become negative. However, since all the surface deflection measurements are strongly influenced by the subgrade modulus, the estimate of the subgrade modulus is greatly improved after a single iteration, irrespective of the initial seed moduli. Equation 6 is therefore used once in the beginning to obtain an accurate initial estimate of the subgrade modulus.

MODIFIED NEWTON METHOD

Consider the Newton method for solving a single nonlinear equation (e.g., estimating a single layer modulus from a single surface deflection measurement). The method is shown in Figure 1. The nonlinear deflection versus modulus curve is approximated by a straight line that is tangent to it at the estimate $\hat{E}^i$. The slope of the straight line, $(dw/dE)|_{E=\hat{E}^i}$, is used to obtain the increment, ΔE^i, which is added to $\hat{E}^i$ to obtain the improved modulus estimate $\hat{E}^{i+1}$. Since the slope is not known analytically, it must be obtained numerically through

$$\left.\frac{dw}{dE}\right|_{E=\hat{E}^i} \approx \frac{w[(1+r)\hat{E}^i] - w(\hat{E}^i)}{r\hat{E}^i} \tag{7}$$

where r is sufficiently small (say 0.05). This requires the additional deflection arising from a modulus of $(1 + r)\hat{E}^i$ to be computed.

For m sensors and n layers, the "slope" is represented by the gradient matrix

$$[G]^i = \left[\frac{\partial\{w\}}{\partial\{E\}}\right]_{\{E\}=\{\hat{E}\}^i} = \left[\begin{matrix} \frac{\partial w_1}{\partial E_1} & \frac{\partial w_1}{\partial E_2} & \cdots & \frac{\partial w_1}{\partial E_n} \\ \vdots & & & \vdots \\ \frac{\partial w_m}{\partial E_1} & \frac{\partial w_m}{\partial E_2} & \cdots & \frac{\partial w_m}{\partial E_n} \end{matrix}\right]_{\{E\}=\{\hat{E}\}^i} \tag{8}$$

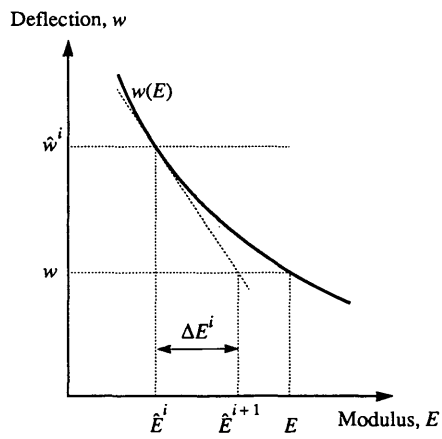

FIGURE 1 Newton's method.

and the element on the jth row and kth column of the matrix is estimated numerically as

$$\left.\frac{\partial w_j}{\partial E_k}\right|_{\{E\}=\{\hat{E}\}^i} \approx \frac{w_j([R]\{\hat{E}\}^i) - w_j(\{\hat{E}\}^i)}{r\hat{E}_k^i}$$

where $[R]$ is a diagonal matrix with the kth diagonal element being $(1 + r)$ and all other diagonal elements being 1 [i.e., the partial derivative is estimated numerically by taking the difference in the jth deflection arising from the use of the moduli $\hat{E}_1^i, \hat{E}_2^i, \ldots, (1 + r)\hat{E}_k^i, \ldots, \hat{E}_n^i$ and the use of the moduli $\hat{E}_1^i, \hat{E}_2^i, \ldots, \hat{E}_k^i, \ldots, \hat{E}_n^i$]. Thus, a separate call to a mechanistic analysis program is required to compute the partial derivatives in each column of the gradient matrix. Increments to the moduli, $\{\Delta E\}^i$, can then be obtained by solving the m equations in n unknowns.

$$\{\hat{w}\}^i + [G]^i\{\Delta E\}^i = \{w\} \tag{9}$$

and the revised moduli are obtained through

$$\{E\}^{i+1} = \{E\}^i + \{\Delta E\}^i \tag{10}$$

One technique for solving the least-squares problem is to solve the $n \times n$ normal equations

$$[G]^T[G]\{\Delta E\}^i = [G]^T\{\{w\} - \{\hat{w}\}^i\} \tag{11}$$

However, the condition number of the matrix $[G]^T[G]$ is the square of the condition number of $[G]$, and hence solving the normal equations can magnify the effect of errors in the elements of $[G]$, errors in $\{w\}$, and round-off errors that accumulate during calculations. The recommended method for solving linear least-squares problems is by using orthogonal factorizations or singular value decomposition (*5*).

The iteration is terminated when the changes in the layer moduli are sufficiently small, that is,

$$\frac{\hat{E}_k^{i+1} - \hat{E}_k^i}{\hat{E}_k^i} < \varepsilon \qquad k = 1, 2, \ldots, n \tag{12}$$

In addition, if the computed and measured deflections match closely, the root-mean-square error defined by

$$\text{RMS error in deflections} = \sqrt{\frac{1}{m}\sum_{j=1}^{m}\left(\frac{\hat{w}_j^i - w_j}{w_j}\right)^2} \tag{13}$$

will also be small. Only for theoretical deflection basins generated by an elastic layer program can the iteration be carried on until the RMS error in the deflections is smaller than a value requested by the analyst. For deflection basins measured in the field, it will usually not be possible to obtain an arbitrarily close match between the computed and measured deflections.

The initial formulation of the Newton method for backcalculating layer moduli was also conceived and first suggested to the research team by Raab (unpublished data). A literature search has revealed that the method was conceived previously and published by Hou (*6*).

In the Newton method, the number of calls made to a mechanistic analysis program is $(n + 1)$ for each iteration. The total number of forward calculations can be reduced by using a modified Newton approach in which several iterations are performed with a gradient matrix before it is revised. The modified Newton method usually converges more slowly than the normal method but saves n forward calculations required to compute the gradient matrix during each iteration. Experience has shown that performing three iterations before revising the gradient matrix yields good convergence with fewer calls to the mechanistic analysis program.

The Newton method is a rapidly convergent algorithm but can sometimes diverge for badly behaved functions if the initial guesses for the solutions are poor. For the pavement backcalculation problem, however, the surface deflections (which are functions of the layer moduli and thicknesses) appear to be well behaved, and for most problems convergence is obtained even for very poor initial guesses (i.e., seed moduli). The modified Newton algorithm is applicable to flexible or rigid pavements as long as an appropriate mechanistic program is used for the forward calculations.

IMPROVING LAYER THICKNESSES

In many situations the thickness of some pavement layers may only be known approximately. Incorrect thickness specifications usually lead to larger errors in the predicted layer moduli. For example, if a layer thickness smaller than the actual one is specified, the modulus backcalculated for that layer will usually be larger than the correct one in order to yield an equivalent layer stiffness. In such situations the analyst may wish to have the backcalculation program improve the incorrect layer thicknesses. Layer thickness improvement has been successfully accomplished for theoretical deflection basins using the EVERCALC program (*2*). The modified Newton method can also be readily extended to include such capability as long as the total number of unknown layer moduli and layer thicknesses does not exceed the number of sensors. For improving l layer thicknesses, Equation 9 is expanded to

$$\{\hat{w}\}^i + [G]^i\begin{Bmatrix}\{\Delta E\}^i \\ \{\Delta t\}^i\end{Bmatrix} = \{w\} \tag{14}$$

where $\{\Delta t\}^i$ is the vector of thickness increments and the augmented gradient matrix is

$$[G]^i = \left.\left[\frac{\partial\{w\}}{\partial\{E\}}\ \frac{\partial\{w\}}{\partial\{t\}}\right]\right|_{\substack{\{E\}=\{\hat{E}\}^i \\ \{t\}=\{\hat{t}\}^i}}$$

$$= \left.\begin{bmatrix} \frac{\partial w_1}{\partial E_1} & \cdots & \frac{\partial w_1}{\partial E_n} & \frac{\partial w_1}{\partial t_1} & \cdots & \frac{\partial w_1}{\partial t_l} \\ \vdots & & \vdots & \vdots & & \vdots \\ \frac{\partial w_m}{\partial E_1} & \cdots & \frac{\partial w_m}{\partial E_n} & \frac{\partial w_m}{\partial t_1} & \cdots & \frac{\partial w_m}{\partial t_l} \end{bmatrix}\right|_{\substack{\{E\}=\{\hat{E}\}^i \\ \{t\}=\{\hat{t}\}^i}} \tag{15}$$

A column of the gradient matrix corresponding to a partial derivative with respect to a thickness is estimated numerically

by computing the surface deflections due to a slight increase in that thickness. The number of forward calculations during each iteration now increases to $(n + l + 1)$.

It has been found that better overall convergence is achieved if the layer moduli are first estimated with fixed layer thicknesses as discussed in the previous section, and then additional iterations are performed to improve both the layer moduli and thicknesses as outlined in this section.

In principle the technique outlined above can be used to predict any layer property, including Poisson's ratio, as long as the number of unknown quantities does not exceed the number of sensor locations. All that is required is that the partial derivatives of the surface deflections with respect to the unknown quantities be estimated. However, at present the method has only been tested for estimation of layer moduli and thicknesses. Preliminary results indicate that at times the iteration does not converge as the number of unknown quantities is increased.

MICHBACK PROGRAM

The algorithm presented in this paper is being implemented in a new computer program named MICHBACK. The forward calculation program used by MICHBACK is an extended precision version of the CHEVRON program, henceforth called CHEVRONX.

Several elastic layer analysis programs are currently being used in practice for flexible pavement analysis. The CHEVRON program has been widely used, partly because it is in the public domain, and many newer programs are based on it. However, it has been discovered by various researchers that the numerical integration performed in CHEVRON is not sufficiently accurate for stiff pavements, and differences have been observed between results obtained from the BISAR (*7*) and CHEVRON programs, especially in surface deflections close to the applied load. The four-part Legendre-Gauss quadrature used in our version of the original CHEVRON program was extended to 16- and 18-part Legendre-Gauss quadrature over different intervals by L. Irwin of Cornell University to obtain the extended precision program CHEVRONX (which yields results identical to those of the version of the CHEVRON program distributed by Cornell University, CHEVLAY2). Results from CHEVRONX very closely match those produced by the BISAR (*7*) program.

NUMERICAL EXAMPLES AND COMPARISONS

The real test of any backcalculation program should ultimately be based on how well it can predict the properties of real pavements using surface deflections measured in the field. The actual in situ properties of real pavements, however, are seldom known accurately and often sound engineering judgment must be used to ascertain whether the backcalculated properties are reasonable. Whereas backcalculations based on field measurements will be performed in due course using MICHBACK, the initial results presented in this paper are based on "theoretical" deflections basins generated by the elastic layer program CHEVRONX. Note that deflection basins generated by BISAR or CHEVLAY2 would essentially be identical to those generated by CHEVRONX.

Several examples of backcalculation using MICHBACK are given in this section. All the examples are due to a wheel load of 40.034 kN (9,000 lbf) applied to a circular area of radius 150.1 mm (5.91 in.) and seven surface deflections calculated at radial distances of 0, 203.2, 304.8, 457.2, 609.6, 914.4, and 1524 mm (0, 8, 12, 18, 24, 36, and 60 in.) from the center of the loaded area. Surface deflections were rounded to the nearest hundredth of a mil (1 mil = 0.001 in.) before being input to all programs. The moduli backcalculated by MICHBACK are compared with the values obtained from the MODULUS 4.0 and EVERCALC 3.0 programs. Attention was given to making the comparisons as fair and equitable as possible. The forward calculation program used by EVERCALC is the original CHEVRON, whereas that used by MODULUS is WES5 (whose precision is comparable to that of CHEVRONX). To assess whether the results obtained with EVERCALC were sensitive to the difference in precision between the program used to compute the deflection basins (CHEVRONX) and its own forward calculation program (CHEVRON), backcalculations were also performed with EVERCALC using deflection basins generated by the original CHEVRON program. Two sets of backcalculation results are therefore presented for EVERCALC: results tabulated under "EVERCALC" were based on deflection basins generated by CHEVRONX, and the results tabulated under "EVERCALC-Alt" were based on alternative basins generated by CHEVRON.

The MICHBACK and EVERCALC programs require the same types of input parameters. The convergence criterion for the moduli (Equation 12) specified for these programs was $\varepsilon = 0.001$ (0.1 percent), and the seed moduli used in each example are given.

The MODULUS program is somewhat different in its approach, does not allow the anlayst to specify a convergence measure, and requires slightly different input parameters:

1. The most probable value of the subgrade modulus and lower and upper values indicating the range of all other layer moduli are required as input so that a data base of deflection basins can be generated. It was found that the moduli backcalculated by MODULUS were quite sensitive to the initial value of the subgrade modulus and somewhat sensitive to the moduli ranges. To give it a more than fair start, a subgrade seed modulus of 48.26 MPa (7,000 psi) was used for MODULUS, whereas a poorer seed modulus of 20.68 MPa (3,000 psi) was used for the other two programs in all examples. The lower moduli for layers other than the subgrade and concrete slab (in composite pavements) were specified as the seed moduli used for the MICHBACK and EVERCALC programs, whereas for the concrete slab the lower modulus was specified as 13 789.5 MPa (2,000,000 psi). The upper moduli were specifed as 5515.8, 413.69, 275.79, and 41 368.8 MPa (800,000, 60,000, 40,000 and 6,000,000 psi) for AC, base, subbase, and concrete slab moduli, respectively, for the appropriate examples.
2. MODULUS was allowed to automatically select appropriate weights to be applied to the readings of each sensor.
3. Use of a rigid bedrock was suppressed for all examples except for those in which bedrock was present. For the examples in which bedrock was present, MODULUS does not

allow the bedrock modulus to be specified, but assigns it internally (*3*).

4. The "RUN A FULL ANALYSIS" option was used for all examples, so that material types were not required as input.

Three-Layer Pavements

Typical configurations of three-layer pavements with thin, medium, and thick AC layers are given in Table 1. Backcalculation of the layer moduli from the surface deflections were performed using seed moduli of 689.48, 103.42, and 20.68 MPa (100,000, 15,000, and 3,000 psi) for the AC, base, and subgrade layers, respectively. Exact Poisson's ratios and thicknesses were input.

The moduli backcalculated by the MICHBACK, MODULUS, and EVERCALC programs are given in Table 2, together with the maximum percentage error in the backcalculated moduli and the RMS error in the surface deflections described in Equation 13 (multiplied by 100). The MICHBACK program yields excellent results. Whereas the specified tolerance in two consecutive modulus estimates was $\varepsilon = 0.1$ percent, the backcalculated moduli actually have larger errors when compared with the actual moduli. Hence, the specified tolerance, ε, should usually be smaller than the error desired in the backcalculated moduli (perhaps by an order of magnitude). The MODULUS program yields significantly larger errors than MICHBACK, with the error in the base modulus being as much as 4 percent for the "thick" pavement. The EVERCALC program backcalculates progressively poorer results as the pavement becomes stiffer. However, when the alternative deflection basins generated by the original CHEVRON program are used, EVERCALC gives excellent results. This implies that improving the forward calculation program within EVERCALC should enable it to yield excellent results for three-layer pavements.

Four-Layer Pavement

Backcalculated moduli for a four-layer pavement are given in Table 3. The actual properties of the pavement and the seed moduli were thicknesses = 152.4, 254, 152.4, and ∞ mm (6, 10, 6 and ∞ in.); actual moduli = 3447.38, 310.26, 103.42, and 51.71 MPa (500,000, 45,000, 15,000 and 7,500 psi); Poisson's ratios = 0.35, 0.4, 0.4, and 0.45; and seed moduli = 689.48, 103.42, 48.26, and 20.68 MPa (100,000, 15,000, 7,000 and 3,000 psi). The results show that MICHBACK yields more accurate results than the other programs. The error in the subbase modulus backcalculated by MODULUS is very large

TABLE 1 "Typical" Three-Layer Pavements

Layer	Thickness (mm[a])			Poisson's Ratio	Modulus (MPa[b])
	Thin	Medium	Thick		
AC	50.8	127.0	228.6	0.35	3447.38
Base	152.4	203.2	152.4	0.40	310.26
Subgrade	∞	∞	∞	0.45	51.71

[a] 1 mm = 0.03937 in
[b] 1 MPa = 145.038 psi

TABLE 2 Backcalculation: Three-Layer Pavements

Program	Pavement Type	Backcalculated Modulus (MPa[a])			Max. Error in Moduli (%)	RMS Error in Deflections (%)
		AC	Base	Subgrade		
MICHBACK	Thin	3432.95	310.40	51.71	0.42	0.019
	Medium	3446.66	310.24	51.71	0.02	0.032
	Thick	3455.93	307.67	51.74	0.84	0.014
MODULUS	Thin	3346.79	316.47	51.71	2.92	0.370
	Medium	3468.75	307.51	51.71	0.89	0.110
	Thick	3346.71	322.67	51.71	4.00	0.139
EVERCALC	Thin	3472.48	309.54	51.71	0.73	0.020
	Medium	3294.06	317.25	51.71	4.45	0.065
	Thick	3030.65	399.84	51.66	28.87	0.126
EVERCALC-Alt	Thin	3448.97	309.93	51.72	0.11	0.020
	Medium	3467.17	308.71	51.72	0.57	0.024
	Thick	3450.86	315.52	51.72	0.17	0.148

[a] 1 MPa = 145.038 psi

TABLE 3 Backcalculation: Four-Layer Pavement

Program	Backcalculated Modulus (MPa[a])				Max. Error in Moduli (%)	RMS Error in Deflections (%)
	AC	Base	Subbase	Subgrade		
MICHBACK	3448.07	310.93	102.75	51.72	0.65	0.012
MODULUS	3756.95	248.21	153.75	52.34	48.67	0.162
EVERCALC	3282.99	319.28	101.55	51.74	4.77	0.092
EVERCALC-Alt	3413.06	319.04	98.64	51.77	4.62	0.063

[a] 1 MPa = 145.038 psi

(49 percent). Whereas the AC modulus backcalculated by EVERCALC improves significantly when the alternative deflection basin generated by the original CHEVRON program is used, the backcalculated subbase modulus becomes poorer. It has been found that for pavements with more than three layers, MICHBACK generally yields better results than EVERCALC, whereas the MODULUS program yields a poor estimate for at least one layer modulus.

Four-Layer Pavement with Incorrect AC Thickness

The ability of MICHBACK to improve incorrectly specified thicknesses is illustrated by performing a backcalculation of the four-layer pavement analyzed above assuming that the thickness of the AC layer was known only approximately. The AC layer thickness was input as 101.6 mm (4 in.), whereas the actual thickness was 152.4 mm (6 in.), and the MICHBACK program was used to backcalculate the layer moduli as well as the AC thickness. The program backcalculated layer moduli of 3454.83, 312.08, 102,42, and 51.73 MPa (501,081, 45,263, 14,855, and 7,503 psi) for the AC, base, subbase, and subgrade layers, and a thickness of 152.11 mm (5.989 in.) for the AC layer. The maximum error in the backcalculated moduli is 0.97 percent, the error in the thickness is 0.18 percent, and the RMS error in the compound surface deflections is 0.012 percent.

Four-Layer Composite Pavements

Backcalculated moduli for two four-layer composite pavements having a stiff concrete slab as one layer are given in Tables 4 and 5. The actual properties of the pavements and the seed moduli used were as follows:

- Stiff composite pavement (slab above base layer): thicknesses = 152.4, 254.0, 203.2, and ∞ mm (6, 10, 8, and ∞ in.); actual moduli = 3447.38, 31 026.4, 172.37, and 51.71 MPa (500,000, 4,450,000, 25,000, and 7,500 psi); Poisson's ratios = 0.35, 0.25, 0.40, and 0.45; and seed moduli = 689.48, 3447.38, 48.26, and 20.68 MPa (100,000, 500,000, 7,000, and 3,000 psi);
- Flexible composite pavement (slab beneath base layer): thicknesses = 152.4, 203.2, 254.0, and ∞ mm (6, 8, 10, and ∞ in.); actual moduli = 3447.38, 172.37, 31 026.4, and 51.71 MPa (500,000, 25,000, 4,450,000, and 7,500 psi); Poisson's ratios = 0.35, 0.40, 0.25, and 0.45; and seed moduli = 689.48, 48.26, 6894.8, and 20.68 MPa (100,000, 7,000, 1,000,000, and 3,000 psi).

The results indicate that whereas MICHBACK converges reasonably well for both composite pavements, the other programs yield significantly poorer results, especially for the stiff composite pavement. The moduli backcalculated by EVERCALC are extremely poor for the stiff composite pavement when the deflection basin generated by CHEVRONX is used. When the alternative basin generated by CHEVRON is used with EVERCALC, although the error in the backcalculated base modulus is 131 percent for the first composite pavement, the RMS error in the deflections is only 0.06 percent, indicating that the deflections computed by EVERCALC are very close to the input deflections. This implies that EVERCALC converged to a local minimum that does not represent the correct solution. For some other composite pavement sections that were analyzed EVERCALC was able to backcalculate more accurate moduli, but its accuracy was generally poorer than MICHBACK's.

Whereas surface deflections were rounded to the nearest hundredth of a mil in all the examples presented here, improved accuracy was obtained with MICHBACK when the surface deflections were input to greater precision, especially for very stiff composite pavements. The MODULUS and EVERCALC programs do not allow surface deflections to be input to precision greater than a hundredth of a mil. Whereas a precision greater than a hundredth of a mil is usually unrealizable in practice, the observation with MICHBACK indicates the difficulty that can occur when backcalculating moduli of composite pavements owing to sensitivity arising from even rounding of the surface deflections.

TABLE 4 Backcalculation: Stiff Composite Pavement

Program	Backcalculated Modulus (MPa[a])				Max. Error in Moduli (%)	RMS Error in Deflections (%)
	AC	Slab	Base	Subgrade		
MICHBACK	3443.03	31131.9	158.59	51.75	7.99	0.007
MODULUS	3639.74	30827.1	67.57	52.40	60.80	0.068
EVERCALC	10908.93	15838.0	90.95	51.83	216.44	1.526
EVERCALC-Alt	3410.81	29075.9	398.29	51.52	131.07	0.064

[a] 1 MPa = 145.038 psi

TABLE 5 Backcalculation: Flexible Composite Pavement

Program	Backcalculated Modulus (MPa[a])				Max. Error in Moduli (%)	RMS Error in Deflections (%)
	AC	Base	Slab	Subgrade		
MICHBACK	3444.31	172.29	30839.3	51.67	0.60	0.030
MODULUS	3392.90	175.13	30354.1	51.71	2.17	0.078
EVERCALC	4293.42	190.71	27300.9	51.39	24.54	0.753
EVERCALC-Alt	3388.46	176.00	30423.6	51.79	2.10	0.105

[a] 1 MPa = 145.038 psi

TABLE 6 Backcalculation: Three-Layer Pavements over Bedrock

Program	Bedrock Location	Backcalculated Modulus (MPa[a])			Max. Error in Moduli (%)	RMS Error in Deflections (%)
		AC	Base	Subgrade		
MICHBACK	Deep	3459.07	309.76	51.69	0.34	0.037
	Shallow	3446.14	309.68	51.75	0.19	0.087
MODULUS	Deep	3460.72	308.88	51.71	0.44	0.187
	Shallow	3505.29	299.23	53.09	3.55	0.074
EVERCALC	Deep	5493.76	215.07	51.90	59.36	1.150
	Shallow	4123.02	278.06	52.34	19.60	0.600
EVERCALC-Alt	Deep	3435.39	311.54	51.69	0.41	0.016
	Shallow	3456.94	309.20	51.76	0.34	0.041

[a] 1 MPa = 145.038 psi

TABLE 7 Performance Comparison of MICHBACK and EVERCALC for Four-Layer Flexible Pavement

Program	Number of Times Operation was Performed		
	CHEVRON Called	Gradients Computed	Iterations
MICHBACK (Newton)	27	5	5
MICHBACK (Modified Newton)	23	3	9
EVERCALC	21	4	4

Three-Layer Pavements Over Bedrock

Backcalculated moduli for two three-layer pavements overlying bedrock are given in Table 6. The only difference in the two pavements was the bedrock depth of 6.096 m (20 ft) for the deep bedrock pavement and 1.219 m (4 ft) for the shallow bedrock pavement. The true location of the bedrock was specified as input to all programs, and the true modulus of the bedrock, 34 473.8 MPa (5,000,000 psi), was input to MICHBACK and EVERCALC (the MODULUS program does not allow the bedrock modulus to be input). All other layer properties and the seed moduli used were identical to the three-layer pavement of "medium" thickness analyzed above (see Table 1). The moduli backcalculated by MICHBACK are somewhat better than those obtained by the other programs. Note that EVERCALC yields excellent results when alternative deflection basins generated by CHEVRON are used.

Performance Comparison

The performances of MICHBACK and EVERCALC are compared in Table 7 for backcalculation of the moduli of the four-layer flexible pavement considered earlier. Both the Newton method (in which the gradient matrix was calculated for each iteration) and the modified Newton method (in which four iterations were performed before updating the gradient matrix) were used in MICHBACK. Four more iterations are required for the modified Newton method than for the Newton method, but the total number of calls to the CHEVRONX program is fewer for the former (i.e., 23 as opposed to 27) since the gradient matrix is computed fewer times. The actual savings varies from problem to problem, but typically the modified Newton method requires about five fewer calls to CHEVRONX. The EVERCALC program calls CHEVRON only 21 times and is therefore marginally more efficient than MICHBACK (EVERCALC also computes a gradient matrix similar to the one computed by MICHBACK). For more complex problems, such as those involving composite pavements, the difference in the number of forward calculations performed by EVERCALC and MICHBACK can be greater, but MICHBACK usually yields more accurate results. In view of MICHBACK's accuracy, its slightly poorer performance appears justifiable. EVERCALC's performance was the same even if a deflection basin generated by CHEVRON was used.

CONCLUSIONS

An algorithm based on the efficient Newton method for the solution of simultaneous nonlinear algebraic equations is presented for the backcalculation of pavement layer properties from measured surface deflections. The method is capable of backcalculating layer thicknesses in addition to the layer moduli and has been implemented in a new backcalculation program named MICHBACK.

Comparisons of moduli backcalculated by the MICHBACK, MODULUS 4.0, and EVERCALC 3.0 programs, using deflection basins generated by an extended precision CHEVRON elastic layer analysis program, are presented for a variety of pavement sections. The results indicate that MICHBACK usually backcalculates more accurate moduli than the other programs. EVERCALC is also able to backcalculate moduli very accurately for three-layer flexible pavements, but it is handicapped by its use of the original CHEVRON program, the accuracy of which is poor for stiff pavements. Even for deflection basins generated by its own forward calculation program (i.e., original CHEVRON), EVERCALC's backcalculation deteriorates for four-layer flexible pavements and stiff composite pavements. MODULUS tends to produce a large error in at least one backcalculated modulus for four-layer flexible and stiff composite pavements.

ACKNOWLEDGMENT

The authors would like to express their gratitude to the Michigan Department of Transportation and the University of Michigan Transportation Research Institute for providing the financial support for this work. We are also grateful to Lynne Irwin for improving the quadrature in our version of the CHEVRON program and to Robert L. Lytton, NCHRP, and Joe Mahoney for providing us copies of the MODULUS 4.0 and EVERCALC 3.0 programs for evaluation purposes.

REFERENCS

1. A. J. Bush III. *Computer Program BISDEF*. U.S. Army Corps of Engineers Waterways Experiment Station, 1985.
2. N. Sivaneswaran, S. L. Kramer, and J. P. Mahoney. Advanced Backcalculation using a Nonlinear Least Squares Optimization Technique. Presented at the 70th Annual Meeting of the Transportation Research Board, Washington, D.C., 1991.
3. J. Uzan, R. L. Lytton, and F. P. Germann. General Procedure for Backcalculating Layer Moduli. In *Nondestructive Testing of Pavements and Backcalculation of Moduli, ASTM STP 1026* (A. J. Buch III and G. Y. Baladi, eds.), American Society for Testing and Materials, Philadelphia, Pa., 1989, pp. 217–228.
4. K. M. Chua and R. L. Lytton. Load Rating of Light Pavement Structures. In *Transportation Research Record 1043*, TRB, National Research Council, Washington, D.C., 1984.
5. D. Kahaner, C. Moler, and S. Nash. *Numerical Methods and Software*. Prentice-Hall, Englewood Cliffs, N.J., 1989.
6. T. Y. Hou. *Evaluation of Layered Material Properties from Measured Surface Deflections*. Ph.D. thesis. University of Utah, Salt Lake City, 1977.
7. D. L. DeJong, M. G. F. Peutz, and A. R. Korswagen. *Computer Program BISAR*. Koninklijkel/Shell-Laboratorium, Amsterdam, the Netherlands, 1973.

New Scenario for Backcalculation of Layer Moduli of Flexible Pavements

A. SAMY NOURELDIN

A new backcalculation scenario that uses falling weight deflectometer (FWD) deflection bowl data to directly backcalculate subgrade modulus and overall pavement modulus and predict effective structural number of the pavement is presented. The procedure allows for decomposing measured maximum deflection into two components: subgrade deflection and pavement deflection. Execution of the scenario accounts for conditions when thickness data are not available, not reliable, or not representative. The scenario depends on a concept that is not related to selection of seed values. The concept is that there is a unique location on the surface of the pavement at a radial distance r_x from the loading center that deflects with a value D_x exactly equal to the deflection of the point on the top of subgrade underneath the loading center. The scenario was field tested using FWD deflection measurements representing newly constructed roads, roads with considerable deterioration, top of compacted subgrade, top of subbase, top of base, and top of wearing surface. General observations on field applications and a field testing example are introduced.

Calculation of load-related pavement surface deflections at specific points, using material properties of pavement layers (modulus, Poisson's ratio, and thickness), is well established. Backcalculation of pavement layer moduli is a reversed procedure. Pavement layer moduli are calculated using load-related pavement surface deflection measurements (actual deflection bowl) and available thickness or coring data and making reasonable assumptions for Poisson's ratios.

The scenario of this backcalculation process usually takes the form of assuming acceptable values of pavement layer moduli (seed values), predicting a theoretical deflection bowl, comparing the theoretical deflection bowl with the actual deflection bowl, and accepting moduli values when the difference between the theoretical bowl and the actual bowl is not significant.

This technique has passed through many adjustments and modifications. Adjustments are usually made to avoid obtaining excessive modulus values for the pavement surface layer. Seed values are forced to be in certain ranges. A rigid base is sometimes assumed. Actual deflection measurements are sometimes adjusted for seasonal variations before the backcalculation procedure is conducted instead of investigating the effect of seasonal variations on the backcalculated moduli values.

Several questions are still to be answered. How can backcalculated data be used to compare between pavement sections? How can backcalculated data be used to identify deficient pavement layers? Is it possible to bypass the requirement of thickness data in the backcalculation procedure, especially when these data are not reliable and field coring is not representative?

This paper presents a new scenario for the backcalculation process. Seed values will not be required to predict a theoretical deflection bowl and compare it with the actual deflection bowl. Instead, an effective total thickness value is computed directly from the actual deflection bowl and is compared with the actual total thickness existing on the top of the subgrade. Computed moduli associated with the actual total thickness are the resulting backcalculated moduli. In addition, an alternative backcalculation process predicting the in situ effective total thickness is introduced for cases where thickness data are not available, not reliable, or not representative.

UNDP Ministry of Communications, Riyadh 11178, Saudi Arabia.

METHODOLOGY

Equipment and Loading Conditions

The scenario presented herein is based on two-layer elastic analysis and applicable to falling weight deflectometers (FWDs). The FWD used has a plate radius of 6.0 in. (15 cm) and seven geophones located at distances 0, r_1, r_2, r_3, r_4, r_5, and r_6 from the loading center. These geophones measure the deflections D_0, D_1, D_2, D_3, D_4, D_5, and D_6 at the surface of the flexible pavement due to a 9,000-lb load. If a different load is used, deflection measurements should be normalized to the load of 9,000 lb.

Concept

The concept of the procedure is that a unique location exists on the surface of the pavement at a radial distance r_x from the loading center that deflects with a value D_x exactly equal to the deflection of a point on the top of the subgrade underneath the loading center (Figure 1). If this unique location is found, the overall pavement modulus (E_p), the subgrade modulus (E_{SG}), the effective total thickness (T_x), the subgrade deflection underneath the loading center (D_x), and the pavement deflection underneath the loading center ($D_0 - D_x$) can be determined. The following section indicates how this unique location is found and how the backcalculation scenario is executed for two cases. The first case applies when pavement thickness data are available, and the second case applies when thickness data are not available.

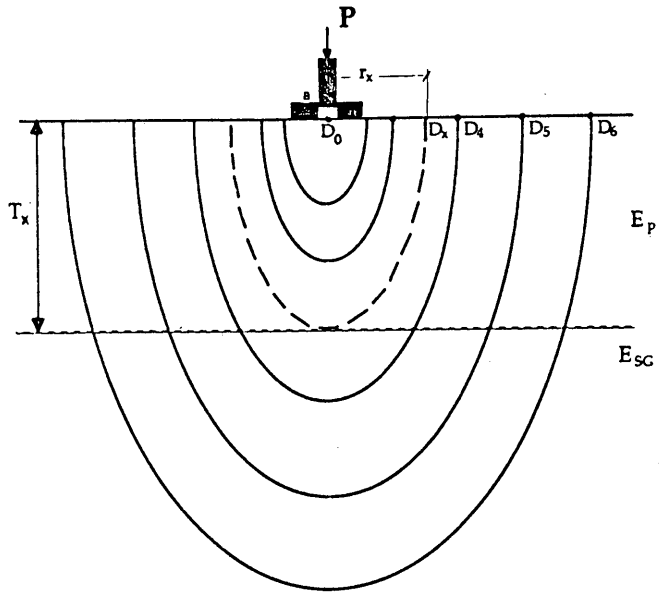

FIGURE 1 Contour lines of equal vertical deflections within the pavement system.

Execution of Backcalculation Scenario

Thickness Data Available

When thickness data are available and reliable through records or field coring, the unique location described above can be determined and the backcalculation scenario can be executed as follows:

1. The outer geophone location is assumed to be the unique location (i.e., $r_x = r_6$ and consequently $D_x = D_6$).
2. Determine subgrade modulus (E_{SG}) using r_6 and D_6 values for r_x and D_x using the following equation:

$$E_{SG} = \frac{2{,}149}{r_x D_x} \tag{1}$$

where D_6 and r_6 are in inches and E_{SG} is in psi. This equation is based on Boussinesq's deflection equation (*1*). This method of determining the subgrade modulus was proposed by Ullidtz (*2,3*) for deflections measured outside the loading plate. The method was also reported previously by Noureldin and Sharaf (*4*) and Hall et al. (*5*).

3. Determine the overall pavement modulus (E_p) using r_6 and D_6 for r_x and D_x values and using the following equation:

$$E_p = \frac{716 - \dfrac{2{,}149}{r_x}}{D_0 - D_x} \tag{2}$$

where E_p is in psi and D_0, D_6, and r_6 are in inches. This equation is based on Burmister's method of deflection in two-layer systems (*6*). The equation was reported by Noureldin and Sharaf (*4*).

4. Determine the effective total thickness, T_x, using r_6 and D_6 for r_x and D_x and using the following equation:

$$T_x = \left[\frac{D_0 - D_x}{D_x\left(\frac{r_x}{3} - 1\right)}\right]^{1/3} * (4r_x^2 - 36)^{1/2} \tag{3}$$

where D_0, D_6, r_6, and T_x are in inches.

This equation is also based on the Burmister and Odemark method of deflection in a two-layer system (*6,7*) and the concept of equivalent thicknesses described by Barber (*8*). The equation was reported by Noureldin and Sharaf (*4*).

5. Repeat Steps 1 through 4 for each geophone outside the loading plate.
6. Draw the relationships r_x versus T_x, r_x versus E_{SG}, and r_x versus E_p, where the horizontal axis coordinates are for r_x equal to r_1, r_2, r_3, r_4, r_5, and r_6 (Figure 2).
7. The backcalculated subgrade modulus and the overall pavement modulus are those associated with the unique location at the radial distance r_x (Figure 2).
8. Subgrade deflection underneath the center of the loading plate is the deflection of the unique location (D_x). Pavement deflection is the difference between the maximum deflection and the deflection of the unique location ($D_0 - D_x$).

Table 1 presents a sample of deflection measurements obtained by the FWD on a 16-in. flexible pavement. Table 2

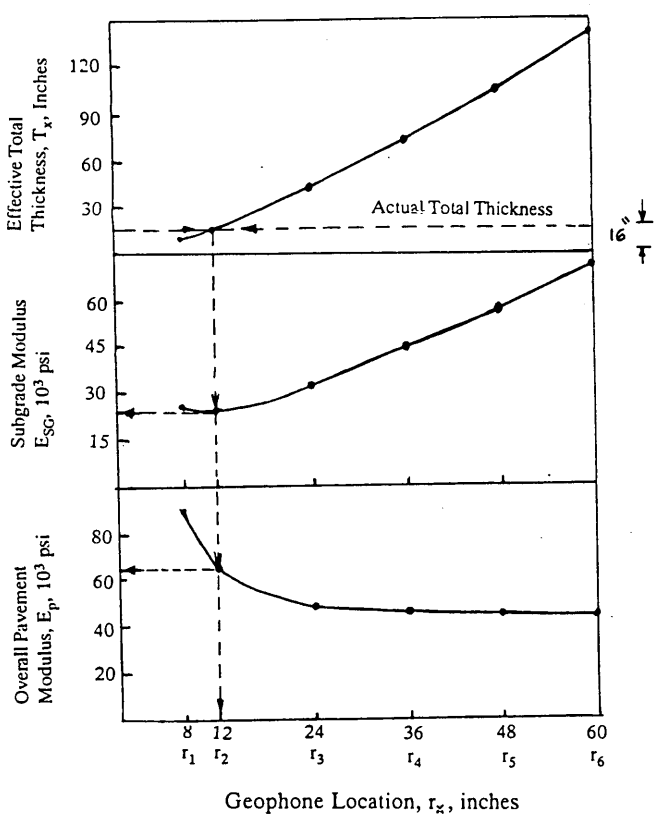

FIGURE 2 Determination of unique location.

TABLE 1 FWD Deflection Measurements on a 16-in. Flexible Pavement (Load = 9,000 lb; Plate Radius = 6.0 in.)

Location	0	1	2	3	4	5	6
Radius, r_x, inches	0	8	12	24	36	48	60
Deflection, D_x, mils	D_0	D_1	D_2	D_3	D_4	D_5	D_6
	15.9	10.9	7.6	2.8	1.3	0.8	0.5

TABLE 2 Subgrade Modulus (E_{SG}), Overall Pavement Modulus (E_p), and Effective Total Thickness (T_x) Computation Steps

		E_{SG} (psi)	E_p (psi)	T_x (inches)
rx = r6 = 60 in	Dx = r6 = 0.5 mils	71,600	44,200	140.8
rx = r5 = 48 in	Dx = r5 = 0.8 mils	56,000	44,500	103.4
rx = r4 = 36 in	Dx = r4 = 1.3 mils	45,900	45,000	72.3
rx = r3 = 24 in	Dx = r3 = 2.8 mils	32,900	47,800	41.6
rx = r2 = 12 in	Dx = r2 = 7.6 mils	23,600	64,700	16.6
rx = r1 = 8 in	Dx = r1 = 10.9 mils	24,700	89,500	9.6

gives the computation steps for determining subgrade modulus (E_{SG}), overall pavement modulus, and effective total thickness (T_x). In addition Figure 2 shows r_x versus T_x, r_x versus E_{SG}, and r_x versus E_p relationships. The unique location is at $r_x = r_2 = 12$ in., corresponding to an actual total thickness of 16 in. Subgrade modulus and overall pavement modulus are 23,000 psi and 65,000 psi, respectively (Figure 2). The subgrade deflection underneath the loading center is $7.6 * 10^{-3}$ in. (surface deflection at the unique location). The pavement deflection underneath the loading center is $8.3 * 10^{-3}$ in. ($15.9 * 10^{-3}$ in. $- 7.6 * 10^{-3}$ in.).

Thickness Data Not Available

When thickness data are not available through design records or field coring, a need exists for an alternative scenario for the backcalculation process. The need also exists when nondestructive deflection coverage is conducted at a network level (and not at a project or research level).

The total pavement thickness is defined as the sum of individual thicknesses of pavement layers above the subgrade layer. An alternative definition is that total pavement thickness is the vertical distance between the surface of the pavement and the top of the weakest pavement layer within the pavement system. As long as pavement layers are stiffer than the subgrade, the two definitions are equivalent. However, if the subbase, base, or surface layer is less stiff than the subgrade, the alternative definition yields an effective total thickness that is less than the actual total thickness. Conversely, if the top portion of the subgrade layer is compacted (or consolidated) more than deeper portions, the alternative definition yields an effective total thickness that is more than the actual total thickness.

Using the concept of effective total pavement thickness described above, the layer of lowest modulus can be searched, and the distance between the pavement surface and the top of this layer is considered the effective total pavement thickness. The alternative backcalculation scenario is, then, executed as follows:

1. Find the unique location of the geophone at a distance r_x from the center of the loading plate measuring a deflection D_x such that $r_x * D_x$ is maximum. This means that r_6D_6, r_5D_5, r_4D_4, r_3D_3, r_2D_2, and r_1D_1 values should be calculated, and the maximum value is to be selected. If r_4D_4 is the largest value, for example, $r_x = r_4$ and $D_x = D_4$.
2. Determine the subgrade modulus (E_{SG}), overall pavement modulus (E_p), and effective total thickness (T_x) using Equations 1, 2, and 3.
3. The subgrade deflection underneath the loading center is D_x, and the pavement deflection underneath the loading center is $(D_0 - D_x)$.

In the computation example previously introduced,

- $r_2 * D_2$ represents the largest $r_x * D_x$ multiplication value; hence $r_x = r_2 = 12$ in. and $D_x = D_2 = 7.6 * 10^{-3}$ in.;
- $E_{SG} = 23{,}000$ psi, $E_p = 65{,}000$ psi, and effective total thickness = 15.8 in.; and
- Subgrade deflection is $7.6 * 10^{-3}$ in. and pavement deflection is $8.3 * 10^{-3}$ in. ($15.9 * 10^{-3}$ in. $- 7.6 * 10^{-3}$ in.).

Assumptions and Limitations

The scenario has the following assumptions and limitations:

1. The pavement is an idealized elastic two-layer flexible system.
2. The material is weightless, homogeneous, and isotropic.
3. The pavement layer has a uniform thickness and an infinite width in all horizontal directions. The bottom layer (subgrade) has an infinite thickness.
4. Poisson's ratios of the two layers are equal to 0.5.
5. The top of subgrade is the top of the layer of lowest modulus in the pavement system (when thickness data are not available).
6. The total pavement thickness is considered to be the distance between the top of the pavement and the top of the layer of lowest modulus in the pavement system (when thickness data are not available).
7. Thin pavements that are less than the radius of the loading plate in thickness will yield inaccurate results.

Determination of AASHTO Effective Structural Number

The *AASHTO Guide for Design of Pavement Structures* (*9*) recommended a nondestructive deflection testing procedure for determination of the effective structural number, SN_{eff}. This procedure follows an assumption that the structural capacity of the pavement (represented by its structural number) is a function of its total thickness in inches (T_x) and overall modulus in psi, (E_p), such that

$$SN_{eff} = \sqrt[3]{\frac{E_p}{11 * 10^6}} * T_x \quad (4)$$

Equation 4 was not explicitly introduced in the AASHTO guide and was originally reported by Noureldin and Al Dhalaan (*10*) and later by Hall et al. (*5*). The equation presented by Hall et al. (*5*) was

$$SN_{eff} = 0.0045\ D \sqrt[3]{E_p} \quad (5)$$

where D is the total pavement thickness and E_p is the effective modulus of the pavement. As can be easily noted, Equations 4 and 5 are practically the same.

After substituting Equations 2 and 3 into Equation 4 (or 5) to determine the effective structural number (SN_{eff}) as a function of r_x and D_x (radii and deflection associated with the unique location described in this paper), the SN_{eff} equation becomes

$$SN_{eff} = \frac{(4r_x^2 - 36)^{1/2}}{17.234(r_x * D_x)^{1/3}} \quad (6)$$

This equation can be easily executed as a part of the backcalculation scenario presented in this paper, whether or not thickness data are available. In addition, the simplicity of the equation allows its use at the research, project, or network level.

APPLICATION

General Observations

The availability of long roadway segments in Saudi Arabia that are still in the construction stages provided the opportunity to test the backcalculation scenario presented in this paper under real conditions. The FWD was used to obtain measurements on top of compacted subgrade, subbase, base, and wearing surface layers for the same locations on a number of roadway segments. The following observations were obtained:

1. Maximum deflection (D_0) decreased after the construction of any layer.
2. Effective structural number (SN_{eff}) and effective total thickness (T_x) estimated by the backcalculation process presented in this paper increased after the construction of any layer.
3. The unique location defined in this paper got away from the loading center (r_x increased) after the construction of any layer.
4. The backcalculated subgrade modulus (E_{SG}) remained practically the same after construction of each individual layer.
5. The backcalculated subgrade modulus was predicted by the first geophone outside the loading plate in all tests conducted on top of subgrade.
6. The computation of subgrade modulus, using the measurement of maximum deflection (D_0) and assuming one-layer analysis, always resulted in a value larger than that predicted by other geophones. This was true even when the deflection measurements were taken on top of the compacted subgrade.

Effect of Seasonal Variations

The backcalculation process presented in this paper was applied using nondestructive deflection measurements representing fall, winter, spring and summer conditions on specific roadway sections in Saudi Arabia. Although this research work is still in its early stages, preliminary results were obtained. The results suggest that under the dry conditions prevailing in Saudi Arabia, backcalculated subgrade modulus (E_{SG}) is slightly affected by changes in air temperature, whereas backcalculated pavement modulus (E_p) is significantly affected. In addition the estimated effective total thickness (T_x) remained the same during the four seasons and was practically equal to the actual total pavement thickness. However, the estimated effective structural number (SN_{eff}) was shown to drop considerably during the hot conditions of summer.

Demonstrative Field Testing Example

Table 3 presents FWD measurements on a 1,300-ft roadway segment. Deflection measurements were taken at a lateral distance of 3 ft from the pavement edge each 100 ft. The roadway segment exhibited low to medium severity, wheelpath longitudinal cracking, and frequent transverse cracking. The pavement cross section consists of 6-in. full-depth asphalt on top of a 10-in. subbase layer (i.e., total pavement thickness is 16 in.). The design structural number was originally 3.74.

The backcalculation scenario presented previously was executed assuming that thickness data were not available.

Table 4 gives the backcalculated modulus values, effective total thickness, and effective structural number (SN_{eff}) along

TABLE 3 FWD Data on 1,300-ft Segment (Load = 9,000 lb; Plate Radius = 6.0 in.)

Location	0	1	2	3	4	5	6	Temperature	
Radius (in.)	0	8	12	24	36	48	60		
Dist. Feet	D_0 mils	D_1 mils	D_2 mils	D_3 mils	D_4 mils	D_5 mils	D_6 mils	Air °F	Pave °F
0	13.1	9.1	6.4	2.6	1.2	0.6	0.4	93	97
100	14.1	10.1	7.3	2.8	1.3	0.8	0.5	93	100
200	15.9	10.9	7.6	2.6	1.1	0.7	0.5	94	100
300	10.3	7.9	6.0	2.8	1.6	1.0	0.6	92	100
400	12.8	8.9	6.3	2.5	1.2	0.7	0.4	92	99
500	12.2	7.6	5.1	1.5	0.5	0.3	0.1	93	99
600	11.1	8.3	6.3	2.7	1.3	0.8	0.5	93	100
700	12.1	8.1	5.6	1.9	0.8	0.4	0.2	91	96
800	15.6	10.6	7.3	2.8	1.4	0.9	0.5	91	98
900	11.3	7.5	5.1	2.2	1.3	0.8	0.5	91	96
1000	13.0	9.4	6.9	2.5	1.0	0.5	0.2	91	98
1100	8.5	6.2	4.8	2.3	1.2	0.8	0.5	91	96
1200	14.1	10.1	7.4	3.0	1.5	1.0	0.6	91	97
1300	13.6	9.1	6.4	2.4	1.2	0.7	0.5	91	96

Deflections are in mils (1/1000 inch)

TABLE 4 Backcalculated Moduli, Effective Total Thickness, and Effective Structural Number

Distance Feet	Subgrade Modulus E_{SG} psi	Overall Pavement Modulus E_P, psi	Effective Total Thickness T_x, inches	Effective Structural Number SN_{eff}
0	28,000	80,100	16.36	3.17
100	24,500	79,000	15.74	3.04
200	23,600	64,700	16.59	3.00
300	29,800	124,900	14.42	3.24
400	28,400	82,600	16.28	3.19
500	35,100	75,600	17.99	3.42
600	28,400	111,900	14.72	3.19
700	32,000	82,600	16.93	3.32
800	24,500	64,700	16.82	3.04
900	35,100	86,600	17.20	3.42
1000	26,000	88,000	15.46	3.09
1100	37,300	145,100	14.77	3.49
1200	24,200	80,100	15.59	3.02
1300	28,000	74,600	16.76	3.17
Mean	28,900	88,600	16.12	3.20
Std. Dev.	4,400	23,000	1.04	0.16
Coeff. of Var.	15.20%	26%	6.45%	5.00%

the roadway segment. The variability in overall pavement modulus values, as represented by the coefficient of variation, was more than the variability in the subgrade modulus, possibly because of cracking observed on the pavement surface. Computed effective total thickness was practically equal to the actual total thickness (16.0 in.) and exhibited relatively low variability. The mean value of the effective structural number (SN_{eff}) was lower than the design value (3.74). However, the SN_{eff} values had shown the lowest variability.

Figures 3, 4, and 5 show moduli, effective total thickness, and effective structural number profiles along the 1,300-ft roadway segment.

Table 5 presents the maximum deflection, subgrade deflection, and pavement deflection values underneath the center of the FWD loading plate along the roadway segment. Figure 6 shows the profiles of these deflection values. The

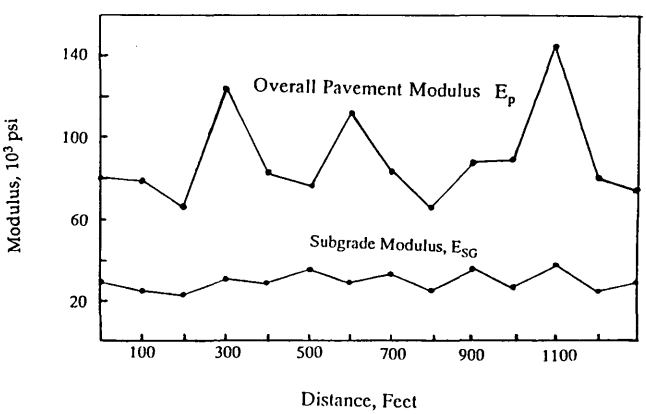

FIGURE 3 Backcalculated moduli values.

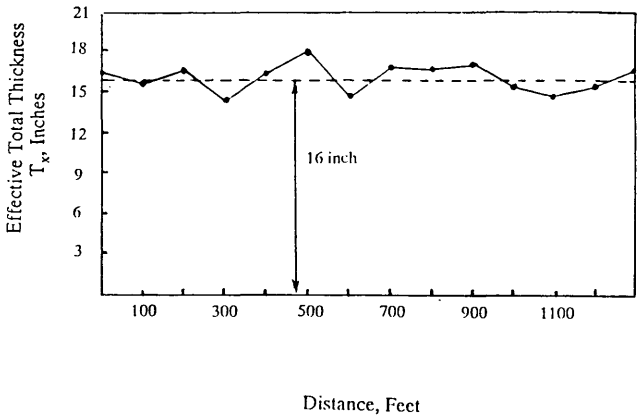

FIGURE 4 Effective total thickness.

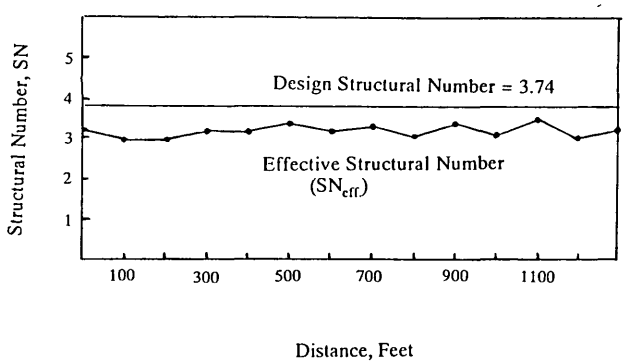

FIGURE 5 Effective structural number (SN_{eff}).

TABLE 5 Deflection Values Underneath the Center of the FWD Loading Plate

Distance Feet	Maximum Deflection D_o, mils	Subgrade Deflection D_x, mils	Pavement Deflection ($D_o - D_x$), mils
0	13.1	6.4	6.7
100	14.1	7.3	6.8
200	15.9	7.6	8.3
300	10.3	6.0	4.3
400	12.8	6.3	6.5
500	12.2	5.1	7.1
600	11.1	6.3	4.8
700	12.1	5.6	6.5
800	15.6	7.3	8.3
900	11.3	5.1	6.2
1000	13.0	6.9	6.1
1100	8.5	4.8	3.7
1200	14.1	7.4	6.7
1300	13.6	6.4	7.2
Mean	12.7	6.32	6.37
Std. Dev.	2.0	0.92	1.33
Coeff. of Var.	15.80%	14.50%	20.90%

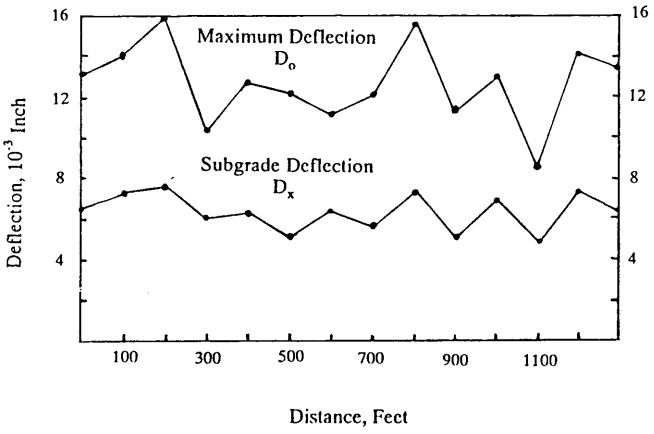

FIGURE 6 Deflection profiles underneath the center of the FWD loading plate.

variability in pavement deflection was higher than the variability in subgrade deflection (Table 5 and Figure 6). This also might be attributed to the observed cracks on the pavement surface.

SUMMARY

A new scenario for backcalculation of layer moduli of flexible pavements was introduced. It allows for the determination of subgrade modulus, overall pavement modulus, and effective structural number. In addition, it enables decomposition of measured maximum deflections into two components: subgrade deflection and pavement deflection. The scenario can be executed whether or not thickness data are available. Necessary computations are directly made using deflection bowl data on a seven-geophone FWD. The new scenario is suggested as a simple, quick, and reliable backcalculation approach for evaluation of flexible pavements.

REFERENCES

1. J. Bousinesq. *Application des Potentials à l'Étude de l'Equilibre et du Mouvement des Solides Elastiques*. Gauthier-Villars, Paris, 1885.
2. P. Ullidtz. *Pavement Analysis*. Elsevier Science Publishers B. V., 1987.
3. P. Ullidtz. Overlay and Stage by Stage Design. *Proc. Fourth International Conference on Structural Design of Asphalt Pavements*, Ann Arbor, Mich., 1977.
4. A. S. Noureldin and E. A. Sharaf. A Simplified Mechanistic Algorithm for Pavement Analysis. Presented at 71st Annual Meeting of Transportation Research Board, Washington, D.C., 1992.
5. K. T. Hall, M. I. Darter, and R. P. Elliot. Revision of AASHTO Pavement Overlay Design Procedures. Presented at 71st Annual Meeting of Transportation Research Board, Washington, D.C., 1992.
6. D. M. Burmister. The Theory of Stresses and Displacements in Layered Systems and Application to the Design of Airport Runways. *HRB Proc.*, 1943.
7. N. Odemark. *Investigations as to the Elastic Properties of Soils and Design of Pavements According to the Theory of Elasticity*. Meddelande 77, Statens Vägenstitut, Stockholm, Sweden, 1949.
8. E. S. Barber. Discussion. *HRB Proc.*, Vol. 20, 1940.
9. *AASHTO Guide for Design of Pavement Structures*. Vol. 2. American Association of State Highway and Transportation Officials, Washington, D.C., 1986.
10. A. S. Noureldin and M. A. Al Dhalaan. Establishment of Some Structural Parameters to Pavement Evaluation Using the Falling Weight Deflectometer. Presented at 70th Annual Meeting of the Transportation Research Board, Washington, D.C., 1991.

Stiffness of Asphalt Concrete Surface Layer from Stress Wave Measurements

MARWAN F. AOUAD, KENNETH H. STOKOE II, AND ROBERT C. BRIGGS

The spectral analysis of surface waves (SASW) method is an in situ seismic technique used to evaluate the stiffness of the asphalt concrete (AC) surface layer as well as the stiffnesses of lower layers in a pavement profile. Measurements are made at low strain levels; hence testing is nondestructive. A key element in performing SASW measurements is the generation and detection of surface waves. To sample the AC surface layer, wavelengths less than the surface layer thickness need to be generated. This requirement can only be accomplished with sources generating high frequencies (frequencies generally above 20 kHz). Two high-frequency sources, a small hammer and a piezoelectric generator, were used. Results show that the piezoelectric generator performed better than the small hammer as a high-frequency source, especially for temperatures above 80°F. SASW measurements made at the pavement test facility in Bryan, Texas, indicated how it is possible to quantify changes in the stiffness of the AC surface layer with ambient temperature changes. These in situ measurements along with similar measurements made on Route 1 in Austin, Texas, show how Young's modulus, E, of the AC surface layer changes with temperature in the manner predicted by the AASHTO guide for temperatures below 100°F. However, for temperatures above 100°F, the AASHTO guide overpredicts the decrease in E with increasing temperatures based on the in situ SASW results. In the case of thin AC surface layers, layers with a thickness on the order of 1 in. (2.5 cm) or less, wavelengths shorter than the thickness of the surface layer could not be generated so that the surface layer could not be evaluated with SASW tests. In such cases, compressional stress wave measurements are suggested.

The spectral analysis of surface waves (SASW) method is a nondestructive and nonintrusive method for evaluating stiffness profiles of pavement systems using stress (seismic) waves. General application of the SASW method to pavement systems can involve extensive testing and analytical modeling. However, the method is readily applied to measurements of surface layers when the layer thickness is on the order of several inches. This application is demonstrated herein by tests performed on AC surface layers at the Texas Transportation Institute (TTI) Annex in Bryan, Texas, and on Route 1 in Austin, Texas. The effectiveness of the test in determining in situ changes in AC surface layer stiffness due to changes in ambient temperature is shown, and limitations of the method on thin AC surface layers are noted.

SASW testing was performed at three sites at the TTI facility [Sites 4, 9, and 12 as designated by Scrivner and Michalak (*1*)]. These sites have AC surface layers that are about 5 in. (12.5 cm) in thickness. Such surface layers are considered "thick" layers in the context of SASW testing. Each site was tested at two different seasons of the year. The first series of tests involved measurements in the summer (during the last week of July 1988) when the temperature of the surface layer ranged from 80°F to 143°F. The second series involved measurements during the cold season, in the first week of March 1989, when the temperature ranged from 30°F to 81°F. SASW tests were also performed at Sites 10 and 11 at the TTI facility, which have an AC layer thickness of 1 in. (2.5 cm). These sites are considered to have a "thin" surface layer in the context of SASW testing. In this case, compressional wave testing was also performed during the cold season of the year to evaluate the stiffness of the surface layer.

A suite of SASW and compressional wave tests was also performed on the AC surface layer of Route 1 in Austin, Texas. This pavement is composed of a thick surface layer, which was tested within 1.5 years after placement, in contrast with the AC surface layers at TTI, which are about 25 years old.

The objectives of testing at TTI and Route 1 were to study the effects of temperature, thickness, and age of the AC layer on the measurement of stiffness, to determine whether the SASW method ceases to perform adequately at some surface layer thicknesses, to recommend when other techniques (such as compression wave testing) should be used in place of the SASW method to characterize the AC surface layer, and to evaluate the importance of frequency in these measurements. Stiffness variations of AC with temperature and frequency are dependent on asphalt type. This variable was not studied because the thrust of this work dealt with developing the methodology needed to apply SASW and compression wave testing to AC surface layers.

SASW METHOD

The SASW method was initiated at the University of Texas at Austin in the early 1980s with funding from The Texas State Department of Highways and Public Transportation (*2–4*). Key elements in the SASW technique are the generation and detection of surface waves using a source and two receivers placed on the pavement surface. Two strengths of the SASW method are (*a*) all measurements are made from the pavement surface and (*b*) a pavement stiffness profile in terms of Young's modulus can be obtained without knowing the layer thicknesses. These two strengths make the SASW method effective in testing pavement systems where the pavement surface layer is intact. In addition, research has been conducted at several universities during the last decade to

M. F. Aouad and K. H. Stokoe II, Department of Civil Engineering, The University of Texas at Austin, Austin, Tex. R. C. Briggs, Texas Department of Transportation, Austin, Tex.

improve the theoretical and practical aspects of the method (*5–11*).

When SASW measurements are performed, a source and two receivers are placed on the pavement surface such that the distance from the source to the first receiver is equal to the distance between the two receivers. A dynamic signal analyzer is used to capture and process the receiver outputs denoted by $x(t)$ and $y(t)$ for Receivers 1 and 2, respectively. Then $x(t)$ and $y(t)$ are transformed to the frequency domain [$X(f)$ and $Y(f)$] through the use of a Fast Fourier Transform. $X(f)$ and $Y(f)$ are used to calculate the cross power spectrum between the two receivers, denoted by G_{XY} [$G_{XY} = X(f)^* \cdot Y(f)$, where * denotes the complex conjugate]. The surface wave velocity and wavelength as a function of frequency, $V_R(f)$ and $\lambda(f)$, are determined from these results by

$$\Theta_{XY}(f) = \tan^{-1}[\mathrm{Im}(G_{XY})/\mathrm{Re}(G_{XY})] \quad (1)$$

$$t(f) = \Theta_{XY}(f)/(360° \cdot f) \quad (2)$$

$$V_R(f) = D/t(f) \quad (3)$$

$$\lambda(f) = V_R(f)/f \quad (4)$$

where

$\Theta_{XY}(f)$ = phase shift of the cross power spectrum in degrees at each frequency,
Im = imaginary part of the cross power spectrum at each frequency,
Re = real part of the cross power spectrum at each frequency,
f = frequency,
$t(f)$ = time delay between receivers as a function of frequency, and
D = distance between receivers.

In addition, values of a coherence function are calculated in these measurements. The coherence function, $\gamma^2(f)$, is defined as

$$\gamma^2(f) = |G_{XY}|^2/(G_{XX} \cdot G_{YY}) \quad (5)$$

where

$\|$ = magnitude of the cross power spectrum,
G_{XX} = power spectrum of Receiver 1, and
G_{YY} = power spectrum of Receiver 2.

The coherence will be equal to unity where the input and output signals are correlated (noise free). Typical functions for Θ_{XY} and γ^2 are shown in Figure 1 for receivers spaced 6 in. (15.2 cm) apart.

In an elastic, isotropic medium, the elastic constants are determined from the surface wave velocity according to the following relationships:

$$V_S = C \cdot V_R \quad (6)$$

$$G = (\gamma/g) \cdot V_S^2 \quad (7)$$

$$E = 2G(1 + \nu) \quad (8)$$

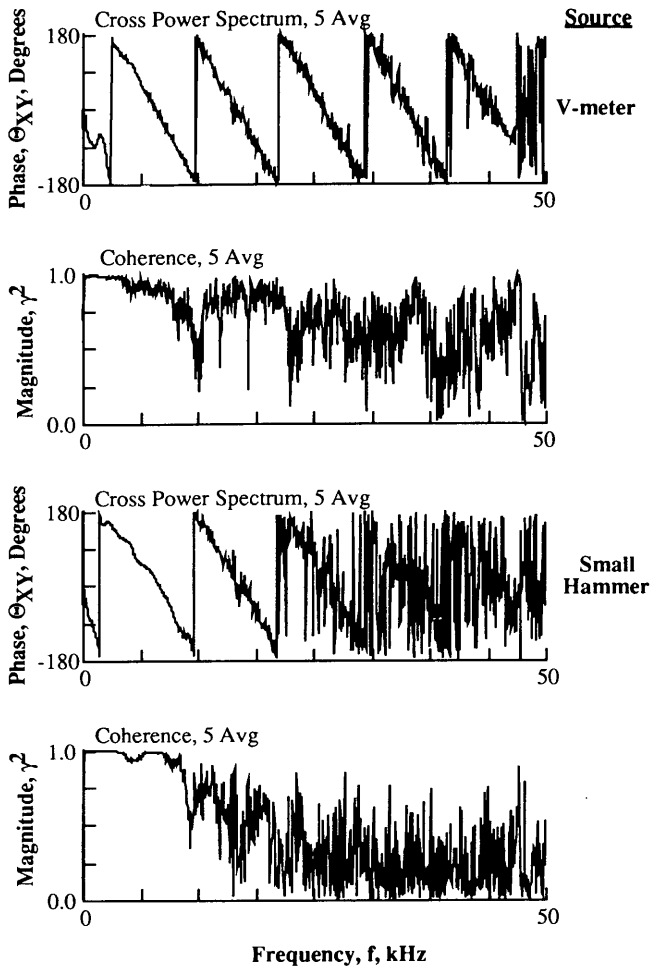

FIGURE 1 Comparison of phases of the cross power spectra and coherence functions using two sources, Site 12 at TTI Annex (T = 97°F, receiver spacing = 6 in., AC thickness ≈ 5 in.).

where

V_S = shear wave velocity,
C = $1.135 - 0.182 \cdot \nu$ (for $\nu \geq 0.1$),
G = shear modulus,
γ = total unit weight,
g = acceleration of gravity,
E = Young's modulus, and
ν = Poisson's ratio.

A Poisson's ratio of 0.27 was assumed unless compression wave measurements were made.

SASW MEASUREMENTS AT SITES 4, 9, AND 12

The asphalt concrete pavement stiffness (E) is dependent on temperature and frequency because of the viscous nature of asphalt. The modulus of the pavement can change significantly with temperature and frequency. To quantify in-place changes in E of the AC layer with temperature, SASW tests were performed at Sites 4, 9, and 12 at the TTI Annex.

The first series of tests was conducted during July 1988 when the surface temperature varied from 80°F in the morning (5:30 a.m.) to about 143°F in the afternoon (2:15 p.m.). Two sources were used. A small ball-peen hammer [weight about 2 oz (57 gm)] and a V-meter (piezoelectric source with central output frequency of 54 kHz) were compared as high-frequency generators. The surface waves were monitored with two PCB Model 308B02 accelerometers placed on the pavement surface. The accelerometers have a resonant frequency of 25 kHz and a calibration factor of 1 V/*g*. The accelerometers were coupled to the asphalt concrete by attaching 10-32 threaded rods to the bottom of the accelerometers, which, in turn, were attached to 10-32 nuts glued to the AC surface. This approach was used so that exactly the same points could always be tested.

The small hammer and V-meter were evaluated to determine whether they could provide the high frequencies required to evaluate the AC layer. A comparison of the cross power spectra and coherence functions [$\Theta_{XY}(f)$ and $\gamma^2(f)$ in Equations 1 and 5] from SASW measurements at Site 12 using both sources is shown in Figure 1. The V-meter generated energy up to 45 kHz, as opposed to the maximum 20-kHz energy generated by the small hammer as noted in the cross power spectra. Despite the poor coherence at frequencies above 20 kHz due to attenuation and background noise interference, the cross power spectrum using the V-meter as a source could be easily interpreted to obtain the experimental dispersion curve. As the temperature of the surface layer rose, the surface layer became too soft to allow impact sources such as the small hammer to be used as a high-frequency source. On the basis of this comparison, the V-meter was adopted as the better source for the generation of high frequencies and was used for the remainder of the first test series.

The second series of SASW tests was conducted during Mach 1989, when the surface temperature varied from 30°F early in the morning (5:50 a.m.) to 81°F in the early afternoon (12:45 p.m.). The source used to generate the high frequencies in the second series of tests was the small ball-peen hammer because of its simplicity. The performance of this source was checked against the V-meter for low surface temperatures. A comparison of the cross power spectra and coherence functions at Site 12 using both sources is shown in Figure 2. The small hammer performed well over the range of temperatures and frequencies required to sample the surface layer. Both sources generated energy up to 50 kHz. The generated surface waves were detected by two WR (Wilcoxon Research) Model 736 accelerometers placed on the pavement surface. These accelerometers have a resonant frequency above 50 kHz and a calibration factor of 0.1 V/*g*. The accelerometers were coupled to the asphalt concrete by attaching a magnet to a steel plate at the bottom of the accelerometers, which, in turn, was attached to a nail driven into the surface layer. This coupling method was faster and more convenient than the approach used in the first series of tests and represents the method of choice.

A comparison of the phases of the cross power spectra for a temperature range from 30°F to 143°F using the V-meter as a source and a receiver spacing of 6 in. (15.2 cm) at Site 12 is shown in Figure 3. This comparison shows the deterioration of the phase shift of the cross power spectrum as the surface

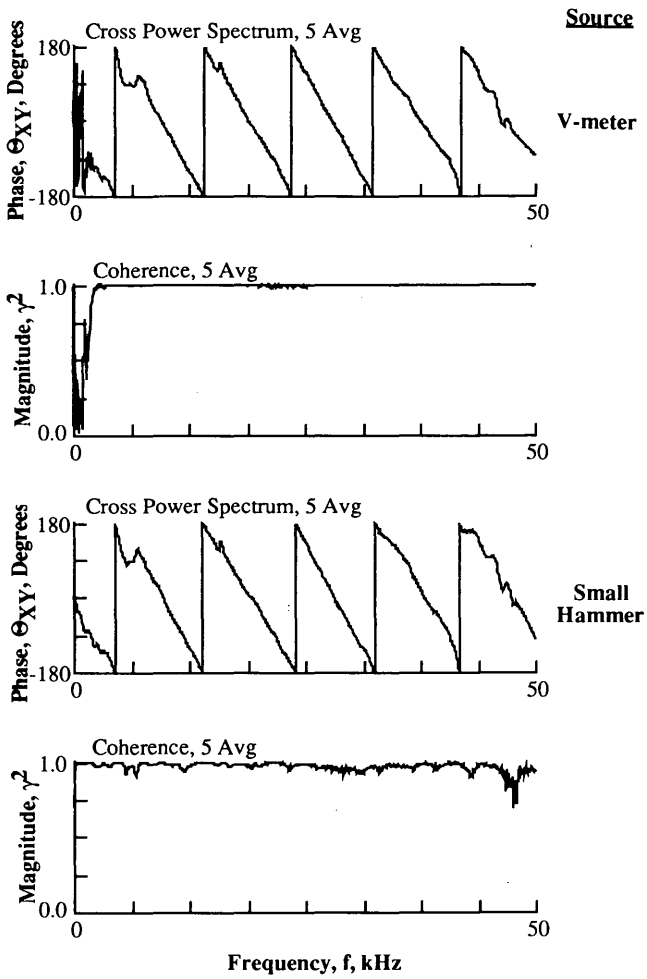

FIGURE 2 Comparison of phases of the cross power spectra and coherence functions using two sources, Site 12 at TTI Annex (T = 59°F, receiver spacing = 6 in., AC thickness ≈ 5 in.).

layer warms. At a temperature of 30°F, frequencies up to 50 kHz were generated, as opposed to frequencies of about 18 kHz when the temperature rose to 143°F. The same behavior was observed at Sites 4 and 9.

Experimental Dispersion Curves

The phase shifts of the cross power spectra and the coherence functions were used to obtain the experimental dispersion curves shown in Figures 4a and 4b for Sites 4 and 12, respectively. The dispersion curves for Site 9 were similar to those for Site 12. The experimental dispersion curves shown are the composite dispersion curves based on receiver spacings of 0.5 and 1 ft (0.15 and 0.3 m). The 1-ft (0.3-m) spacing was used to sample the base layer. However, that measurement was used only slightly in these tests. To illustrate how the measured phase shifts, Θ_{XY}'s, are used to calculate wave velocities, consider Points A and B on each curve in Figure 4b. These points are shown in the field measurements in Figure 3. Point A corresponds to a surface wave velocity and wave-

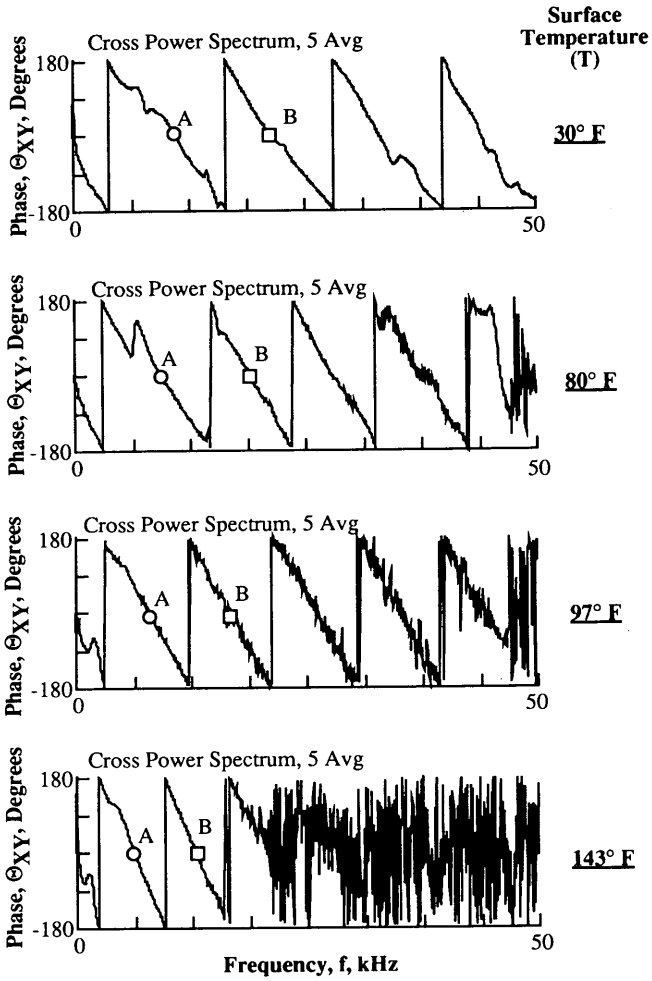

Note: Points A and B shown in dispersion curves in Fig. 4b

FIGURE 3 Variation in phase of the cross power spectrum as the asphalt concrete surface layer warms from 30°F to 143°F, Site 12 at TTI Annex (V-meter source, receiver spacing = 6 in., AC thickness ≈ 5 in.).

length calculated from Equations 1 through 4 for a phase shift of 360 degrees between receivers. This phase shift gives different wave velocities for different temperatures because the frequency at which the 360°-degree phase shift occurred decreased as temperature increased. Point B corresponds to a surface wave velocity and wavelength for a phase shift of 720 degrees between receivers.

Figures 4a and 4b indicate that the stiffness of the surface layer can be determined with great precision as it warms or cools. This value is simply calculated from the average of all values of V_R at wavelengths shorter than the layer thickness [6 in. (15.2 cm) in this case]. At a temperature of 30°F, an average value of the surface wave velocity of the asphalt layer was found to be 5,430 fps (1655 m/sec) as opposed to the value of 3,370 fps (1025 m/sec) at a temperature of 143°F. These values correspond to Young's moduli of 2,735 ksi (18.8 × 10^3 MPa) and 1,055 ksi (7.3 × 10^3 MPa) at 30°F and 143°F, respectively. These values of E correspond to an average measurement frequency of 15 kHz and, thus, must be corrected for frequency for use in design or for comparison with

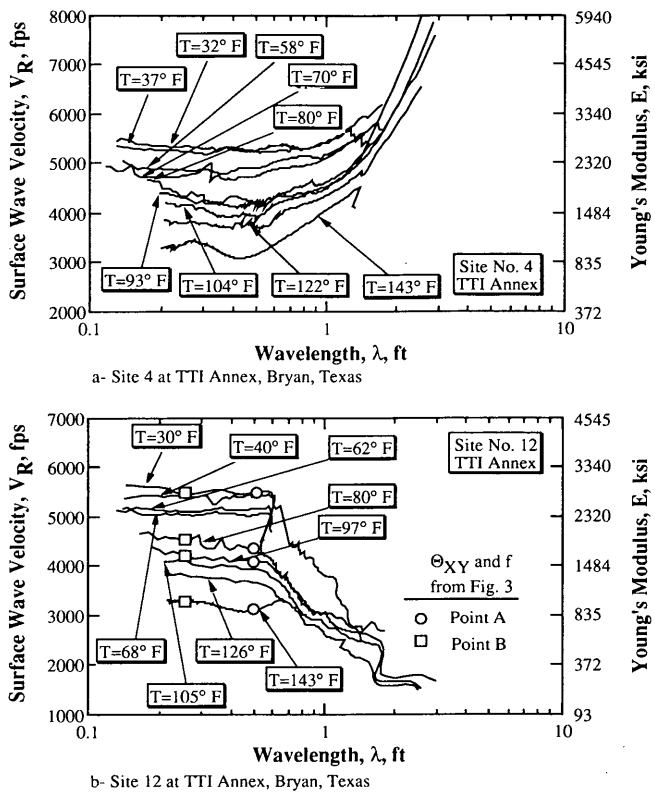

FIGURE 4 Change in stiffness of the asphalt concrete surface layer (thickness ≈ 5 in.) as a result of solar heating or cooling.

results from other tests such as the falling weight deflectometer (say at about 30 Hz). The SASW-determined moduli values should, therefore, be divided by the correction factor shown in Figure 5. The solid data points in Figure 5 represent extrapolated values from curves obtained by Sousa and Monismith (*12*). Additional testing has been conducted by the first author in the laboratory with field cores (*13*), and these results are shown by the open symbols. The solid curve represents a potential frequency correction curve to adjust high-frequency SAW measurements to those at a frequency of 30 HZ.

Figure 4 also indicates a slight decrease in velocity with increasing wavelength in the surface layer, suggesting a frequency dependence of the stiffness of the AC layer (most

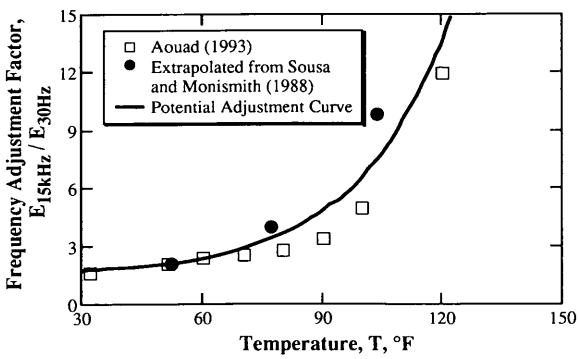

FIGURE 5 Variation of frequency adjustment factor with temperature for asphalt concrete.

easily seen in Figure 4b above temperatures of 68°F). Finally, the base material was sampled with SASW measurements using a 1-ft (0.3-m) receiver spacing. Without any further analysis of the data, it is clear that the base material of Site 4, which consists of 4 percent cement-stabilized crushed limestone, is stiffer than the surface layer because the surface wave velocity increases as wavelength increases above 0.55 ft (0.17 m) (Figure 4a). On the other hand, surface wave velocity decreases at wavelengths greater than 0.55 ft (0.17 m) at Site 12, indicating a softer material below the surface layer. This is further shown in Figure 6, which shows a comparison of the dispersion curves of Sites 4 and 12 for measurements at two different temperatures. From the SASW measurements, the thickness of the surface layer was determined to be about 0.55 ft (0.17 m), which is in reasonable agreement with the thickness of 0.42 ft (0.13 m) shown on the construction drawings. The layer thickness was determined as equaling the wavelength at which the surface wave velocities begin to change from the nearly constant value representing the surface layer (*14*).

Adjustment of Modulus for Frequency

Values of surface wave velocities determined from the SASW measurements were used to calculate Young's moduli of the surface layer using Equations 6 through 8. A unit weight of 140 pcf (22 kN/m^3) and a Poisson's ratio of 0.27 were assumed for the AC layer. Table 1 gives surface wave velocities and Young's moduli for wavelengths of 0.25 and 0.42 ft (0.08 and 0.13 m). The wavelength of 0.25 ft (0.08 m) was selected because it was the minimum wavelength measured when the surface temperature rose to 143°F. The wavelength of 0.42 ft (0.13 m) was selected because it corresponds to the as-built thickness of the AC surface layer. Figure 7 shows the variation of the surface layer modulus with temperature. At a wavelength of 0.25 ft (0.08 m), the modulus exhibits a slightly higher value than at a wavelength of 0.42 ft (0.13 m), primarily because of the effect of frequency.

As an initial attempt to remove the effect of frequency, the moduli of the surface layer were calculated using surface wave velocities at a frequency of 15 kHz and were normalized to a modulus at 70°F [$E_{70°F} \approx 2{,}140$ ksi (14.8×10^3 MPa)]. The

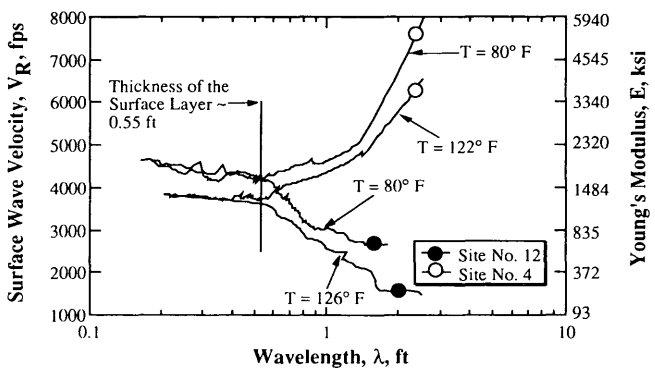

FIGURE 6 Comparison of experimental dispersion curves determined at Sites 4 and 12 for two temperatures.

TABLE 1 Surface Wave Velocities and Young's Moduli of the Asphalt Concrete Surface Layer at Wavelengths of 0.25 and 0.42 ft Determined from SASW Measurements at Sites 4, 9, and 12

Temp. (°F)	Site 4				Site 9				Site 12			
	λ = 0.25 ft		λ = 0.42 ft		λ = 0.25 ft		λ = 0.42 ft		λ = 0.25 ft		λ = 0.42 ft	
	V_R (fps)	E (ksi)	V_R (fps)	E (ksi)	V_R (fps)	E (ksi)	V_R (fps)	E (ksi)	V_R (fps)	E (ksi)	V_R (fps)	E (ksi)
30	-----	-----	-----	-----	5482	2788	5355	2661	5545	2853	5471	2777
32	5359	2665	5249	2557	-----	-----	-----	-----	-----	-----	-----	-----
37	5251	2559	5190	2500	-----	-----	-----	-----	-----	-----	-----	-----
40	-----	-----	-----	-----	-----	-----	-----	-----	5246	2553	5195	2504
43	-----	-----	-----	-----	5292	2598	5190	2499	-----	-----	-----	-----
56	-----	-----	-----	-----	5098	2411	5010	2329	-----	-----	-----	-----
58	4878	2208	4920	2246	-----	-----	-----	-----	-----	-----	-----	-----
62	-----	-----	-----	-----	-----	-----	-----	-----	5146	2457	5142	2453
68	-----	-----	-----	-----	-----	-----	-----	-----	5036	2353	5034	2351
70	4811	2148	4737	2082	-----	-----	-----	-----	-----	-----	-----	-----
72	-----	-----	-----	-----	4782	2122	4736	2081	-----	-----	-----	-----
80	4368	1770	4216	1649	-----	-----	-----	-----	4484	1865	4286	1704
81	-----	-----	-----	-----	4495	1874	4191	1629	-----	-----	-----	-----
89	-----	-----	-----	-----	4433	1823	4170	1613	-----	-----	-----	-----
93	4326	1736	4199	1636	-----	-----	-----	-----	-----	-----	-----	-----
97	-----	-----	-----	-----	-----	-----	-----	-----	4193	1631	4090	1552
104	4171	1614	3937	1438	3984	1472	3822	1355	-----	-----	-----	-----
105	-----	-----	-----	-----	-----	-----	-----	-----	4120	1575	3917	1423
117	-----	-----	-----	-----	3870	1389	3770	1318	-----	-----	-----	-----
122	3821	1354	3729	1290	-----	-----	-----	-----	-----	-----	-----	-----
126	-----	-----	-----	-----	-----	-----	-----	-----	3828	1359	3648	1234
139	-----	-----	-----	-----	3436	1095	3330	1029	-----	-----	-----	-----
143	3417	1083	3193	946	-----	-----	-----	-----	3272	993	3105	894

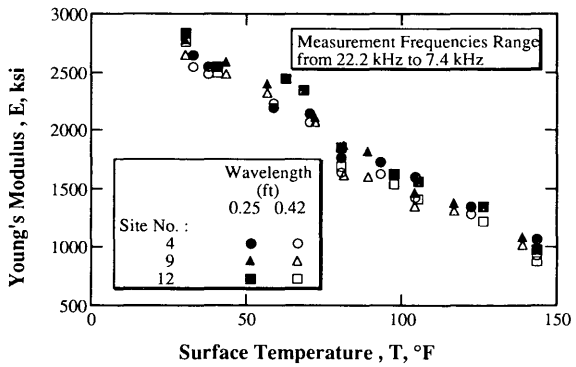

FIGURE 7 Variation in low-strain Young's modulus with temperature for wavelengths of 0.25 and 0.42 ft at the TTI Annex, Bryan, Texas.

frequency of 15 kHz was selected because it was about the highest frequency generated when the temperature rose to 143°F. Table 2 gives the surface wave velocities and normalized moduli at a frequency of 15 kHz. The variation of normalized modulus with temperature is presented in Figure 8. A change in modulus by a factor of about 2.6 was observed for the change in temperature from 30°F to 143°F. When such correlation curves become well established, thin pavements, which are especially difficult to test at high temperatures as discussed in the next section, could be tested when cool, and

TABLE 2 Surface Wave Velocities and Normalized Young's Moduli of the Asphalt Concrete Surface Layer Determined from SASW Measurements at Sites 4, 9, and 12; Measurement Frequency ≈ 15 kHz

Site 4			Site 9			Site 12		
T (°F)	V_R (fps)	$E/E_{70°F}$	T (°F)	V_R (fps)	$E/E_{70°F}$	T (°F)	V_R (fps)	$E/E_{70°F}$
32	5316	1.2266	30	5431	1.2802	30	5545	1.3345
37	5254	1.1981	43	5250	1.1963	40	5246	1.1945
58	4880	1.0336	56	5081	1.1205	62	5146	1.1494
70	4800	1.0000	72	4817	1.0071	68	5063	1.1126
80	4400	0.8403	81	4440	0.8556	80	4474	0.8688
93	4223	0.7740	89	4380	0.8327	97	4160	0.7511
104	4100	0.7296	104	3984	0.6889	105	4050	0.7119
122	3821	0.6337	117	3870	0.6500	126	3800	0.6267
143	3378	0.4953	139	3440	0.5136	143	3291	0.4701

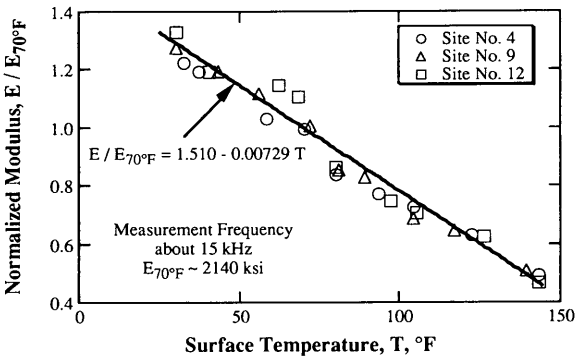

FIGURE 8 Variation in normalized low-strain Young's modulus (normalized to a modulus at a temperature of 70°F) with temperature for three sites at the TTI Annex, Bryan, Texas.

values of moduli at higher temperatures could be obtained from correlation curves such as the one in Figure 8.

Normalized moduli of the asphalt concrete layer obtained from SASW measurements and corrected to a frequency of 30 Hz are shown in Figure 9. These corrected values are compared with values suggested by the *AASHTO Guide for Design of Pavement Structures* (*15*) in Figure 10. Figure 10

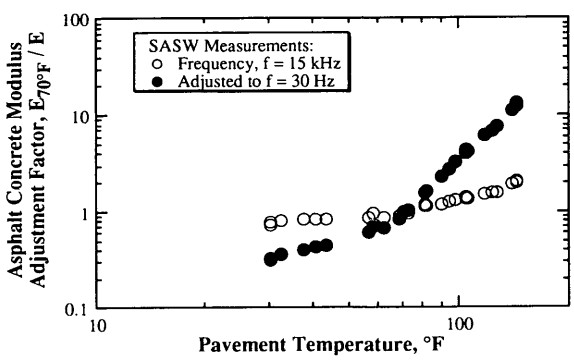

FIGURE 9 Normalized modulus determined from SASW measurements at the TTI Pavement Facility and adjusted for frequency using Figure 5.

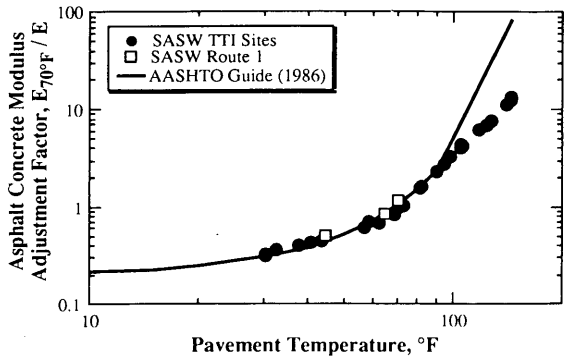

FIGURE 10 Comparison of the variation of AC modulus with temperature from SASW measurements with that suggested by the *AASHTO Guide for Design of Pavement Structures* (*15*).

indicates that the normalized moduli of the surface layer determined by SASW measurements at temperatures less than 100°F compare closely with normalized moduli suggested by the AASHTO guide. However, at temperatures above 100°F, in situ moduli determined by SASW testing are underestimated using the AASHTO guide. The SASW measurements were made at small strains (less than 0.001 percent). It is assumed that the lower values of moduli determined at high temperatures for the AASHTO guide are due to the higher strains associated with stress-controlled laboratory testing of soft AC specimens. At high temperatures, the behavior of asphalt is quite strain dependent. In addition, to accommodate the frequency effect in the SASW test, different adjustment factors are applied at different surface temperatures, as shown in Figure 5. The factor at high temperatures is large, and small errors in this factor could also contribute to the differences seen in Figure 10.

SASW tests similar to those performed at the TTI Annex were also performed on Route 1 in Austin, Texas. Testing was performed during February 1991, approximately 1.5 years after the AC layer 7 in. (17.8 cm) thick was placed. Results similar to those shown in Figures 3, 4b, and 8 were obtained. At a temperature of 70°F, an average value of the surface wave velocity of the AC layer was 5,410 fps (1650 m/sec). This value corresponds to a Young's modulus of 2,715 ksi (18.7×10^3 MPa), representing a stiffer AC layer than that encountered at the TTI facility, where $E_{70°F} \approx 2{,}140$ ksi (14.8×10^3 MPa). Normalized moduli of the AC surface layer obtained from SASW measurements on Route 1 and corrected to a frequency of 30 Hz at temperatures of 70°F, 63°F, and 43°F are shown in Figure 10. The normalized values agree well with the curve suggested by the AASHTO guide at these temperatures.

TESTING OF THIN ($t \approx 1$ in.) AC SURFACE LAYERS

Sites 10 and 11 at the TTI Annex were selected as representative pavement with thin AC surface layers. These sites consist of an AC layer 1 in. (2.5 cm) thick underlain by crushed limestone base and subbase. SASW measurements were performed at the two sites to evaluate the material profiles at

temperatures ranging from 70°F to 110°F. The stiffness of the surface layer could not be determined from the SASW measurements because wavelengths less than the thickness of the surface layer could not be generated. Therefore, no zone of short wavelengths, essentially constant velocities, was determined. The generation of short wavelengths was limited by the maximum aggregate size and the relatively high surface temperature. In this case, compression wave measurements should be performed in conjunction with the SASW measurements to determine the stiffness of the AC surface layer as discussed elsewhere (*13*).

CONCLUSIONS

The SASW method was used at the TTI pavement facility in Bryan, Texas, and on Route 1 in Austin, Texas, to evaluate the stiffness of AC surface layers under different climatic conditions. The method proved to be effective in determining in situ changes in stiffness (E) over temperatures ranging from 30°F to 143°F. The method was most effective at sites where the thickness of the surface layer was greater than 2 in. (5 cm) (referred to as "thick" surface layers herein). Young's moduli measured by the SASW tests represent high-frequency values and should be adjusted for frequency using Figure 5. The adjusted in situ moduli change with temperature in the same manner as predicted by the AASHTO guide (*15*) for temperatures below 100°F but show less sensitivity at temperatures above 100°F.

An essential element when performing SASW measurements to evaluate the stiffness of the AC surface layer is the generation of high frequencies, frequencies generally above 10 kHz. Two sources, a small hammer and a piezoelectric generator, were used, and the performance of each source was evaluated. The piezoelectric generator performed better than the small hammer as a high-frequency source, especially for temperatures of the AC surface layer above 80°F.

The SASW method was also used to determine the stiffness profiles of pavement sites where a "thin" AC surface layer was encountered [AC layer thickness $\approx$ 1 in. (2.5 cm)]. The stiffness of the AC surface layer could not be determined from SASW measurements because wavelengths shorter than 1 in. (2.5 cm) could not be generated. In such cases, direct compression wave measurements are suggested for use in characterizing the stiffness of the surface layer.

ACKNOWLEDGMENTS

This work was supported by the Texas Department of Transportation. The authors wish to express their appreciation for this support.

REFERENCES

1. F. Scrivner and C. H. Michalak. *Linear Elastic Layered Theory as a Model of Displacements Measured Within and Beneath Flexible Pavement Structures Loaded by the Dynaflect.* Research Report 123-25. Texas Transportation Institute, Texas A&M University, College Station, 1974.
2. J. S. Heisey, K. H. Stokoe II, W. R. Hudson, and A. H. Meyer. *Determination of In Situ Shear Wave Velocities from Spectral Analysis of Surface Waves.* Research Report 256-2. Center for Transportation Research, The University of Texas at Austin, Austin, 1982.
3. J. S. Heisey, K. H. Stokoe II, and A. H. Meyer. Moduli of Pavement Systems from Spectral Analysis of Surface Waves. In *Transportation Research Record 852*, TRB, National Research Council, Washington, D.C., 1982, pp. 22–31.
4. S. Nazarian. *In Situ Determination of Elastic Moduli of Soil Deposits and Pavement Systems by Spectral-Analysis-of-Surface-Waves Method.* Ph.D. dissertation. The University of Texas at Austin, Austin, 1984.
5. S. Nazarian and K. H. Stokoe II. *In Situ Determination of Elastic Moduli of Pavement Systems by Spectral-Analysis-of-Surface-Waves Method (Practical Aspects).* Research Report 368-1F. Center for Transportation Research, The University of Texas at Austin, Austin, 1985.
6. S. Nazarian and K. H. Stokoe II. *In Situ Determination of Elastic Moduli of Pavement Systems by Specvtral-Analysis-of-Surface-Waves Method (Theoretical Aspects).* Research Report 437-2. Center for Transportation Research, The University of Texas at Austin, Austin, 1986.
7. J. C. Sheu. *Applications and Limitations of the Spectral-Analysis-of-Surface-Waves Method.* Ph.D. dissertation. The University of Texas at Austin, Austin, 1987.
8. I. Sánchez-Salinero. *Analytical Investigation of Seismic Methods Used for Engineering Applications.* Ph.D. dissertation. The University of Texas at Austin, Austin, 1987.
9. G. J. Rix. *Experimental Study of Factors Affecting the Spectral-Analysis-of-Surface-Waves Method.* Ph.D. dissertation. The University of Texas at Austin, Austin, 1988.
10. D. R. Hiltunen and R. D. Woods. Influence of Source and Receiver Geometry on the Testing of Pavements by the Surface Waves Method. In *Nondestructive Testing of Pavement and Backcalculation of Moduli*, STP 1026 (A. J. Bush III and G. Y. Baladi, eds.), ASTM, Philadelphia, Pa., 1989, pp. 138–154.
11. D. R. Hiltunen and R. D. Woods. Variables Affecting the Testing of Pavements by the Surface Waves Method. In *Transportation Research Record 1260*, TRB, National Research Council, Washington, D.C., 1990, pp. 42–52.
12. J. B. Sousa and C. L. Monismith. Dynamic Response of Paving Materials. In *Transportation Research Record 1136*, TRB, National Research Council, Washington, D.C., 1988, pp. 57–68.
13. M. F. Aouad. *Evaluation of Flexible Pavements and Subgrades Using the Spectral-Analysis-of-Surface-Waves (SASW) Method.* Ph.D. dissertation. The University of Texas at Austin, Austin, 1993 (in progress).
14. J. M. Roesset, D. W. Chang, K. H. Stokoe II, and M. F. Aouad. Modulus and Thickness of the Pavement Surface Layer from SASW Tests. In *Transportation Research Record 1260*, TRB, National Research Council, Washington, D.C., 1990, pp. 53–63.
15. Temperature-Deflection Corrections for Asphalt Pavements. Appendix L. *AASHTO Guide for Design of Pavement Structures*, AASHTO, Washington, D.C., 1986.

Rutting Rate Analyses of the AASHO Road Test Flexible Pavements

MARSHALL R. THOMPSON AND DAVID NAUMAN

Asphalt concrete (AC) fatigue cracking, AC low-temperature cracking, and pavement surface rutting are the flexible pavement distress modes normally considered in flexible pavement analysis and design. AC fatigue cracking and rutting in component pavement layers (AC surface, granular base and subbase layers, and subgrade) are related to structural responses (stress-strain-deflection). Pavement rutting is discussed. One practical and applied pavement rutting approach is to correlate structural responses (stress-strain-deflection) with field distress measurements. The forms of laboratory-based material/soil distress models are helpful in establishing the general parameters that best define the structural response–field distress measurement relationships. The NCHRP 1-26 Phase 1 Final Report indicated that the log permanent strain (ε_p)–log load repetitions (N) phenomenological model was an appropriate, versatile, and practical approach. Paving materials (AC and granular base/subbase) and subgrade soils generally follow the model. It is assumed that a phenomenological pavement surface rutting model would be of the same form. An analogue, a proposed pavement surface rutting rate (RR) model, is evaluated: $RR = RD/N = A/N^B$, where RR is the rutting rate, RD is the rut depth in inches, N is the number of repeated load applications, and A and B are terms developed from field calibration testing data. The RR model was validated by analyzing selected AASHO Road Test data and rutting performance information from Illinois Department of Transportation rehabilitated sections of the AASHO Road Test flexible pavement tangent sections. The analyses indicated that the RR concept is valid. Stable pavement rutting trends were related to ILLI-PAVE estimated pavement structural responses, particularly the subgrade stress ratio. Similar RR performance (the B values in the RR equation) was noted for the original AASHO sections, reconstructed sections built with salvaged AASHO materials, and new sections constructed with similar paving materials. The RR approach can be effectively used in a priori pavement analysis and design and pavement management system activities. For the typical "generic specification" flexible paving materials used by a highway agency, the B terms and relationships relating structural responses to A can be established from a flexible pavement performance data base.

Flexible pavement distress modes normally considered in flexible pavement analysis and design are fatigue cracking, rutting, and low-temperature cracking. Asphalt concrete (AC) fatigue cracking and rutting in component pavement layers are significant considerations related to structural responses (stress-strain-deflection). Pavement rutting is the focus of this paper.

To limit pavement surface rutting to acceptable levels, careful attention must be directed to all of the various paving layers and the subgrade. The AC surface, the granular base and subbase layers, and the subgrade may contribute to the accumulation of pavement surface rutting. High-strength stabilized base materials, such as cement-treated aggregate and pozzolanic-stabilized base, do not significantly contribute to rut depth accumulation.

Mechanistic-based distress models for fatigue and rutting use stress-, strain-, or deflection-related parameters to estimate fatigue life or permanent deformation accumulation under repeated loading. The development of acceptable flexible pavement distress models includes the successful integration of structural modeling concepts and the material/soil testing procedures used in establishing laboratory-based fatigue or permanent deformation accumulation models. Field calibration (reconciling of actual distress development under field conditions with predicted distress development) and the establishment of shift factors are required.

An alternative approach is to directly correlate structural response outputs (stress/strain/deflection) determined from a selected standard structural analysis model with field distress measurements. The forms of laboratory-derived material/soil distress models are helpful in establishing the general parameters that best define the structural response–field distress measurement relationships.

In this paper, the application of the log permanent strain–log number of load repetitions phenomenological model and a pavement surface rutting rate (RR) model is evaluated. The primary data are from the AASHO Road Test data base.

PERMANENT DEFORMATION MODELS

Material permanent strain accumulation models (AC, granular materials, and cohesive soils) and pavement system rutting models and algorithms were considered in Phase 1 of NCHRP 1-26 (*1*). The log permanent strain–log load repetitions phenomenological model appeared to be an appropriate, versatile, and practical approach. The model is expressed as follows:

$$\log \varepsilon_p = a + b \log N \quad (1)$$

or

$$\varepsilon_p = AN^b \quad (2)$$

M. R. Thompson, Department of Civil Engineering, University of Illinois at Urbana-Champaign, Newmark Civil Engineering Laboratory, 205 North Mathews Avenue, Urbana, Ill. 61801-2352. D. Nauman, Department of Civil Engineering, University of Illinois at Urbana-Champaign, Newmark Civil Engineering Laboratory, 205 North Mathews Avenue, Urbana, Ill. 61801-2352. Current affiliation: Crawford, Murphy, & Tilly, Inc., 2750 West Washington Street, Springfield, Ill. 62702.

where

ε_p = permanent strain,
a and b = experimentally determined factors, and
A = antilog of a.

Ohio State University (OSU) researchers have proposed a permanent strain accumulation prediction model for use in a pavement design system developed for the Ohio Department of Transportation (*2*). The OSU permanent strain accumulation model is

$$\varepsilon_p/N = AN^m \quad (3)$$

where

ε_p = plastic strain at N load repetitions,
N = number of repeated load applications,
A = experimental constant dependent on material and state of stress conditions, and
m = experimental constant depending on material type.

If the b term from the log permanent strain–log N model is known, m is equal to $b - 1$.

Soils and Granular Materials

Various data considered elsewhere (*1*) indicate that for reasonable stress states (considerably below material failure strengths), the b term for soils and granular materials is generally within the range of 0.12 to 0.2 (*3–6*). The lower values are for the soils. The a term is variable and depends on material/soil type, repeated stress state, and factors influencing material shear strength. Stress state is generally expressed in such terms as repeated deviator stress ($\sigma_D = \sigma_1 - \sigma_3$), principal stress ratio (σ_1/σ_3), and deviator stress ratio (σ_D/σ_3). In these terms, σ_1 is the major principal stress and σ_3 is the minor principal stress.

The OSU study (*4*) indicated that A is "dependent on soil type and structure, moisture content, dry density, and dynamic stress level." Extensive University of Illinois data (*6*) confirm that A is influenced by many factors. The Illinois study indicated that for a given soil the parameter "log A" was significantly correlated with repeated deviator stress. Examination of the A data indicated that most of the soils also exhibit a "threshold stress level," which is defined as the stress level above which the permanent deformation of the soils under repeated loading is rapid and below which the rate of cumulative deformation from additional stress applications is very small. In most cases the threshold stress level is 50 to 60 percent of the ultimate strength of the soil.

The stress ratio (repeated stress/ultimate strength) approach has good potential. In relative terms, low A values are noted for reduced stress ratios, and large A values are noted for increased stress ratios. Since stress ratio is a valid indicator of rutting potential (as evidenced by the A term), the factors influencing the stress state and strength of in situ granular materials and soils are important considerations.

Asphalt Concrete

Khedr's AC permanent deformation model (*7*) (in the form of Equation 3) was based on repeated load compression tests. The study summarized data for a series of AC mixtures (three crushed limestone aggregates, 85/100 AC-20 asphalt cement) and a range of testing temperatures and stress levels.

Khedr's analyses showed that the m term ($m = b - 1$) does not show considerable variability as influenced by temperature and stress state. Although in Khedr's statistical analyses "m was found to be constant," the m values tended to decrease for higher temperatures (i.e., for decreased AC stiffness). Khedr's average b for the AC mixtures tested was 0.22. The A term was dependent on the repeated deviator stress and the AC mixture modulus. Log A decreased as a function of the log of the AC modulus/repeated deviator stress (i.e., 1/AC strain).

Leahy (*8*) and Leahy and Witczak (*9*) have recently reported on a comprehensive AC permanent deformation study. Two hundred fifty-one asphalt concrete specimens were tested under varying conditions. Temperature, deviator stress, asphalt type and content, aggregate type, and compactive effort were considered. The study confirmed the general applicability of the log permanent strain-log N phenomenological model (Equation 1).

They concluded that a and b were affected by test conditions and mixture properties. a was influenced to a greater extent than b. For the data base considered, the a term varied considerably (coefficient of variation of 97 percent), but the b term showed less variability (average was 0.44 with a coefficient of variation of 27 percent).

Some of Leahy's more specific relevant conclusions are as follows (*8*):

- The slope coefficient, b, was moderately influenced by temperature, asphalt content, and compaction/air voids. It was not affected by deviator stress or aggregate or asphalt type.
- The intercept coefficient, a, was heavily influenced by temperature, deviator stress, and asphalt type and moderately influenced by asphalt content and compaction/air voids. The aggregate had no effect on the intercept coefficient.

Recent Texas A&M studies by Mahboub and Little (*10–12*) include the development of proposed procedures for considering AC rutting in the mixture design process. AC mixture rutting potential is evaluted by laboratory creep testing, and a modified SHELL procedure is used to estimate rutting. The following expression is used to characterize AC permanent deformation:

$$\varepsilon_{vp} = at^b \quad (4)$$

where

ε_{vp} = viscoplastic strain,
t = time, and
a and b = regression constants.

The exponent b from creep testing is generally considered to be comparable with the b term in the log permanent strain–log N relation established from repeated load testing. Mah-

boub and Little (*10–12*) found from their data and various literature sources that the average b (six values based on creep testing data) was about 0.226, with a standard deviation of 0.031. They indicate that b can be "treated as a constant."

The average b value (0.44) for Leahy and Witczak's data base does not compare favorably with the 0.226 value from Mahboub and Little or the 0.22 value from Khedr. However, the test parameters in the Leahy study represent a much wider data set. For example, Leahy's data for AC Mixture 2 (4.8 percent AC-20, crushed aggregate) indicates that b may change significantly at extremes of temperature or stiffness.

PAVEMENT RUTTING RATE MODEL

The OSU researchers (*2*) indicated that "this relation [Equation 3] is also valid for describing rutting progress in all pavement layers—asphalt, granular base course, subbase materials and subgrade support soils." The references cited in this paper support the general validity of that statement.

If all of the paving materials (AC and granular base/subbase) and the subgrade soils generally follow the log ε_p–log N phenomenological model (Equation 1) and the OSU model (Equation 3), it is reasonable to assume that a phenomenological pavement surface rutting model would be of the same form. A pavement system rutting rate (RR) analogue can be obtained by substituting rut depth for the permanent strain term. The resulting equation is

$$RR = RD/N = \mathbf{A}/N^{B} \quad (5)$$

where

RR = rutting rate,
RD = rut depth (in.),
N = number of repeated load applications, and
A and B = terms developed from field calibration testing data.

To evaluate the validity of the concept, the RR model (Equation 5) was used to analyze selected AASHO Road Test data.

RUTTING RATE ANALYSES OF AASHO ROAD TEST DATA

AASHO Road Test rut depth data for the single-axle lanes of the conventional flexible pavement sections (AC/granular) of Loops 3 through 6 and the bituminous wedge sections in Loops 3, 5, and 6 were analyzed to

1. Establish the RR parameters (**A** and B),
2. Evaluate the validity of the RR model, and
3. Identify the pavement structural responses that most influence **A** and B.

Typical rut-depth development data are shown in Figure 1 for AASHO Section 591 (outer wheelpath) of Loop 4. Section 591 is 5-in. AC surface, 6-in crushed stone base, and 8-in. gravel subbase. Loop 4 single-axle loading was 18 kips. Figure 2 shows the log RR–log N relation.

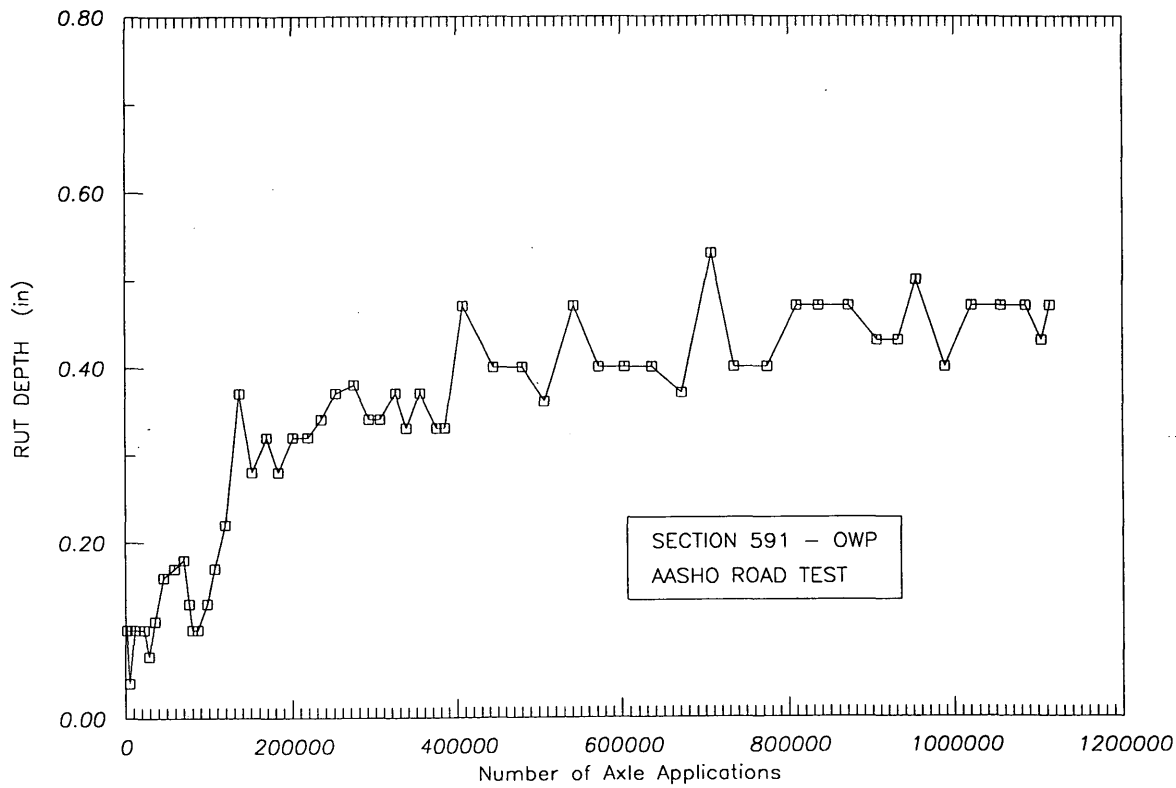

FIGURE 1 Rut depth versus N for Section 591.

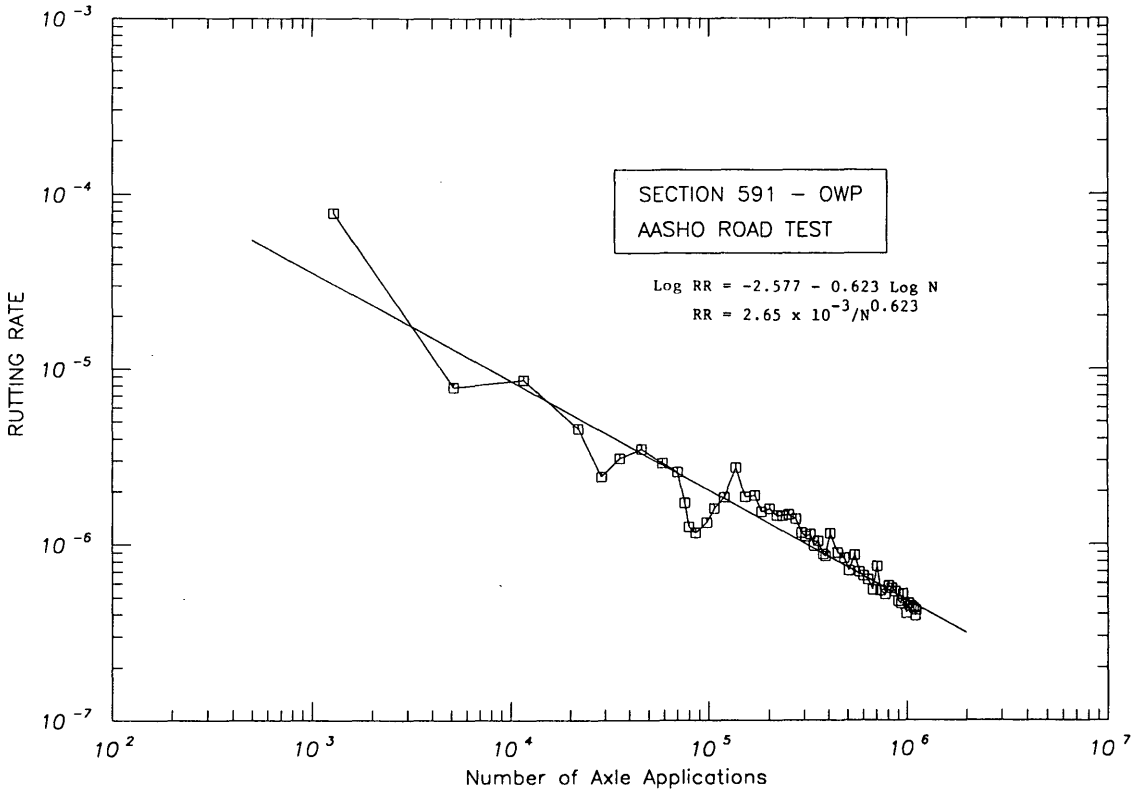

FIGURE 2 Log rutting rate versus log N for Section 591.

Table 1 is a summary (for all of the sections analyzed) indicating the veracity of the RR model. Statistically significant ($\alpha = 0.05$) relations were obtained for 182 of the 192 cases (95 percent).

A strong relation (see Figure 3) was noted for the AC/granular sections on an arithmetic plot between B and **A**, regardless of axle loading. A B–log **A** plot and related regression equation are shown in Figure 4.

Figure 4 is for the entire data base summary including the bituminous wedge sections. The data in Figure 4 are for a range of single-axle loads (12 to 30 kips), pavement cross sections (surface, base, and subbase thicknesses), and pavement types (conventional flexible and full-depth type AC wedge sections).

TABLE 1 Rutting Rate Analysis Results

AASHO Loop	Axle Load (kips)	Number of Sections	Number of Significant Relations*
3	12.0	26	25
3-wedge	12.0	16	15
4	18.0	60	59
5	22.4	40	39
5-wedge	22.4	16	11
6	30.0	18	17
6-wedge	30.0	16	16
		192	182

*Statistically significant regression at $\alpha = 0.05$.

The effects of axle load on the **A** parameters are shown in Figure 5 for similar AC/granular pavement sections. Note that for the 5-in. surface, 6-in. base, and 12-in. subbase section (the strongest section), **A** values do not increase with axle loading.

If the **A** term in the RR model can be related to pavement structural responses (stress, strain, and deflection), the B term can be estimated from the regression equation shown in Figure 4. Thus, a viable rutting algorithm can be developed for use in a priori design and pavement management system activities.

Thompson and Elliott (*13*) have developed algorithms based on ILLI-PAVE for estimating the 9-kip wheel loading structural responses of conventional flexible pavements. Extensive analyses of the Loop 4 AASHO Road Test data were conducted by Elliott and Thompson (*14*) in the development of mechanistic design concepts and procedures for the Illinois Department of Transportation. Representative seasonal values for AC moduli and subgrade moduli (E_{Ri}) were established, as indicated in the following table:

Season	*AC Modulus (ksi)*	*Subgrade E_{Ri} (ksi)*	*Estimated Unconfined Strength (psi)*
Spring	1,340	1.4	8
Summer	340	3.1	12
Fall	700	5.4	17

Pertinent structural reponses [surface deflection, subgrade deflection, subgrade strain, subgrade deviator stress, and subgrade stress ratio (SSR = deviator stress/unconfined strength)] were estimated for all of the Loop 4 sections for spring, summer, and fall conditions. Winter conditions were

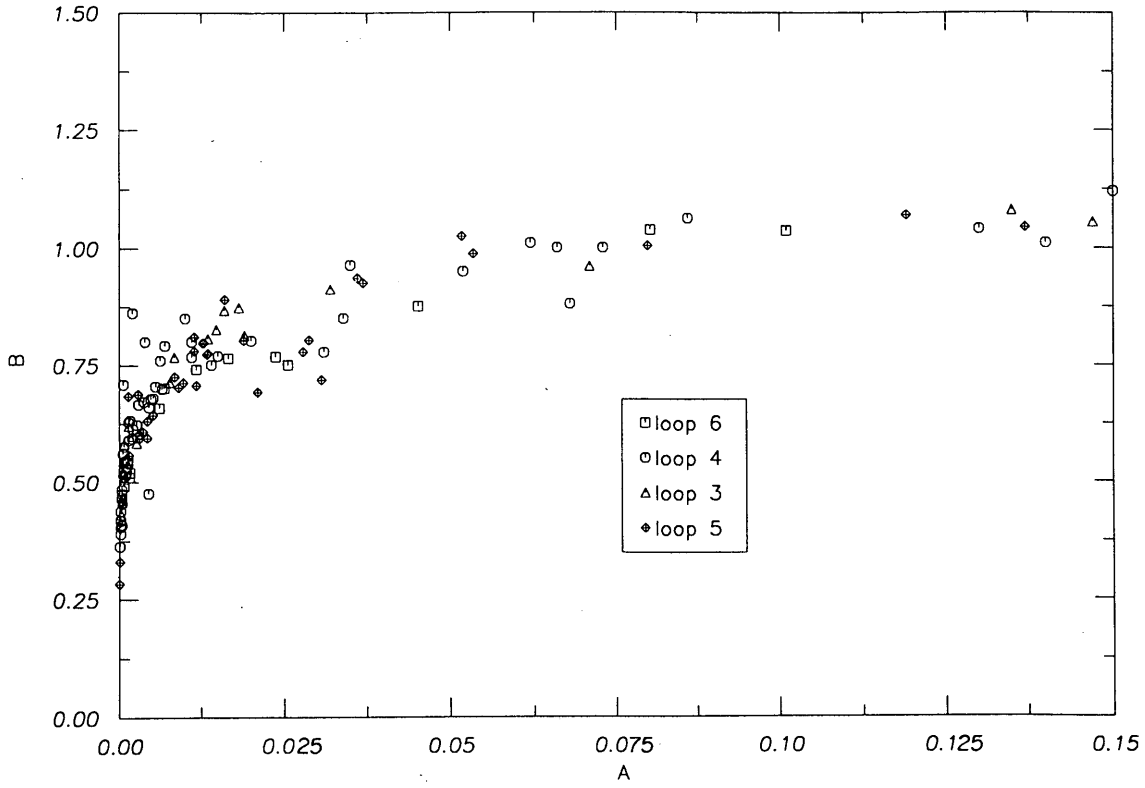

FIGURE 3 *B* versus A for AASHO Loops 3 through 6.

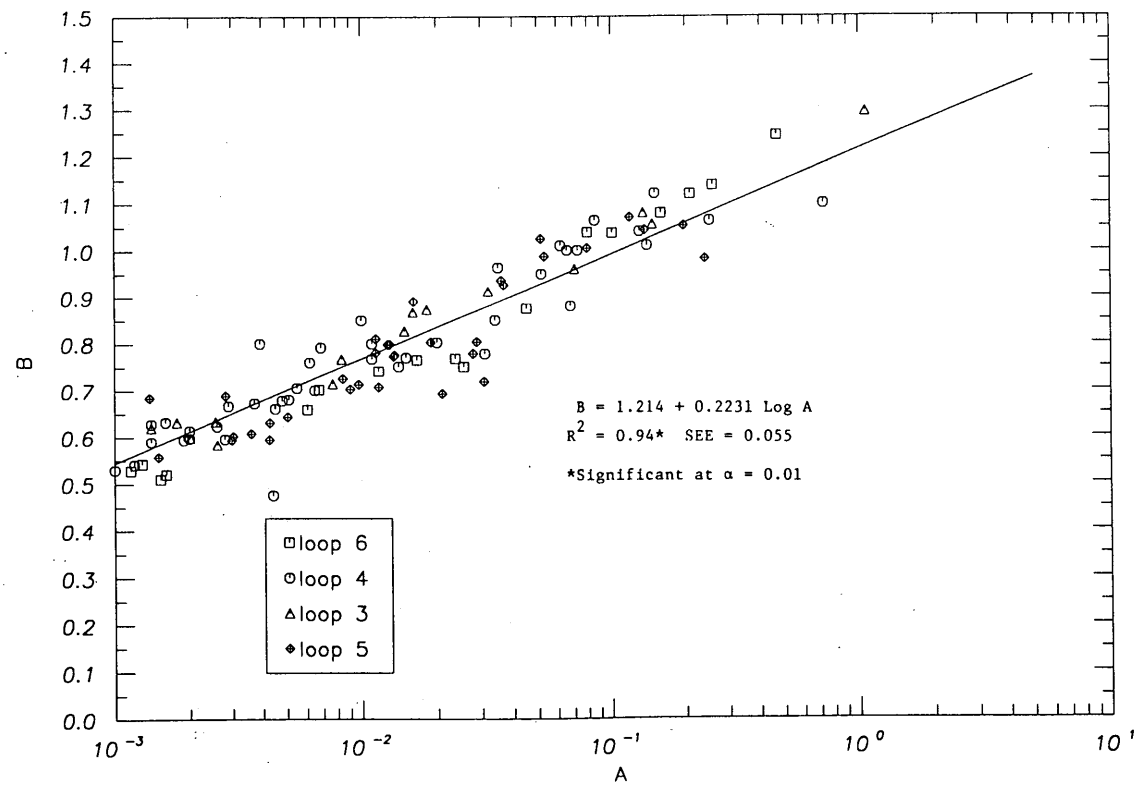

FIGURE 4 *B* versus log A for AASHO Loops 3 through 6.

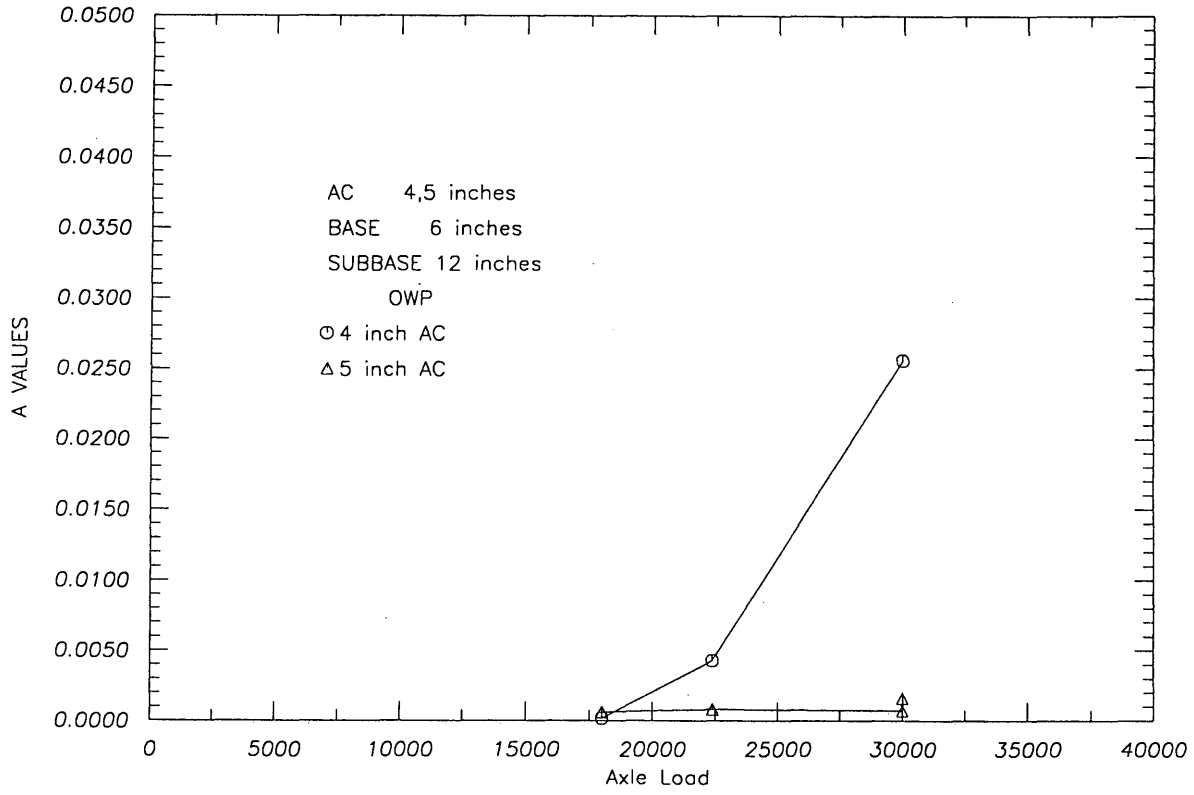

FIGURE 5 A versus axle load.

not considered. Rutting generally does not significantly increase during the winter period since, compared with other seasons, the AC stability is large and the modulus and shear strength of the frozen base/subbase materials and frozen subgrade are very high. It is generally conceded that the stress states calculated for the granular base and subbase layers are not particularly accurate. However, the response factors listed above are indicators of the stress state in the granular layers.

Selected plots of **A** versus subgrade stress ratio, surface deflection, and subgrade strain were examined. The plots (as shown in Figure 6 for the **A**–subgrade stress ratio relation for Loop 4) all indicate threshold type relations. For pavement structural responses less than a certain value, low **A**'s are noted. As the structural response values increase above the threshold value, erratic and inconsistent trends are noted, and the **A** relation is not well defined.

The data base was analyzed using the SPSS statistical package. Simple correlation results indicated that the spring structural responses are the most effective indicators of **A**.

Figure 7 indicates that low **A**'s are typical for spring subgrade stress ratios less than about 0.4. For the Loop 4 data base and subgrade stress ratios < 0.4, the average **A** is 1.08×10^{-3} (standard deviation of 1.29×10^{-3}) and the average B is 0.512 (standard deviation of 0.09).

Stepwise linear regression was used to establish relations between **A** and spring pavement structural reponses for those cases where the subgrade stress ratio was > 0.4. The subgrade stress ratio term was the first and only variable selected. Figures 8 and 9 show **A**–subgrade stress ratio relations and regression equations. Note the large standard errors of estimate associated with the regression equations. The equations are not good predictive equations even though they are statistically significant. Significant ($\alpha = 0.05$) regression equations were also obtained for **A**–surface deflection and **A**–subgrade strain relations, but their associated standard errors of estimate were equal to or greater than those for the **A**–subgrade stress ratio relations.

Figures 10 and 11 are plots (Loop 4 data) of number of load applications to a PSI of 1.5 versus **A**. For those sections that survived the total traffic (1.1×10^6 for Loop 4), the terminal PSI was greater than 1.5. Those sections with large **A**'s did not sustain more than about 100,000 load repetitions before reaching a PSI of 1.5. A plot for the combined data base (Loops 3 through 6) is shown in Figure 11. Similar trends are noted for all of the loops. It is apparent that high levels of early life rut depth development (quantified by large **A**'s) are indicative of reduced functional life as measured by PSI. Note that low **A**'s do not ensure long pavement life. A broad range (70,000 to 1.1×10^6) of load applications to failure was obtained with **A** values less than about 0.01. Other factors such as AC fatigue obviously contributed to the varied pavement performance achieved.

RUTTING RATE ANALYSES OF REHABILITATED AASHO ROAD TEST SECTIONS

The RR model was further evaluated by applying it to rutting data from various flexible pavement sections constructed by

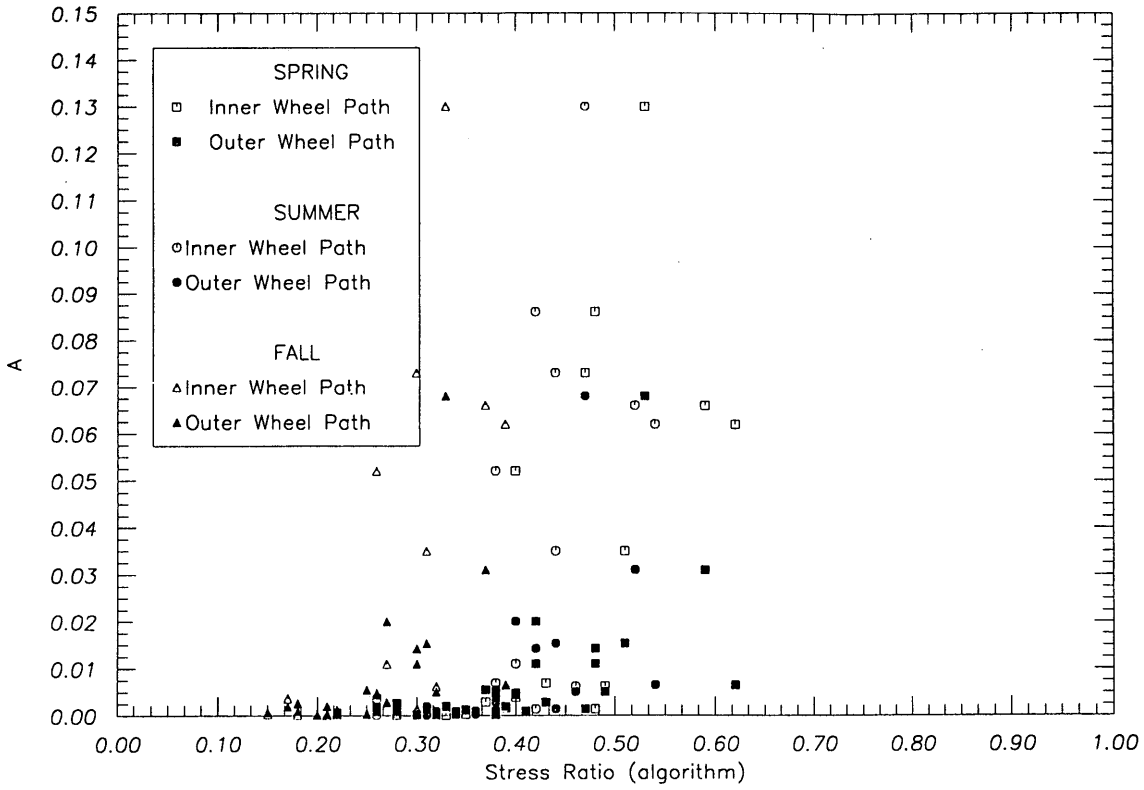

FIGURE 6 A versus subgrade stress ratio for Loop 4.

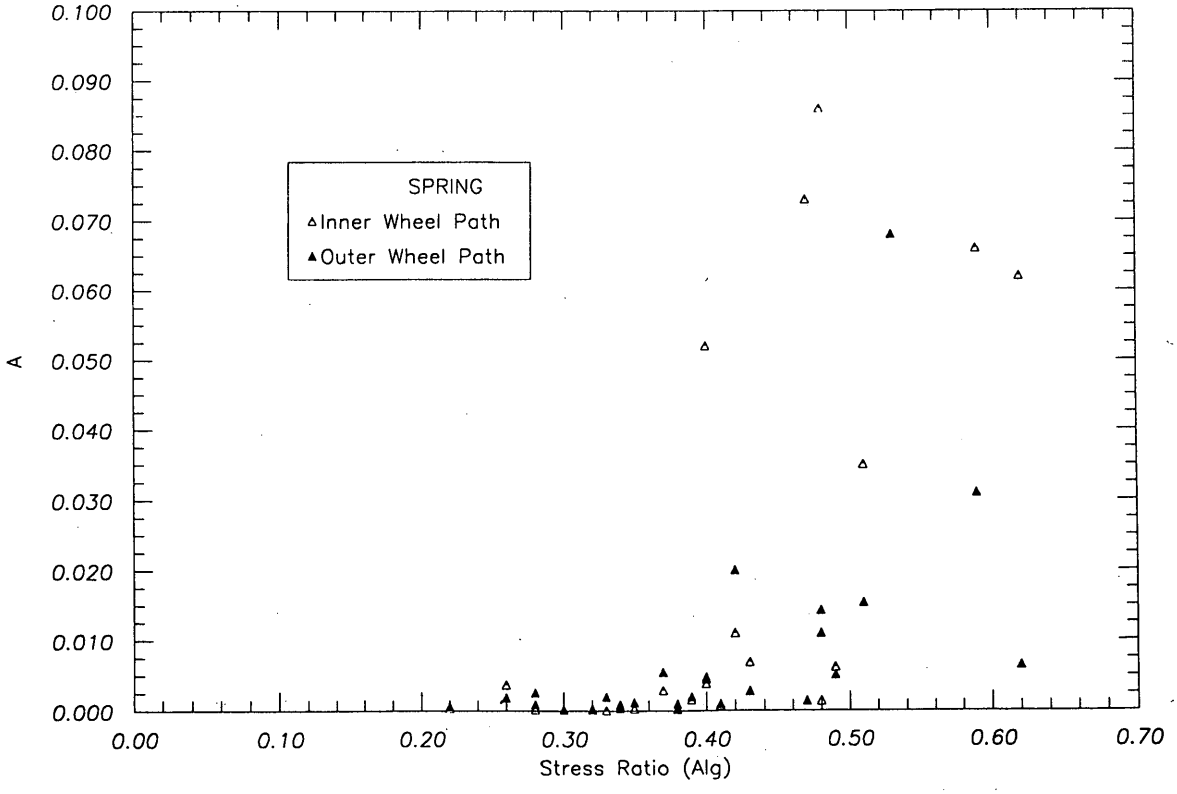

FIGURE 7 A versus spring subgrade stress ratio for Loop 4.

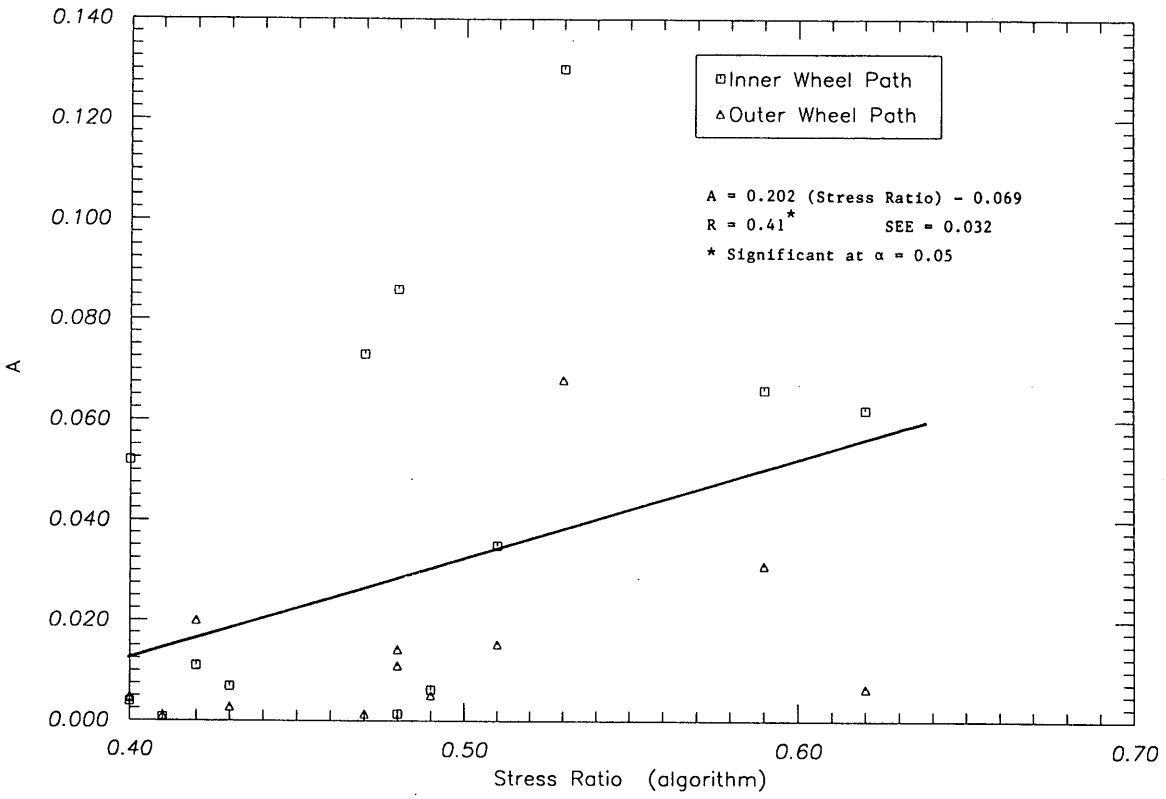

FIGURE 8 A versus spring subgrade stress ratio for stress ratios > 0.4 (Loop 4 data).

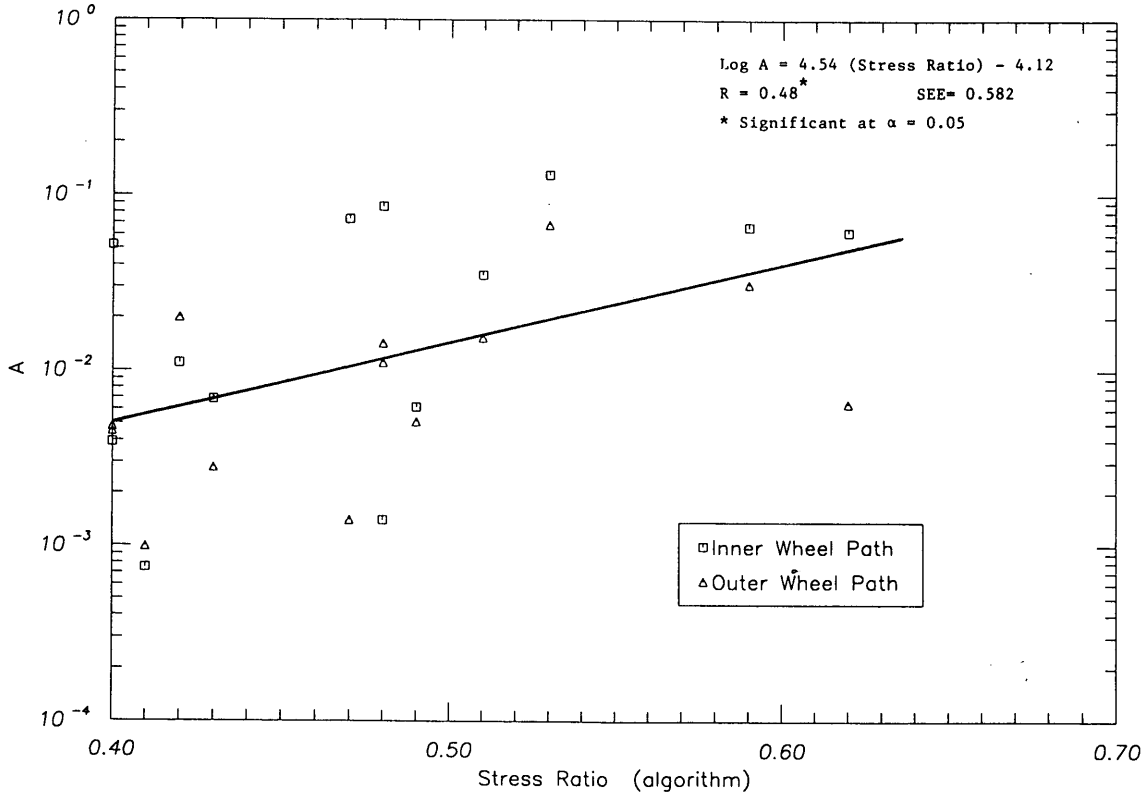

FIGURE 9 Log A versus spring subgrade stress ratio for stress ratios > 0.4 (Loop 4 data).

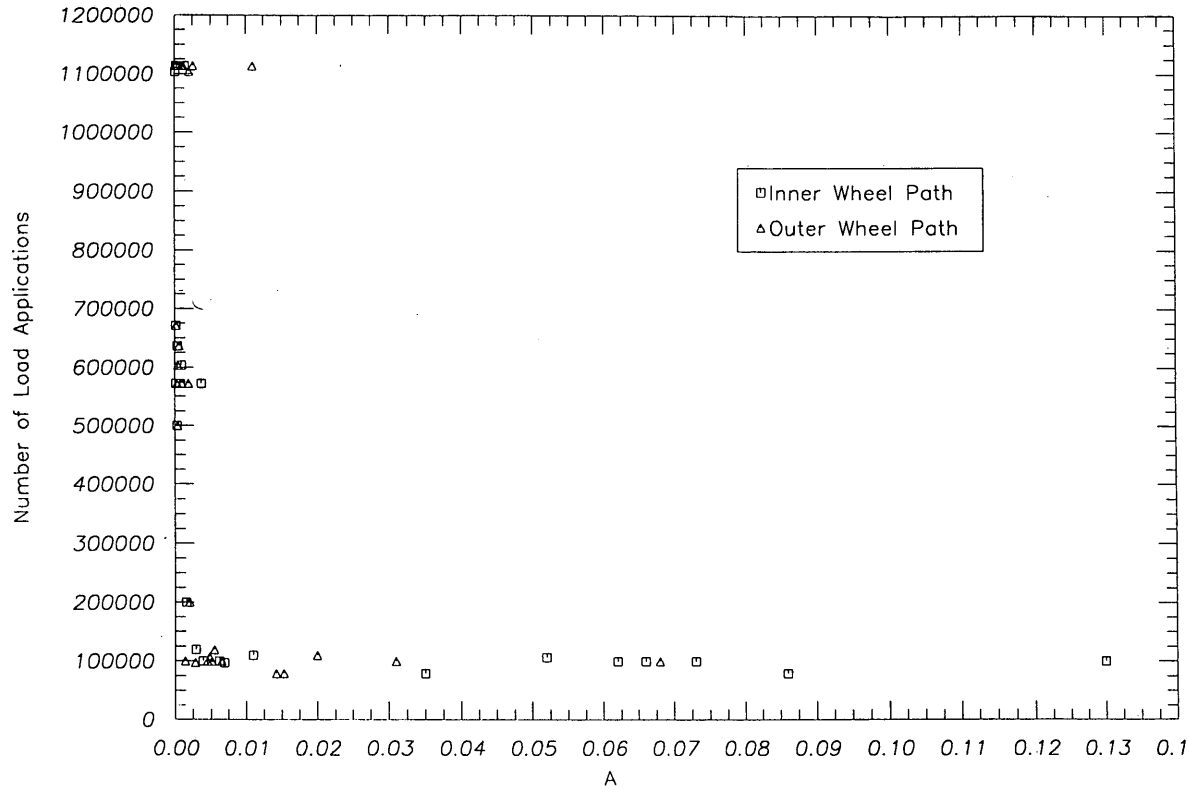

FIGURE 10 Number of load applications to failure (PSI = 1.5) versus A (Loop 4 data).

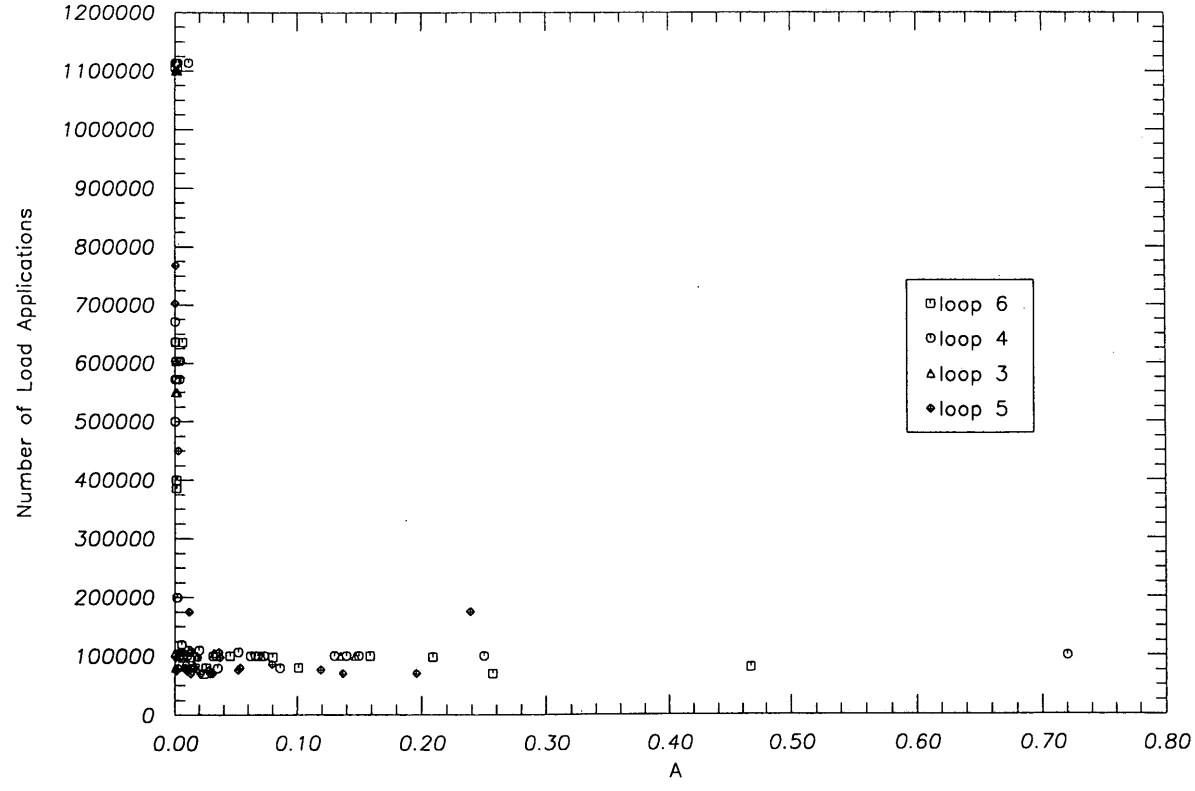

FIGURE 11 Number of load applications to failure (PSI = 1.5) versus A (entire data base).

the Illinois Department of Transportation as part of the AASHO Road Test rehabilitation program. Before incorporating the Road Test tangent sections into current I-80, considerable pavement rehabilitation and reconstruction were required (*15*).

Two new flexible pavement sections were built as duplicates of original flexible pavement designs (Sections 581 and 625) in Loop 4. Section 581 was 5-in. AC surface, 6-in. crushed stone base, and 12-in. sandy gravel subbase. Section 625 was 4-in. AC surface, 6-in. crushed stone base, and 12-in. sandy gravel subbase.

Salvaged crushed stone and sandy gravel subbase from the AASHO pavement sections were used in the reconstruction. The AC surface was a standard (for the 1960 era) Illinois Class I material. A new section of conventional flexible pavement was also constructed. The pavement section was 4.5 in. of Class I AC, 8.5 in. of dense-graded crushed stone base (Illinois Specification Grade 8), and 23 in. of dense-graded gravel subbase (Illinois Grade 7).

Annual pavement condition surveys were conducted by the Illinois Department of Transportation from 1962 to 1974, when the sections were overlaid to correct surface rutting conditions. Mixed traffic data were also collected. Mixed traffic was converted to 18-kip ESALs on the basis of AASHO equivalency factors for a terminal PSI of 2.5.

Rut depth development data for the reconstructed duplicate sections were analyzed using the RR model. Figure 12 shows the rut depth–ESAL relations for the various sections. The data are for the outer wheelpath (OWP). OWP rutting data for the original AASHO sections are also shown for comparison. Rutting rate–ESAL relations are shown in Figure 13. The RR model **A** and *B* parameters are shown in Figures 14 through 16 for the various sections (the regression relations are significant at $\alpha = 0.05$).

The excellent agreement of RR between the performance of the original and reconstructed sections is encouraging. The average *B* value was 0.504 (standard deviation = 0.027), and the average **A** was 4.44×10^{-4} (standard deviation = 3.4×10^{-4}). The **A** term showed more variability since the pavement section (and thus the pavement structural responses) are different. The original AASHO traffic (1.1×10^6 axle loads) was applied over a short period (September 1958 to March 1961) with 18-kip single axles, whereas the reconstructed sections received mixed traffic over a 12-year study period.

SUMMARY

Analyses of relevant portions (rut depth and number of load repetitions) of AASHO Data Base 7322 (*16*) and field performance data from the AASHO Test Site (I-80) rehabilitated and new flexible pavement sections (*15*) demonstrate that the rutting rate concept is valid. The Road Test data show that stable pavement rutting trends were related to estimated pavement structural responses, particularly the subgrade stress

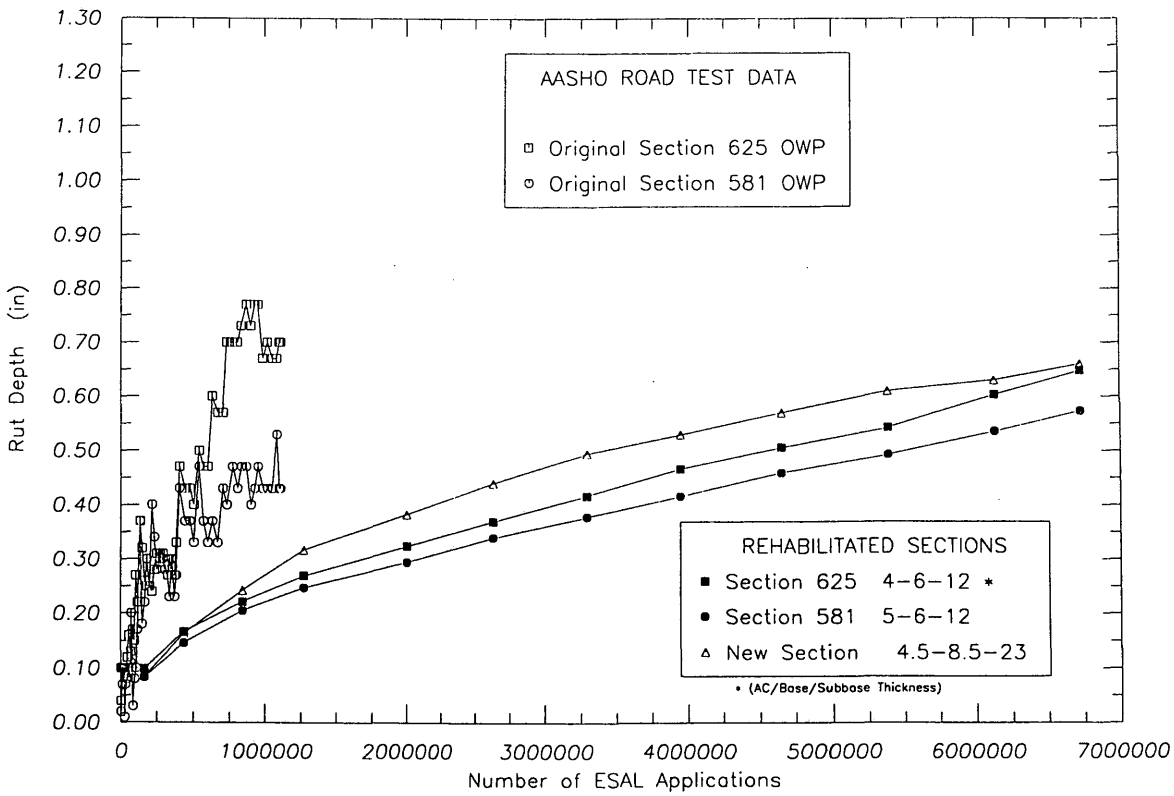

FIGURE 12 Rut depth versus 18-kip ESAL applications for rehabilitated AASHO Road Test.

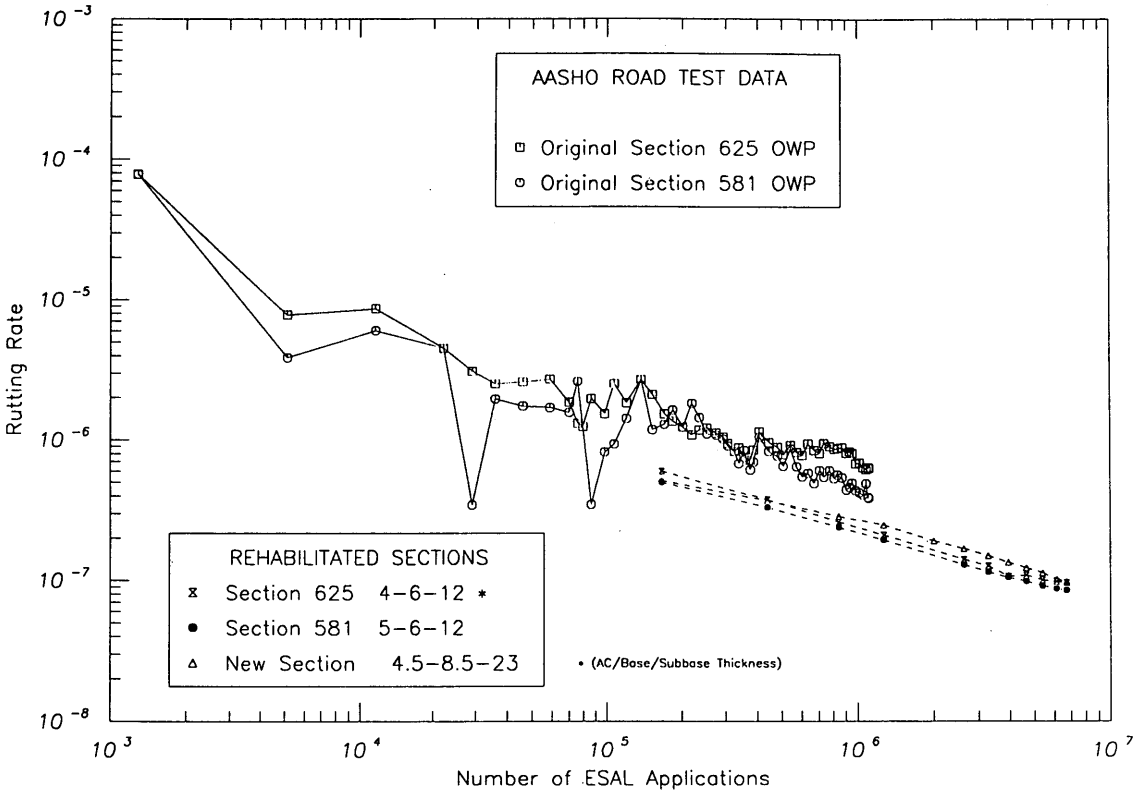

FIGURE 13 Rutting rate versus 18-kip ESAL applications for rehabilitated AASHO Road Test.

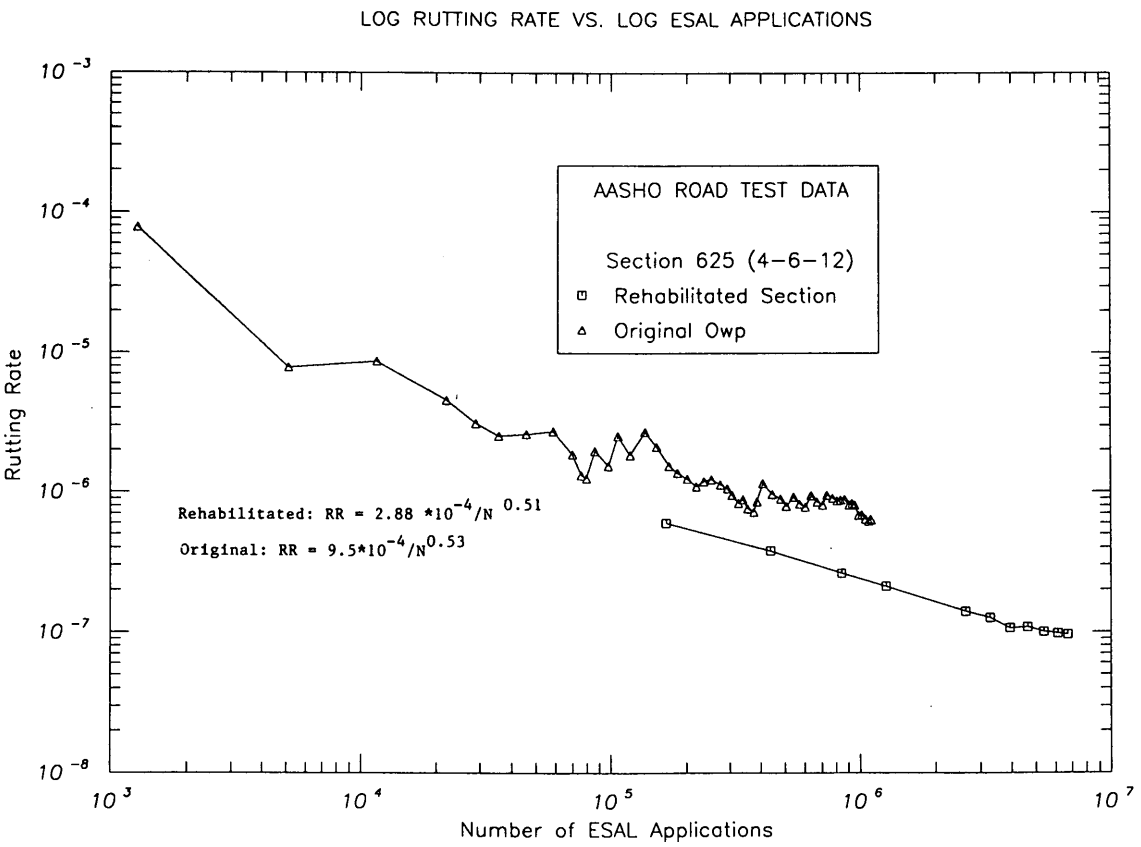

FIGURE 14 Rutting rate versus 18-kip ESAL applications for Section 625.

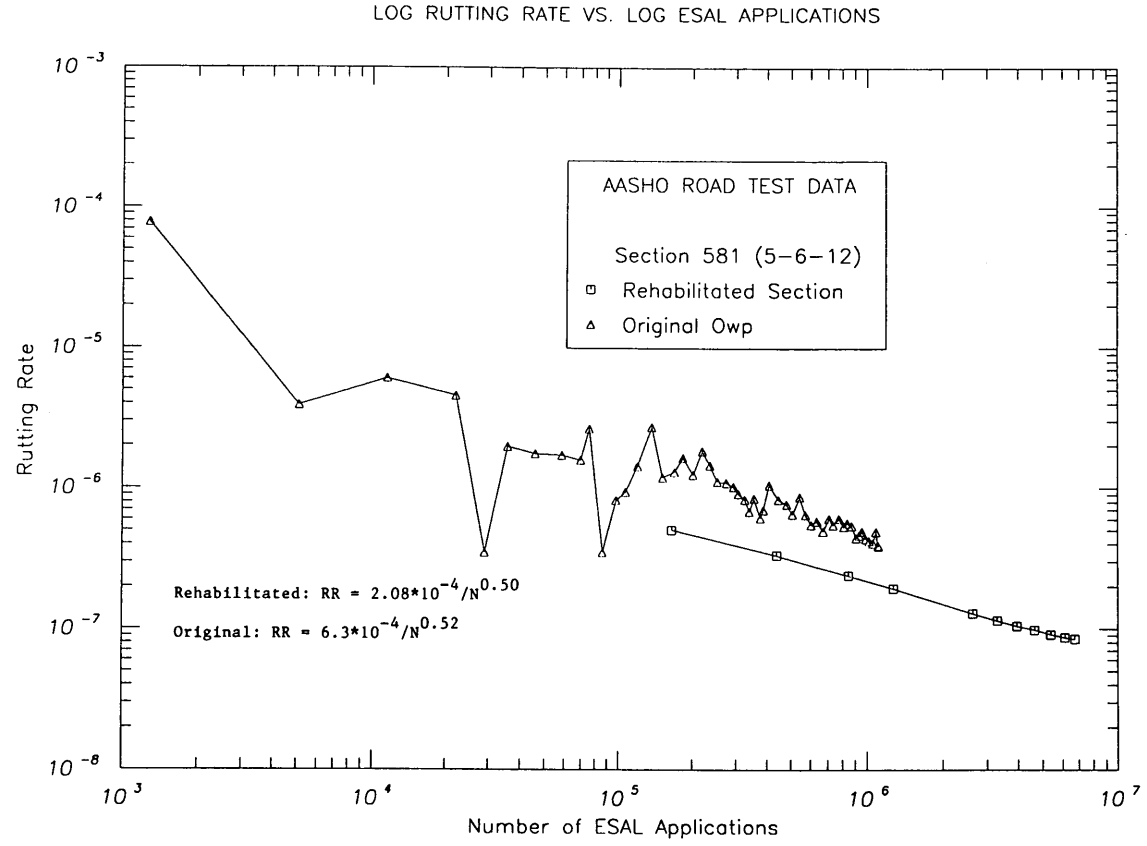

FIGURE 15 Rutting rate versus 18-kip ESAL applications for Section 581.

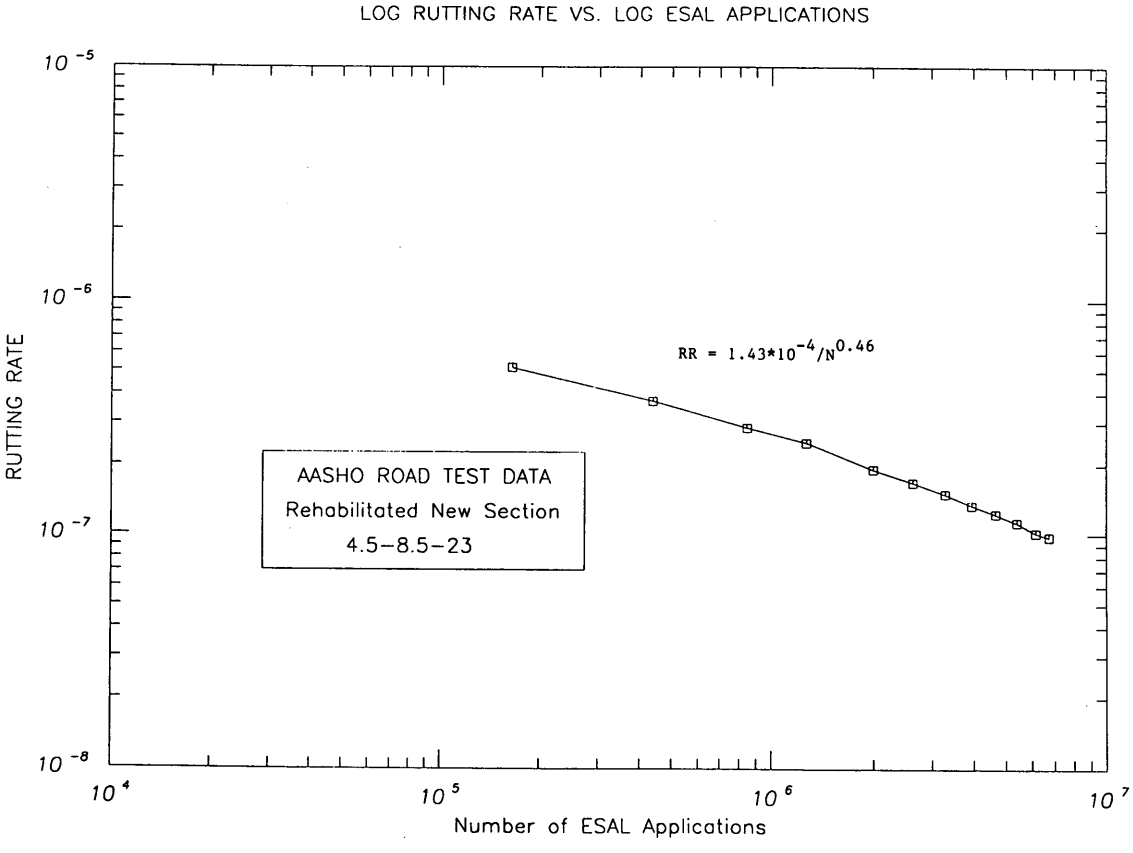

FIGURE 16 Rutting rate versus 18-kip ESAL applications for new section.

ratio. If the SSR was below a threshhold level, low **A**'s were noted. For SSRs > 0.4, a statistically significant trend (but rather inaccurate predictive equation) between SSR and **A** is noted (see Figure 9).

It is particularly encouraging to note the similarity between the rutting rate performance (the *B* values in the RR equation) of the original AASHO sections (AASHO Data Base 7322) and structurally similar sections constructed with AASHO materials (or very similar materials) included in the I-80 rehabilitation.

The RR approach can be effectively used in a priori pavement analysis and design and pavement management system activities. For the typical "generic specification" flexible paving materials used by a highway agency, the *B* terms and relationships relating structural responses to **A** can be established from a flexible pavement performance data base. In a pavement management system, the actual traffic and the development of pavement distresses are monitored. The monitoring data can be used to establish pavement distress/performance trends (i.e., rut depth–ESAL relations). The RR model is particularly helpful in analyzing the pavement rutting data for a specific pavement section and estimating future rutting for pavement management system use. As more rutting data are collected for the section, they can be used to update and refine the RR model and thus improve pavement management system predictions for the development of pavement rutting.

The concepts, principles, and analyses presented in this paper are for the specific materials and soils used in the AASHO Road Test. The approach is considered to be generally applicable to flexible pavement systems. The RR approach is a practical and easily used procedure.

REFERENCES

1. *Calibrated Mechanistic Structural Analysis Procedures for Pavements.* Final Report, Volume II—Appendices. National Cooperative Highway Research Program Project 1-26. TRB, National Research Council, Washington, D.C., March 1990.
2. K. Majidzadeh et al. *Implementation of a Pavement Design System.* Final Report, Research Project EES 579. Ohio State University, Columbus, 1981.
3. K. Majidzadeh, S. Khedr, and H. Guirguis. Laboratory Verification of a Mechanistic Subgrade Rutting Model. In *Transportation Research Record 616*, TRB, National Research Council, Washington, D.C., 1976.
4. K. Majidzadeh, F. Bayomy, and S. Khedr. Rutting Evaluation of Subgrade Soils in Ohio. In *Transportation Research Record 671*, TRB, National Research Council, Washington, D.C., 1978.
5. S. A. Khedr. Deformation Characteristics of Granular Base Course in Flexible Pavements. In *Transportation Research Record 1043*, TRB, National Research Council, Washington, D.C., 1985.
6. R. M. Knutson, M. R. Thompson, T. Mullin, and S. D. Tayabji. *Materials Evaluation Study—Ballast and Foundation Materials Research Program.* FRA-OR&D-77-02. Federal Railroad Administration, 1977.
7. S. A. Khedr. Deformation Mechanism in Asphaltic Concrete. *Journal of Transportation Engineering,* ASCE, Vol. 112, No. 1, Jan. 1986.
8. R. B. Leahy. *Permanent Deformation Characteristics of Asphalt Concrete.* Ph.D. thesis. University of Maryland, 1989.
9. R. B. Leahy and M. W. Witczak. The Influence of Test Conditions and Asphalt Concrete Mix Parameters on Permanent Deformation Coefficients Alpha and Mu. *Journal, Association of Asphalt Paving Technologists,* Vol. 59, 1991.
10. K. Mahboub and D. Little. *An Improved Asphalt Concrete Mix Design Procedure.* Research Report 474-1F. Texas Transportation Institute, College Station, July 1987.
11. K. Mahboub and D. Little. An Improved Asphalt Concrete Mix Design Procedure. *Journal, Association of Asphalt Paving Technologists*, Vol. 59, 1990.
12. K. Mahboub. Asphalt Concrete as Related to Rutting. *Journal of Materials in Civil Engineering,* ASCE, Vol. 2, No. 3, Aug. 1990.
13. M. R. Thompson and R. P. Elliott. ILLI-PAVE Based Response Algorithms for Design of Conventional Flexible Pavements. In *Transportation Research Record 1043,* TRB, National Research Council, Washington, D.C., 1985.
14. R. P. Elliott and M. R. Thompson. *Mechanistic Design Concepts for Conventional Flexible Pavements.* Civil Engineering Studies, Transportation Engineering Series No. 42, University of Illinois at Urbana-Champaign, 1985.
15. R. J. Little and L. J. McKenzie. *Performance of Pavement Test Sections in the Rehabilitated AASHO Road Test.* Physical Research Report 76. Bureau of Materials and Physical Research, Illinois Department of Transportation, 1977.
16. *AASHO Road Test Data Base 7322.* TRB, National Research Council, Washington, D.C.

Heavy-Duty Asphalt Pavements in Pennsylvania: Evaluation for Rutting

PRITHVI S. KANDHAL, STEPHEN A. CROSS, AND E. RAY BROWN

Thirty-four heavy-duty asphalt pavements encompassing poor to excellent rutting performance were evaluated. The objective was to identify the pavement properties (materials, mixture design, construction, and postconstruction) that typify good- and bad-performing pavements. Eleven pavement cores were obtained from each pavement to determine in-place voids in the total mix, mix composition, coarse aggregate fractured face count, fine aggregate particle shape and texture, and recovered asphalt cement properties. The mix from the pavement cores was heated and recompacted using three compactors: gyratory testing machine, rotating base/slanted foot mechanical Marshall compactor, and static base conventional mechanical Marshall compactor. All project data such as job-mix formula, construction data, and traffic data were obtained. Rut depths were measured on each project using a profilograph device. Some 60 independent variables covering the mix design, construction, and postconstruction for each pavement were selected to determine their effect on the rut depth (dependent variable). The extensive data were analyzed using correlation analysis, linear regression analysis methods, and stepwise multiple variable analysis methods. A rutting model was also developed. Recommendations were made to the Pennsylvania Department of Transportation to improve and optimize the resistance of asphalt paving mixtures to rutting for heavy-duty pavements. The main recommendations are (*a*) use at least 75 percent crushed sand in the fine aggregate, (*b*) use 75 blows per side compactive effort using a rotating base/slanted foot Marshall compactor, (*c*) design mix with at least 4.0 percent air voids, and (*d*) improve production quality control to ensure that the mixes "as placed" are reasonably close to the mixes "as designed."

Premature rutting of hot mix asphalt (HMA) pavements has been experienced in several states in the United States in recent years due to increased traffic loads and truck tire pressures. Recent surveys in Illinois and Texas indicate that the tire pressures have increased substantially. Tire pressures averaged 661 kPa (96 psi) and 689 kPa (100 psi) in Illinois and Texas surveys, respectively.

The Pennsylvania Department of Transportation's (PennDOT's) first major asphalt pavement rutting was experienced on I-70 in Washington County during early summer 1986. Additional cases of rutting have occurred since. A special provision for designing the HMA pavements for heavy-duty pavements was developed by PennDOT and implemented in 1987. The salient features contained in the special provisions are use of (*a*) larger size (38-mm or 1½-in.) aggregate in binder and base courses, (*b*) coarse aggregate with at least 85 percent two or more fractured faces, (*c*) at least 75 percent manufactured sand in the fine aggregate, and (*d*) Marshall specimens made with 75 blows on each side. However, there was a need to evaluate several heavy-duty pavements constructed in the past with and without the special provision so that the pavement properties (materials, mixture design, construction, and postconstruction) that typify good and bad pavements could be identified. This will facilitate changes to PennDOT's current material specifications, mix design, and construction procedures to cope with the increased truck loads and tire pressures.

P. S. Kandhal and E. R. Brown, National Center for Asphalt Technology, 211 Ramsay Hall, Auburn University, Ala. 36849-5354. S. A. Cross, Civil Engineering Department, University of Kansas, 2006 Learned Hall, Lawrence, Kans. 66045.

DATA COLLECTION, SAMPLING, AND TESTING PLAN

Thirty-four heavy-duty pavements encompassing poor to excellent rutting performance were identified by PennDOT. All Interstate highways and highways with average daily traffic of more than 20,000 or more than 1,000 daily 8,172-kg (18-kip) equivalent single-axle load (ESAL) applications are defined as heavy-duty pavements.

Data Collection

The following data were collected for all projects:

1. Average climatic conditions;
2. Average daily traffic, percent trucks, and 8,172-kg (18-kip) ESALs per day;
3. Details of underlying pavement structure and overlay;
4. Job-mix formula (JMF) including the Marshall design data; and
5. Construction data such as mix composition, Marshall test data, and field compaction.

These data are contained elsewhere (*1*).

Sampling and Testing Plan

Eleven cores 152.4 mm (6 in.) in diameter were obtained during spring 1989 from a representative 1 lane-mi segment (travel lane) of each project (Figure 1). Five cores (numbered C1 through C5) were obtained at random locations longitudinally from the inside wheel track of this segment. The five

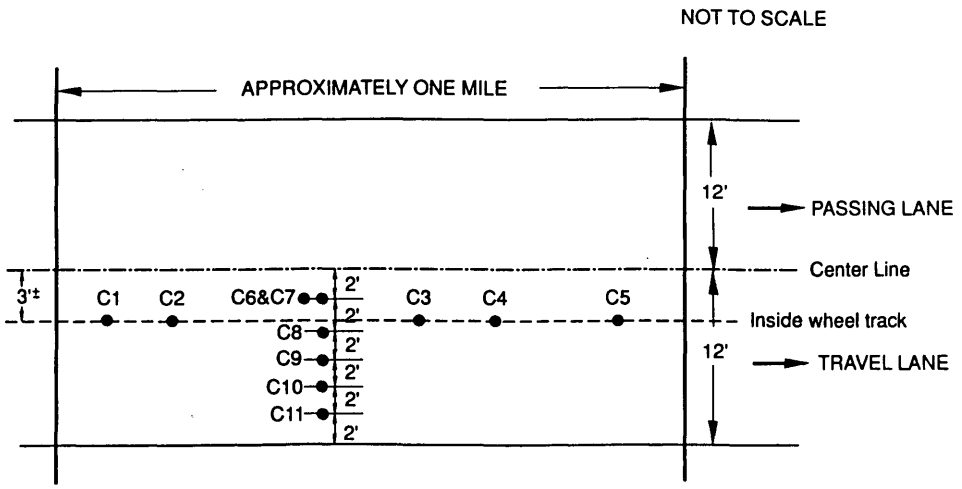

FIGURE 1 Core sampling plan.

cores from each project (total of 170 cores) were tested as follows:

1. Thickness of layers (all cores),
2. Bulk specific gravity (all cores),
3. Theoretical maximum specific gravity,
4. Extraction—asphalt content and gradation (all cores),
5. Coarse aggregate (retained on No. 4 sieve)—fractured face count (one core), and
6. Fine aggregate—particle shape and texture [determined in terms of percent void content using the National Aggregate Association procedure (*1*)].

Five additional cores 152.4 mm (6 in.) in diameter (C7 through C11) were obtained across the pavement, 2 ft center to center, at the worst (maximum rutting) location of the selected segment, as shown in Figure 1. The testing program for these transverse cores is shown in Figure 2. Essentially, the following tests were run:

1. Bulk specific gravity of layers (all cores) to determine in-place voids in the total mix (VTM);
2. Static unconfined creep test (two cores); and
3. Bulk specific gravity, stability, and flow tests on two specimens recompacted by three compaction methods: (*a*) gyratory testing machine (GTM), (*b*) rotating base, slanted foot mechanical Marshall compactor, and (*c*) static base conventional mechanical Marshall compactor.

The thickness of all layers in Cores C7 through C11 was accurately measured before sawing the layers and used to obtain the profiles of the underlying layers once the surface profile was established. One core (C6) was taken beside Core C7 as shown in Figure 1. Aged asphalt cement was recovered by the Abson method from this core and tested for penetration at 25°C (77°F) and viscosity at 60°C (140°F).

Measurements of Rut Depth

A transverse surface profile of the lane adjacent to Cores C7–C11 (Figure 1) was obtained using a profilograph device. Cores taken transversely across the pavement were used to help determine the amount of rutting in the top layer and the

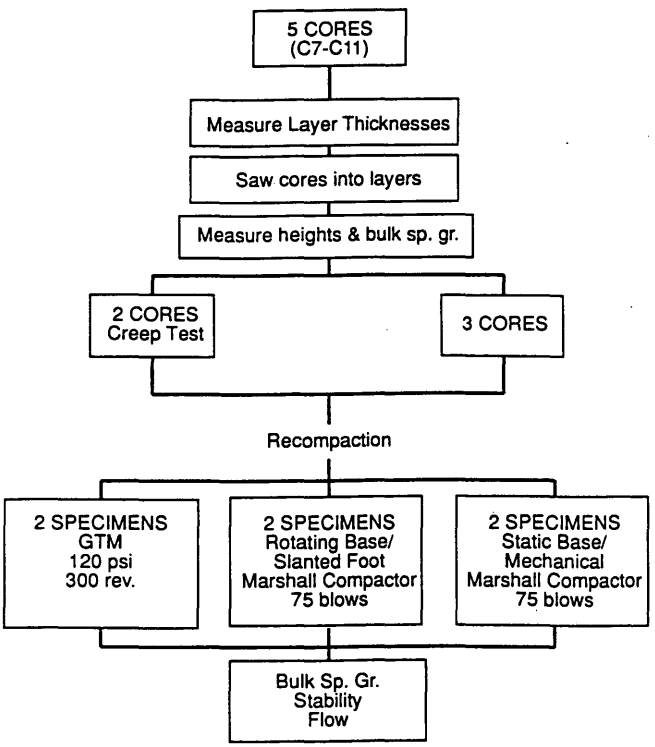

FIGURE 2 Flowchart for testing cores C7 through C11.

underlying layers. This was done by drawing a profile of the layers using the core layer thicknesses. The amount of rutting was determined for the top layer by subtracting the rut depth in the second layer from the rut depth at the surface. The rut depth in the second layer was determined by subtracting the rut depth in the third layer from the rut depth in the second layer.

PROJECT DETAILS AND TEST DATA

Project Location Details

It was planned to evaluate 35 sites. However, Site 21 was deleted by PennDOT, and there are no data for that site. The

locations of the 34 project sites scattered across Pennsylvania are given elsewhere (*1*). The pavement condition rating was subjectively determined for each pavement as follows:

Maximum Rut Depth (in.)	*Age of Overlay (years)*	*Rating*
0–⅛	—	Excellent
⅛–¼	>3	Excellent
⅛–¼	≤3	Good
¼–⅜	>3	Good
¼–⅜	≤3	Fair
⅜–¾	>3	Fair
⅜–¾	≤3	Poor
>¾	—	Poor

The subjective rating proved to be fairly reasonable on subsequent rut depth/traffic load data analyses, which will be discussed later. Only 4 of the 34 projects did not have concrete pavements underneath the HMA overlay. The age of the HMA overlays as of 1990 summer ranged from 2 to 19 years. On the basis of the subjective rating of the 34 projects, 10 were excellent, 9 were good, 12 were fair, and 3 were poor.

Traffic and Climatological Data

Detailed traffic and climatological data for the projects are given elsewhere (*1*). The average daily traffic ranged from 5,925 to 41,000 vehicles per day, and the ESALs ranged from 440 to 9,288 per day. The total estimated traffic carried by the pavements in this study ranged from less than 1 million ESALs to more than 30 million ESALs. The average yearly temperature ranged from 8.6°C (47.6°F) to 12°C (53.7°F), which is a very narrow range.

Mix Design Data

Detailed mix design data obtained from the JMF of the wearing course (Layer 1) and the binder course (Layer 2) are given elsewhere (*1*). The data include asphalt content, gradation, mix design compactive effort, specimen specific gravity, theoretical maximum specific gravity, VTM, voids in the mineral aggregate (VMA), percent voids filled with asphalt (VFA), Marshall stability, and flow. An ID-2W mix (a dense-graded wearing course mix with 12.5-mm or ½-in. top size) was used in Layer 1 of most projects. Similarly, an ID-2 B (a dense-graded binder course mix with 25.4-mm or 1-in. top size) was used in Layer 2 of most projects. The average mix design data for the mixtures for Layers 1 and 2 are given in Table 1.

All mixes were designed using the Marshall method. The number of blows per face used for the Layer 1 mixtures was 50 for 24 projects, 65 for 3 projects (Pennsylvania Turnpike), and 75 for 7 projects. The number of blows per face for the Layer 2 mixtures was 50 for 21 projects and 75 for 7 projects, with no data being available for 6 projects. The average VTM of the Layer 1 mixtures is below the midpoint of the 3 to 5 percent range generally recommended for the mix design. The average VTM is less than 4.0 percent for the Layer 2 mixtures. Only 7 of the 34 projects had design VTM equal to or greater than 4.0 percent. The Layer 1 design stability values are generally very high, and the flow values are within the acceptable range of 6 to 16. The average Layer 2 design stability value is 2,318 lb. Although satisfactory, this is lower than that of the wearing courses. The average flow value is slightly higher than the wearing courses.

TABLE 1 Average Mix Design Data

	Layer 1		Layer 2	
	Average	Range	Average	Range
Asphalt Content	6.2	5.0 to 8.75	4.7	4.0 to 5.2
VTM or Air Voids, %	3.6	2.8 to 4.5	3.7	2.6 to 4.4
VMA, %	16.6	14.5 to 22.4	13.6	12.2 to 14.3
VFA, %	78.5	73.9 to 83.9	72.7	67.2 to 79.0
Stability, lbs.	2514	2019 to 3666	2318	1477 to 3100
Flow, 0.01 inches	10.9	8 to 15	11.6	9 to 14
Passing No. 8	42.6	35 to 50	28.3	19 to 30
Passing No. 200	4.6	3.0 to 6.0	4.3	2.5 to 5.0

Construction Data

Detailed project construction data on VTM, asphalt content, and the material passing 12.5-mm (½-in.), 2.36 (No. 8), and 75-μm (No. 200) sieves are given elsewhere (*1*). The statistical analysis of VTM data obtained at the time of construction in HMA pavement is as follows.

	Wearing Course	*Binder Course*
Number of projects	29	19
Mean VTM	5.79	4.75
Standard deviation (VTM)	1.01	1.32
95 percent confidence limits	3.8–7.8	2.1–7.4

The data indicate that the level of compaction in both layers was generally acceptable. Lower voids (about 1 percent) were achieved in the binder course than in the wearing course.

Longitudinal Core (C1–C5) Test Data

Mix Composition

The detailed test data are given elsewhere (*1*). Mix composition was determined by extracting core samples. Generally the asphalt content measured from the cores was deficient from the JMF asphalt content for both wearing and binder courses. The percentage of material passing the 2.36-mm (No. 8) sieve was also generally higher than the JMF values for both wearing and binder courses. As expected, these values are higher than those obtained on loose mixes at the time of construction because some degradation takes place under rolling, under subsequent traffic, and from coring and sawing operations. The percentage of minus 75 μm (No. 200) was also significantly higher than the JMF values for both courses.

VTM

The statistical analysis of VTM data obtained by testing cores C1 through C5 is as follows.

	Wearing Course	*Binder Course*
Number of projects	34	27
Mean VTM	3.17	3.02
Standard deviation (VTM)	1.54	1.38
95 percent confidence limits	0.0–7.4	0.3–5.9

The average VTM values in both courses are very low. According to past experience, HMA pavements approach the

potential for rutting when the VTM is approximately 3 percent or less. Since these are average values, obviously there are many projects that have VTM less than 3 percent. The average mix design VTM values were 3.6 and 3.7 percent, respectively, for wearing and binder courses as reported earlier. Further examination of VTM data obtained on projects in service for 3 or more years (at the time of coring in 1989) indicates even lower values. The older projects have average VTM values of 2.61 and 2.85 percent, respectively, for wearing and binder courses. Thus, the VTM data indicate that the Pennsylvania HMA mixtures are compacted by traffic generally to a higher degree than by laboratory compaction. Therefore, the laboratory compaction effort needs to be increased.

Recovered Aggregate Properties

The summary of the recovered aggregate properties is as follows:

	Wearing		*Binder*	
	Average	*Range*	*Average*	*Range*
Coarse aggregate (%)	48	32–57	68	53–78
Crushed faces (%)	93	66–100	100	100
Fine aggregate (%)	52	43–68	32	22–47
Natural sand (%)	24	0–100	23	0–100

Transverse Core (C7–C11) Test Data

The following observations were made on the basis of the statistical analysis of the detailed data obtained from Cores C7–C11 and reported elsewhere (*1*).

1. Average VTM values of 3.75 and 3.83 percent, respectively, were obtained for wearing and binder courses. The average VTM values are higher than those obtained from cores C1 through C5 sampled longitudinally. This can be attributed to the location of cores—cores C1 through C5 were obtained in the inside wheel track (where most densification occurs), whereas cores C7 through C11 were obtained transversely across the pavement, including areas other than wheel tracks. Cores C7 through C11 were taken at a location where the most rutting had occurred. Previous work at NCAT (*2*) showed that rutting was related to low air voids. However, the low void content did not always occur exactly in the wheel paths. As a result the 20th percentile air void content (80 percent higher and 20 percent lower) from voids obtained across the pavement lane were used in correlations with rutting. The results indicated that the use of the 20th percentile air void content was reasonable when compared with the use of the average or minimum air void content.

The average 20th percentile VTM values are 3.01 and 3.10 percent for wearing and binder courses, respectively, and are very close to the average values obtained from cores C1 through C5. As discussed earlier in the case of test data from cores C1 through C5, these values of VTM are considered low and will increase the potential for rutting.

2. The average percentages of VTM obtained in recompacted specimens are as follows:

	Average VTM in Recompacted Specimens	
Compactor	*Wearing Course*	*Binder Course*
Gyratory	2.44	2.00
Marshall Rotating Base	1.74	1.96
Marshall Static Base	2.04	2.46

The Marshall compactor with rotating base and slanted foot gave the highest density (least VTM) for both wearing and binder courses and thus can be used to obtain near maximum potential compaction of mixes, which is likely to be achieved under 2 to 3 years' traffic. Surprisingly, the gyratory compactor gave the least density (lower than the conventional Marshall method using static base) for the wearing course. However, the gyratory compactor provided samples with higher density than the conventional static base mechanical Marshall compactor in the case of binder course mixes containing larger aggregates (25 to 38 mm or 1 to 1½ in. maximum size). This indicates that the gyratory compaction is more effective in densifying the mix when the maximum aggregate size is increased. On the basis of the preceding data it appears that the mechanical Marshall compactor with rotating base and slanted foot should be used for both wearing and binder course mixes to minimize the potential of overasphalting mixes designed for heavy-duty pavements and high-pressure truck tires.

3. Average gyratory shear index (GSI) values were 1.35 and 1.26 for wearing and binder courses, respectively. Whereas a value of 1.00 is considered ideal to prevent rutting, values up to 1.20 may be acceptable. Therefore, both average values are on the high side and indicate a high potential for rutting.

4. Average 60-min permanent deformation values (static unconfined creep test at 40°C or 104°F) for wearing and binder courses were observed to be close: 11.90×10^{-4} and 11.27×10^{-4} in./in., respectively. No reliable deformation threshold values are available in the literature. A stress level of 103.5 kPa (15 psi) was used in the creep test. The static unconfined creep test as used in this study did not indicate the potential for rutting.

Rut Measurement Data

Maximum surface rut depth at the worst location of all projects ranged from 1.0 mm (0.04 in.) to 40 mm (1.66 in.), averaging 10.9 mm (0.43 in.). The average rut depth in the wearing course is 2.5 mm (0.10 in.) greater than in the binder. On most projects, the thicknesses of wearing course and binder course were 38 mm (1.5 in.) and 51 mm (2 in.), respectively. There are several projects where the underlying layers contributed significantly to the total surface rut depth. The 15 poor to fair projects can grouped into three general categories as shown below. It appears that in a majority of cases the underlying layers (including the binder course) contributed to the surface rut depth.

Type	*No. of Project*
1. Projects in which the underlying layers contributed significantly (in addition to the wearing course) toward the total surface rut depth.	10
2. Projects in which the underlying layers were primarily responsible for the total surface rut depth.	2
3. Projects in which most rutting was contributed by the wearing course only.	3

STATISTICAL ANALYSIS OF DATA AND DISCUSSION OF RESULTS

Independent Variables

Five broad categories of 60 independent variables covering the mix design, construction, and postconstruction data for each pavement were selected to determine the effect these variables might have on rutting. The 60 variables are listed elsewhere (*1*). The data were analyzed using correlation analysis, linear regression analysis methods, and stepwise multiple variable analysis methods. The objective was to identify the independent variables that significantly affect rutting and to establish their threshold values, if possible. Rutting is a complex phenomenon. It is doubtful that any single independent variable could predict rutting reliably. In addition, within each layer one bad property (for example, excessive asphalt content) can nullify other good properties (such as 0 percent natural sand and 100 percent fractured face count). There are also numerous interactions between the properties. Therefore, very low correlation coefficients were obtained when only one independent variable at a time was examined (*1*).

The stepwise multiple variable analysis method appeared more promising in obtaining a reasonable correlation to the dependent variable. Two stepwise procedures were used to analyze the groups of independent variables. The dependent variable used is the average surface rut depth in inches divided by the square root of total traffic, as discussed later.

The two stepwise procedures used were the forward and backward methods. In the forward selection procedure, the single variable that is most correlated to the dependent variable in a step is added to the multiple regression equation until no variables remain that, when added to the model, reduce the deviations sum of squares at a 0.5 significance level. In the backward procedure, the single variable that is least correlated to the dependent variable in a step is deleted from the multiple regression equation. The procedure stops when all variables remaining in the model are significant at the 0.1 level. Only the data from the forward selection method will be discussed in this paper.

Dependent Variables

The dependent variable selected for analysis was rut depth. It is well established that traffic affects rutting in pavements. The total estimated traffic experienced by the pavements in this study ranged from less than 1 million ESALs to more than 30 million ESALs. By dividing the rut depth by some function of traffic, the pavements could be normalized to a rate of rutting that would allow, for example, two pavements with 12.7-mm (½-in.) ruts of differing age to be compared on the basis of this rate of rutting. The initial densification for a rutted pavement follows a direct relationship with traffic. However, after initial densification the rate of rutting decreases with an increase in traffic until a condition of plastic flow occurs and the rate of rutting again increases. Previous work by Brown and Cross (*2*) and Parker and Brown (*3*) has shown that expressing the rate of rutting as a function of the square root of total traffic better models pavement behavior when compared with other expressions for the rate of rutting.

Figure 3 is a histogram showing all sites with increasing rate of rutting. The sites have been labeled E (excellent), G (good), F (fair), or P (poor) on the basis of the subjective performance rating discussed earlier. A value of 0.00020 for rut depth in inches divided by the square root of ESALs generally divides E and G sites from F and P sites. Therefore, the value 0.0002 can reasonably be considered as a threshold above which

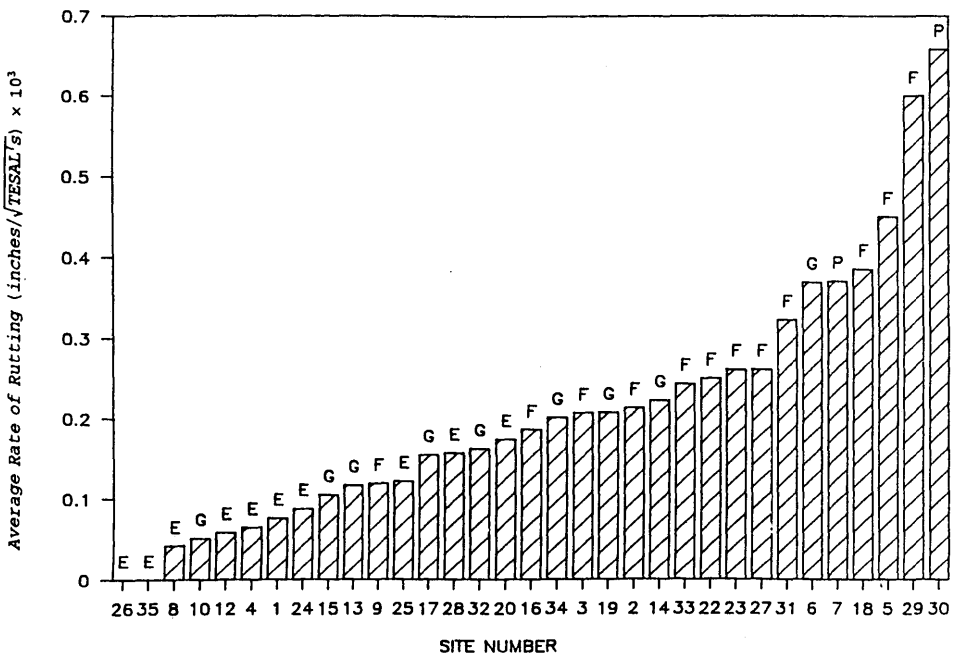

FIGURE 3 Pavement rutting and rate of rutting.

pavements are expected to develop undesirable amounts of rutting. This value also agrees with similar values established by Parker and Brown for Alabama highways (*3*).

Statistical Analysis

Mix Design Variables

The 10 mix design variables investigated included the mix composition (asphalt content and gradation) and Marshall mix design parameters such as VTM, VMA, number of blows per side, stability, flow, stability/flow, and Metcalf's bearing capacity calculated from stability and flow values (*4*). The results of the correlation analysis for the 10 mix design variables are given elsewhere (*1*). Generally, poor correlations were obtained. This is probably due to the difference between the mix "as designed" and the mix "as placed" in terms of both mix composition and compacted density. The in-place unit weights after traffic exceed the mix design unit weight, which indicates that the mix design compactive effort is inadequate. This could account for the poor correlations between mix design variables and rutting. Because of the change in mix composition, the recompacted mix properties were investigated to determine trends.

Table 2 gives the significant independent variables obtained from stepwise regression analysis using the forward selection procedure. However, the R-square values are considered low because of the difference between the mix "as designed" and the mix "as placed."

Construction Variables

These variables included data obtained at the time of construction such as mix composition (asphalt content and gradation) and VTM in as-constructed mat. According to stepwise regression analysis (Table 3), the percentages passing the 2.36-mm (No. 8) and 75-μm (No. 200) sieves, VTM, and the asphalt content (binder mix only) were selected as significant independent variables, although the R-square values are low.

Postconstruction Longitudinal Variables (Cores C1–C6)

The percentages of material passing the 2.36-mm (No. 8) and 75-μm (No. 200) sieves, the percentage of crushed particles in the coarse aggregate, the percentage of natural sand, average VTM, and the asphalt content were selected as the most significant independent variables (Table 4). There is a significant improvement in R-square values compared with those in mix design and construction variables.

TABLE 2 Summary of Stepwise Regression Analysis for Mix Design Variables

Step	Variable Entered	Number In	Partial R-square	Model R-square
Wearing Mix (All Variables R-square = 0.33)				
1	Passing #8	1	0.2445	0.2445
2	# Blows	2	0.0280	0.2725
3	Stability	3	0.0190	0.2915
4	Flow	4	0.0124	0.3040
Binder Mix (All Variables R-square = 0.43)				
1	Flow	1	0.1382	0.1382
2	Passing #200	2	0.0469	0.1852
3	VMA	3	0.0666	0.2517
4	Passing #8	4	0.0792	0.3308
5	% Asphalt Cement	5	0.0726	0.4035

TABLE 3 Summary of Stepwise Regression Analysis for Construction Variables

Step	Variable Entered	Number In	Partial R-square	Model R-square
Wearing Mix (All Variables R-square = 0.34)				
1	Passing #8	1	0.2787	0.2787
2	Passing #200	2	0.0385	0.3172
3	VTM	3	0.0272	0.3444
Binder Mix (All Variables R-square = 0.47)				
1	Passing #8	1	0.1895	0.1895
2	VTM	2	0.0788	0.2684
3	Passing #200	3	0.1678	0.4362
4	% AC	4	0.0346	0.4708

Postconstruction Transverse and Longitudinal Variables

The transverse variables (C7–C11 core test results) and the longitudinal variables (C1–C6 core test results) were combined to create a new data set. The new data set included the variables that could be performed during mix production quality control to determine whether a quality control test program using recompacted samples of the produced mix could predict rutting. The variables were divided into three groups for analysis on the basis of the recompactive method used. The three groups included GTM recompaction, static base Marshall recompaction, and rotating base Marshall recompaction. The variables selected were asphalt content, average in-place VTM, percent passing the 2.36-mm (No. 8) and 75-μm (No. 200) sieves, recovered asphalt penetration and viscosity, percent crushed particles, percent natural sand in the fine aggregate, creep, and the recompacted properties of stability, flow, stability/flow ratio, bearing capacity, VTM, and VMA. The stepwise regression analysis results using the three recompactive methods are similar (*1*). Table 5 gives the significant independent variables when the rotating base Marshall compactor was used for recompaction.

TABLE 4 Summary of Stepwise Regression Analysis for Postconstruction Longitudinal Variables

Step	Variable Entered	Number In	Partial R-square	Model R-square
Wearing Mix (All Variables R-square = 0.55)				
1	Passing #8	1	0.4373	0.4373
2	Passing #200	2	0.0341	0.4714
3	Crushed Particles	3	0.0206	0.4920
4	% Natural Sand	4	0.0122	0.5042
5	Average VTM	5	0.0161	0.5203
6	%AC	6	0.0189	0.5392
Binder Mix (All Variables R-square = 0.64)				
1	% AC	1	0.2435	0.2435
2	Passing #8	2	0.0873	0.3308
3	Crushed Particles	3	0.0811	0.4119
4	Average VTM	4	0.0857	0.4976
5	Viscosity	5	0.1008	0.5985
6	Passing #200	6	0.0369	0.6354

TABLE 5 Summary of Stepwise Regression Analysis for Rotating Base Recompacted Variables

Step	Variable Entered	Number In	Partial R-square	Model R-square
Wearing Mix (All Variables R-square = 0.73)				
1	Passing #8	1	0.4393	0.4393
2	Stability	2	0.1333	0.5726
3	Rotating VMA	3	0.0544	0.6270
4	Average VTM	4	0.0649	0.6919
5	% Natural Sand	5	0.0144	0.7063
6	Rotating VTM	6	0.0087	0.7151
Binder Mix (All Variables R-square = 0.93)				
1	Rotating VTM	1	0.3970	0.3970
2	Viscosity	2	0.1794	0.5764
3	Passing #8	3	0.0553	0.6317
4	Crushed Particles	4	0.0448	0.6765
5	Average VTM	5	0.0424	0.7189
6	Rotating VMA	6	0.0473	0.7662
7	Creep	7	0.0343	0.8005
8	Stability	8	0.0380	0.8385
9	Stability/Flow	9	0.0617	0.9002
10	Penetration	10	0.0160	0.9162
11	% Natural Sand	11	0.0130	0.9292

Rutting Model

The preceding analyses indicate that many variables contribute to rutting and that no one variable adequately predicts rut depths. Many of the variables used, such as recovered penetration and viscosity, contribute to rutting. However, they cannot be controlled or predicted during design and construction. A meaningful model to predict rutting would contain variables that both significantly contribute to the model and can be controlled during design and construction. Eight variables were selected to represent mix properties that are controllable during design and construction. The mix design variables were not used because they were not representative of the mix "as placed." These eight variables are the 20th percentile VTM from cores C7–C11 to represent the mix design VTM; the VMA calculated from recompacted samples to represent mix design VMA; the percent passing the 12.5-mm (½-in.), 2.36-mm (No. 8), and 75-μm (No. 200) sieves and the percent crushed faces from the in-place cores (C1–C5); the recompacted flow to represent the mix design flow; and the recompacted mix stability. Two models for each mix type, wearing and binder, were developed for each of the three compaction methods (*1*). Only the rotating base Marshall model will be discussed here.

Rotating Base Marshall Model

The eight selected variables for predicting rutting have an R-square of 0.38 for the wearing mix and 0.49 for the binder mix. The stepwise procedure selected all variables as significant except recompacted flow for the wearing mix with an R-square of 0.37. The model is shown in Figure 4. For the

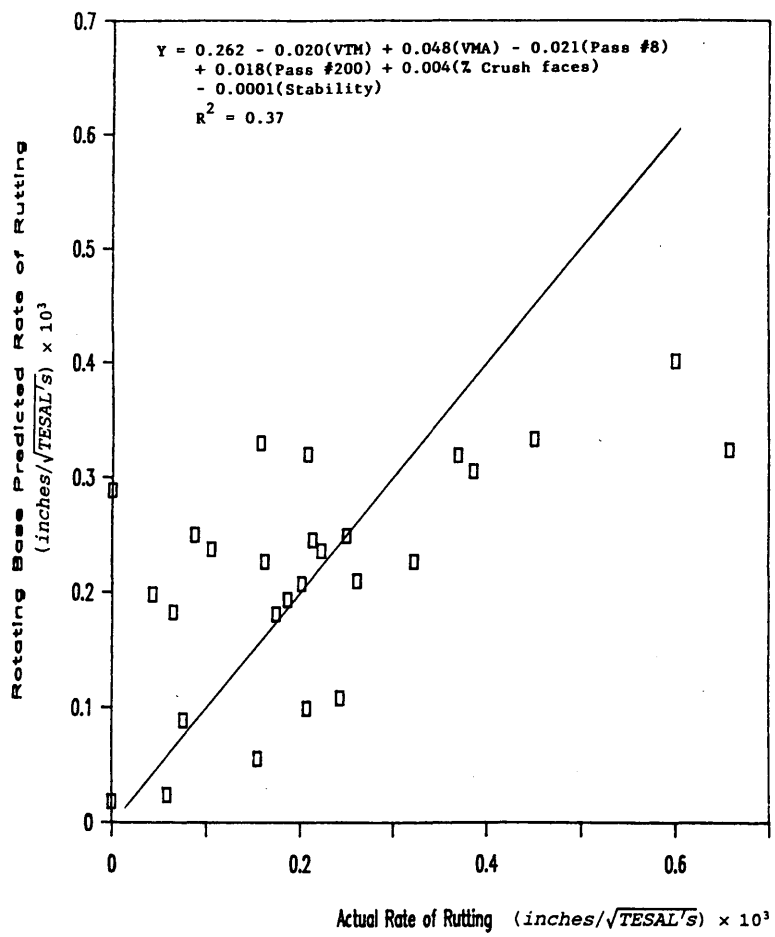

FIGURE 4 Rate of rutting model for rotating base Marshall compaction (wearing course mix).

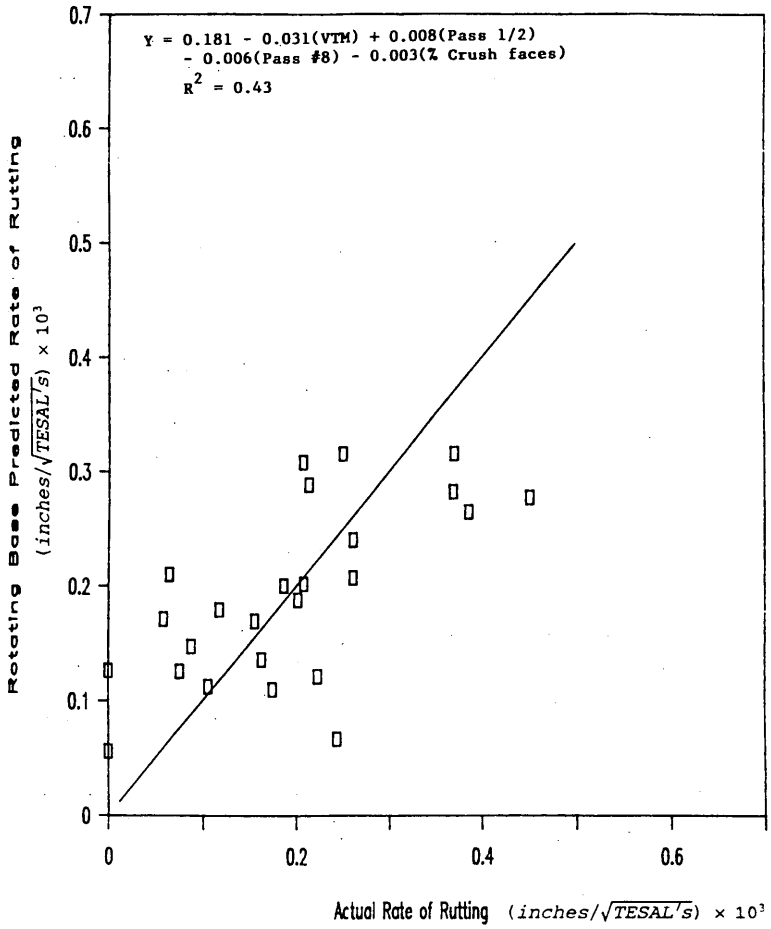

FIGURE 5 Rate of rutting model for rotating base Marshall compaction (binder course mix).

binder mix the 20th percentile VTM, the percent crushed faces, and the percent passing the 12.5-mm (½-in.) and the 2.36-mm (No. 8) sieves contributed significantly with an R-square of 0.43 as shown in Figure 5.

Heavy-Duty Specifications

As mentioned earlier, 7 of the 34 projects evaluated were constructed using the heavy-duty specifications implemented by PennDOT in 1987. The seven projects were in service for only 2 to 3 years at the time of this evaluation. Four of the seven heavy-duty pavements were rated good to excellent. The remaining three pavements rated poor to fair were designed with low mix design VTM (less than 4 percent). Maximum mix design VTM of 4.0 percent was incorporated in the specification later. The average rate of rutting for all seven pavements is 0.00010 in. per square root ESALS, and 0.00005 when the latter three are excluded. Both of these values are well below the threshold value of 0.00020 determined earlier. Therefore, it appears that the current PennDOT heavy-duty specifications have minimized the rutting problem.

Summary

Obviously, rutting is a complex phenomenon, as evidenced by the many independent variables selected by the stepwise procedure as significantly contributing to rutting. Each selected variable must be considered in designing the HMA mix and controlling HMA construction quality. Ideally, a simple, end-result test method capable of determining rutting potential is needed that can be used to design the HMA mix in the laboratory and control its quality on a daily basis in the field. Until such a test method is available, it is prudent to minimize the rutting problem by using specifications for mix composition, mix design, and construction quality control that are based on significant independent variables and their respective recommended values.

THRESHOLD ANALYSIS

Threshold values were identified for mix design variables and postconstruction variables (*1*). The various threshold values were determined for the preceding parameters by examining plots of the percent fair to poor pavements occurring at greater than or less than a given value of that parameter. A change in the slope of the line indicates an increase or decrease in the occurrence of fair to poor pavements, giving a threshold value. If a change in slope was not very apparent, the values corresponding to about 10 percent fair/poor sites were considered. Threshold values identified for in-place VTM (at the time of coring), percent natural sand in the fine aggregate, and GSI only will be discussed here. Figure 6 shows the per-

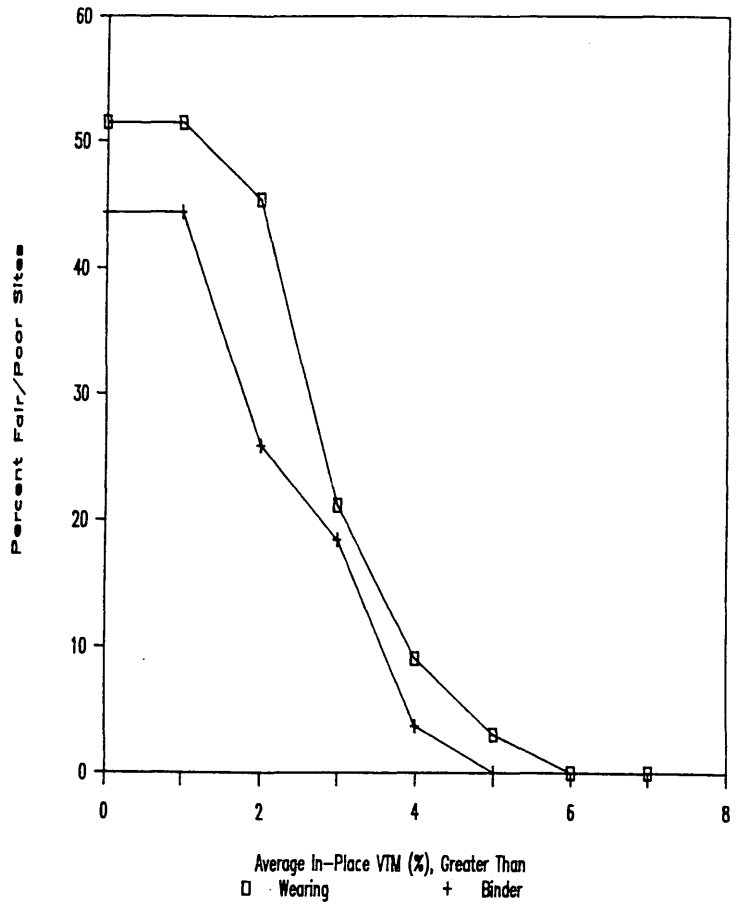

FIGURE 6 Average in-place VTM versus percent fair and poor pavements.

centage of pavements rated fair to poor at greater than a given air void content versus rutting for the wearing and binder mixes. The plot shows a change in the slope of the line at 3.0 percent VTM for the wearing mixes and 2.0 percent VTM for the binder mixes. Below these threshold values, the occurrence of fair to poor pavements increased.

Figure 7 shows the relationship between the percent natural sand in the fine aggregate and the percent fair to poor pavements. It appears that mixes with less than 20 percent natural sand in the fine aggregate contained fewer fair to poor pavements than mixes with more than 20 percent natural sand in the fine aggregate. Ten pavements had no natural sand in either wearing or binder course mixes. Of these 10 pavements, 8 were good to excellent and 2 were fair in performance.

Similarly, a GSI threshold plot showed a significant increase in the percentage of fair to poor pavements when the GSI exceeded 1.2 for both wearing mixes and binder mixes. Average GSI values of 1.35 and 1.26 for wearing and binder courses, respectively, obtained in this study are on the high side and indicate potential for rutting.

RECOMMENDATIONS

The following recommendations were made to improve and optimize the resistance of PennDOT HMA mixes on heavy-duty pavements.

Materials

1. Coarse aggregate retained on the 4.75-mm (No. 4) sieve should continue to have at least 85 percent of particles with two or more fractured faces for wearing and binder courses.
2. Fine aggregate should continue to have at least 75 percent crushed sand in the fine aggregate for both wearing and binder courses. Encourage use of 100 percent crushed sand if possible.

Mix Design

1. Use 75 blows per side compactive effort using a rotating base/slanted foot Marshall compactor. This will minimize the potential overasphalting of mixes designed for heavy-duty pavements and high-pressure truck tires.
2. Design mixes with at least 4.0 percent air voids.

Mix Production Quality Control

1. The mixes "as placed" were generally finer than mixes "as designed." Better mix gradation control is necessary during production.
2. Air void content in laboratory-compacted samples of "produced mix" is more important than that of the "designed

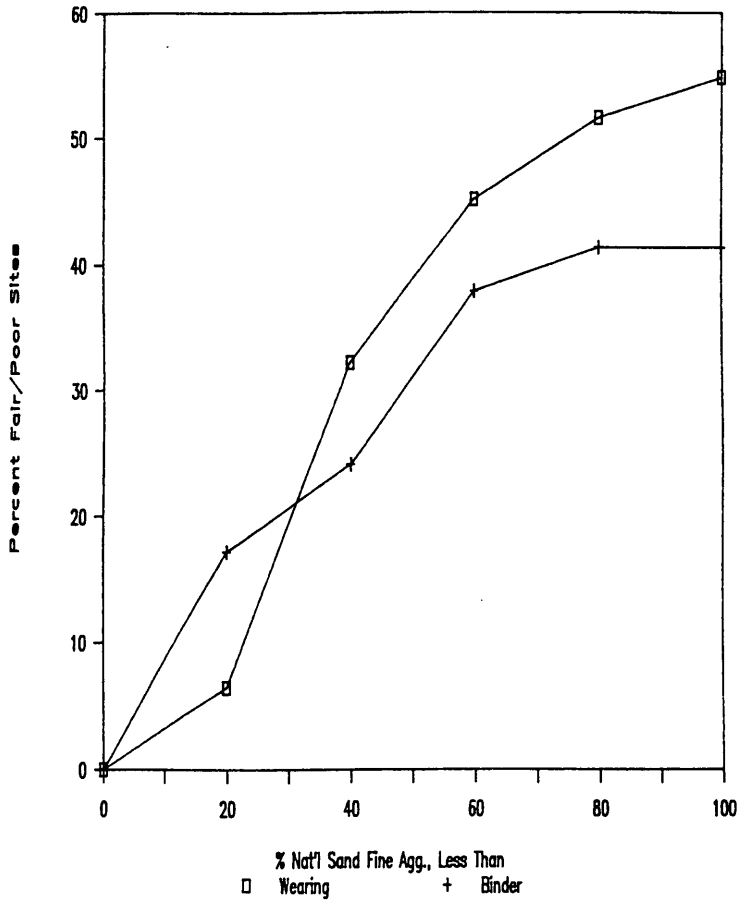

FIGURE 7 Percent natural sand in fine aggregate versus percent fair and poor pavements.

mix." Air void content should not be allowed to fall below 3.0 percent.

ACKNOWLEDGMENT

This research was sponsored by PennDOT in cooperation with FHWA.

REFERENCES

1. P. S. Kandhal, S. A. Cross, and E. R. Brown. *Evaluation of Bituminous Pavements for High Pressure Truck Tires.* Report FHWA-PA-90-008-87-01. Pennsylvania Department of Transportation, 1990.
2. E. R. Brown and S. A. Cross. A Study of In-Place Rutting of Asphalt Pavements. *Proc., Association of Asphalt Paving Technologists,* Vol. 58, 1988.
3. F. Parker and E. R. Brown. *A Study of Rutting of Alabama Asphalt Pavements.* Final Report, Project ST 2019-9. Alabama Highway Department, 1990.
4. C. T. Metcalf. Use of Marshall Stability Test in Asphalt Paving Mix Design. In *Highway Research Board Bulletin 234,* HRB, National Research Council, Washington, D.C., 1959.

The opinions, findings, and conclusions expressed here are those of the authors and not necessarily those of PennDOT, FHWA, the National Center for Asphalt Technology, or the University of Kansas.

Use of LPC Wheel-Tracking Rutting Tester To Select Asphalt Pavements Resistant to Rutting

YVES BROSSEAUD, JEAN-LUC DELORME, AND RENÉ HIERNAUX

The last survey carried out in 1991 on the French road network shows that, for the last 15 years, the roads have behaved very well as far as surface rutting is concerned. Less than 1.5 percent of the motorway network is affected by rutting defects. The phenomenon is limited and confined to particular areas. The explanation of this favorable situation lies in the awareness as early as 1970 of the rutting problem due to heavy traffic, which led to the design of a laboratory test, the Laboratoires des Ponts et Chaussées (LPC) wheel-tracking rutting tester. This test, whose mechanical and dynamical conditions are as close as possible to those generated in the pavement, is performed at a rather high temperature (60°C). The test has allowed the determination of different types of material behaviors and the definition of limit values (used in standards) allowing a good quality of the road. These specifications have been confirmed by correspondence between performance in the wheel-tracking rutting test and behavior on site. Moreover, the influence of test parameters and the mixture on the stability level of the mixes has been estimated. Interlaboratory tests, carried out in 1992 in conformity with ISO Standard 5725, confirmed the first estimates obtained in pretests, that is, very good repeatability values. New applications of the test have been used for the study of special asphalt mixes, study of the behavior of waterproofing systems for bridge decks, and analysis of the evolution of the macrotexture of very thin surface layers (20 or 30 mm). However, because of a significant increase in heavy traffic, new studies will be performed this year on the LPC circular fatigue test track in Nantes, France. At the same time, comparison studies on test devices and rutting depth prediction calculation models will be made, particularly on the finite element computation model CASTOR.

For nearly 20 years, the performance of French pavements with respect to rutting has been rather good: the latest surveys of the technical network by the Laboratoires des Ponts et Chaussées (LPC) (1991) and by motorway operators (Union des Sociétés d'Autoroutes à Péage, USAP, 1990) show that less than 1 percent of high-traffic roads have ruts exceeding 1 cm depth.

These highly encouraging results are attributed to

- Awareness by highway engineers of the negative impact of rutting on users' safety and comfort, which has led to the introduction of a loading simulation test based on the LPC wheel-tracking rutting tester for the selection of mixtures that resist permanent deformation;
- Arrangements in the design (alignment rules), construction (selection of materials, powerful production and compaction plant), and inspection (checks that the properties of the materials conform with the mixture design) of road structures; and
- The development of specific mixtures to combat rutting effectively at particularly sensitive sites (use of special polymer-based binders, "structuring" fibers, and plastic).

Y. Brosseaud, Laboratoire Central des Ponts et Chaussées, Route de Pornic, BP 19, Bougenais, France 44340. J.-L. Delorme, Laboratoire Régional des Ponts et Chaussées de Melun, 19 Avenue Clemenceau, Melun, France 77015. R. Hiernaux, Laboratoire Régional des Ponts et Chaussées de Saint-Quentin, 151 rue de Paris, Saint Quentin, France 02100.

DESCRIPTION OF EQUIPMENT AND TEST PRINCIPLES

The rutting test is described in AFNOR Standard 98253, in application since December 1991.

For practical mix design studies, a wheel-tracking rutting test (*1*) is used; it measures the rut created by the repeated passage of a wheel over a prismatic bituminous concrete sample. The laboratory simulation of the rutting phenomenon must approach actual pavement stress conditions so that the result obtained can provide one of the selection criteria for a mix design. The test is associated with the LPC wheel-tracking rutting tester (Figure 1), which can test two samples simultaneously, on two separate frames, at a fixed temperature.

There are 72 such testers in service, most of them in France (23 in government laboratories and 22 used by road contractors and oil companies). The rest are abroad, in Europe (Germany, Switzerland, Austria, Italy, etc.), the Americas (United States and Brazil), and Africa (Morocco, Saudi Arabia, Cameroon, etc.).

Presentation of the Test

Sample

The sample (Figure 2) is a plate measuring 500 × 180 mm with a thickness of 100 mm or 50 mm. It is placed in a metal frame and rests on a steel base plate. The assembly is placed in the rutting tester. The test may be carried out on a sample taken from an actual pavement; however, the test plate is generally prepared in the laboratory and compacted in its frame by using the LPC laboratory-tired compactor using two level compaction procedures.

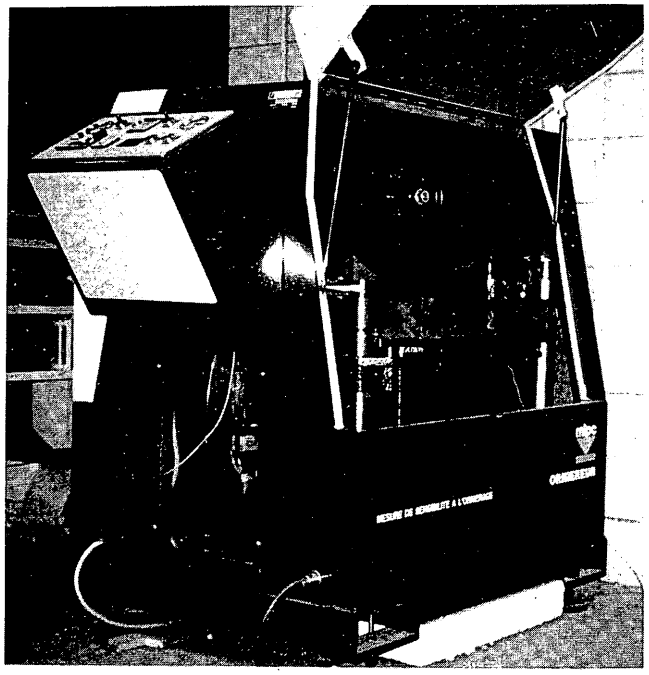

FIGURE 1 Wheel-tracking rutting test machine.

FIGURE 2 Detail of wheel and sample.

Two samples are compacted and tested for each compaction level. Density is measured with great precision at three depth levels before the test, often using the LPC vertical gamma densitometer bench; different points are measured for each depth. However, another measurement can be made (geometric density or density in water). This criterion is very important in evaluating the results.

Wheels

The wheels of the tester are fitted with smooth tires (400 × 8) inflated to a pressure of 6×10^5 Pa and loaded to 5,000 N. The wheels pass over the center of the sample twice per second, executing an alternating movement with an amplitude of 205 mm. Load time at the center of the plate is approximately 0.1 sec, comparable with roadway loading conditions. Pressure readings should not deviate from specified pressure by more than 5 percent.

Temperature

Temperature is regulated by circulating hot air through a probe placed in the sample. The variation of temperature scatter in the sample plate does not exceed ±2.0°C for bituminous concrete. The test temperature selected is 60°C for all bituminous concrete, but the equipment has a range of 35°C to 65°C. The test temperature is chosen to be relatively high to reproduce the most unfavorable pavement conditions. In summer, temperatures close to 60°C can be frequently observed for 4 to 6 hr.

A rut is defined by the relative percentage of reduction in the thickness of the plate in the wheelpath. Measurements are taken by using a depth gauge with a resolution of 0.1 mm; the gauge reference point is linked to the sample-holder frame. Measurements are taken for five transverse profiles spaced at 75-mm intervals, each characterized by three points in the rut 25 mm apart. For the test sample, the rut is represented by the mean of 15 measurements. The initial profiles are obtained after 1,000 cycles cold, giving good contact between sample, frame, and base plate. The test is terminated after 30,000 cycles unless rut depth exceeds 15 percent, but the test can be carried out for a greater number of cycles (e.g., 100,000). The test is stopped after different numbers of cycles to measure the rut.

Results

Figure 3 shows an example of results obtained 1 week after procurement of the materials. To evaluate rutting sensitivity, the mix designer takes into account not only the rut depth occurring after a certain number of cycles at a specified job site void content, but also the shape of the rutting curve (Figure 3) used to calculate the model CASTOR and the sensitivity of this curve to variation in void content.

Precision of the Test

An interlaboratory test organized in the second quarter of 1992 in accordance with ISO Standard 5725 was performed with the participation of 12 government and private (road contractors' and oil companies') laboratories, including two outside France (Switzerland and Austria). The test program consisted of four repetitions of the test (with one repetition being the mean of two elementary tests). The material tested was a bituminous concrete used in the wearing course, maximum size 10 mm (0/10), that demonstrated average behavior in the rutting tester, namely, a rut depth of 7 to 8 percent at 30,000 cycles.

The statistical processing of the data from the test program has been only partially completed at this writing (the analysis

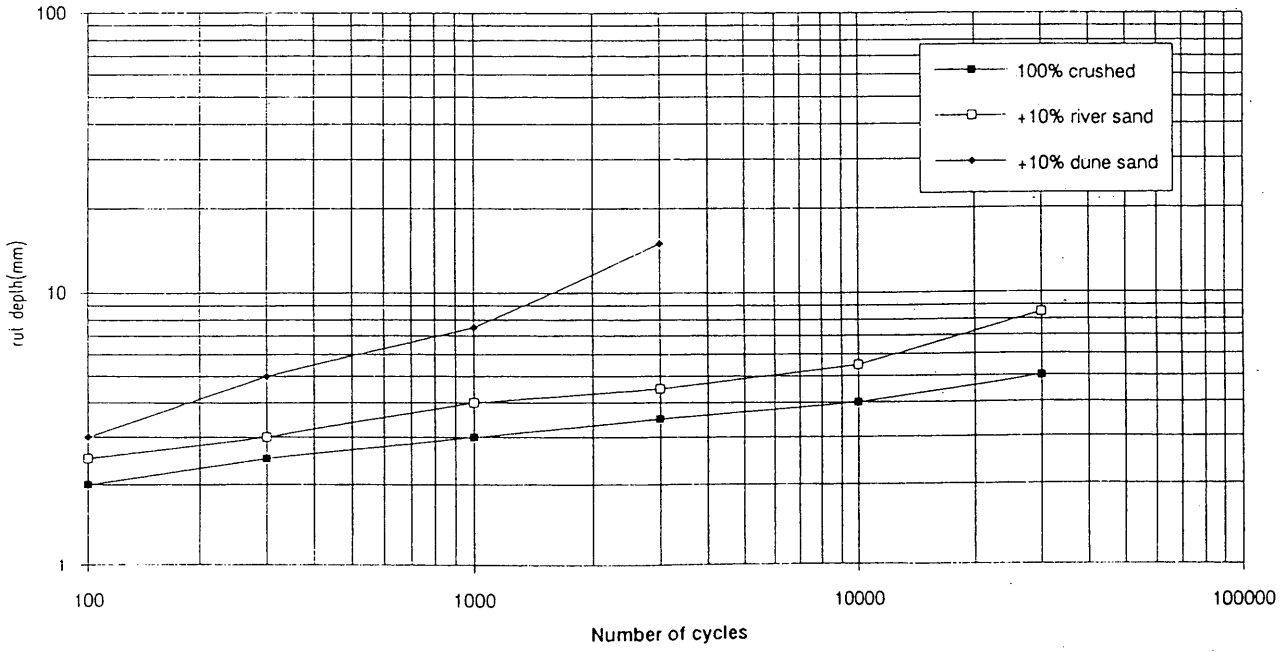

FIGURE 3 Example of results—effect of the addition of dune sand or river sand on rut depth.

covers only nine laboratories). The following values have been found: repeatability, $r \approx 1.1$ (percent of rut); reproducibility, $R \approx 1.4$.

The significant difference between two tests is 15 to 20 percent in relative value for a rut depth of 7 percent (or, more precisely, a difference of 1.5 mm of rut is needed to differentiate two materials tested on a plate 100 mm thick with 8 mm rutting).

This level of precision is equivalent for rut depths between 5 and 7 percent. But the dispersion is a little higher for the start of the test (at 30 cycles, the depth of rutting is 2.7 percent, $r \approx 0.7$, and $R \approx 0.9$); this result appears logical since it corresponds more closely to placement of a material in a phase where rutting is practically nonexistent.

In these results, which qualify only the rutting test (all production and compaction in a single laboratory using LPC equipment, insulated 80-L mixer, LPC laboratory-tired compactor), it can be seen that the reproducibility of the test is very good. These results confirm the preliminary cross-tests performed 10 years ago.

Measurement of Evolution of Macrotexture

Very thin bituminous concrete (VTBC) materials (applications 20 to 30 mm thick) are used in new pavements or for the maintenance of correctly designed pavements that are in good structural condition to obtain good skidding resistance. This resistance must last as long as possible under repeated loads. To assess the evolution of VTBC macrotexture and to guide the choice of the characteristics of VTBC composition, these materials are subjected to a test simulating passages of loads using the LPC rutting tester, with slightly modified operating arrangements.

The plates are prepared on a nonrutting substrate that generally consists of a coated material with a high modulus (including a very hard binder of penetrability class 10/20 in 1/10 mm). After bonding by a tack coat, the VTBC material is applied in the thickness planned for the site.

The test sample is prepared in the LPC plate compactor using a high level of compaction and a smooth tire tread at the end of the test to produce a macrotexture that closely resembles the one that will be obtained on site. The sand patch texture depth (SPTD) method is used to measure the texture depth on the plate. Half the quantity of sand specified in Standard NFP 98-216-1 is used.

The simulation is performed with 3,000 cycles at 60°C. The change in geometrical roughness is measured by another SPTD test in the wheel track under the conditions defined above. This measurement is valid only if the deformation of the plate is less than 5 mm.

The specifications concerning the change in macrotexture of VTBC defined in Standard NFP 98137 limit the reduction of the sand patch texture depth to 50 percent to ensure adequate durability of the structure in service.

Three classes of material are defined: rutting, nonrutting with unacceptable change of texture, and nonrutting with preservation of texture. Examples of results are as follows:

- On VTBC with a 0/6 mixture, 2/6 gap, including 0.3 percent organic fibers and 6.3 percent grade 60/70 bitumen: initial SPTD, 0.9 mm; SPTD at 3,000 cycles, 0.8 mm;
- On antirutting-coated materials with a 0/14 mixture, structured by addition of 1 percent plastic waste, coated with 5.2 percent grade 40/50 bitumen (Figure 4, transverse section): initial SPTD, 0.9 percent; SPTD at 30,000 cycles, 0.88 mm; and rut depth, 5 percent.

This coated material exhibited very good resistance to rutting while maintaining its surface texture.

APPLICATIONS OF LPC WHEEL-TRACKING RUTTING TESTER

Studies and Mixture Design

The French mixture design methodology calls for the rutting test to be performed in the following cases: (*a*) study of an entirely new design and (*b*) use of designs on pavements where the loadings are large (large heavy-vehicle traffic, more than 500 vehicles of more than 5 tonnes payload per direction), where traffic is channeled, and on gradients (exceeding 3 percent), winding roads, and so forth.

The rutting test is also recommended if the mixture of the coated materials entails a high compactibility, for example, when certain sands are used (e.g., ground sand, round sand).

Checks of Conformity

The rutting test can be used as a quality control for coated materials when work is started at a site where there is a risk of rutting, to check that there are no great differences between the design mixture and the site that might be caused by

- Components (aggregates, binder) different from those of the design,
- Storage conditions (in particular for sands with high fines content), or
- Means of production that favor workability (some drum mixer-dryer plants use porous materials).

These checks, always very useful, can in some cases lead to adjustments of the mixture to meet rutting resistance requirements.

The rutting test has been used successfully several times to determine the corrective action necessary to change the behavior of a material susceptible to rutting, which may be detected either in the course of the job or after commissioning. The treatment has consisted of hot recycling of the coated rutting-susceptible materials by the addition of precoated aggregates, with the composition being adjusted on the basis of rutting test results.

Mixture Design for Special Coated Materials

The rutting test is widely used to analyze the effect of changing the characteristics of the binder or the mastic on the stability of a coated material in the development of mixture designs for special coated materials or for coated materials with a high modulus and very good antirutting properties. The classifications that have been established in the laboratory have been checked in some cases by work at sites where a control or reference formula could be found.

For example, coated materials were reinforced by the incorporation of plastic waste (see Figure 4); it was found that the division of the rut depth in the rutting test by a factor of 2 to 3 with respect to the control formula (without plastic waste) was borne out on site by the total absence of deformation, whereas the control exhibited deformations of 1 to 1.5 cm (findings made after 2 years on a bus lane at the approach to traffic lights). These many observations have clearly shown the utility of antirutting coated materials (i.e., those exhibiting a rut depth of less than 5 percent at 30,000 cycles and 60°C).

However, the comparative studies performed on special coated materials with regard to the effects of special binders, their composition, their proportion, and the level of compaction of the materials have not necessarily led to systematic improvements in rutting. It appears that the so-called "special" binders (bitumen polymers/bitumen fibers) must exceed a minimum threshold of modification to be able to endow the coated material with reinforced stability properties.

Tests on Waterproofing Layers

The rutting test is used to study deformation of "high-speed" waterproofing layers developed by road contractors. These sand-bitumen complexes, extensively filled with polymers and covered with thick surface dressing of polymer binder, are applied on bridges using conventional equipment (paver, spreader, compactor). Given the deformation properties of the material, it is appropriate that its behavior in the presence of the definitive wearing course be examined in advance (*2*).

The test is performed on a plate that has the following composition: concrete substrate, waterproofing complex to be tested, and wearing course. The test is performed at 45°C.

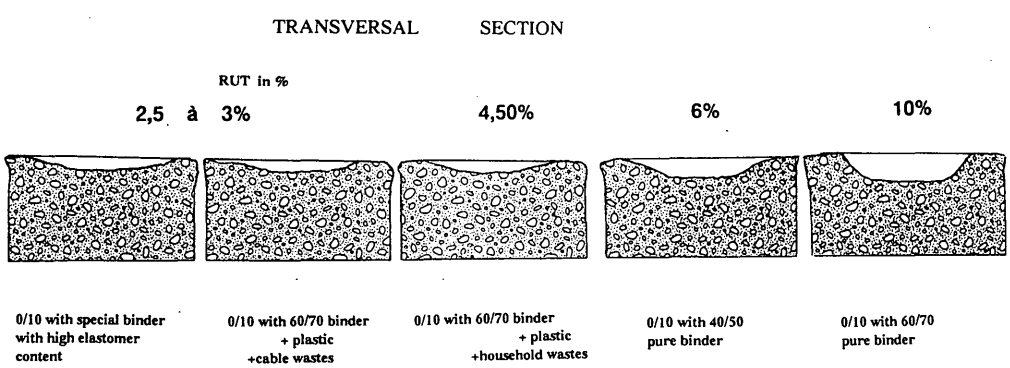

FIGURE 4 Influence of special bituminous mixes.

This temperature was selected to allow for the particular thermal environment on a bridge and the thermal protection provided by the wearing course and with a view to using the same specification as for semigranular coated materials (thickness placed 60 mm), namely, less than 10 percent rutting at 30,000 cycles.

Currently, the complexes (five different contractors' products) that meet these specifications perform very well on site. The oldest jobs now date back 4 or 5 years.

RUTTING SPECIFICATIONS FOR BITUMINOUS PRODUCTS

Specifications for the allowable percentage of rutting for different coated materials appear in the Product Standards, Series NFP 98 130 to 98 141, issued in 1990–1991.

The characteristics of the test and the selection criteria are as follows:

- The test is performed at only one temperature, 60°C;
- The thickness of the plate is 10 cm for layers >5cm thick, 5 cm for layers ≤5 cm thick, and equal to the thickness of use (2 to 2.5 cm) for VTBC materials (the specification concerns the durability of the macrotexture); and
- The maximum values (Table 1) are fixed at a given number of cycles, which depends on the type of coated material for the site density. These values are obtained by interpolating the percentage of rutting measured between two plate compaction energy levels (most often determined in the LPC laboratory-tired compactor) that bracket the site density. This is to allow for the density effect on rutting resistance.

These specification thresholds are the result of the correspondence that has been established among the many laboratory findings using the rutting tester and observations made in the field.

Analyses have determined, as a function of the characteristics of the site (heavy traffic, type of environment), the degree of deformation that should not be exceeded to ensure good stability of a given type of coated material. This empirical approach has led to the specification of characteristics for bituminous materials taking into account the position of the material in the structure, the thickness of placement of the surface layers, and the distribution of loads.

Position of the Material in the Structure

A road base is subjected to lower temperatures (about 10°C) than a surface course. Previously, the rutting test was performed at 50°C and the specification was 10 percent at 30,000 cycles. Knowledge of the influence of temperature on the test result and the aim of improving rutting resistance slightly have led to the threshold of 10 percent at 10,000 cycles but at 60°C.

High-modulus coated materials must have very good rutting resistance, so a specification a little more demanding than that for surface layers has been devised. These materials are often covered with thin or very thin layers, so thermal protection is slight, and the temperature conditions are close to those of the surface (number of cycles, 30,000).

In reality, these materials exhibit a better rutting resistance than specified by the standard; it is common to attain less than 5 percent at 30,000 cycles. This value is often used in certain motorway contracts requiring an antirutting solution.

Thickness of Placement of the Surface Layers

The level of deformation from which there may be safety problems for users starts at 1 cm. In consequence, the percentage of rutting should be judged against this criterion. For thin bituminous concrete, larger percentages of rutting are acceptable because the plate is thinner; thus, the depth of rutting will still be at an acceptable level (less than 1 cm or 25 percent with a layer thickness of 4 cm; two limits are defined, 1,000 and 3,000 cycles).

On VTBC, coated materials that have surface characteristics similar to those of the German stone mastic asphalt, good skidding resistance is obtained by means of a marked macrotexture that must be durable. The rutting test, simulating the passage of rolling loads, is performed to evaluate the durability of the texture. The first test consists of limiting the maximum deformation to 5 mm to allow measurement of the sand patch texture depth and characterize its evolution. Beyond this deformation, it is believed that VTBC materials lack the stability needed to preserve a durable roughness.

Distribution of the Loads

Bituminous concretes for airfield pavements are subjected to a small number of loads and are not channeled, so materials that are less stable with respect to rutting can be accepted; the level of 10 percent is required for 10,000 cycles only.

Currently, studies are in progress to evaluate the effects of the increasing aggressiveness of the loads generated by single wheels and the steady increase of truck (HGV) traffic. The results may lead to more stringent specifications for singular zones (such as HGV lanes on gradients, which are especially vulnerable).

INFLUENCE OF TEST AND MIXTURE DESIGN PARAMETERS

It is very difficult to establish correlations between the test and mixture design parameters and the sensitivity to rutting evaluated by the rutting tester that are valid for all materials studied. However, it has been possible to identify broad trends, the variation of which should be adjusted according to the degree of sensitivity to rutting of the material but the direction of variation of which is the same in all cases. The results described below constitute orders of magnitude that serve to qualify the pertinence of the test and to guide choices in the composition of materials that are not subject to rutting or that have a slight tendency to rutting.

Temperature

The main studies conducted (*3*) concern bitumen-treated granular materials with good rutting resistance (the test can

TABLE 1 Maximum Values of Allowable Rutting Percentage in Coated Materials

Type	Domain of use	Number of cycles	Maximum % rutting
Bitumen-treated granular, 0/20 or 0/14	subbase roadbase	10,000	≤ 10
Bituminous concrete, 0/14 or 0/10, thickness 60 to 80 mm	base course wearing course	30,000	≤ 10
Bituminous concrete thin layer, thickness 30 to 40 mm	wearing course	1,000 3,000	≤ 10 ≤ 20
High-Modulus Coated Material, 0/14 or 0/10, thickness 80 to 100 mm (generally based on hard grade 10/20 binder)	base course roadbase	30,000	≤ 8
Bituminous concrete, 0/14 or 0/10 for airfield pavement, thickness 50 to 70 mm	base course wearing course	10,000	≤ 10
Very Thin Bituminous Concrete (VTBC), 0/14, 0/10, or 0/6, thickness 20 to 25 mm	wearing course	3,000	deformation < 5 mm reduction of SPTD < 50%

be continued up to 100,000 cycles without rutting exceeding 8 percent). An increase in the test temperature of 10°C (measured in the core of the material) causes a lateral translation of the rutting curve (percentage of rutting versus number of cycles in log-log coordinates) representing a factor of 10 in number of cycles; the same percentage of rutting is found at 50°C and 100,000 cycles as at 60°C and 10,000 cycles. This is for a temperature range from 42°C to 60°C. Regulation of the enclosure makes it possible to hold the temperature to within ±2°C (value confirmed in the interlaboratory tests).

Tests on bituminous concretes that are slightly more sensitive to rutting are under way to evaluate the influence of a smaller variation in temperature (5°C, for example).

Thickness of Plate

Thickness does not have a direct influence, since at the same level of voids content, the same value of the percentage of rutting (depth of rut/initial thickness of plate) is found to within 1 percent, whatever the thickness of the plate. Thickness is only a secondary parameter acting on the more or less great ease of arrangement of the internal skeleton and therefore of the voids content and the texture of the sample. Thus, to avoid getting too far away from the domain of use of the materials and, for a given energy of compaction, to keep the voids contents in the sample fairly close to those at the site, two standard thicknesses have been selected.

Voids Content for a Given Composition and Compaction Force

The voids content is one of the factors that most influences a material's sensitivity to creep. Generally, the graph of the percentage of rutting versus the voids content has a parabolic shape whatever the type of material, and there is a range of voids content (often between 3 and 7 percent voids) for which the material is most stable. Therefore, there exists an optimal level of filling of the intergranular voids by the bitumen, where deformation resistance is obtained by effective immobilization of the grains with no lubrication effect by the binder.

The curves on the graphs will be more or less accentuated according to the degree of sensitivity of the material to creep (an unstable material yields a curve that changes rapidly). Figure 5 shows these tendencies. For different thicknesses and forces of compaction, it is indeed the voids content that determines the material's response to creep.

Given the importance of the voids content to the results of the test, it can be understood why the tests are performed at two voids content levels that bracket the level expected at the site to interpolate the percentage of rutting. This method does not, therefore, lead to underestimating the risk of rutting (as might an overly bold extrapolation).

Mode of Production of Sands

A 1989 study of the use of bar mills in quarry crushing installations to produce a sand containing between 16 and 18 percent filler showed that this mode of crushing affects, as a function of the percentage of ground sand, the sensitivity to rutting of the coated materials produced. A 0/14 mixture consisting of 28 percent crushed sand undergoes a 50 percent increase in the percentage of rutting when this sand is replaced by a ground sand made from the same rock. The level of rutting reached was in this last case very close to the specification threshold (9 percent rutting at 30,000 cycles).

Increasing the proportion of ground sand is very harmful to the stability of this coated material. Exceeding a critical threshold of 32 percent leads to a very sharp amplification in rutting (12 to 18 percent rutting at only 3,000 cycles). This sudden change of behavior shows that the zone of transition between a stable material and a material liable to rutting is very narrow.

Further tests consisting of changing the type of 2/14 gravel while preserving the 0/2 ground sand have led to the same conclusions, indicating that it is in fact the mode of preparation of the sand, as well as the critical proportion of sand, that underlies the phenomenon of rutting in coated materials (results confirmed by assessments of behavior on site).

This material was selected for the investigation (on the LPC's circular fatigue test track at Nantes in 1992) of the influence of the mode of loading (single wheel or paired wheels) on the behavior of four coated materials differentiated by type of binder.

Similar effects have been found with rotary table crushers, the principle of which is to reduce the size of the materials by mutual attrition of the grains. The aggregates have highly blunted edges, and their spherical shape makes the granular skeleton less resistant to permanent deformation.

Angularity

For a given composition, the rutting test clearly reveals the degree of crushing of alluvial materials (see Figure 5), and it can be used to determine the degree of crushing of a material for its behavior to be judged adequate (further crushing contributing no significant gain of stability) (*4*).

For coated materials, this means reduction of all of the blocks entering the crusher [crushing index 100 (IC100)]. The

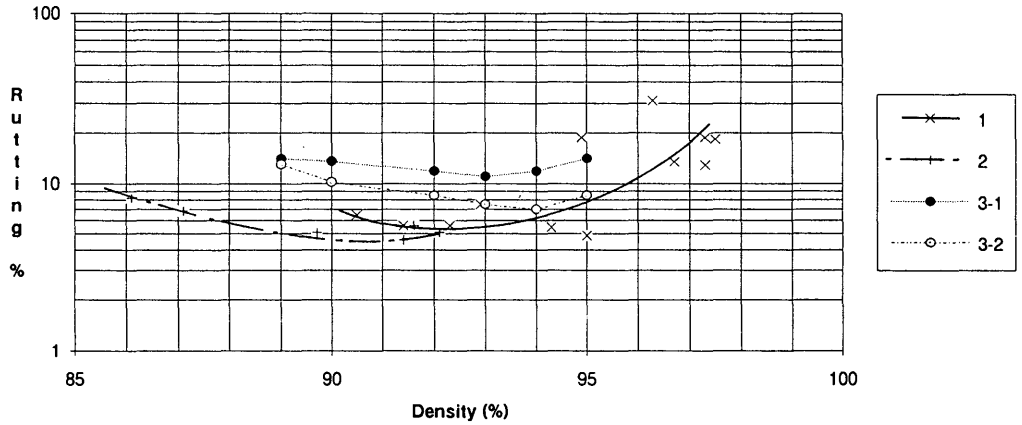

Key	Number of cycles	Formula	Composition	Sensitivity
1	1000	BC 0/6 for chip coating (solid rock)	0/3 limestone 68%; 4/6 Diorite 32%; total fines 11%; 60/70 bitumen 7,0%	very high
2	30000	BC 0/10 Semi-granular(solid rock)	Continuous grading; 0/2 sand 35%; total fines 7,5%; 60/70 bitumen 5,7%	low
3-1	30000	BC 0/14 Semi-granular (Moselle alluvial)	Continuous grading; 0/5 sand 50%; total fines 8%; 60/70 bitumen 5,8%; crushing index IC30	high
3-2	30000	" "	" crushing index IC100	moderate

FIGURE 5 Effect of density and angularity on rutting.

material is then called fully crushed. There is a reduction in rutting of 30 to 50 percent when the crushing index changes from 30 to 100. For bitumen-treated granular materials, this reduction of blocks may be limited to 30 percent (IC30). However, the use of these alluvial materials should be avoided when the site is especially vulnerable to the problems of rutting, because even if means to improve the rutting behavior of these materials are available, they are still more sensitive to deformations than materials made from massive rock. This shows that it is possible to adjust the aggregate parameter of mixtures both by mode of preparation and by recomposition.

Grading Curve

With regard to grading, the results (*3*) are only fragmentary, and no general conclusion can be drawn concerning the effects of the respective proportions of the different grading classes.

However, the following tendencies have been observed:

- Reducing the 0/2 sand content approximately 5 percent (and slightly increasing the voids content) reduces the rutting depth at the end of the test by 15 to 25 percent.
- Increasing the proportion of coarse aggregates systematically results in better rutting behavior.
- Introducing a gap in the grading curve, even a small one (2/4 or 4/6), generally contributes to instability, a reason why these mixtures are restricted to use in thin and very thin layers, where their great workability promotes optimal placement, leading to good cohesion properties.

Studies using the rutting tester can help optimize these gap-graded mixtures in two ways. The first is by evaluating the increase in the risk of rutting that results from the attempt to achieve better compactibility through the size of the gap. For example, a 0/14 coated material of the same mineral type and with the same type and proportion of binder but in one continuous mixture, another having a 2/6 gap, and a third having a 2/10 gap with highly variable voids content (5.8, 3.9, and 2.1 percent, respectively) exhibited very different sensitivities to rutting. At 100,000 cycles the depths of rutting are 35 percent greater for the second mixture and more than 250 percent greater for the third mixture than for the first. The second way is by classifying mixtures of the same compactibility according to their rutting resistance. For example, mixtures with similar voids content, obtained by different granular recompositions (gap, fines content, percentage of sand), but the same binder content can lead to depths of rutting that vary by a factor of 1 to 2, making it possible to optimize the mixture with respect to its rutting resistance. Moreover, the combination of two factors, such as the introduction of a 4/6 gap and the incorporation of 10 percent round sand, makes the material very unstable (Figure 6).

Type and Proportion of Binder

In the example mentioned previously, it was shown that the use of special binders could significantly correct a material's sensitivity to rutting. The use of a bitumen highly modified by an SB polymer—grafted in the same proportion as the

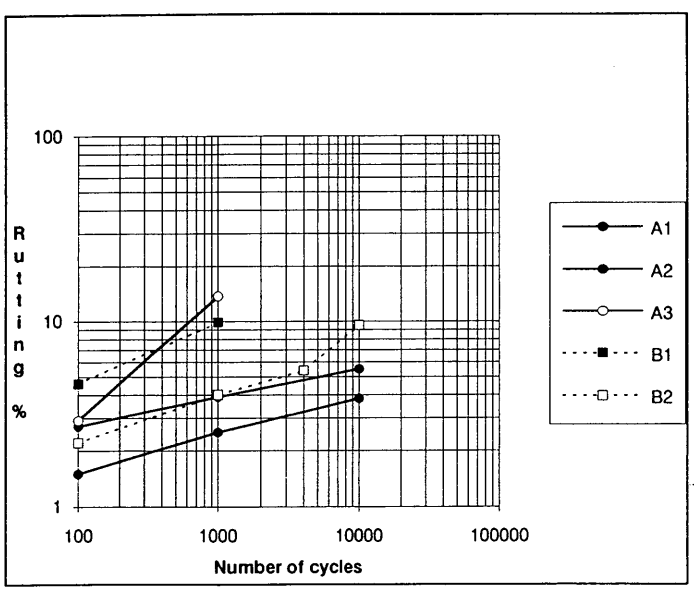

Key	Formulation	% Sand	River sand	% Filler	Binder	Percentage
A1	0/14 continuous - solid rock (La Noubleau)	32	/	7,7	Pure 60/70	4
A2	"	"	"	"	"	5,3
A3	"	"	"	"	"	6,6
B1	0/14, 2/4 gap - solid rock (La Noubleau)	36	10%	7,9	Pure 60/70	5,35
B2	"	"	"	"	Modified SB	"

FIGURE 6 Influence of grading curve and binder type and content.

basic binder (60/70 class)—although failing to duplicate the properties of a material suitably formulated to resist rutting, helped to halve rutting at 1,000 cycles, allowing the use of this material for applications in thin layers (Figure 6).

It would therefore seem always to be possible to improve rutting behavior to some extent by using a modified binder, but one should first attempt to study improving stability by action on the aggregates to optimize the mixtures, since the aggregate parameter has in some cases more influence than the binder, whether through its proportion or its type.

These are the conclusions of a study performed in 1987 (*5*) on three aggregates and three pure bitumens, in which it was shown that for a straight-run bitumen, one of the criteria of characterization was the ring and ball temperature (RBT), which in some cases should be completed by the thermal susceptibility (Penetration Index IP), in particular when the value of the RBT is far from 60°C (temperature of the rutting test). The value of the RBT seems in this case to correlate rather well with the depth of rutting for a given mixture that is at all sensitive to rutting (upper limit of specifications).

It has been found that a variation in RBT of 5°C to 6°C (range of consistency of a class of bitumen) can have a significant effect on the behavior of the mixture, since it can account for up to 20 percent additional rutting. This indicator is necessary but far from sufficient to evaluate the behavior, especially since the evolution of the RBT of the binder during coating and placement is also a factor of influence. The rolling thin-film oven test seems to provide useful information about some responses to the rutting tester and under traffic when the aggregate is somewhat porous or the binder changes rapidly (rapid evaporation of some solvents).

Since the effect on rutting of increasing the binder content is not proportional, there exists a critical level of filling of the voids by the binder beyond which the material becomes unstable. But any increase necessarily leads to an increase in the depth of rutting (Figure 6).

LABORATORY AND SITE CORRESPONDENCE

It is not possible to establish a correlation (in the statistical sense of the term) between the results obtained in the laboratory and the behaviour in situ for the following reasons:

- The rutting test was developed to reproduce the most severe loading conditions encountered on roads and to reject or correct mixtures judged unstable, whose use might lead to a risk of rutting. There are therefore rather few cases of rutting allowing statistical analysis.
- Loading conditions on the road are not known with enough precision to define the degree of aggressiveness (there are no recorded data on the temperature at various levels of the structure of coated materials, the number and distribution of loads, the effects of dynamic loads, the configuration of speeds, etc.).
- The means of measuring deformations were relatively cumbersome and could not be used in the continuous mode. Only isolated and therefore fragmentary information could be obtained. (The situation has evolved thanks to the SIRANO multifunction investigation system, in particular with a laser profile measurement device.)

However, sufficiently detailed analyses have been done in a few cases to establish correspondences between the observed effects and identify tendencies deduced from laboratory tests on samples that had rutted on site. The main conclusions are the following:

- In general, when the specifications concerning the rutting of a coated material are met in the mixture design, no rutting is found on site.
- In the opposite case (i.e., when rutting of these formulations is observed), it is found that one or more parameters have changed with respect to the laboratory study. The change may be a change in the source of the bitumen, accidental pollution of the binder, materials from a quarry having large heterogeneities (presence of fault or weathering of the rock), or an "evolutive" production process (for example, mixture of materials from a jaw crusher and a bar mill or a gyratory crusher), or a poor evaluation of the density of the material.

This makes it necessary to use in the test procedure the materials that will actually be used on the site (checks at the start of the job sometimes prove necessary) and to comply with the values specified in the standards, which are minimum values; the design engineer may impose more stringent requirements for a site where there is a high risk of rutting.

Samples taken from rutted zones (rutting of 15 to 25 mm on sections of 1 to 4 km) systematically give values that are substantially below specifications, and often rutting is between 12 and 18 percent after only 3,000 cycles, sometimes even less in a few cases of particularly unstable materials (the test must be stopped at 300 cycles).

The classification established by the rutting tester between stable and rut-sensitive materials is in fact found to be valid in the field.

Currently, the criteria defined in the standards for traditional conditions and those recommended by some project engineers or laboratories in very special cases (based mainly on experience with the materials and with the conditions of exposure and evaluation of HGV traffic and its rate of growth) satisfy the managers of the road network.

CONCLUSION AND PROSPECTS

For a score of years (the LPC rutting tester in its current form was introduced in 1973), many laboratory studies and findings using the rutting test have made it possible to correctly specify the proper selection criteria for mixtures resistant to rutting, specification thresholds for the different domains of use of the mixtures, and the main evolutionary tendencies in the factors of influence bearing on the test and the composition of the mixtures.

The test is covered by a French standard (AFNOR). It is currently used by government laboratories and by road contractors and oil companies for mixture studies of bituminous materials.

All of these factors help to explain the good performance of French pavements with respect to the phenomenon of surface rutting on all high-traffic roads. However, given the very large and regular increase of heavy-vehicle traffic (*6*), both in number (by a factor of 3 in 5 years) and in level of ag-

gressiveness (modification in the last 3 to 5 years of the distribution of loads, larger payloads, and the shift to the single wheel), in the last few years there has been a growth in rutting of bituminous materials (base and wearing courses) at difficult sites (gradients, truck lanes, intersections with traffic lights) on French high-traffic pavements.

This change in behavior has led to a comparative study at the LPC's circular fatigue test track at Nantes with a view to examining

- The influence of a single wheel compared with that of dual wheels,
- The influence of the composition of the material on rutting resistance [four materials are tested differing only in type of binder: straight-run, conventional (60/70 grade); hard (10/20 grade); modified by SBS polymer; and special to combat rutting], and
- The possibilities offered by various test methods for characterizing rutting (static, dynamic creep, rutting tester) and calculation models that predict rutting on site.

In the course of this program, new experiments will be performed on the LPC rutting tester to improve knowledge of the influence of the mode of loading (pressure, load, and speed of passage). A new process of continuous measurement of the evolution of the rut during the test will be developed using the technique of laser sensors with image analysis.

A procedure to validate the CASTOR design program associated with the LPC rutting test will be undertaken (*7,8*). This design program is a two-dimensional finite-element model describing the passage at constant speed of a wheel on a structure with viscoplastic behavior. The solution methods yield the pavement surface deformation of the courses. These mechanical analysis methods use the elementary properties of the material (reversible and irreversible constitutive laws); the LPC rutting tester is used as an element in the linear fitting of the creep curve for the bituminous materials in the structure [the curve of evolution of rut depth versus the number of loadings is linear in log-log coordinates, having the form $P_0 = A(N/1000)^a$].

Applications include studies to check the design of pavement structures or their predicted behavior and studies of maintenance for rutted pavements by regraveling or partial replacement of the pavement. The various simulations allow selection by comparative analysis of the best arrangements given the residual characteristics of the old pavement modeled and the viscoplastic properties of the new material.

This calculation tool must today be regarded as a complementary means of investigation. The studies and methods will add to our knowledge of the laws of behavior of bituminous materials in permanent deformation, allowing a judicious choice of techniques according to the stresses expected to be imposed on the structures.

REFERENCES

1. J.-P. Grimaux and R. Hiernaux. Utilisation de l'orniéreur type LPC. *Bulletin de liaison des Laboratoires des Ponts et Chaussées,* numero spécial V, 1977.
2. *Surfaçage de tablier, entretien et réparation.* Guide de chantier. STER, 1981.
3. R. Hiernaux. L'orniéreur type LPC. *Journée des LPC.* Dijon, France, 1989.
4. A. Panis et al. Stabilité des enrobés bitumineux pour couches d'assise ou de liaison, réalisés avec des granulats alluvionnaires plus ou moins anguleux. *Bulletin de liaison des Laboratoires des Ponts et Chaussées,* No. 174, Juillet 1991.
5. B. Barbe. Effet des facteurs bitume, granulats, et composition des mélanges sur la résistance à l'orniérage des enrobés en laboratoire. *Revue Générale des Routes et Aérodromes,* 1988.
6. M. Faure et al. Orniérage des mélanges bitumineux. *Revue Générale des Routes et Aérodromes,* Juin 1992.
7. J. P. Marchand et al. Cracking in Wearing Courses. *Proc., 5th International Conference, Structural Design of Asphalt Pavements,* Vol. 1, Delft, the Netherlands, pp. 741–757.
8. M. Goacoulou. Calcul de structure à l'orniérage: Programme CASTOR—Méthode de prévision des déformations permanentes dans la structure bitumineuse. *Bulletin de liaison des Laboratoires des Ponts et Chaussées,* No. 156, 1988.

Sensitivity of Strategic Highway Research Program A-003A Testing Equipment to Mix Design Parameters for Permanent Deformation and Fatigue

JORGE B. SOUSA, AKHTARHUSEIN TAYEBALI, JOHN HARVEY, PHILIP HENDRICKS, AND CARL L. MONISMITH

A new comprehensive mix design methodology using compaction and mix evaluation procedures developed as part of the Strategic Highway Research Program A-003A research endeavor is presented. The methodology can be used within the framework of an analysis system to estimate the likely performance of the selected mix in service. Descriptions of specimen preparation using rolling wheel compaction, mix evaluation in fatigue using a third-point loading controlled-strain flexural fatigue test, and rutting (permanent deformation) evaluation using a newly developed simple shear test capable of testing specimens 0.15 m (6 in.) in diameter and 0.05 m (2 in.) high or 0.20 m (8 in.) in diameter and 0.076 m (3 in.) high in repetitive loading are included. The mix design framework is presented as a matrix that allows the effects of asphalt content and air void content to be evaluated separately. The results of an example mix design within this framework demonstrate the sensitivity of the new tests to these variables.

The scope of Strategic Highway Research Program (SHRP) Project A-003A, Performance-Related Testing and Measuring of Asphalt-Aggregate Interactions and Mixtures, included the development of laboratory tests for asphalt-aggregate mixes. The tests permit the estimation of mix performance in situ. This paper presents some of the recommended procedures and equipment for specimen fabrication and evaluation of rutting and fatigue characteristics of an asphalt-aggregate mixture. It proposes that the effects of asphalt content and void content be individually evaluated and presents a mix design matrix for this purpose.

BACKGROUND

Specimen Preparation

For test results to be meaningful, specimens prepared in the laboratory must resemble as closely as possible in-service mixtures (i.e., those produced by mixing, placement, and compaction in the field and subsequently conditioned by traffic loads and aged by environmental influences).

The compaction method has been found to significantly affect the permanent deformation properties of dense-graded mixtures (*1,2*). Among the three compaction methods examined (California kneading, Texas gyratory, and rolling wheel), kneading specimens were generally most sensitive to aggregate characteristics and least sensitive to asphalt characteristics. Gyratory specimens were least sensitive to aggregate characteristics and only slightly more sensitive than rolling wheel specimens to asphalt characteristics.

The rolling wheel compactor has been recommended for use by the SHRP Project A-003A team, since it generally produces specimens whose permanent deformation characteristics lie between those of specimens produced by gyratory and kneading compaction and are within the range of those produced by field compaction. Moreover, specimens have homogeneous aggregate and air void structures and have all cut surfaces, and air void contents of compacted mixes can be reasonably controlled.

Rolling wheel compaction is a comparatively easy procedure to accomplish and enables rapid fabrication of a large number of specimens and a wide range of shapes and dimensions. Specimens for fatigue and permanent deformation can be cut or cored from the same slab. The procedure is also appealing because of its intuitive similarity to field compaction.

Fatigue

Fatigue resistance of an asphalt mixture is the ability to withstand repeated bending without fracture. Fatigue is one of the common forms of distress in asphalt concrete pavements and manifests itself in the form of cracking under repeated traffic loading. Cracking may initiate at either the top or bottom of an asphalt concrete layer, depending on the relative stiffness of the layers, tire pressure distribution and magnitude, pavement temperature profile, and so forth. In all cases fatigue has been directly associated with repeated application of tensile stresses or strains at a particular point in the asphalt-aggregate mixture.

Whereas there have been attempts to develop simplified representations of fatigue response (e.g., representative fatigue relationships, surrogate methods based on measurements of stiffness or dissipated energy, etc.), it is generally accepted that the fatigue resistance of a mix can be reasonably defined by the third-point bending beam fatigue test. In this

Institute of Transportation Studies, University of California at Berkeley, 1301 S. 46th St., Bldg. 452, Richmond, Calif. 94804.

test an imposed strain or stress is applied repetitively until failure occurs, either by complete fracture or by a significant reduction in stiffness. The fatigue behavior of a specific mixture can then be characterized by the relationship between level of stress or strain and the number of load repetitions to failure.

In the third-point bending beam repetitive flexure test used herein, a sinusoidally varying strain level is imposed in such a way that permanent deformation cannot occur. Variation of the magnitude of the stress is monitored, and failure occurs when an arbitrary but predefined reduction of stiffness occurs.

This test has been selected for the following reasons:

1. Specimen geometry: Beams 0.05 m (2 in.) by 0.063 m (2.5 in.) by 0.38 m (15 in.) can be readily obtained either from slabs sawed from existing pavements or from slabs prepared by rolling wheel compaction. With this geometry a relatively large section of the beam is subjected to a uniform flexural bending moment. The beam section is sufficiently large to accommodate maximum particle sizes used in actual mixes. The contribution to the deformation by shear stresses is negligible.
2. Repetitively applied loads: Although considerable progress has been made in fracture mechanics, given the relative magnitude of particle size and specimen size for the mixes used herein, a phenomenological approach is believed to produce more reliable results. Accordingly, application of repetitive strains (at different levels) has been used to define the fatigue mechanism experienced by pavements under traffic.
3. Mode of loading: Much discussion has been directed to the relative performance of mixtures in controlled-stress versus the controlled-strain mode of loading, with controlled-stress loading conditions applicable to comparatively thick and stiff asphalt-bound layers and the controlled-strain mode of loading applicable to thinner and more flexible asphalt-bound layers. Tayebali et al. suggest that the relative ranking of the mixtures in both modes of loading is the same when comparisons are made of the performance of various mixes in representative pavement structures (*3*). The controlled-strain mode of loading was selected for use in this investigation since the testing is easier to control in the laboratory (i.e., fatigue tests can easily be programmed and executed without accumulation of permanent deformation). (It is necessary to use a shift factor to translate the laboratory results to estimate field performance regardless of the mode of loading selected. The magnitude of this factor therefore can be defined according to the specific mode used.)

It was therefore necessary to develop a testing device that could be used in laboratories for routine fatigue testing. Such a device needed to provide for easier positioning and removal of specimens than existing equipment to minimize overall testing time, as well as provide more reliable results than have been obtained thus far (i.e., a lower coefficient of variation).

Rutting

Rutting (permanent deformation) in an asphalt-concrete layer is caused by a combination of densification (volume change) and shear deformations, both resulting from repetitive application of traffic loads. For properly compacted pavements, shear deformations caused primarily by large shear stresses in the upper portions of the asphalt-aggregate layers and below the edges of the passing tire are dominant. Repetitive loading in shear is considered essential to properly measure, in the laboratory, the influence of mixture composition on resistance to permanent deformation. Because the rate of permanent deformation accumulation increases rapidly at higher temperatures, laboratory testing should be conducted at the higher temperatures.

To predict permanent deformation, laboratory tests must be capable of measuring properties under states of stress that are encountered within the entire rutting zone, particularly near the pavement surface. Since there are an infinite number of states of stress, it is impossible to simulate all of them with a single test. Moreover, the nonlinear behavior of the material makes the estimation of stress conditions more difficult. Accordingly, several tests have been proposed to determine a constitutive law for asphalt concrete, which are necessary to determine these stresses for a range in traffic conditions (see paper by Sousa, Weissman et al. in this Record). To rapidly screen and evaluate the resistance of various mixtures to permanent deformation, it appears desirable to use a single test rather than the battery of tests noted above, with the requirement that it be sensitive to the most important aspects of mix behavior.

A test that appears to meet this requirement is the constant height repetitive simple shear test on cylindrical specimens, for the following reasons:

1. Specimen geometry: A specimen 0.15 m (6 in.) in diameter by 0.05 m (2 in.) high can be obtained readily from a pavement section by coring or can be produced by compaction methods proposed by SHRP (i.e., gyratory or rolling wheel compaction). The state of stress is relatively uniform for the loads applied. The magnitude of loads required to test specimens of this size is easily attained by servohydraulic loading equipment.
2. Rotation of principal axes: It is the simplest test that permits controlled rotation of principal axes of strain and stress, which are important in studying rutting.
3. Repetitively applied loads: Studies have suggested that repetitive rather than creep loading is required to define the propensity of mixes to permanent deformation. The difference has, in part, been attributed to the viscoelastic characteristics of different asphaltic binders.
4. Dilation: An important factor controlling the resistance of a mix to permanent deformation is dilation. Under shear strains, densely compacted mixes tend to dilate (as to dense sands). If dilation is constrained (as it is to some degree by the adjacent material in the pavement), confining stresses are generated. It is in part due to the development of these confining stresses that a mix derives its resistance to shear strains, and mixes with little tendency to dilate will have a higher propensity for rutting. In the constant height simple shear test the development of axial stresses is dependent on the dilatancy characteristics of the mix, with the amount of axial stress depending on the aggregate type, structure, texture, and void level. The two primary mechanisms that resist permanent deformation of a mix during the test are the stiffness of the asphalt binder and the increased stability in the aggregate

structure imparted by axial stress generated by dilation. (It is possible that mixes containing some modified binders can have additional dilation forces caused by modifier dilatancy resulting from shear strain rates.)

A well-compacted mix with a good granular aggregate will develop a high axial stress at very small shear strain levels. Poorly compacted mixes can generate similar levels of axial stresses but require much higher shear strains to do so.

Stiff binders assist in resisting permanent deformation, since the magnitude of the shear strain is less for each load application compared with mixes containing low stiffness binders, and the rate of permanent deformation accumulation is directly related to the magnitude of the shear strain.

Because both of these mechanisms contribute to the resistance of a mix to permanent deformation in the constant height simple shear test as well as in the field, evaluation of the permanent deformation resistance of an asphalt-aggregate mix is believed to be a suitable test.

The execution of a constant height repetitive simple shear test required the design and fabrication of totally new equipment. Taking into consideration that this test would be performed on a routine basis, considerable effort was made to ensure the easiest possible interface with the user.

EQUIPMENT AND TEST DESCRIPTIONS

Compaction Equipment

Two types of compaction equipment have been proposed for inclusion in the SHRP mix design specimen preparation procedure: (*a*) gyratory compaction for the majority of mix evaluations and (*b*) rolling wheel compaction for situations in which prismatic (fatigue specimens) might be required. Two slightly differing methods have evolved from the SHRP A-003A research program, one at the University of California at Berkeley (UCB) and the other at Oregon State University (*4*). The UCB rolling wheel compaction method was used to prepare all specimens for the investigation reported herein.

The UCB rolling wheel compactor, shown in Figure 1, is a commercially available single steel wheel roller weighing approximately 550 kg (1,200 lb). The roller is operable as a vibratory compactor but is only used in the static mode in the UCB method.

The compaction mold used at UCB is made of layers of plywood covered with ¼-in. steel plates for durability. The height of the one lift is .075 m (3 in.), with the length and width being adjustable. The sides of the mold have a 4:1 slope to prevent material being trapped uncompacted in the bottom corners of the slab. For compaction as a part of the mix design process a steel plate insert is used to divide the mold into three cells 0.15 by 0.60 m (6 by 24 in.).

All aggregates are assembled in 7-kg (14.5-lb) batches and mixed using a commercially available mixer. The mixed materials are placed in steel pans until heated for compaction. Each cell or "ingot" weighs approximately 20 kg (45 lb) and provides two fatigue beams and one permanent deformation specimen, or three permanent deformation specimens.

After the compacted mix has cooled overnight, specimens are obtained by coring or cutting (see Figure 2). Commercially

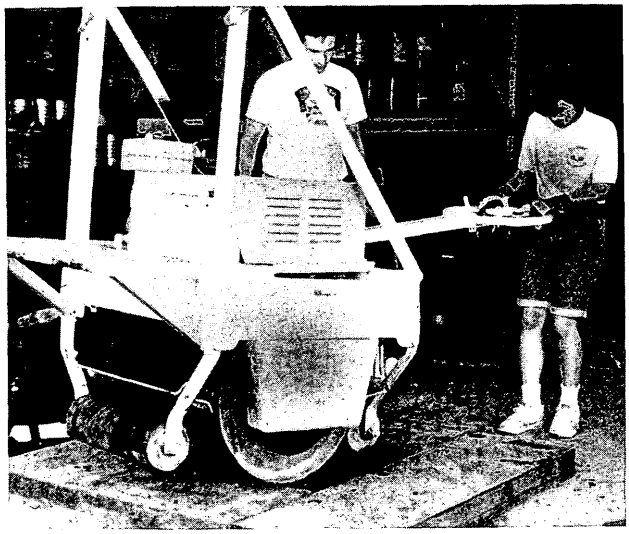

FIGURE 1 View of the mold and rolling wheel as part of the UCB compaction procedure.

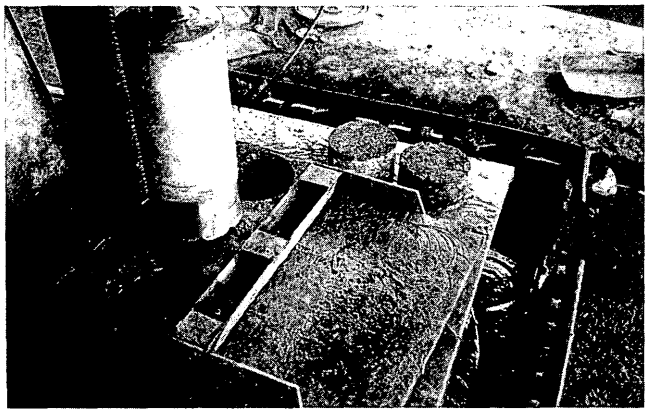

FIGURE 2 View of a small asphalt-aggregate mixture slab "ingot" being cored.

available coring machines and saws are used to obtain the cores and make the first cut on the fatigue beams. A double-blade saw developed at UCB, shown in Figure 3, is used to cut the cores and fatigue beams to their final dimensions. The use of two simultaneously operating blades results in greater precision in making the faces of the cores and beams parallel, a requirement to ensure good test results. (However, acceptable precision has been obtained using a conventional single-blade saw.)

Compaction Procedure

Rolling wheel compaction involves calculation of the mass of material to be compacted within a mold of known volume. First, the maximum specific gravity of the mixture is determined by the Rice method (ASTM D 2041). Second, the volume of the compaction mold is measured. These two values are then used with the desired air void content to determine

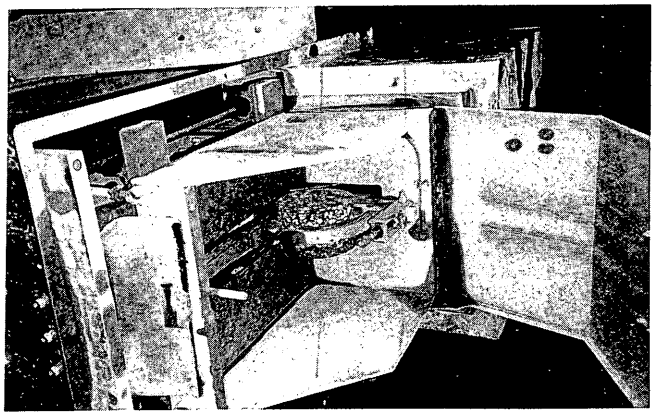

FIGURE 3 Two-blade saw used in the fabrication of cylindrical and beam specimens.

FIGURE 4 General view of the UTM constructed by James Cox and Sons, Inc.

the mass of material to be placed in the mold, rodded, and compacted to the measured volume. The compactor is passed repeatedly over the mixture until it is compacted level with the top of the mold. Several mixtures of different air void contents or different asphalt contents can be compacted simultaneously in the three cells of the mold.

Alternatives

If no fatigue beams were required for the mix design analysis, the amount of material required to produce 36 permanent deformation specimens using rolling wheel compaction would be approximately 250 kg (550 lb), with 3 days of preparation time. Approximately 2 additional days of preparation time would be required to produce the 16 fatigue beams.

In comparison, and assuming that each specimen had the correct measured air void content, approximately 200 kg (440 lb) of material would be required to produce the same 36 specimens using a gyratory compactor. The compaction time for the gyratory compactor would depend on the number of compaction molds available. The mixing, coring, cutting and air void content measurement time would be approximately the same as for rolling wheel compaction.

Testing Equipment

SHRP Project A-003A has developed and installed a newly designed materials testing system termed the Universal Testing Machine (UTM) because of its comprehensive testing capabilities and accommodation of add-on testing modules (see Figure 4). The equipment, manufactured by James Cox and Sons, Inc., Colfax, California, accommodates testing modules for permanent deformation, fatigue, and stiffness testing. A microcomputer using the ATS software (*5*) provides feedback closed-loop control to the servohydraulic system, confining pressure, test temperature, and data acquisition.

Fatigue

The beam testing module can be hydraulically clamped in the UTM for testing beam fatigue specimens, which are placed in the device and secured by electric geared motors. The fatigue module allows testing of beams with maximum dimensions of 0.05 by 0.063 by 0.38 m (2 by 2.5 by 15 in.), as shown in Figure 5.

The fatigue beam device can also be used as a stand-alone system using the same hydraulic pump and control console. This approach frees the UTM for stiffness testing (frequency and strain sweeps) and permanent deformation testing.

Specimen temperature is maintained by circulating air directly around the specimens, minimizing the time required to reach equilibrium temperature. The environmental chamber unit, an integral part of the stand-alone equipment, can provide accurate temperature control over a wide range of temperatures, −20°C to 70°C (−4°F to 158°F), with an accuracy of 0.5°C (0.9°F), as does the UTM. [Fatigue testing would normally be done at temperatures less than 30°C (85°F).]

The fatigue beam device allows the fatigue characteristics of mixes to be defined over a wide range of temperatures and loading conditions. The loading conditions include both the controlled-load and controlled-deformation modes under step, haversine, sinusoidal, or other predefined loading patterns at frequencies up to 20 Hz. In addition, this equipment can be used to define the frequency response of a material over a wide range of temperatures, frequencies, and strains in flexure.

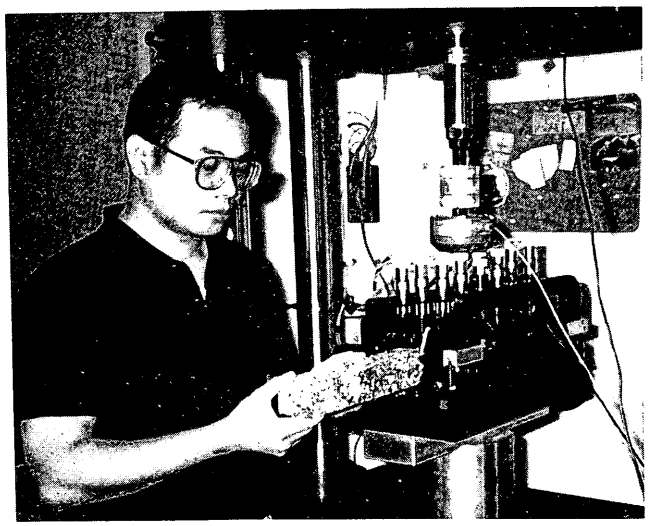

FIGURE 5 Four-point bending beam fatigue test module for the UTM.

Results from SHRP Project A-003A associated with characterization of fatigue behavior of mixtures suggest that use of the new equipment has considerably improved the reliability of results compared with those obtained with earlier devices. For example, the coefficient of variation in the fatigue data has improved from about 70 percent using the old equipment to 40 percent using this new device. Good reliability can be obtained with as few as 4 specimens, compared with the 21 to 26 reported in the literature.

Permanent Deformation

One of the developments resulting from SHRP Project A-003A is the capability of determining properties of an asphalt-concrete mixture in the simple shear mode. The device is capable of determining stiffness and permanent deformation characteristics in shear over temperatures from 0°C to 60°C (32°F to 140°F), a range in which stiffness moduli vary by three orders of magnitude.

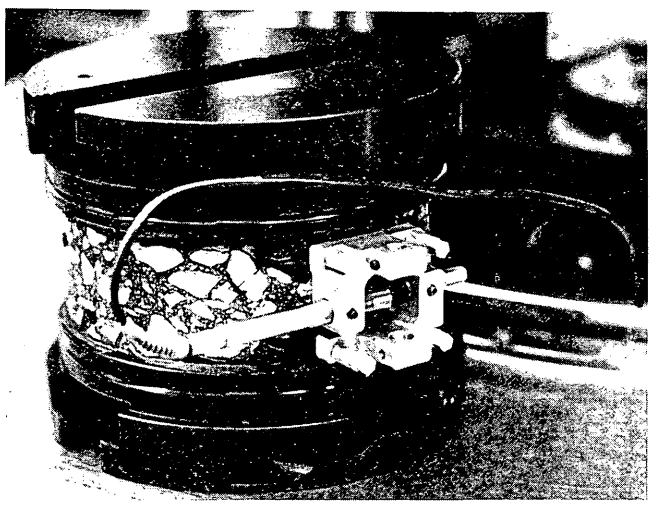

FIGURE 6 Shear specimen (6 in. in diameter by 2 in. high) with caps glued.

The testing system consists of two orthogonal tables mounted on bearings. The tables are connected to two hydraulic actuators, which are controlled using servovalves under feedback closed-loop digital algorithms. To ensure that the shear and axial forces are transmitted to the specimen, aluminum caps are glued to the parallel faces of the specimen. A gluing device developed by James Cox and Sons, Inc., is used to ensure that the faces of the caps are glued parallel. Hydraulic clamps ensure an easy interface with the user by eliminating the need to use tools to fasten the specimens to the loading tables (Figure 6).

To execute a repetitive simple shear test at constant height, the vertical actuator maintains the height of the specimen using as feedback the output of an LVDT, which measures the relative displacement between the specimen caps. The horizontal actuator applies haversine loads under control by the shear load cell. For this study a loading time of 0.1 sec and a rest period of 0.6 sec were used with a shear stress level of 69 kPa (10 psi). For this study a temperature of 60°C (140°F) was used.

EXPERIMENT DESIGN

In the Marshall and Hveem mix design methods, a fixed compaction effort is applied to mixtures with varying asphalt contents, resulting in a test program involving combinations of asphalt content and air void content, as indicated in Table 1. The two variables cannot be evaluated individually because they are dependent on each other. The disadvantage of this

TABLE 1 Typical Values of Asphalt Content and Void Content Obtained from a Mix with Watsonville Aggregate and Valley Asphalt Using the Hveem or Marshall Method of Compaction

void content %	asphalt content %						
	A	B	C	D	E	F	G
	4.00	4.25	4.75	5.25	5.75	6.25	6.50
0 (0%-3%)						Marshall 2.6	
1 (3%-4%)				Marshall 3.6	Marshall 3.2		
2 (4%-5%)							
3 (5%-6%)			Marshall 5.5				
4 (6%-8%)		Marshall 7.7					

TABLE 2 Matrix of Asphalt Content and Void Level Used in the New Mix Design Framework

void content %	asphalt content %						
	A	B	C	D	E	F	G
	3.1	4.2	4.5	4.9	5.3	5.5	6.0
0 (0%-2.5%)							
1 (2.5%-4%)			M1C 2.9	M1D 2.9		M1F 3.0	M1G 2.6
2 (5%-6%)			M2C 5.0	M2D 4.9		M2F 5.3	M2G 5.0
3 (6%-7%)							
4 (7%-9%)			M4C 7.8	M4D 7.6		M4F 8.1	M4G 8.9

type of approach is that the standard compaction method used for specimen preparation may be less or more than can be achieved by the contractor under the circumstances of the individual project. The effects on pavement performance of higher or lower degrees of compaction, and to some extent the effects of the variations in asphalt content, cannot be evaluated from the mix design. To overcome these problems a new mix design procedure is proposed in which both the asphalt content and air void content are varied, resulting in a rectangular matrix, as indicated in Table 2. This framework allows the effects of asphalt content and air void content to be evaluated individually and allows for a range of possible combinations. In this approach the compaction effort is varied for each cell (asphalt content–void content combination).

An example experiment design was carried out for this paper for two reasons: to determine (*a*) whether SHRP Project A-003A testing equipment and test procedures were sensitive to variation in mix parameters and (*b*) whether significant changes in fatigue and permanent deformation performance could be detected using the new mix design procedure when air void content and asphalt content are varied independently.

SPECIMEN FABRICATION

Materials

Aggregate RB (Watsonville granite) and an AR-4000 asphalt (asphalt AAG-1) were the materials selected for this example. The RB aggregate is completely crushed, has an angular shape, and is composed mostly of medium-grained quartz with dark areas of feldspar. It has been used in a large number of SHRP experiments.

The asphalt contents included in the design for this paper were 4.5, 4.9, 5.5, and 6.0 percent (by weight of aggregate), and the air void contents were 2 to 4.5 percent, 5 to 7 percent, and 8 to 10 percent [measured using parafilm (*6*)] (see Table 2). The materials were mixed at 137°C (280°F) and compacted at 116°C (240°F).

Three shear specimens 0.10 m in diameter by 0.05 m high (4 in. by 2 in.) were prepared for each cell using the UCB rolling wheel compaction method. Three or four fatigue beams were prepared for four of the cells around the perimeter of the matrix. [Shear specimens 0.10 m (4 in.) in diameter were used because the permanent deformation testing machine was still being fabricated for the proposed standard specimens 0.15 m (6 in.) in diameter.]

Material Quantities

Assuming that all of the specimens compacted for each of the 12 cells of the design matrix had the target air void content, approximately 420 kg (900 lb) of mix would be required to provide the 36 permanent deformation specimens [0.15 m (6 in.) in diameter] and 16 fatigue beams. In practice, some small adjustments may be required in the weight-volume calculations to achieve the desired air void content of some cells. The amount of adjustment required is reduced as experience is gained with a given aggregate.

Duration

For this investigation specimens were prepared in only two of the three cells in the compaction mold to prevent material passing from one cell to another (a slightly greater distance between cells in the mold will eliminate this problem). Thus, using two molds and allowing for overnight cooling, all specimens could be compacted in 5 days, assuming no adjustments were required. Coring and cutting require approximately 1 hr, and air void content measurement using parafilm requires approximately 30 min for each cell.

TEST RESULTS

Air Void Content

The air void contents for the specimens used in this study measured using parafilm and the maximum effective specific gravity (ASTM D 2041) are given in Table 2. The use of parafilm, or some other suitable method, is required for the high air void content specimens included in the design matrix. Otherwise, with water entry and the interconnection of pores in these specimens, the weight-in-water measurement for bulk specific gravity would be meaningless.

Fatigue

The fatigue characteristics of asphalt mixtures are usually expressed as relationships between the initial stress or strain and number of load repetitions to failure. An energy approach—based on a relationship between the cumulative dissipated energy and the number of cycles to failure—has also been used to characterize fatigue behavior of asphalt mixtures. Conventionally, in order to establish these relationships repeated flexure, direct tension or diametral tests are performed at several stress or strain levels requiring up to 36 specimens and 3 to 4 weeks of testing time.

The new fatigue device enables characterization of any given mix within a relatively short time and requires fewer specimens without sacrificing the reliability of the results. With this short procedure, fatigue tests would be performed at a given temperature and at relatively higher frequency (10 Hz) over a range of strain levels (strain levels that will give a fatigue life varying between 5,000 and 500,000 cycles), permitting fatigue response to be developed. Interpretation of the results can be established by either the conventional method (i.e., log-strain versus log-cycles to failure relationship) or by use of dissipated energy expressed in terms of log-initial dissipated versus log-cycles to failure or log-cumulative dissipated energy versus log-cycles to failure.

For typical mixtures containing conventional asphalt binders, this procedure requires approximately 24 hr to ascertain whether a mix is suitable for the intended pavement application. It is conducted by testing a minimum of four beam specimens in the controlled-strain mode of loading at 10 Hz. For atypical mixtures (e.g., mixtures with gap-graded aggregates) or mixtures containing modified binders, full fatigue testing with more than four specimens is recommended.

The short test procedure is as follows:

1. Conduct a test at a fairly high strain level such that the specimen will last for 5,000 to 10,000 cycles. For example, one could start a test at a strain level in the range 800×10^{-6} to 1000×10^{-6} in./in. and determine the life. If the life is higher than 10,000 cycles, increase the strain level for the second specimen. If it is lower, reduce the strain level. Two tests at these strains will take about 2 hr.
2. From the first two tests a crude estimate of the slope of the log-strain versus log-cycles relation can be determined. Use this relationship to estimate the strain level that will provide a fatigue life around 100,000 cycles. This test will take about 4 hr.
3. Reestablish the log-strain versus log-cycles relationship from Step 2 and estimate the strain required for the test to fail at 400,000 to 500,000 cycles. This test will take 13 to 15 hr. However, this long test can be done at the end of the day (about 5 p.m. or earlier if the other three tests have been completed) and be left to run overnight. The specimen will have reached its fatigue life by the next morning.

Figures 7 to 9 show the results of the fatigue tests for mixes containing 4.5 and 6.0 percent asphalt content (by weight of aggregate) and different air void contents. Figure 7 shows the plot of strain versus number of cycles, Figure 8 shows the initial dissipated energy per cycle versus the number of cycles, and Figure 9 shows the cumulative dissipated energy (*7*) versus the number of cycles. Table 3 compares fatigue life for these mixtures at the 400×10^{-6} in./in. strain level. It can be seen that by increasing the asphalt content from 4.5 to 6.0 percent, the fatigue life increased by about 70 percent. Increasing the air void content from the range of 4 to 5 percent to 7 to 9 percent resulted in a reduction of fatigue life of about 40 percent.

The fatigue test results illustrate that the fatigue performance of mixes can be evaluated in a relatively short time period using the improved fatigue equipment and procedure without compromising the reliability of the test results.

Permanent Deformation

Simple shear repetitive load tests wherein specimen height was maintained constant were performed, and for each of the tests the number of load repetitions to reach 3 percent permanent shear strain was computed. A plot of the accumulation of permanent deformation with load repetitions is shown in Figure 10 for some of the cells of the new mix design matrix. The slopes and intercepts of the lines vary with air void content and asphalt content. The best performance was obtained between cells M1D and M1F, indicating an optimum asphalt content between 4.9 and 5.5 percent by weight of aggregate. Interestingly, 4.9 percent was the asphalt content previously obtained from the Hveem mix design method for this aggregate and asphalt, and 5.5 percent was the asphalt content obtained from the Marshall method.

A three-dimensional plot of the variation of repetitions to reach 3 percent permanent shear strain with air void content and asphalt content is shown in Figure 11. The air void content is an important mix variable in the design process. Asphalt content plays a role in optimizing that performance not only by the viscosity level at a given test temperature and rate of loading, but also during specimen fabrication (*2*). These results show that the constant height repetitive simple shear test is sensitive to mixture variables and that asphalt content and air void content influence the results in accordance with experience. It is particularly interesting to note the sharp decease in resistance to permanent deformation for mixes with very low void contents.

Recognizing that the results of the constant height repetitive simple shear test suggest an optimum asphalt content similar to that which would be obtained from the Hveem method in this instance, one could ask, Why use this more comprehensive procedure? There are cases in which the Hveem stabi-

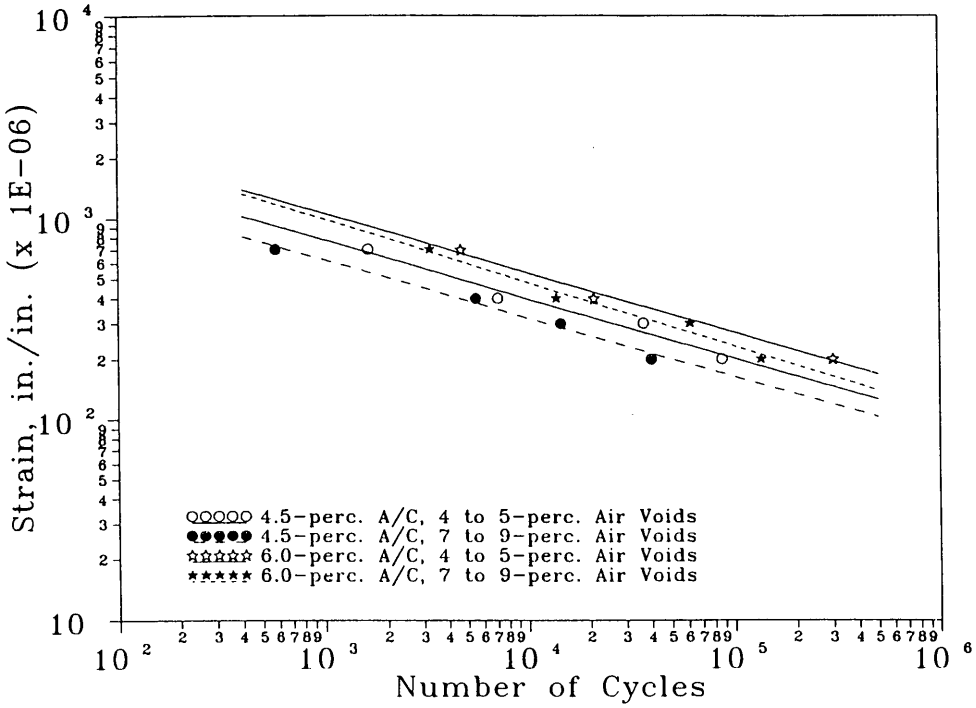

FIGURE 7 Comparison of fatigue life in terms of strain level versus the number of cycles to failure for four asphalt-aggregate mixtures.

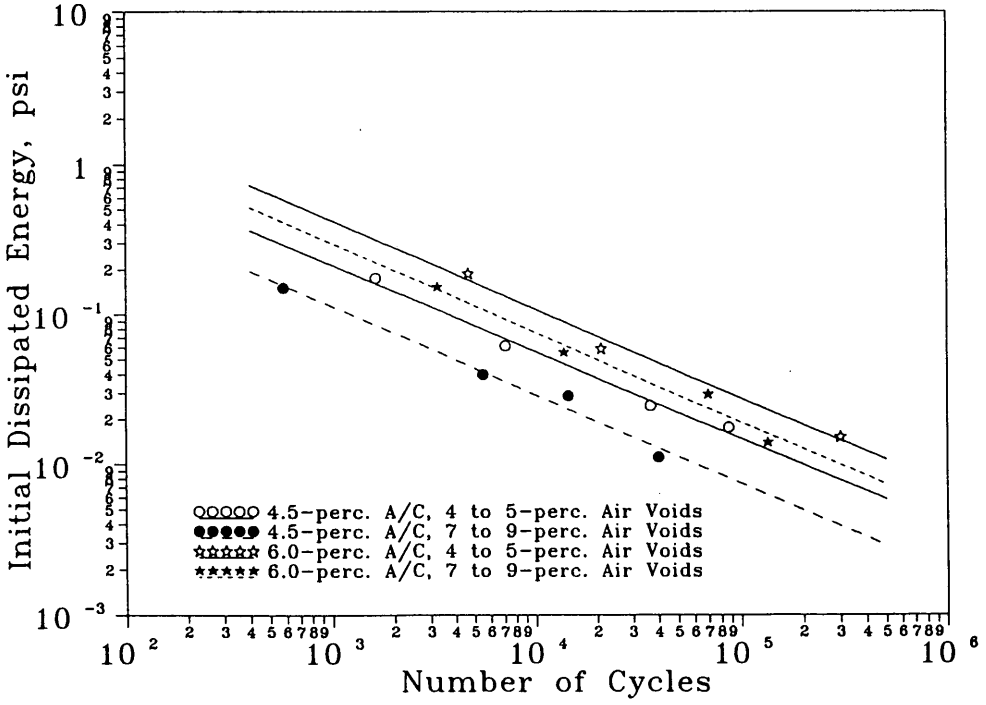

FIGURE 8 Comparison of fatigue life in terms of initial dissipated energy versus the number of cycles for four asphalt-aggregate mixtures.

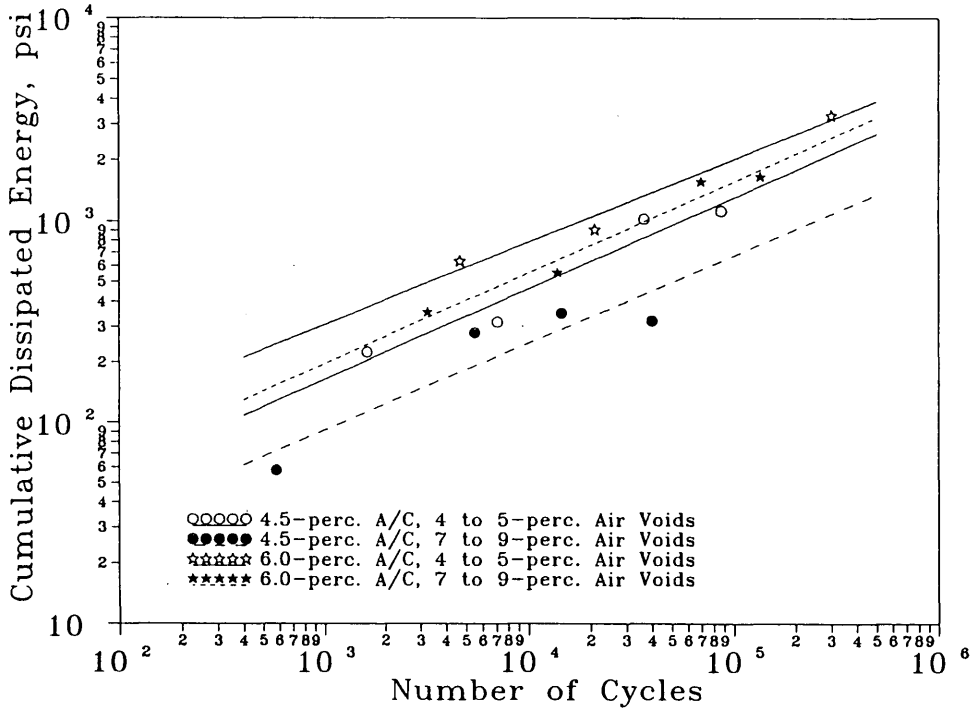

FIGURE 9 Comparison of fatigue life in terms of cumulative dissipated energy versus the number of cycles for four asphalt-aggregate mixtures.

TABLE 3 Fatigue Life (Number of Cycles to Failure) at 400 μin./in. Strain Level

		Air Voids (%)		Percentage Diff.
		4-5	7-9	
Asphalt Content (% by wt. of mix)	4.5	9700	4500	54
	6.0	26500	18100	32
Percentage Diff.		63	75	

Note: percentage difference is the difference expressed as a percentage of larger value

lometer test has shown no difference in performance when modifiers have been used, while the constant height repetitive simple shear test produces results that follow engineering expectations (*2,8,9*). This test can also be used for evaluating large stone mixtures, since specimens 0.20 m (8 in.) in diameter by 0.076 m (3 in.) high can be accommodated. Another major advantage of the new procedure is the capability of obtaining properties in engineering units, which can in turn be used in performance prediction models.

INTEGRATION OF MIX DESIGN PARAMETERS INTO STRUCTURAL DESIGN AND PERFORMANCE ESTIMATION

Figure 12 shows a framework for a mix design and analysis system that has been suggested by SHRP researchers (*10*). Essentially the procedure requires that the specific distress mode under consideration—fatigue, rutting, or thermal cracking—be evaluated using the results of the accelerated performance test within the context of a specific pavement section, environment, and anticipated traffic loading.

To examine the propensity for fatigue cracking, data like those shown in Figures 7 through 9 can be used in a performance prediction model (such as those being developed as part of SHRP Project A-005) that is analytically based. If the results of the computations show that the mix exhibits cracking before the expected performance life is obtained, either the thickness of the layer can be increased or the mix can be redesigned.

In the case of rutting, results of the accelerated performance test (e.g., constant height repetitive simple shear test) would initially be used within the framework of an abridged analysis system to ensure that the estimated rut depth does not exceed

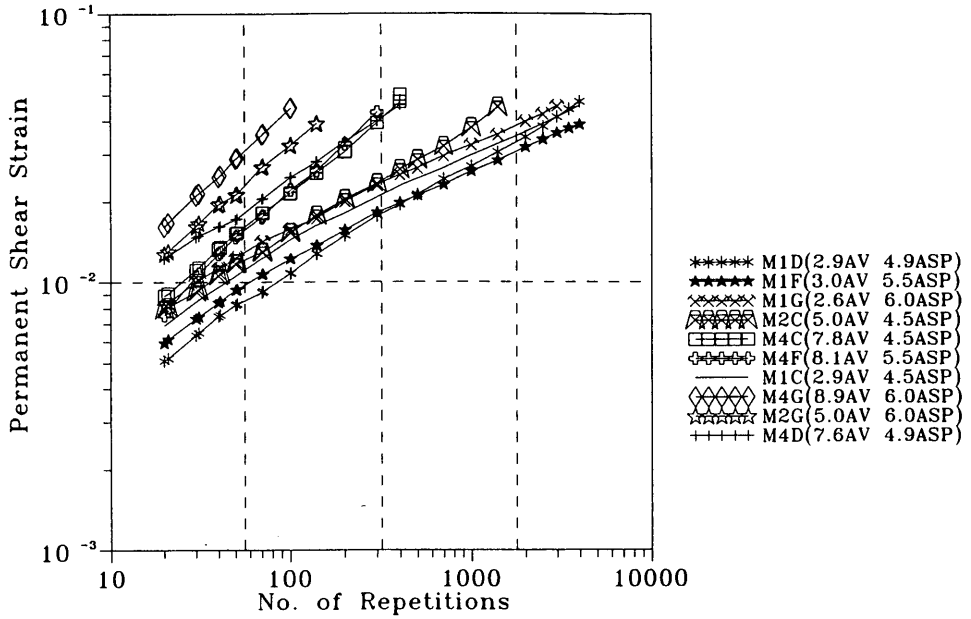

FIGURE 10 Variation of permanent shear strain with the number of load applications for some of the cells in the new mix design framework.

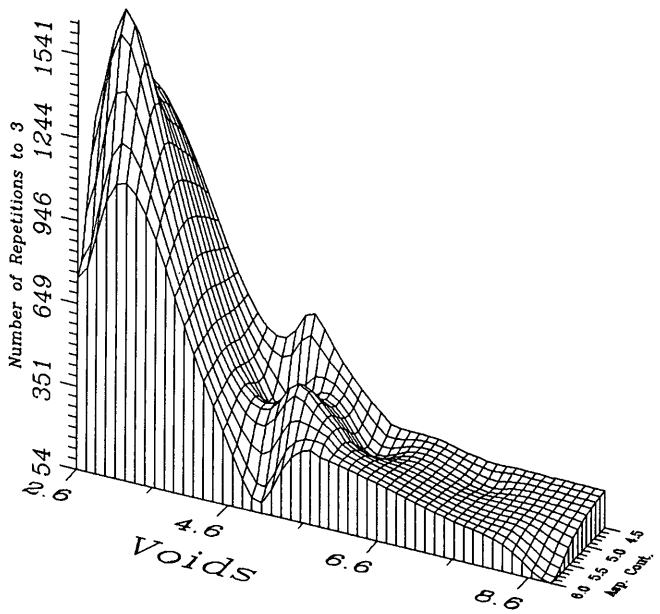

FIGURE 11 Variation of the number of repetitions to reach 3 percent permanent shear strain with asphalt and void content (maximum at 3.0 void content and 4.9 asphalt content).

some level of rutting associated with the specific pavement conditions. [A more comprehensive rutting prediction procedure has also been proposed that includes the simple shear test (see paper by Sousa, Weissman et al. in this Record). This requires a more detailed test program and analysis procedure.] If the rut depth is larger than allowed, the mix must be redesigned.

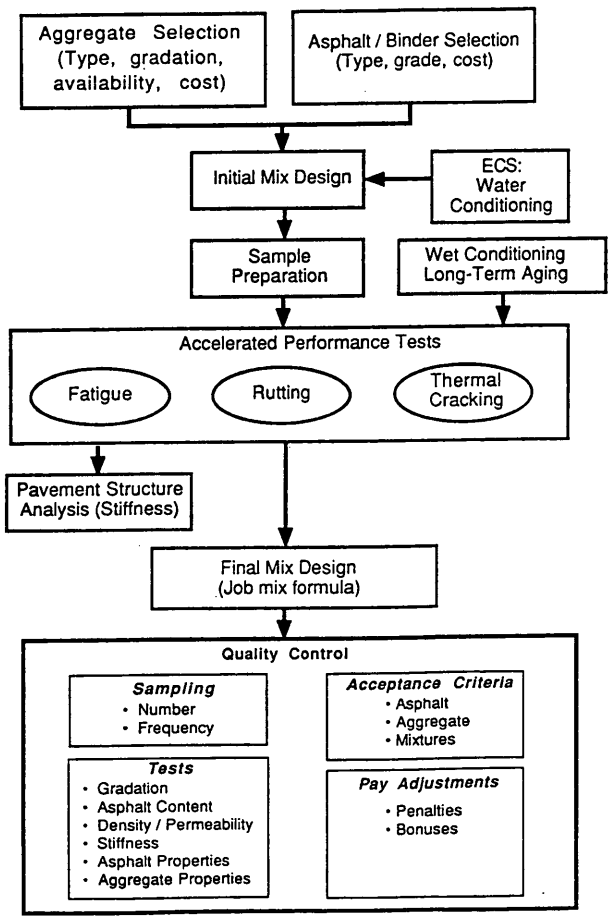

FIGURE 12 Framework for mixture design and analysis system.

In general, the mix design approach described herein emphasizes not only the comprehensive evaluation of mix properties using the accelerated performance tests developed as part of the SHRP research efforts but also the importance of being able to use these results within a suitable analysis framework to estimate performance.

SUMMARY

This paper presents some of the equipment and procedures recommended by the SHRP A-003A contractor for mix evaluation. As part of this research effort, the rolling wheel compactor is recommended for fabrication of asphalt concrete mixes in the laboratory, since beams and cylinders can be produced with the same equipment and at the same time in an efficient manner in terms of time and material quantities.

To characterize the fatigue behavior of asphalt concrete mixtures, a third-point bending fatigue test operating in the controlled-strain mode is recommended. New equipment developed to perform this test, together with a shortened procedure, facilitates the determination of a fatigue relationship at a given temperature in about 24 hr.

To characterize the permanent deformation characteristics of mixes, several tests have been developed. The test selected for an abridged procedure for mix evaluation is the constant height repetitive simple shear test. This test permits the determination of mix characteristics to assess both the relative performance of various candidate mixes and the development of permanent shear deformation in situ.

A new mix design procedure is presented in which air void content and asphalt content are varied independently. To evaluate the sensitivity of the new equipment and procedures to the mix design variables, a 12-cell mix evaluation was undertaken. The proposed design procedure provides more detailed information compared with conventional mix design methodologies. The tests presented discriminated among the different test variables. Moreover, it provides sufficient data so that the influence of expected field compaction conditions, as well as subsequent permanent shear deformation caused by traffic, can be assessed. Finally, the methodology provides information that can be used in prediction models, from which decisions regarding in situ performance can be made.

ACKNOWLEDGMENTS

The work reported herein has been conducted as a part of SHRP Project A-003A. SHRP, a unit of the National Research Council, was authorized by Section 128 of the Surface Transportation and Uniform Relocation Assistance Act of 1987. This project is titled Performance-Related Testing and Measuring of Asphalt-Aggregate Interactions and Mixtures and is being conducted by the Institute of Transportation Studies, University of California, Berkeley. Carl L. Monismith is Principal Investigator.

REFERENCES

1. J. B. Sousa, J. Deacon, and C. L. Monismith. Effects of Laboratory Compaction Method on Permanent Deformation Characteristics of Asphalt Concrete Mixtures. *Asphalt Paving Technology*, Vol. 60, 1991, pp. 533–585.
2. J. Harvey and C. L. Monismith. Effects of Laboratory Asphalt Concrete Specimen Preparation Variables on Fatigue and Permanent Deformation Test Results Using SHRP-A-003A Testing Equipment. Presented at the 72nd Annual Meeting of the Transportation Research Board, Washington, D.C., 1993.
3. A. A. Tayebali, J. A. Deacon, J. S. Coplantz, and C. L. Monismith. Modeling Fatigue Response of Asphalt-Aggregate Mixtures. Presented at the Annual Meeting of the Association of Asphalt Paving Technologists, Austin, Tex., March 1993.
4. *Standard Practice for Preparation of Bituminous Mixture Test Specimens by Means of Rolling Wheel Compactor*. Interim Proposed Standard Practice Specification. SHRP A003-A, Washington, D.C., May 12, 1992.
5. J. B. Sousa and C. K. Chan. Computer Applications in the UCB Geotechnical Laboratories. *ASCE Geotechnical Engineering Congress,* Vol. 1. Geotechnical Special Publication 27, 1991, pp. 531–543.
6. J. Harvey, J. Sousa, J. Deacon, and C. L. Monismith. Effects of Sample Preparation and Air-Void Measurement on Asphalt Concrete Properties. In *Transportation Research Record 1317*, TRB, National Research Council, Washington, D.C., 1991, pp. 61–67.
7. A. Tayebali, J. Deacon, J. Coplantz, J. Harvey, and C. L. Monismith. *Interim Report on Fatigue Response of Asphalt-Aggregate Mixtures*. TM-UCB-A003A-92-1. University of California at Berkeley, Berkeley, 1992.
8. A. Tayebali. *Influence of Rheological Properties of Modified Asphalt Binders on the Load Deformation Characteristics of the Binder-Aggregate Mixtures*. Ph.D. thesis. University of California at Berkeley, Berkeley, 1990.
9. A. Tanco. *Permanent Deformation Response of Conventional and Modified Asphalt-Aggregate Mixtures Under Simple and Compound Shear Loading Conditions*. Ph.D. thesis. University of California at Berkeley, Berkeley, 1992.
10. C. L. Monismith, R. G. Hicks, and F. N. Finn. Accelerated Load Tests for Asphalt-Aggregate Mixtures and Their Role in AAMAS. *Asphalt Paving Technology*, Vol. 60, 1991, pp. 586–631.

Nonlinear Elastic Viscous with Damage Model To Predict Permanent Deformation of Asphalt Concrete Mixes

JORGE SOUSA, SHMUEL L. WEISSMAN, JEROME L. SACKMAN, AND CARL L. MONISMITH

The development and use of a nonlinear elastic, viscous with damage model are discussed. The model is proposed as a constitutive relation for asphalt concrete mixes to permit prediction of permanent deformation. The model is intended to capture the macrobehavior of mixes, including (*a*) the dilatancy observed when the mix is subjected to shear strains, (*b*) the increase of effective shear modulus under increased hydrostatic pressure, (*c*) the significant variation of behavior with changes in temperature and rates of loading, and (*d*) the residual accumulation of permanent deformation under repetitive loading. This model has been developed as part of the Strategic Highway Research Program A-003A efforts to characterize the permanent deformation characteristics of asphalt-aggregate mixes. A new series of tests proposed for the determination of the material properties is presented, modeled and observed responses from a simple validation test are compared, and the use of the model to predict permanent deformation response in an asphalt concrete pavement section is illustrated.

This paper presents the results of a comprehensive investigation to characterize the permanent deformation behavior of asphalt concrete mixes as part of the Strategic Highway Research Program (SHRP) A-003A research program.

Research (*1–4*) has indicated that asphalt concrete demonstrates the following characteristics when subjected to rate-dependent loading over a range of temperatures: (*a*) it dilates under shear loading (i.e., there is a coupling between volumetric and deviatoric behaviors), (*b*) its effective shear modulus increases with increase in hydrostatic pressure, (*c*) it is temperature dependent, (*d*) it is rate dependent, (*e*) volumetric creep is negligible, and (*f*) residual permanent deformation is observed after the load has been removed (i.e., the material exhibits inelastic behavior).

Although most of these observations are not new, very little attention has been directed to the coupling between volumetric and deviatoric behavior and to the importance of deviatoric stresses. However, recent studies (*1*) suggest that permanent deformation is greatest in areas of high shear (near the edge of the tires). For this reason the present study emphasizes this coupling, which plays a significant role in the proposed model.

J. Sousa and C. L. Monismith, Institute of Transportation Studies, University of California at Berkeley, 1301 S. 46th St., Bldg. 452, Richmond, Calif. 94804. S. L. Weissman, Symplectic Engineering, 1350 Solano Avenue, No. 26, Albany, Calif. 94706. J. L. Sackman, Civil Engineering Department, University of California at Berkeley, 733 Davis Hall, Berkeley, Calif. 94720.

In the development of the model, the fact that dilatancy and hardening under hydrostatic pressure are typical of densely compacted aggregates was taken into the consideration. It was also recognized that aggregate behavior is not sensitive to temperature or loading rate, whereas asphalt/binder behavior is very sensitive to both temperature and rate of loading.

In the development of a comprehensive procedure to determine rutting in pavement sections, three aspects have to be considered:

1. Development and selection of a constitutive law that embodies the different aspects of the observed behavior of asphalt-aggregate mixes—recognizing that these mixes are not isotropic linear elastic materials (which can be fully characterized with a Young's modulus and a Poisson's ratio), the definition of a constitutive relationship incorporating the most important aspects of actual mix response is imperative;
2. Development and standardization of new test procedures to determine requisite parameters for the constitutive relationship—for linear elastic materials, determination of a Young's modulus and Poisson's ratio can be accomplished with a simple extension or compression test. On the other hand, determination of material parameters to define the responses of more complex materials requires several tests; and
3. Development of a finite element computer program that permits solution of boundary value problems using the constitutive relationship proposed for the asphalt-aggregate mix.

In this paper three aspects will be discussed: presentation of a constitutive relationship for asphalt-aggregate mixes together with a series of tests required to define the material parameters, preliminary validation of the constitutive relationship by comparing observed and predicted responses from a test other than those used to define the material properties, and use of the constitutive relationship to predict rutting propensity in an asphalt concrete pavement section.

PROPOSED CONSTITUTIVE LAW FOR ASPHALT CONCRETE

A nonlinear elastic viscous with damage constitutive relationship is proposed to represent the response of asphalt-aggregate mixes to stresses leading to permanent deformation. The model consists of a number of three-dimensional

Maxwell elements in parallel; each Maxwell element is composed of a nonlinear spring and dashpot. The dilatancy effect and the increase in effective shear modulus under hydrostatic pressure are due to the aggregate skeleton, whereas temperature and rate dependency are associated with the asphalt binder. Thus dilatancy and hardening are associated with the spring, and temperature and rate dependency are associated with the dashpot.

Consider first the spring in a typical Maxwell element. To achieve the desired coupling and hardening, the strain energy function is expanded in a Taylor series in terms of the strain invariants (i.e., the material is assumed to be initially isotropic) with truncation of terms of an order greater than four. Thus, the strain energy function is approximately (*5,6*)

$$W(\varepsilon^e) = \frac{1}{2} C_1 I_1^2 + C_2 I_2 + \frac{1}{3} C_3 I_1^3 + C_4 I_1 I_2 + C_5 I_3 + \frac{1}{4} C_6 I_1^4 + C_7 I_1^2 I_2 + C_8 I_1 I_3 + \frac{1}{2} C_9 I_2 \quad (1)$$

where

$C_1, C_2, \ldots C_9$ = material constants,
ε^e = elastic strain tensor, and
I_1, I_2, and I_3 = the elastic strain tensor invariants.

The term ε^e is a function of the total strain, ε, and the viscous (i.e., inelastic) strain, ε^i, given by (*5*)

$$\varepsilon^e = \varepsilon - \varepsilon^i \quad (2)$$

The stress tensor, ω, is defined as

$$\sigma = \delta_\varepsilon W(\varepsilon^e) \quad (3)$$

Second, consider the dashpot in a typical Maxwell element. In this case, the equilibrium equation is a rate equation of the following form (*7*):

$$\dot{\varepsilon}^i = \left(1 + \frac{q^n}{\alpha^n}\right) \eta^{-1} \delta_\varepsilon W(\varepsilon^e) \quad (4a)$$

or

$$\dot{\varepsilon}^i = \left(1 - \frac{q^n}{\alpha^n}\right)^{-1} \eta^{-1} \delta_\varepsilon W(\varepsilon^e) \quad (4b)$$

where α and n are material constants. The internal (damage) variable, q, is defined as

$$q = \max_{0 \le \tau \le t} (q_\tau) \quad (5)$$

and q_τ is given by

$$q_\tau = (\varepsilon^i : \varepsilon^i)_\tau^{1/2} \quad (6a)$$

when Equation 4b is used, and by

$$q_\tau = (\dot{\varepsilon}^i : \eta : \dot{\varepsilon}^i)_\tau^{1/2} \quad (6b)$$

when Equation 4a is used. In this expression η, the initial viscosity, is a Rank 4 tensor given in component form by

$$\eta_{ijkl} = \lambda^\nu \delta_{ij} \delta_{kl} + \mu^\nu (\delta_{ik} \delta_{jl} + \delta_{il} \delta_{jk}) \quad (7)$$

where λ^ν and μ^ν are the temperature-dependent material constants.

The thermorheologically simple nature of the asphalt concrete at small strains can be accommodated in the model if η is assumed to be

$$\eta = \eta_0 e^{\frac{C_T(T - T_0)}{T_0 T}} \quad (8)$$

where C_T is a material constant, T and T_0 are the current and reference temperature (in degrees Kelvin), respectively, and η_0 is given by Equation 7 with λ^ν and μ^ν evaluated at the reference temperature.

The two models proposed for Equation 4 differ in the definition of the "damage" parameter q (i.e., they differ in the evolution of the viscosity). The first model is based on the maximum attained strain, whereas the second is based on the maximum attained inelastic strain rate.

The global model is obtained when a number of nonlinear Maxwell elements are assembled in parallel. Note that all Maxwell elements share the same total strain, ε, whereas ε^e and ε^i are evaluated independently for each Maxwell element.

DETERMINATION OF MATERIAL PROPERTIES AND MODEL VALIDATION

Figure 1 shows the framework for permanent deformation prediction using the proposed constitutive equation. The de-

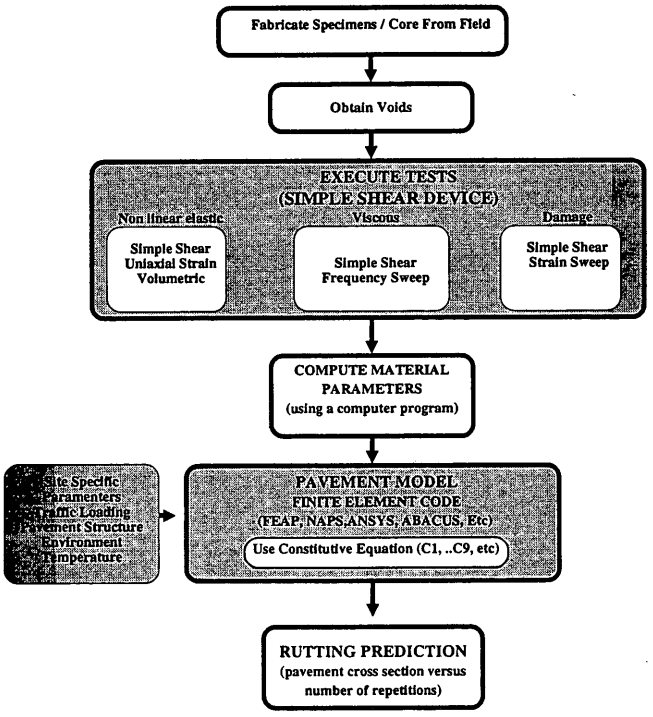

FIGURE 1 Framework to estimate permanent deformation in the asphalt concrete layer of a pavement structure.

termination of the material parameters is one of the first steps in the proposed procedure. It is accomplished by testing four cylindrical specimens 15 cm (6 in.) in diameter by 5 cm (2 in.) high.

With a finite element program capable of incorporating the appropriate constitutive equation for the asphalt concrete material and also constitutive equations for the other materials making up a pavement structure, predictions of rut depth can be made for given traffic and environment conditions.

To illustrate the efficacy of the procedure for permanent deformation determination to discriminate among different asphalt-aggregate combinations, mixes were selected containing Aggregates RB and RL and Asphalts AAK-1 and AAG-1 (materials from the SHRP Materials Reference Library). These mixes included

- V0W0—Aggregate RB, Asphalt AAG-1, low asphalt content, low void content;
- B0W0—Aggregate RB, Asphalt AAK-1, low asphalt content, low void content;
- B1T1—Aggregate RL, Asphalt AAK-1, high asphalt content, high void content; and
- V0T1—Aggregate RL, Asphalt AAG-1, low asphalt content, high void content.

Wheel-tracking tests had been performed by SWK/Nottingham on these mixes. Ranking in order of increasing normalized rutting rate was as follows (*8*): V0W0 < B0W0 < V0T1 < B1T1.

To permit comparisons, the following steps were followed:

1. The nonlinear elastic parameters were determined at 4°C (to minimize viscous effects).
2. The viscous parameters over a range of temperatures (4°C, 20°C, and 40°C) and frequencies (0.01, 0.02, 0.05, 0.1, 0.2, 0.5, 1.0, 2.0, 5.0, and 10 Hz) were determined.
3. The damage parameters were determined.
4. Using the Finite Element Analysis Program (FEAP) developed by Robert Taylor of the Civil Engineering Department at the University of California at Berkeley, the response of the mix in a repetitive simple shear test at 40°C, using 0.1 sec loading time and a time interval between load applications of 0.6 sec was simulated.
5. A repetitive simple shear test was performed at 40°C for the same conditions as in Step 4.
6. Observed and predicted behaviors were compared.
7. Possible causes of discrepancies were evaluated and corrections needed in the model or in the determination of the material parameters were defined.

Evaluation of the model has been accomplished using a test that was not used to obtain the material parameters and that is of a totally different nature from the tests used to determine the material properties (i.e., the validation test was a repetitive test, whereas the tests used to obtain material properties were either constant rate of loading or sinusoidal in nature). It is important not only to be able to match performance at different stress levels but also at varying rates of loading and unloading.

Specimens for testing were fabricated according to the University of California at Berkeley procedure for rolling wheel compaction (*9*). All specimens of one mix were obtained from the same slab by coring. The cores, 15 cm (6 in.) in diameter by 5 cm (2.5 in.) high, were stored at 20°C before testing.

Determination of Nonlinear Elastic Parameters

To determine the nonlinear elastic parameters, the requisite tests were performed at a temperature of 4°C, which was selected to minimize the viscous response of the mixes. Comparisons between measured and computed results are not included for the mix designated V1T0, since not all of the tests were completed.

Simple Shear Constant Height Test

This test permits the direct determination of three of the nine parameters that define the nonlinear elastic response (i.e., C_2, C_4, and C_9). The test required the use of two hydraulic actuators—one to apply the shear stress to the specimen at a rate of 10 psi/sec; the other, under feedback from an LVDT measuring the relative displacement between the specimen caps, to ensure that constant height is maintained in the specimen (within ±0.00005 in.).

The analysis is based on the assumption that a pure shear state of strain is obtained when $\varepsilon_{12} = \varepsilon_{21} = \varepsilon_0$ and all other strain components are zero. For this situation

$$\sigma_{11} = -C_4 \varepsilon_0^2 \tag{9}$$

$$\sigma_{12} = -C_2 \varepsilon_0 - C_9 \varepsilon_0^3 \tag{10}$$

and

$$\sigma_{33} = -(C_4 + C_5)\varepsilon_0^2 \tag{11}$$

where σ_{11} is the axial stress developed to maintain the height constant and σ_{12} is the shear stress imposed. Unfortunately, σ_{33} cannot be measured; thus, C_5 cannot be directly obtained from the test.

The data in Figure 2 show a typical variation of shear strain with shear stress obtained from a test and that predicted from the model (assuming that the measurements contained no viscous response).

Figure 3 shows the typical variation of axial stresses developed during a test as a function of the shear strain for each of the mixes tested. The most significant aspect of these results is that dilation occurred at 4°C, as evidenced by the compressive stresses in the axial direction necessary to maintain constant height. This suggests that the dilation is strain-related and is associated with the granular structure of dense mixes. Its influence can normally be neglected at low temperatures because the asphalt concrete mix is so stiff that conventional traffic loads are not of sufficient magnitude to generate strains large enough to mobilize the dilation component. At higher temperatures, however, strains sufficient to allow dilation to occur become an important aspect in determining the permanent deformation resistance of a mix.

Figure 3 suggests that the model "captures" the dilation observed in the testing.

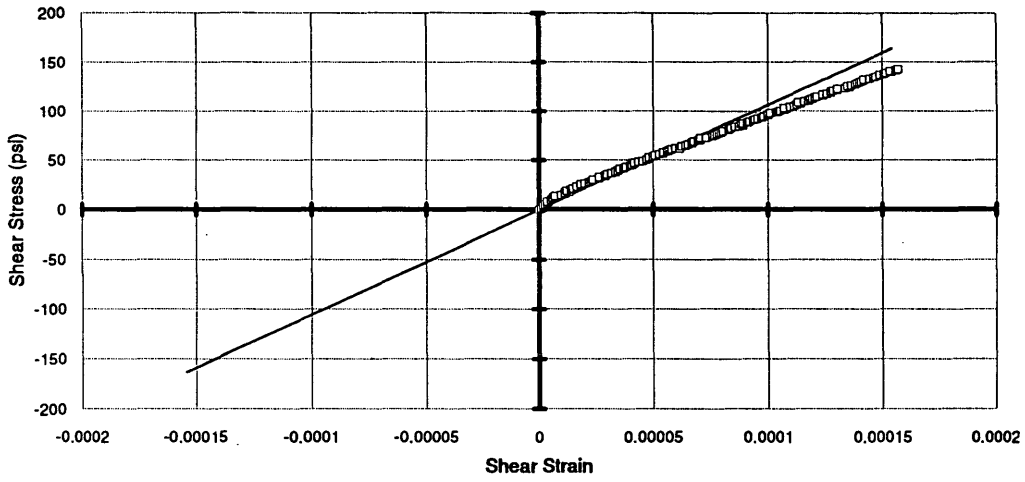

FIGURE 2 Variation of shear stress with shear strain for simple shear tests at 4°C and 10 psi/sec ramping shear stress (model and actual data) (Aggregate RB, Asphalt AAG-1) (V0W0).

Uniaxial Strain Test

The uniaxial strain test permits the direct determination of C_1, C_3, C_6, and C_7 and also provides a check for C_2 and C_4 (obtained from the constant height simple shear test) since the only nonzero strain component is $\varepsilon_{11} = \varepsilon_0$. This assumes that there is no viscous deformation contributing to the response. (If there is viscous deformation, the constant height simple shear and uniaxial strain tests must be executed at the same rate.) In this test the vertical actuator is programmed to ramp the deviatoric axial stress on the sample at a rate of 10 psi/sec while pneumatic servovalves control the confining pressure under feedback from an LVDT measuring the change in perimeter of the specimen. The pneumatic servovalves are programmed to maintain a constant perimeter; thus the change in confining pressure at each instant is just enough to compensate for the bulging of the specimen, ensuring a uniaxial state of strain.

The state of stress is given by

$$\sigma_{11} = C_1 \varepsilon_0 + C_3 \varepsilon_0^2 + C_6 \varepsilon_0^3 \tag{12}$$

and

$$\sigma_{22} = (C_1 + C_2)\varepsilon_0 + (C_3 + C_4)\varepsilon_0^2 + (C_6 + C_7)\varepsilon_0^3 \tag{13}$$

where σ_{11} is the axial stress, σ_{22} is the confining stress, and ε_0 is the axial strain; all other stress components are zero.

Figures 4 and 5 show the typical response of one of the mixes and the best fit obtained with the model parameters.

Figure 6 compares the variation of axial stress with axial strain for the three mixes. Figure 7 compares the variation of the confining stress with the axial strain. In Figure 7 it is interesting to compare the relative performance of the mixes. While the V0W0 mix (Aggregate RB, Asphalt AAG-1, low asphalt content, low voids) only required a confining stress of 17 psi to ensure a state of uniaxial strain, the B1T1 mix (Aggregate RL, Asphalt AAK-1, high asphalt content, high voids) required about 47 psi, even though both were subjected to the same axial stress—approximately 120 psi. This indicated that Mix B1T1 is less stable than Mix V0W0. These results are significant in that they demonstrate that the uniaxial strain test is capable of differentiating between mixes of different stabilities. The Hveem stabilometer would rank the mixes in the same order since that test is similar to the uniaxial strain test.

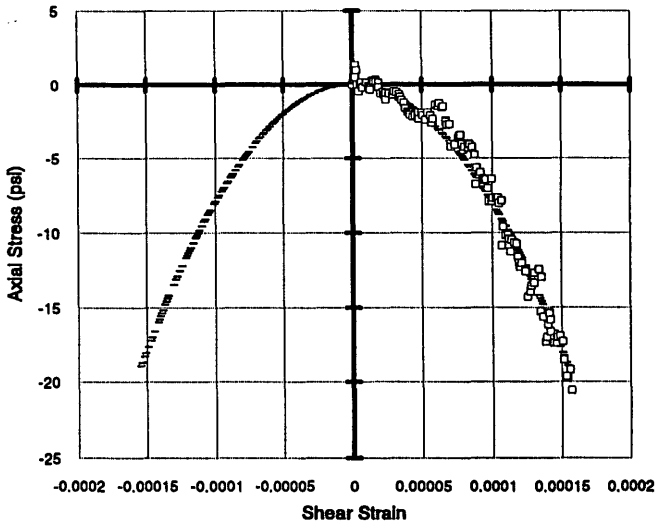

FIGURE 3 Variation of axial stress with shear strain for simple shear tests at 4°C and 10 psi/sec ramping shear stress (model and actual data) (Aggregate RB, Asphalt AAG-1) (V0W0).

Volumetric Test

Results of the volumetric test, together with the constants obtained from the simple shear and uniaxial strain tests, permit the two remaining constants, C_5 and C_8, to be determined. A check of the sum of constants C_1 and C_2 also can be obtained

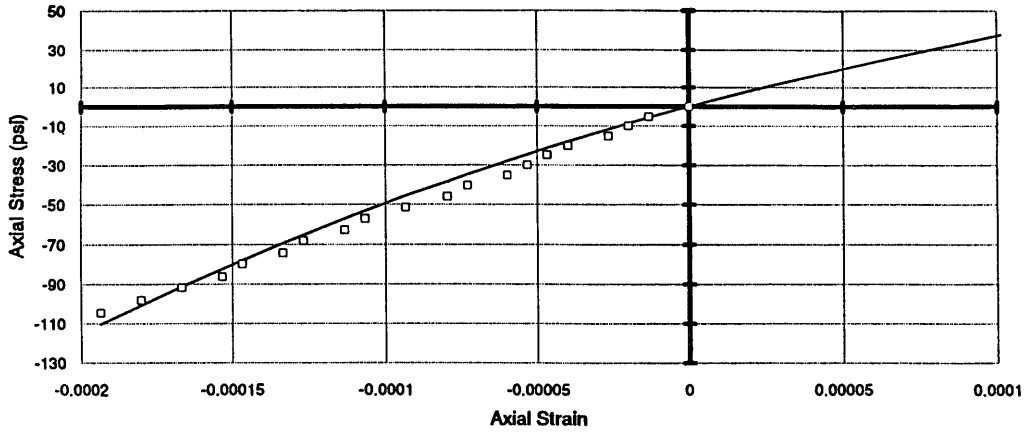

FIGURE 4 Variation of axial stress with axial strain for uniaxial strain tests at 4°C and 10 psi/sec ramping for axial stress (model and actual data) (Aggregate RB, Asphalt AAG-1) (V0W0).

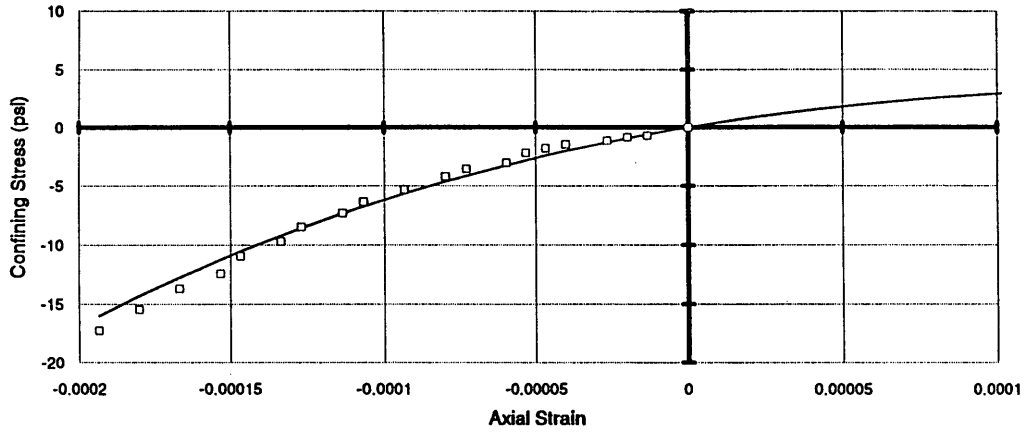

FIGURE 5 Variation of confining stress with axial strain for uniaxial strain tests at 4°C and 10 psi/sec ramping for axial stress (model and actual data) (Aggregate RB, Asphalt AAG-1) (V0W0).

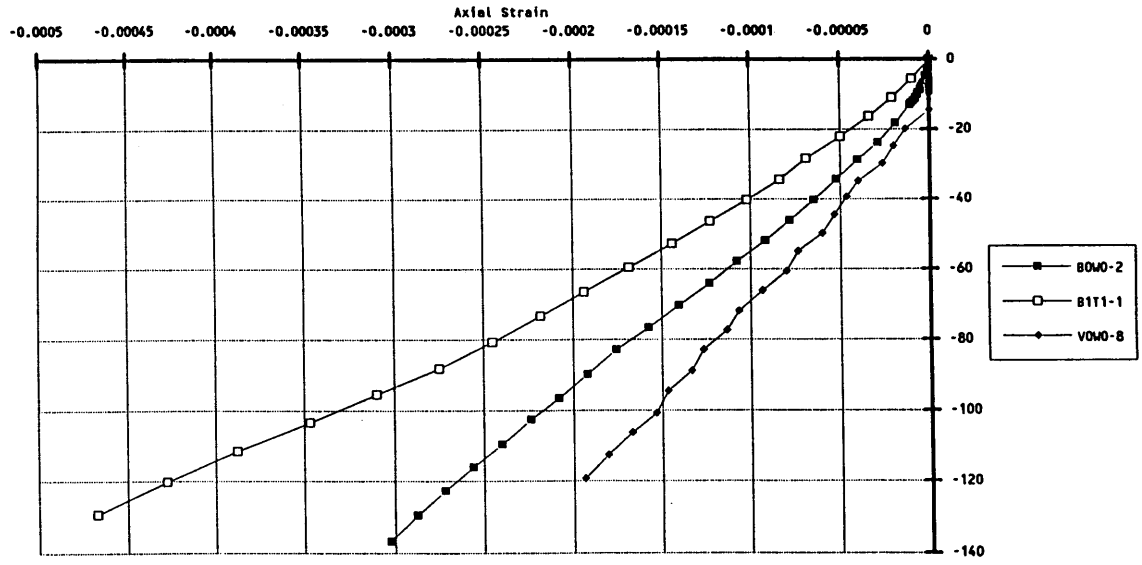

FIGURE 6 Axial stress versus axial strain, uniaxial strain test.

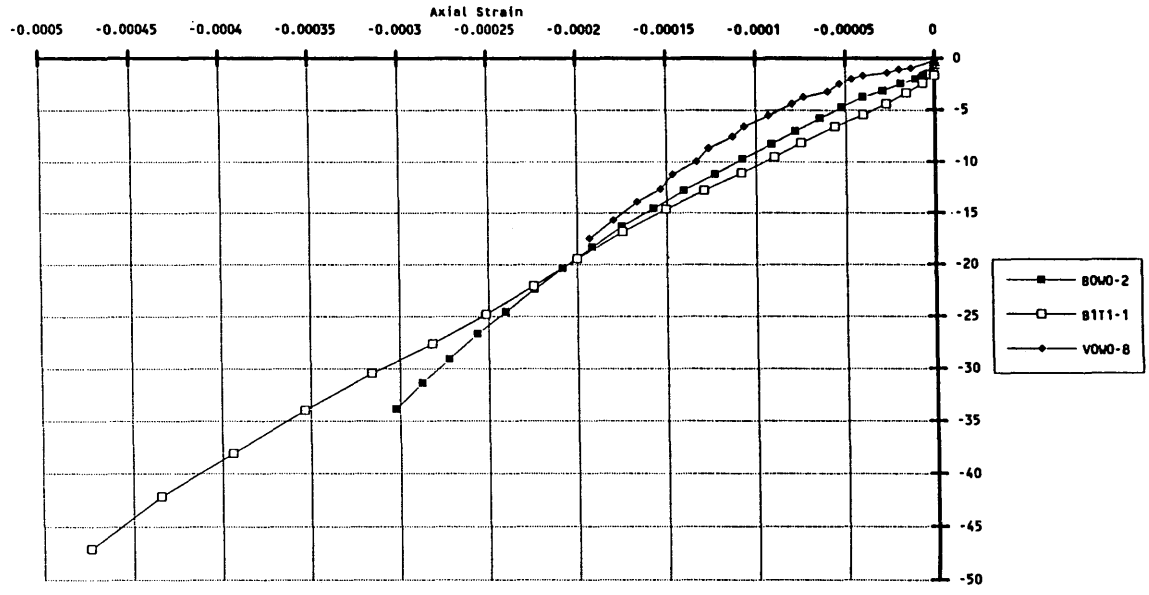

FIGURE 7 Confining stress versus axial strain, uniaxial strain test.

from the volumetric test. In this test the specimen is completely enveloped in a latex membrane and placed inside a pressure cell. The cell pressure is ramped at a rate of 10 psi/sec, and the change in perimeter is measured.

The confining pressure (σ_{22}) and the radial strain ($\varepsilon_0 = \delta/2\pi r$ where δ is the change in perimeter and r is the radius of the specimen) can be computed from the test data. In the volumetric test the state of strain can be stated as $\varepsilon_{11} = \varepsilon_{22} = \varepsilon_{33} = \varepsilon_0$ and the state of stress defined by the following expression:

$$\sigma_{22} = (3C_1 + 2C_2)\varepsilon_0 + (9C_3 + 9C_4 + C_5)\varepsilon_0^2 + (27C_6 + 36C_7 + 4C_8 + 6C_9)\varepsilon_0^3 \quad (14)$$

Figure 8 compares the results obtained from the data with those fitted with the model parameters. Figure 9 compares the response for all four mixes tested.

A summary of the C coefficients obtained from the test results is given in Table 1. All tests were performed at a rate of about 10 psi/sec at 4°C. Whereas that temperature and rate were selected to minimize the viscous deformation, some creep was still present. Accordingly, the C coefficients in Table 1 include some viscous deformation.

The results in Table 1 provide some encouraging comparisons. For example, the values of C_2 and C_4 obtained from the simple shear test for the B0W0 mix compare reasonably well with those obtained from the uniaxial strain test. Also, the value predicted for the coefficient of the linear strain term $(3C_1 + 2C_2)$ in the volumetric test using the values obtained from the uniaxial strain test compares reasonably well with that measured in the volumetric test for all the mixes.

In most instances the comparisons of the C coefficients determined from the tests are reasonable. In the case of C_4 for Mix B1T1, however, a positive value was obtained in the

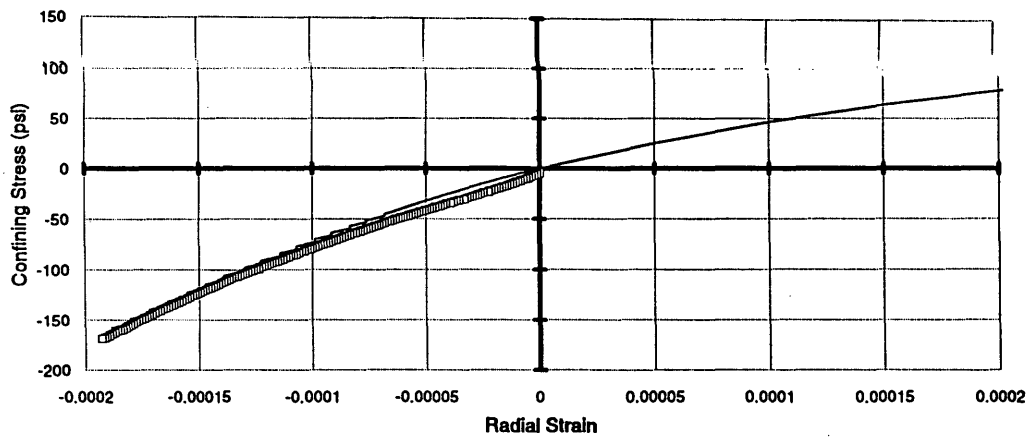

FIGURE 8 Variation of confining stress with radial strain for volumetric tests at 4°C and 15 psi/sec ramping stress (model and actual data) (Aggregate RB, Asphalt AAG-1) (V0W0).

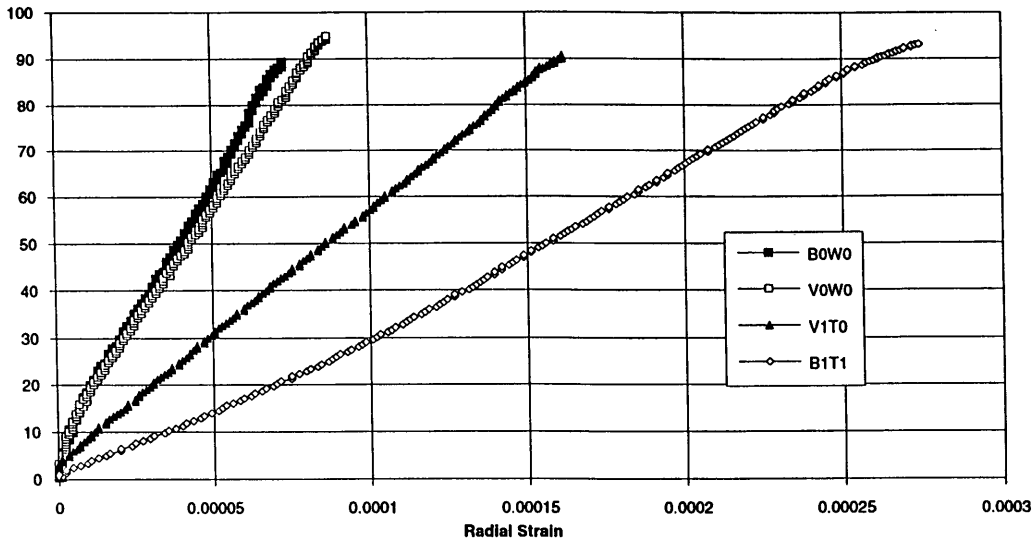

FIGURE 9 Variation of radial strain with confining pressure—volumetric tests.

simple shear test but a negative value was obtained in the uniaxial strain test. Part of this discrepancy might be attributed to the use in the two tests of different specimens whose void contents might have been different.

As stated earlier, some viscous deformations are incorporated in the test data presented herein. Accordingly, the C values are probably smaller than they should be. This has led to the necessity of developing an algorithm that permits determination of the true values for the nonlinear elastic coefficients recognizing that load applications require finite times and are not instantaneous (i.e., values that do not include viscous deformation).

TABLE 1 Summary of C Coefficients Determined from the Simple Shear, Uniaxial Strain, and Volumetric Tests (psi)

		Mix		
		B0W0	V0W0	B1T1
Asphalt type		AAK-1	AAG-1	AAK-1
Asphalt type		RB	RB	RL
Asphalt content (by weight of aggregate)		5.1	4.9	4.3
Compaction method		rolling wheel	rolling wheel	rolling wheel
Air void content (percent)		3.7	3.6	7.9
Simple Shear Test	C_2	-3.88E+05	-1.06E+06	-2.74E+05
	C_4	1.52E+08	7.94E+08	8.14E+07
	C_9	-2.50E+11	-1.00E+10	-2.50E+09
Uniaxial Strain Test	C_1	3.71E+05	4.27E+05	3.11E+05
	C_2	-3.24E+05	-3.83E+05	-2.46E+05
	C_3	-2.94E+08	-6.15E+08	1.39E+07
	C_4	1.17E+08	4.48E+08	-6.84E+07
	C_6	2.91E+11	6.91E+11	-6.73E+10
	C_7	-9.67E+10	-5.01E+11	1.16E+11
Volumetric	C_5	8.97E+08	6.77E+08	8.78E+07
	C_8	-6.50E+11	-6.20E+10	-5.40E+11
From uniaxial strain test:				
$(3C_1 + 2C_2)$		4.66E+05	5.14E+05	4.40E+05
From volumetric test:				
$(3C_1 + 2C_2)$		4.46E+05	5.39E+05	2.52E+05
$(9C_3 + 9C_4 + C_5)$		-6.89E+08	-8.22E+08	-4.03E+08
$(27C_6+36C_7+4C_8+6C_9)$		2.72E+11	3.17E+11	1.65E+11

Determination of Viscous Parameters

The viscous properties of the materials were determined from frequency sweeps at 4°C, 20°C, and 40°C. Strain control shear frequency sweeps were executed at 0.01, 0.02, 0.05, 0.1, 0.2, 0.5, 1, 2, 5, and 10 Hz with an amplitude of 0.0001 in./in. while maintaining the specimen height within ±0.00005 in. Tests were executed from high to low frequency at a particular temperature and from the low temperature to the high temperature.

The imposed sinusoidal strain X at the frequency ω at a strain amplitude X_a,

$$X = X_a \sin(\omega t) \tag{15}$$

will generate a sinusoidal stress P (where t represents time):

$$P = P_a \sin(\omega t + \delta) \tag{16}$$

The complex shear modulus G^* can then be determined as

$$G^* = \frac{P_a}{X_a} \tag{17}$$

At each frequency and temperature, G^* and the phase angle δ were computed from the average of at least three cycles. Using the assumption that the mix is thermorheologically simple, master curves were developed by time-temperature superposition using the IRIS program (*10*). The assumption of a thermorheologically simple response appears reasonable for the small deformations used in the test, as seen in Figure 10.

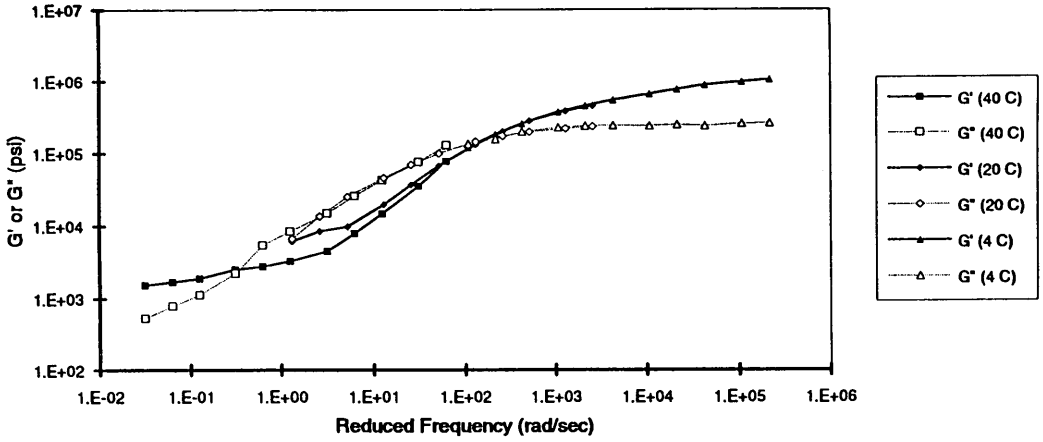

FIGURE 10 Variation of G' and G'' for an asphalt concrete mixture (V0W0) with temperature and frequency. Tests conducted under strain control at 0.0001 shear strain amplitude.

In the determination of the master curve, the C_1 and C_2 coefficients of the WLF equation were also computed:

$$\log a_T = -\frac{C_1(T - T_{ref})}{C_2 + T - T_{ref}} \tag{18}$$

where a_T is the horizontal shift factor and T is the corresponding absolute temperature (degrees Kelvin).

The IRIS program was also used to determine the number (N) of Maxwell elements as well as the values of the constants (g_i and λ_i) required to match the master curves. Table 2 contains the output of IRIS and includes the constants for the WLF equation, which are presented in Table 3. The constants permit the determination of the viscous parameters at any temperature, thus permitting predictions at any pavement temperature.

The N Maxwell elements are defined by their relaxation moduli g_i and their relaxation times λ_i (*11*). Using these values, G' and G'' at any frequency are given by

$$G'(\omega) = G_e + \sum_{i=1}^{N} g_i \frac{(\omega\lambda_i)^2}{1 + (\omega\lambda_i)^2} \tag{19}$$

and

$$G''(\omega) = \sum_{i=1}^{N} g_i \frac{\omega\lambda_i}{1 + (\omega\lambda_i)^2} \tag{20}$$

where G_e is the equilibrium modulus and i refers to the corresponding Maxwell element.

The fitted master curve and the values of G' and G'' obtained from the tests are shown in Figure 11. The results suggest that the assumption of Maxwell elements in parallel represents the dynamic response to a reasonable degree.

The strain control shear frequency sweep test is comparatively easy to perform and provides a reliable measure of the viscous response for a range in temperatures and frequencies at the same strain level. This test may also prove useful in investigating the influence of strain level on the magnitude of the parameters.

To illustrate the influence of asphalt and aggregate type on mix stiffness, variation of $|G^*|$ and phase angle with frequency for four mixes is shown in Figures 12 and 13. The mixes containing Asphalt AAG-1 (V0W0 and V0T1) exhibit different responses from mixes containing Asphalt AAK-1 (B0W0

TABLE 2 Discrete Relaxation Spectra from Computer Program Iris[a]

i	B0W0		V0W0		B1T1		V1T0	
	g_i[b]	λ_i[c]	g_i	λ_i	g_i	λ_i	g_i	λ_i
1	.2489E+07	.1493E-06	.4561E+06	.4763E-05	.2310E+07	.2652E-06	.2676E+06	.2757E-05
2	.2932E+06	.8310E-05	.2565E+06	.4029E-04	.2196E+06	.1240E-04	.2080E+06	.2102E-04
3	.2296E+06	.6178E-04	.2396E+06	.2042E-03	.1949E+06	.7684E-04	.1936E+06	.1144E-03
4	.1314E+-6	.3468E-03	.2482E+06	.1155-02	.1101E+06	.4544E-03	.1818E+06	.6875E-03
5	.8485E+05	.1915E-02	.1439E+06	.5862E-02	.5393E+05	.2643E-02	.1212E+06	.3886E-02
6	.2889E+05	.1064E-01	.7844E+05	.2986E-01	.1694E+05	.1677E-01	.5058E+05	.2087E-01
7	.1929E+05	.4147E-01	.4295E+04	.1758E+00	.2819E+04	.2982E-01	.7978E+04	1037E+00
8	.8068E+04	.3931E+00	.1789E+04	.1199E+01	.4719E+04	.1409E+00	.2923E+04	.8906E+00
9	.2423E+04	.6496E+01	.6061E+03	.1051E+02	.2758E+04	.8117E+00	.5123E+03	.5411E+01
10	.3085E+04	.1859E+03	.1435E+04	.2688E+03	.2085E+04	.5739E+01	.9074E+03	.1698E+04
11					.1240E+04	.1404E+04		

[a]Spectra determination procedure by M. Baumgaertel and H. Winter.
[b]Units of g_i are psi.
[c]Units of λ_i are sec.

TABLE 3 Mix Parameters for Permanent Deformation Model; Three Mixes

MIX TYPE	B0W0		V0W0		B1T1	
Viscous Parameters						
Ref. Temp. (°C)	40		40		40	
C_1 (WLF)	48.02		7.35		53.5	
C_2 (WLF)[K]	-416.57		110.77		583.2	
Viscous Poisson's	0.489		0.489		0.489	
η_0 (psi)	5.94E+05		3.99E+05		1.76E+06	
G_0 (psi)	3.29E+06		1.43E+06		2.92E+06	
α_i	7.57E-01		3.19E-01		7.91E-01	
	8.91E-02		1.79E-01		7.52E-02	
	6.98E-02		1.67E-01		6.68E-02	
	3.99E-02		1.73E-01		3.77E-02	
	2.58E-02		1.01E-01		1.85E-02	
	8.78E-03		5.48E-02		5.80E-03	
	5.86E-03		3.00E-03		9.66E-04	
	2.45E-03		1.25E-03		1.62E-03	
	7.37E-04		4.24E-04		9.45E-04	
	9.38E-04		1.00E-03		7.14E-04	
					4.25E-04	
β_i	6.26E-07		5.45E-06		3.49E-07	
	4.10E-06		2.59E-05		1.55E-06	
	2.39E-05		1.23E-04		8.53E-06	
	7.67E-05		7.19E-04		2.85E-05	
	2.74E-04		2.12E-03		8.12E-05	
	5.18E-04		5.88E-03		1.62E-04	
	1.35E-03		1.89E-03		4.79E-05	
	5.34E-03		5.38E-03		3.79E-04	
	2.65E-02		1.60E-02		1.27E-03	
	9.66E-01		9.68E-01		6.81E-03	
					9.91E-01	
Damage Parameters (Max strain model)						
α_i	0.0003		0.0003		0.0003	
β_i	0.1		0.1		0.1	
n	1		1		1	
Non-Linear Elastic Coefficients		Corrected		Corrected		Corrected
C_1	3.71E+05	7.54E+06	4.27E+05	3.19E+06	3.11E+05	7.37E+06
C_2	-3.24E+05	-6.58E+06	-3.83E+05	-2.86E+06	-2.46E+05	-5.84E+06
C_3	-2.94E+08		-6.15E+08		1.39E+07	
C_4	1.17E+08		4.48E_08		-6.84E+07	
C_5	8.97E+08		6.77E+08		8.78E+07	
C_6	2.91E+11		6.91E+11		-6.73E+10	
C_7	-9.67E+10		-5.01E+11		1.16E+11	
C_8	-6.50E+11		-6.20E+10		-5.40E+11	
C_9	-2.50E+11		-1.00E+10		-2.50E+09	

and B1T1) relative to phase angle variation, as shown in Figure 13. At lower frequencies (higher temperatures) the mixes with Aggregate RB exhibit higher stiffnesses than the mixes with RL material. At higher frequencies the influence of the asphalt (stiffness) predominates.

Determination of Damage Parameters

Damage parameters were estimated from tests performed at 20°C and 1 Hz. Strain control shear tests were executed with strain amplitudes of 0.0001, 0.0002, 0.0005, 0.001, and 0.002 in./in. to investigate the influence of strain level on damage (the specimen height was maintained constant within ±0.00005 in.). In this analysis it was assumed that only 1 Maxwell element out of the 10 or 12 usually obtained from the IRIS program would be significantly influenced for the frequency and temperature used.

The material properties were computed as presented in Equations 15, 16, and 17. Furthermore, the viscosity, η, of the dashpot was computed by

$$\eta = \frac{G''(1 + \tan\delta)}{\omega \tan\delta} \tag{21}$$

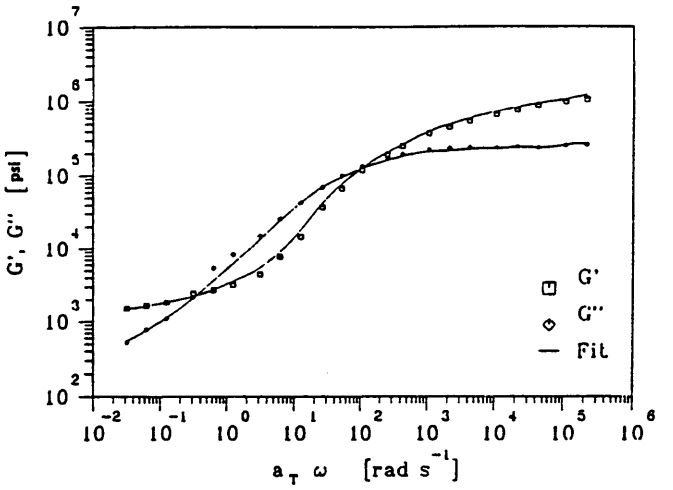

FIGURE 11 Variation of G' and G'' with frequency for Mix V0W0 (Aggregate RB, Asphalt AAG-1) at a reference temperature of 40°C.

where

G'' = loss modulus,
ω = test frequency (rad/sec), and
δ = phase angle.

The stiffness, E, of the spring is given by

$$E = \eta \tan\delta \tag{22}$$

Figure 14 shows the variation of stiffness ratio (stiffness at any strain amplitude divided by stiffness at small strain amplitude) with strain magnitude. It appears that the strain amplitude has comparatively small influence in reducing the spring stiffness, although slight strain softening is observed.

Figure 15 suggests that the dashpot viscosity is strongly influenced by strain amplitude. In this figure the ratio of the viscosity at any strain amplitude to that of a strain level of 0.0001 in./in. is plotted as a function of strain amplitude. Moreover, when the ordinate, termed damage, has a value of 1, the dashpot is considered undamaged. As the value of

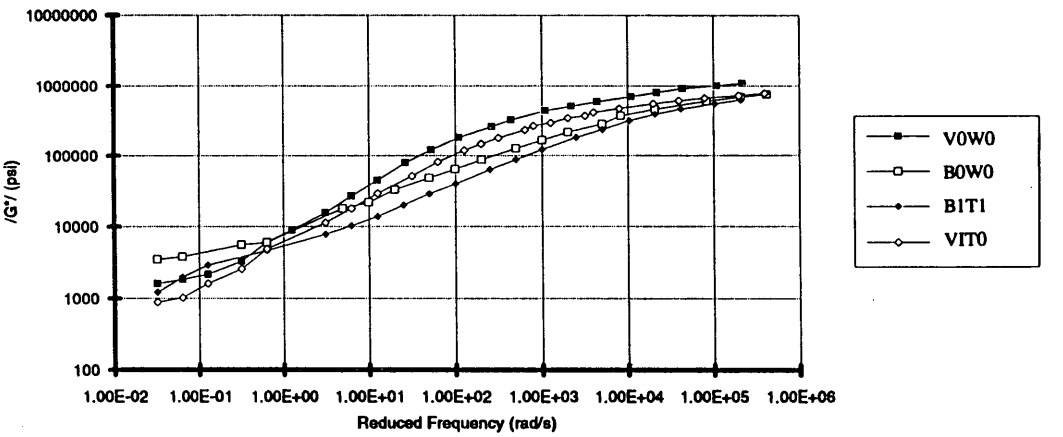

FIGURE 12 Complex shear modulus versus reduced frequency (rad/sec) (40°C reference) from shear frequency sweeps.

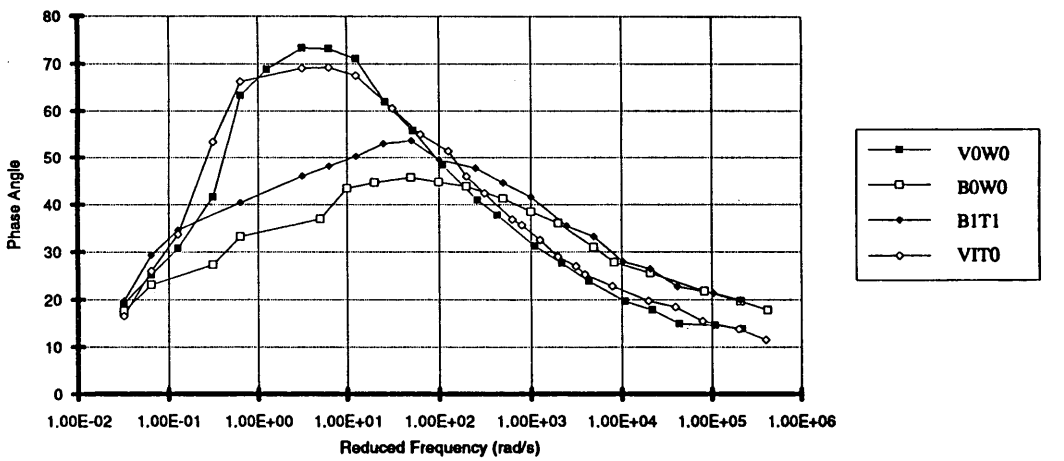

FIGURE 13 Phase angle versus reduced frequency (40°C reference) for shear frequency sweeps.

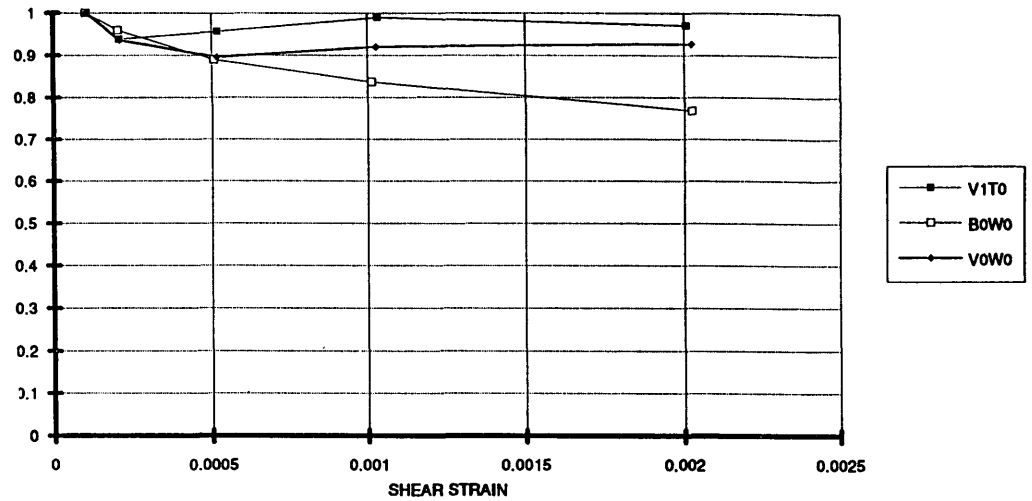

FIGURE 14 Variation of stiffness ratio (E/E_0) with strain amplitude in strain sweep tests at 20°C and 1 Hz.

the ordinate decreases (i.e., approaches 0), the damage to the dashpot increases.

The development of damage with strain level obtained from creep tests is also shown in Figure 15. The variation of the damage parameter with strain magnitude appears to follow a similar path for both strain sweeps and creep tests. The results strongly suggest a highly nonlinear behavior in the dashpots; however, the nonlinearity seems to be independent of the mix.

Material Properties

Table 3 contains a summary of the material properties obtained for three of the four mixes. The values of G_0 represent the instantaneous shear moduli obtained from the IRIS program. The values of C_2 ($C_2 = -2G_0$) obtained from the frequency sweeps (see "corrected" column) are higher than those obtained from the simple shear tests, uniaxial strain tests, and volumetric tests. This is not surprising since the shear frequency sweeps performed at 4°C and 10 Hz yield higher values of G^* than those obtained at 0.1 Hz at the same temperature. Thus it is apparent that the tests conducted at 4°C to determine the nonlinear elastic parameters contain a viscous component.

To match the viscous parameters and the C constants, the C_1 and C_2 values were corrected proportionally. The other C values were not corrected. This fact makes the analysis more linear because the contribution of the nonlinear terms is slightly minimized.

A program to determine all the nonlinear elastic, viscous, and damage parameters, taking each of these factors into consideration by using an iterative procedure with a quadratic convergence, is under development and should rapidly yield consistent and accurate parameters.

The data in Table 3 (using the larger values for C_1 and C_2) provide the basis for predicting the performance of the mixes in some other form of loading and thus serve to provide validation of the permanent deformation model.

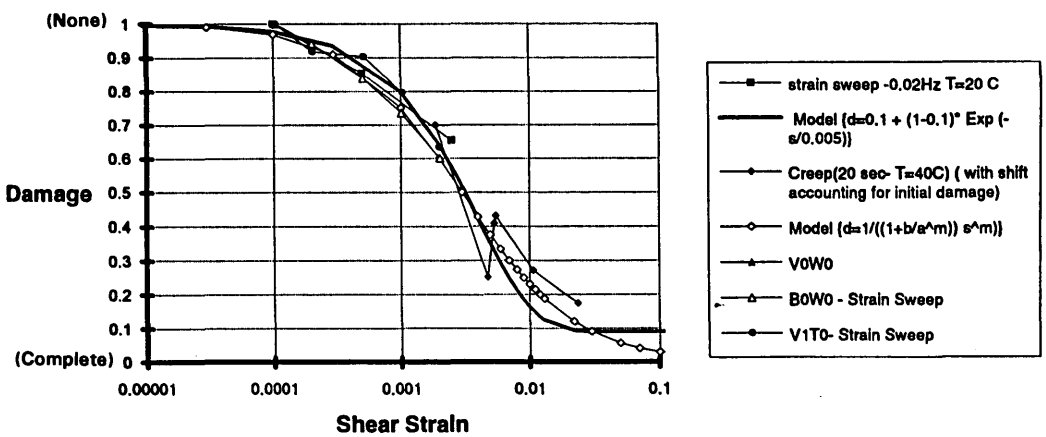

FIGURE 15 Comparison of the shape of the damage function obtained from shear strain sweeps and shear creep tests with a proposed damage model.

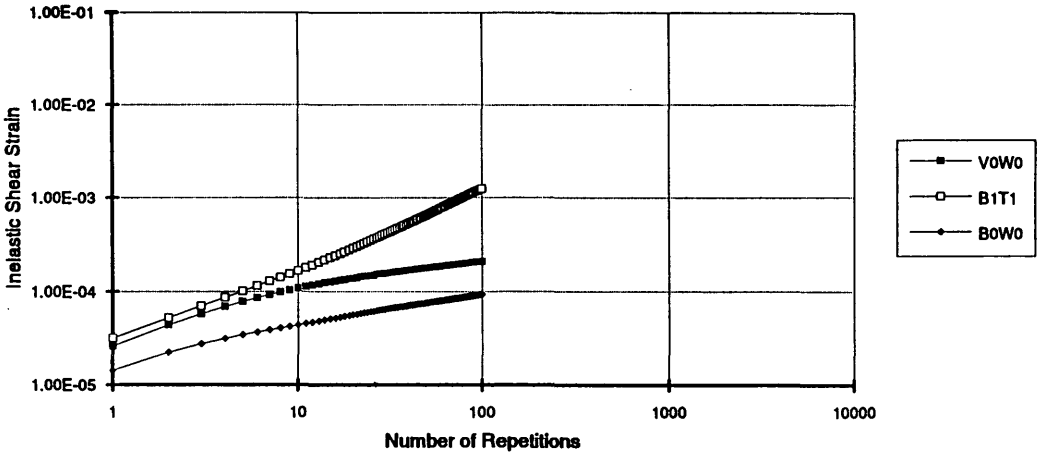

FIGURE 16 Model prediction for accumulation of permanent deformation in the repetitive-load simple shear test.

VALIDATION

A repetitive simple shear test at constant height was selected for validation. This test was conducted at 40°C using a time of loading of 0.1 sec and a time interval between load applications of 0.6 sec. The magnitude of the repetitive shear stress was 7.5 psi. The height of each specimen was maintained within ±0.00005 in.

For validation purposes, a two-element finite element mesh representing half of the cylindrical specimen was used to take advantage of the antisymmetry of the load. The model assumes that the states of stress in the true specimen is perfect (i.e., that a state of pure shear stress exists within the cylindrical specimen).

Using this model and the maerial properties presented in Table 3, 100 cycles of 0.1 sec loading and 0.6 sec unloading were simulated (Figure 16). The simulations accurately ranked the mixes according to their known permanent deformation resistance. This was an important demonstration considering that the mix properties used in the simulations were based on measurements not only at different loading rates but also from totally different types of tests.

Figure 17 compares results obtained from the test of the V0W0 mix with the prediction obtained from the model assuming several levels of damage. Adding a damage component to the mix model significantly improves the ability to accurately simulate test measurements. A relatively good fit between measured and simulated response can be obtained when mix damage is accounted for.

PAVEMENT SECTION EXAMPLE

To illustrate the implementation of the approach outlined in Figure 1, an example of the use of the finite element program is presented. Figure 18 shows a finite element mesh created to represent half of a full-depth, one-lane pavement section. In this simplified two-dimensional model, the loads have been simulated as continuous loading strips consistent with the plane strain assumption. (A full three-dimensional model could have

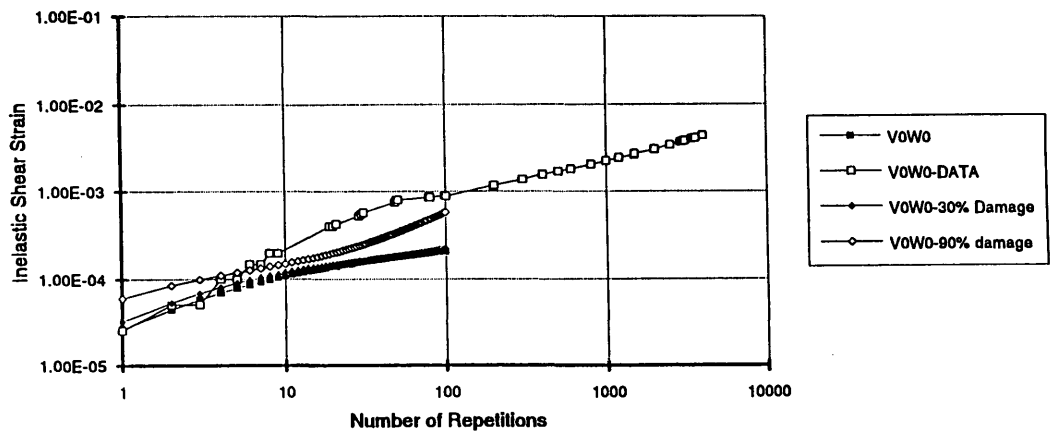

FIGURE 17 Comparison between data and model prediction of accumulation of permanent deformation in the repetitive-load simple shear test.

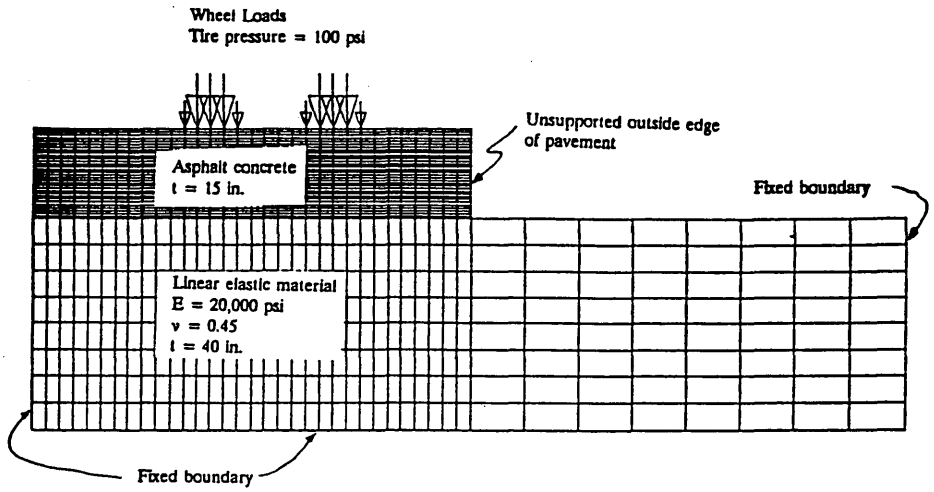

FIGURE 18 Two-dimensional mesh representing a cross section of a pavement section.

been formulated, but because of limited computer resources at the time such a solution could not have been implemented.)

To rapidly achieve significant levels of permanent deformation on the asphalt concrete layer with very few load applications, the material properties used were significantly weakened by reducing the magnitude of both the C constant and the viscous parameters. Moreover, a repetitive haversine load with a 0.3-sec loading time and 0.4-sec rest between load application was used to simulate very slow-moving traffic. The magnitude of the load was selected as 500 psi to increase even more the rate of accumulation of permanent deformation.

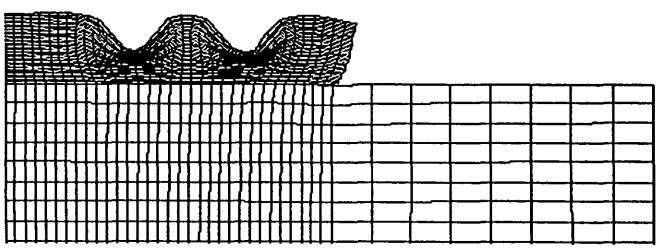

FIGURE 19 Deformed shape of the pavement section after five cycles.

The FEAP program running on an IBM-RS6000 was used. The total cpu time to reach five cycles was about 5 hr. This time could be significantly reduced by using a slightly coarser mesh (without compromising the accuracy of the results) and by increasing the magnitude of the small time steps used to prevent divergence due to such high loads (with tire pressures of 100 psi, the magnitude of the time steps could be increased).

Figure 19 shows the deformed shape at the end of the fifth cycle magnified 100 times. The figure shows the permanently deformed shape without the load being applied. The variation of the pavement profile at the end of the first, second, and fifth cycles is presented in Figure 20. The upheavals due to the shear flow and dilation are similar to those encountered in rutted pavement sections.

This example illustrates the capability of the model to analyze boundary value problems representative of pavement structures and to simulate the general shape of the permanent deformation profile of rutted pavement.

SUMMARY

A nonlinear elastic viscous with damage model for asphalt-aggregate mixes has been proposed. The model is based on

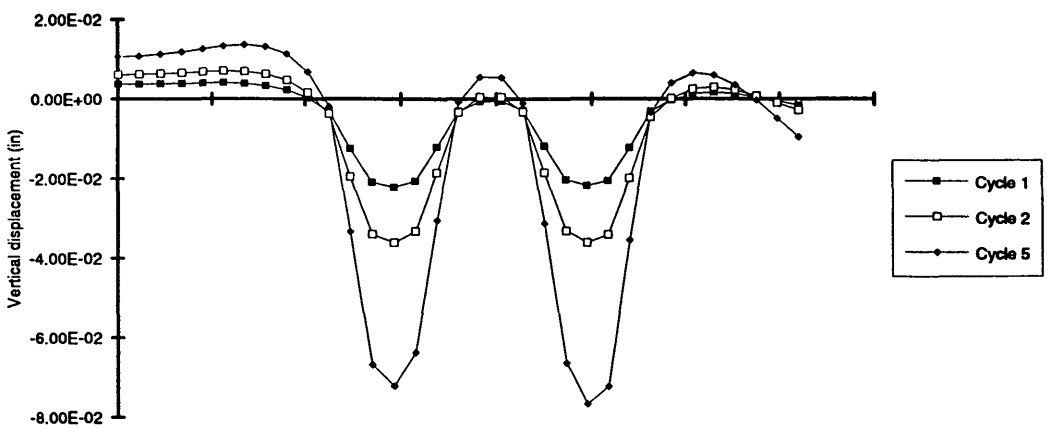

FIGURE 20 Variation of pavement profile with the number of load application, stress level 500 psi, 0.3-sec loading time, 0.4-sec rest period.

principles of mechanics and is directly amenable to finite element approximations.

A new series of tests (i.e., uniaxial strain test, simple shear test at constant height, and volumetric test) has been developed to determine the nonlinear elastic material properties. Simple shear frequency and strain sweep tests at constant height were introduced to determine the viscous and damage parameters for the model.

Results indicate that the model is capable of capturing the most important aspects of the permanent deformation response of asphalt-aggregate mixes. The tests selected for determination of the material parameters were found to be easy to conduct and to yield consistent material properties.

Material properties, obtained for three of the four mixes that had the complete battery of tests performed, were used in simulations that reasonably ranked the mixes according to their known permanent deformation resistance. In this procedure the evaluation of the model behavior was made through a test from which no material parameters were obtained and that is of a totally different nature from those used to determine the material properties (i.e., the validation test was a repetitive test, whereas the tests used to obtain material properties used either a constant rate of loading or were sinusoidal in nature). This was an important demonstration, considering that the mix properties used in the simulations were based on measurements not only at different frequencies and times of loading but from totally different types of tests and stress levels.

Manual determination of material properties from test measurements is a tedious, time-consuming process. A program is being developed to determine requisite properties with minimum user intervention. As a result, testing at 4°C in an effort to minimize the viscous component of the mix response is no longer considered necessary, and standard testing will now be performed at more convenient temperatures and loading rates (e.g., 40°C). Also, as a result of this exercise, a fourth temperature, 60°C, has been added to the frequency sweep tests for some mixes to ensure that the range in loading times required to simulate response is bounded.

Efforts are also being made to refine the model to incorporate a measure of damage capable of capturing inelastic permanent deformation not fully explained by viscous behavior.

The development of a constitutive law for asphalt concrete behavior that can be used in three-dimensional finite element programs is very important to the development of a procedure to accurately predict the permanent deformation response of pavements subjected to moving traffic. For example, tire contact pressures, which vary significantly with tire type and inflation pressure, have a significant influence on the development of permanent deformation. We believe that it is necessary to use a three-dimensional program to properly reflect such effects. The type of model proposed herein can be used in such a finite element idealization.

ACKNOWLEDGMENTS

The work reported herein has been conducted as a part of SHRP Project A-003A. SHRP, a unit of the National Research Council, was authorized by Section 128 of the Surface Transportation and Uniform Relocation Assistance Act of 1987. This project is titled Performance-Related Testing and Measuring of Asphalt-Aggregate Interactions and Mixtures and is being conducted by the Institute of Transportation Studies, University of California, Berkeley. Carl L. Monismith is Principal Investigator. The support and encouragement of Rita B. Leahy of SHRP is gratefully acknowledged.

Special thanks are also due to John Harvey for his efforts in preparing the specimens and editing for publication and to Maggie Paul for the manuscript preparation.

REFERENCES

1. J. B. Sousa, J. Craus, and C. L. Monismith. *Summary Report on Permanent Deformation in Asphalt Concrete*. Report SHRP-A/IR-91-104. Strategic Highway Research Program, Washington, D.C., 1991.
2. A. Tayebali, J. Goodrich, J. B. Sousa, and C. L. Monismith. Relationships Between Modified Asphalt Binders Rheology and Binder-Aggregate Pavement Deformation Response. *Asphalt Paving Technology*, Vol. 60, 1991, pp. 121–159.
3. J. B. Sousa, J. A. Deacon, and C. L. Monismith. Effect of Laboratory Compaction Method on Permanent Deformation Characteristics of Asphalt Concrete Mixtures. *Asphalt Paving Technology*, Vol. 60,. 1991, pp. 533–587.
4. H. S. Papazian. *The Response of Linear Viscoelastic Material in Frequency Domain*. Dissertation. Report 172-2. Transportation Engineering Center, Ohio State University, Columbus, Ohio, Dec. 1961.
5. I. J. Lubliner. *On the Thermodynamic Foundations of Non-linear Solid Mechanics*. Vol. 54, 1972, pp. 259–278.
6. Marsden and Hughes. *Mathematical Foundation of Elasticity*. Prentice-Hall, Englewood Cliffs, N.J., 1983.
7. W. Flugge. *Visoelasticity*. Springer-Verlag, Berlin, 1975.
8. J. M. Gibb, P. S. Pell, and S. F. Brown. *An Evaluation of the Wheel-Tracking Test as a Means of Assessing Resistance to Permanent Deformation*. SWK Pavement Engineering Ltd., Sept. 1991.
9. J. B. Sousa, J. Harvey, L. Painter, J. A. Deacon, and C. L. Monismith. *Evaluation of Laboratory Procedures for Compacting Asphalt-Aggregate Mixtures*. TM-UCB-A-003A-90-5. Institute of Transporation Studies, University of California, Berkeley, 1991.
10. M. Baumgaertel, P. R. Soskey, and H. H. Winter. *IRIS (Innovation Rheological Interface Software)*. User's manual, 1990.
11. M. Baumgaertel and H. H. Winter. Determination of Discrete Relaxation and Retardation Time Spectra from Dynamic Mechanical Data. *Rheologica Acta*, Vol. 28, 1989, pp. 511–519.

Mathematical Model of Pavement Performance Under Moving Wheel Load

PER ULLIDTZ

Vehicle-pavement interaction was studied using the Mathematical Model of Pavement Performance (MMOPP). With MMOPP a length of flexible road is first generated on the computer. Values of layer thicknesses, elastic moduli, plastic parameters, and so forth are generated at points spaced 0.3 m apart in such a way that the pattern of variation is similar to that observed on real pavements. The pavement is then loaded using a quarter car model, and the dynamic load is calculated at each point. The permanent deformation of each layer and the structural deterioration of the asphalt layer resulting from the loads are likewise calculated for each point. The next time increment is then considered, changing the materials characteristics in accordance with climatic changes, applying the loads of that increment, and so on. MMOPP was used on two sections from the AASHO Road Test. The traffic was extended to 20 years, and the effects of varying vehicle characteristics such as spring constant of the tire, damping coefficient of the shock absorber, and use of single or dual tires were studied. It is concluded that the deterioration of pavements is a very complex process, depending on an interaction of pavement parameters, climatic effects, vehicle characteristics, and time. Computer simulation appears to be an efficient and cost-effective means of filling some of the gaps in existing knowledge.

The ride quality of a road pavement is an important indicator of performance. How the ride quality changes over time depends on the longitudinal variation of pavement characteristics as well as on variations in the loading. It is the variation in layer thicknesses, stiffnesses, and plastic and strength parameters in combination with the dynamic effects of the traffic loading that cause a pavement to become rough. Without these longitudinal variations a pavement would remain smooth. It could deteriorate due to rutting and cracking, but it would never get rough.

The Mathematical Model of Pavement Performance (MMOPP) used for this study attempts to model this longitudinal variation on a computer. The first version of the model was developed from 1976 to 1978 (*1,2*), and a later version is described in detail elsewhere (*3*). The model has recently been rewritten for a PC. Only flexible pavements may be simulated by the model.

A brief description of MMOPP is given first, followed by some examples of its application. For this study the model was first used to simulate two of the AASHO Road Test sections. The traffic was then extended over 20 years, for the same sections, and different parameters of the suspension (spring constants, damper coefficients) as well as wheel configuration (dual or single) and traffic mix were used.

Institute of Roads, Transport and Town Planning, Technical University of Denmark, Building 115, DK-2800 Lyngby, Denmark.

MOVING WHEEL LOAD

A road section is first generated on the computer, using a stochastic process, and is then loaded by a moving wheel load, consisting of a mechanical analog of a simple quarter car model (see Figure 1).

The lower system (M2, K2, C2) represents the mass of the axle and the wheel, the spring constant of the tire, and the tire damping. The upper system is the mass of the vehicle and the payload transferred to one wheel, the spring constant, and the damping coefficient of the suspension system. All parameters are considered to be linear, but introducing nonlinear parameters would be easy. The wheel may be either single or dual.

The force exerted at each point of the road surface is calculated using a numerical method. The length of each step in the calculation depends on the resonance frequency and the speed of the vehicle. In most cases a step length of 50 mm could be used.

Parameter values for spring constants and damping coefficients were selected on the basis of information given elsewhere (*4,5*). In the examples given later the following basic parameters were used: spring constant—1242 N/mm for tire and 278 N/mm for suspension; damping coefficients—1 Nsec/mm for tire and 14 Nsec/mm for suspension.

LONGITUDINAL VARIATION OF PARAMETERS

To model the longitudinal variation of the pavement, the road is divided into short lengths, each with a length of only 0.3 m (1 ft). This short length is considered representative of one "point" of the pavement. The layer thicknesses and elastic, plastic, and strength parameters are then varied from point to point. The pattern of variation is very important to the outcome of the simulation.

The variation from point to point is not random. The value at a particular point depends to some extent on the values at preceding points. This may be seen, for example, on the original profile (fall 1958) in Figure 2. This dependency may be described by the autocorrelation function.

An example may illustrate this. Consider a longitudinal road profile where the elevation is measured at points spaced 0.3 m apart and assume that the standard deviation on the elevation is 1 mm. If the values are randomly distributed, this profile would be very rough, with a present serviceability index (PSI) of about 2.5. If, however, the correlation coefficient between consecutive values is 0.9, and 0.8 for points

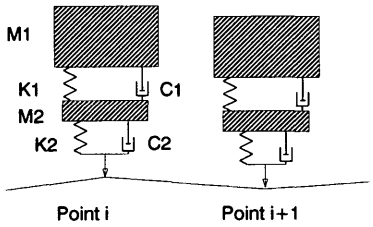

FIGURE 1 Mechanical analog.

0.6 m apart, the profile is very smooth, with a PSI of about 4.0.

A second-order autoregressive process is used to generate the parameters to obtain a distribution with given mean value, standard deviation, and two values of the autocorrelation function.

An example of the variation of layer moduli resulting from the stochastic process is shown in Figure 3. The autocorrelation coefficients for 0.3 and 0.6 m distance were 0.9 and 0.75, respectively, for the asphalt, decreasing to 0.6 and 0.3 for the subgrade.

Very little information is available with respect to actual values of the autocorrelation function for parameters such as elastic modulus, bitumen content, and so forth.

CALCULATION OF PERMANENT DEFORMATION

MMOPP works in increments of time. In the examples below increments of 1 month were used. For each increment the effects of temperature on the asphalt material and seasonal effects, such as spring thaw or wet and dry periods, on the unbound materials (including the subgrade) are first calculated. Then the loads are applied using the mechanical analog described above, and the force (static plus dynamic load) exerted at each point is calculated. The effects of the loads are determined in terms of the permanent deformation of each material and the reduction of the asphalt modulus caused by fatigue.

To calculate the permanent deformations, both the elastic and plastic characteristics of the materials must be known.

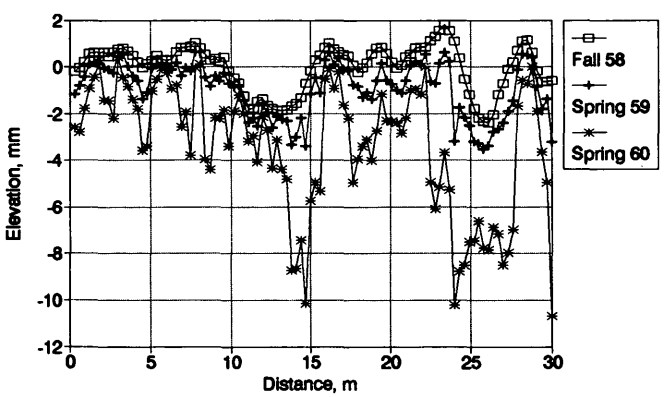

FIGURE 2 Longitudinal profile, simulation of S30, Design 6-9-8.

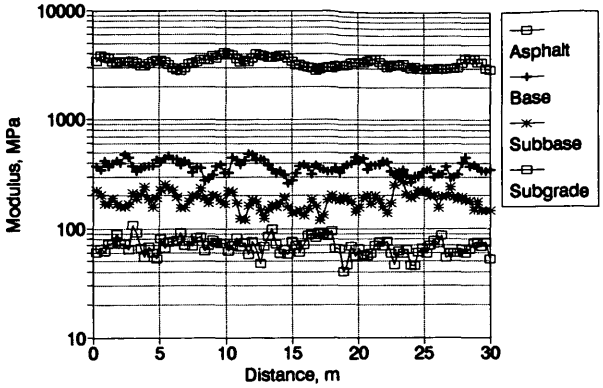

FIGURE 3 Variation of layer moduli, simulation of S30, Design 6-9-8.

The elastic parameters are needed to describe the stress state, and the plastic are needed to get the permanent deformations resulting from the stress state.

The elastic parameters are Young's modulus (E) and Poisson's ratio (ν). For the plastic parameters a decreasing strain rate is assumed as long as the plastic strain is below a critical level. The plastic strain is assumed to be proportional to the number of load repetitions (N) raised to a power (α) (0.1 used as default value) and to the major principal stress (σ_z) raised to another power (β) (1.6 used as default):

$$\varepsilon_p = A \times N^{\alpha} \times \left(\frac{\sigma_z}{\sigma'}\right)^{\beta}$$

A is a constant and σ' is a reference stress.

When the permanent strain reaches the critical level, the strain rate is assumed to be constant, equal to the tangent at the critical level.

The "plastic modulus," E_p, is defined as the ratio of the compressive stress to the plastic strain.

To calculate the permanent deformations Boussinesq's equations are used with Odemark's transformation (*3*). Odemark's equivalent thicknesses, determined from the elastic parameters, define the stress state. The equivalent thickness is calculated from

$$h_{e,n} = f \times \sum_{i=1}^{n-1} \left(h_i \times \sqrt[3]{\frac{E_i}{E_n}}\right)$$

where

h_i = thickness of Layer i,
E_i = modulus of Layer i, and
f = correction factor.

When the equivalent thickness has been calculated, the vertical compressive stress, σ_z, may be found for the centerline of the load from

$$\sigma_z = \sigma_o \times \left\{1 - \frac{1}{\left[\sqrt{1 + \left(\frac{a}{z}\right)^2}\right]^3}\right\}$$

where

σ_o = contact stress under the tire,
a = radius of the loaded area, and
z = depth to the point considered.

For points at a distance R from the center of the loaded area, the vertical compressive stress may be found from the following equation when the distance is larger than the diameter of the loaded area ($R > 2a$):

$$\sigma_z = \frac{3 \times P}{2 \times \pi \times R^2} \times \left(\frac{z}{R}\right)^3$$

where P is the load.

The compressive stress may then be substituted in the equation for the plastic strain, and the permanent, or plastic, deformations can be calculated by integration over the layer thickness. For the center line of the load a closed form solution of the integration exists. The plastic deformation from depth z to infinity may be found from

$$d_p = \frac{(1 + \nu) \times (3 - 2\nu) \times P}{2 \times \pi \times Z \times (2\beta - 1) \times E_p}$$

where ν is Poisson's ratio.

STRUCTURAL DETERIORATION OF ASPHALT

Fatigue of asphalt starts as microcracking in the material. A microcrack reduces the active cross-sectional area of the asphalt layer and thus the modulus of the layer. In the case of uniaxial tension the decrease in modulus is proportional to the loss of area, and the rate of damage may often be expressed by the "kinetic equation" (*6*):

$$\frac{dA}{dN} = K \times \left(\frac{\sigma}{1 - \omega}\right)^n$$

where

dA = decrease in active cross-sectional area caused by dN load repetitions,
σ = mean stress over the area,
ω = damage defined as the lost area divided by the original area, and
K, n = materials constants.

Under a rolling wheel load the stress condition is very complex. To calculate the damage directly would require a sophisticated finite element program. Instead, an empirical relationship with the maximum strain at the bottom of the asphalt layer, ε, is used, having the same format as the kinetic equation:

$$\frac{\Delta E}{E_0} = K \times (\varepsilon)^n \times \Delta N$$

A point is assumed to show a fine crack when the modulus has been reduced to two-thirds the original value and a severe crack at one-third the original value. When the asphalt has reached severe cracking, the modulus is assumed to remain constant. The strain at the bottom of the asphalt is again calculated using Boussinesq's equations with Odemark's transformation.

MMOPP USED ON THE AASHO ROAD TEST

MMOPP produces a graphical output to the screen and stores a number of intermediate values in disk files. At the upper part of the screen the longitudinal road profile is shown as it was generated by the computer and as it changes during loading.

Some examples of longitudinal profiles are shown in Figure 2. The profiles are from a simulation of one of the AASHO Road Test duplicate sections, from Loop 6. The section had 6 in. (152 mm) of asphalt, 9 in. (229 mm) of base, and 8 in. (203 mm) of subbase, and it was loaded by a 30-kip (67 100-N) single-axle load.

The profile from fall 1958 is after 1 month of loading. This profile remains practically unchanged until the spring thaw of 1959, when a considerable permanent deformation occurs. The next major change in the profile is during spring 1960.

In the middle of the screen MMOPP shows the dynamic loading. A horizontal line in the middle indicates the static load (the dead weight), and two other lines indicate a dynamic load of ±20 percent of the static load. The dynamic load is shown for each point of the road.

Static plus dynamic load is shown in Figure 4 at the beginning of a simulation, when the PSI was above 4.0, and toward the end of the experiment, when the PSI was less than 2.0. At the beginning of the test the maximum deviation from the static load level is about 5 percent, and at the end it increases to about 20 percent. The speeds were chosen randomly between 55 and 65 km/hr.

In Figure 5 the asphalt damage is shown for the simulation described above. The values from fall 1958 are after 1 month of loading. The minimum asphalt modulus is assumed to be one-third of the original value. The values shown are at the same reference temperature.

The lower part of the MMOPP screen shows the change in PSI during the duration of the simulation. Figure 6 shows the results of the above simulation of an AASHO Road Test section (Loop 6, design 6-8-9, 30 kips). The AASHO Road Test was started in late 1958 and lasted about 2 years.

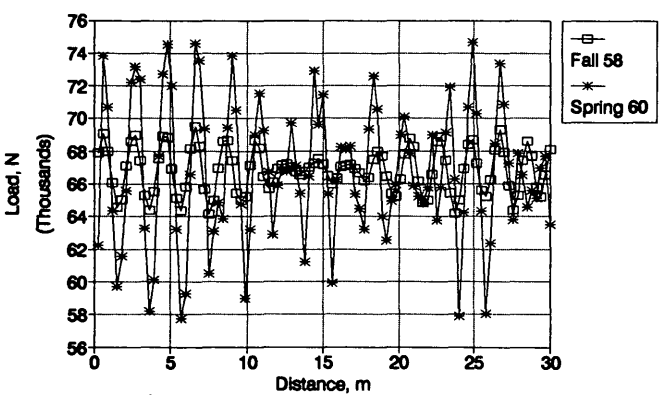

FIGURE 4 Wheel load, simulation of S30, Design 6-9-8.

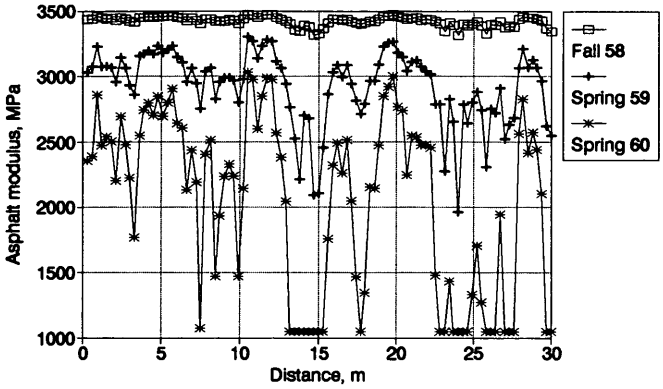

FIGURE 5 Asphalt damage, simulation of S30, Design 6-9-8.

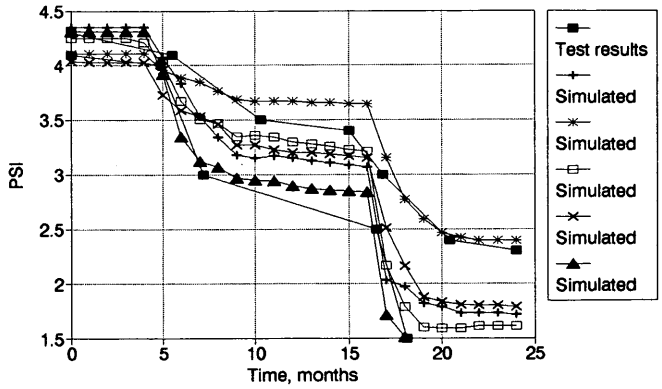

FIGURE 7 Change in PSI, repeated simulations, identical input.

The actual outcome of the road test is also shown for the two identical (duplicate) sections. One section fails in the spring of 1960, whereas the other lasts for the whole experiment. The failure condition was a PSI of 1.5. For both sections most of the damage takes place during spring thaw.

Because the parameters are generated by a stochastic process, the outcome will be different when the program is rerun with the same input parameters, just as was the case for duplicate sections during the actual test. This is shown in Figure 7, where five simulations are compared with the measured performance. Figure 8 shows the corresponding changes in asphalt modulus at a reference temperature. The asphalt modulus is a mean value for the sections. Examples of the variation in modulus along the section are shown in Figure 5.

Another duplicate section, from Loop 2, was also simulated. This section had 2 in. (51 mm) of asphalt, 3 in. (76 mm) of base course gravel, and 4 in. (102 mm) of subbase. The load was a 6-kip (13 360-N) single axle. Figure 9 shows that, again, one of the duplicate sections failed shortly after the spring thaw in 1960, whereas the other lasted to the end of the test.

For both of these simulations the agreement with the performance of the actual test sections is very good. However, a number of input values were unknown and had to be estimated.

EFFECTS OF DIFFERENT LOADING CONDITIONS

The next step in the study was to extend the traffic of the AASHO Road Test over a period of 20 years. During the AASHO Road Test the pavements received approximately 1 million loads, so for a 20-year period this would correspond to 50,000 loads per year.

For the 2-3-4 design from Loop 2 this resulted in a mean life of 3.90 years with a standard deviation 0.81 years, when a PSI of 1.5 was used as the failure criterion. Three simulations are shown in Figure 10. For the 6-9-8 design of Loop 6, the mean life was 3.58 years with a standard deviation of 0.58 years.

Both pavements, in other words, lasted for less than 200,000 loads, although during the AASHO Road Test they had supported more than 600,000 identical loads. This difference is due to the loading rate during the AASHO Road Test, which was much lower during the beginning of the test, including the first spring period, than during the later part of the test. It does, however, emphasize the importance of using a model based on actual distress mechanisms when extrapolating from accelerated tests. A purely statistical extrapolation could lead to very erroneous results.

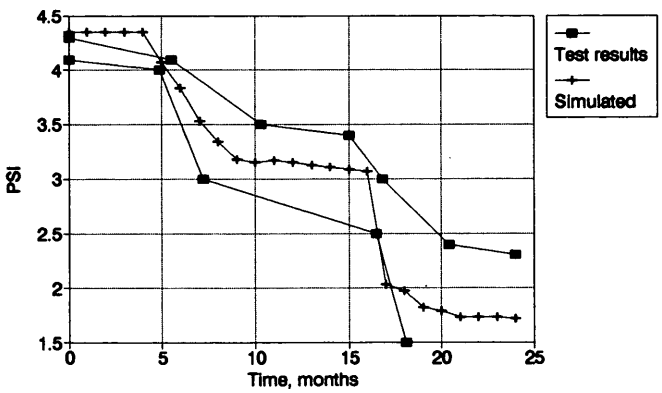

FIGURE 6 Change in PSI, AASHO Road Test results and simulation.

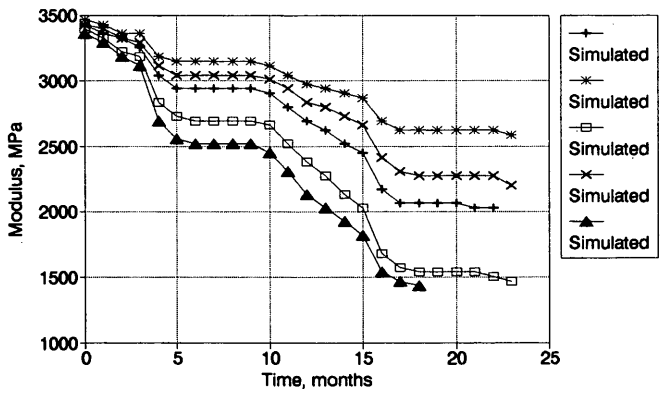

FIGURE 8 Change in asphalt modulus, repeated simulations, identical input.

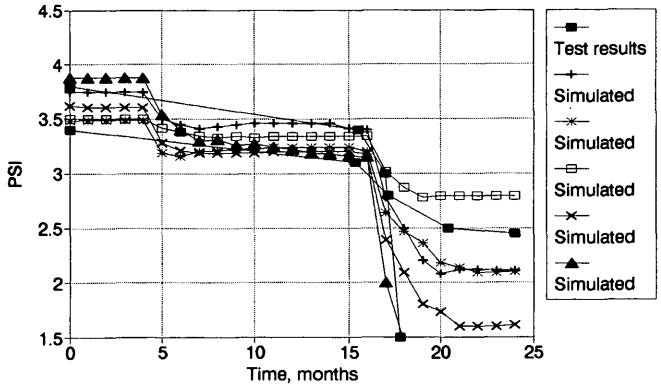

FIGURE 9 PSI, Loop 2, Design 2-3-4, 6 kips.

TABLE 1 Design 2-3-4, 6 kips

	Mean life years	Standard deviation	Light cracking %
AASHO traffic	3.90	0.81	11
½ tire stiffness	5.74	0.99	25
Constant load	4.43	1.08	16
Single wheel	0.62	0.07	0
Mixed traffic	3.12	0.46	26

The amount of light cracking at failure was 11 percent (standard deviation 13 percent) for the 2-3-4 design and 53 percent (standard deviation 17 percent) for the 6-9-8 design.

According to Page (*5*) the tire stiffness is very important to the magnitude of the dynamic load component. Dynamic wheel loads decrease significantly as the tire stiffness is decreased. For the 2-3-4 design a simulation was carried out with the tire stiffness reduced to half the value of the standard wheel. This resulted in a mean life of 5.74 years with a standard deviation of 0.99 years. This corresponds to a 46 percent increase in mean life. The amount of light cracking at the end of the pavement life was 25 percent (standard deviation 10 percent), that is, a larger amount of cracking than observed for the standard wheel, but also after many more load applications. The rate of cracking was 2.2 percent per 100,000 load applications, whereas it was 1.4 percent for the standard load.

Another important parameter is the damping coefficient of the shock absorbers in the suspension system. For a simple damper model it is normally possible to find an optimum value, but actual dampers have very complex characteristics. For the 6-9-8 design a simulation was carried out with a shock absorber having half the damping coefficient of the standard suspension. This resulted in a mean life of 3.13 years (standard deviation 0.70 years), or a decrease of 13 percent. The amount of light cracking was 41 percent at failure, corresponding to a cracking rate of 6.5 percent per 100,000 load applications, whereas it was 7.4 percent for the standard wheel.

Both sections were also simulated using a static wheel load (i.e., without any dynamic effects). This increased the mean life of both sections by about 10 percent and did not change the rate of cracking significantly. It is surprising that the change was not greater. Using the fourth-power rule and a dynamic effect of just 10 percent should result in an increase of about 40 percent.

Changing from a dual to a single wheel on the 2-3-4 design had a very dramatic effect. In all 10 simulations the pavement failed in the first spring period, resulting in a mean life of 0.62 years (−84 percent) (standard deviation 0.07 years). For the 6-9-8 design the change is less dramatic but still important, with a mean life of 2.02 years (−44 percent) (standard deviation 0.37 years).

Finally, the two section were loaded by mixed traffic. For both sections the standard wheel was used as the maximum load and two lighter wheel loads were added. The number of applications of each wheel load were chosen so that the total number of passages would correspond to 50,000 standard wheel loads per year, using a fourth-power relationship.

For both sections mixed traffic reduced the mean life and increased the rate of cracking. For the 2-3-4 design the mean life was reduced by 20 percent to 3.12 years (standard deviation 0.46 years), and for the 6-9-8 by 31 percent to 2.48 years (standard deviation 0.42 years). For the 2-3-4 design the rate

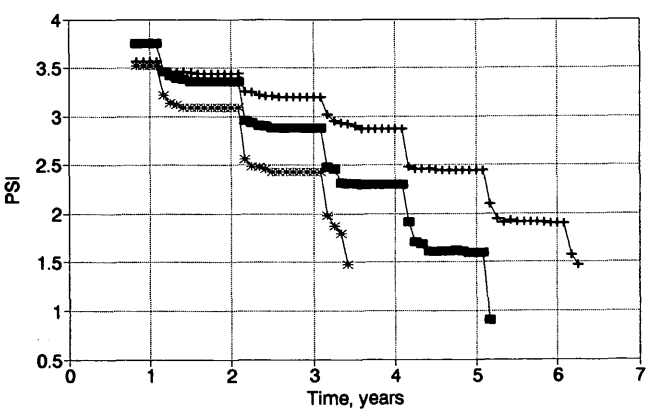

FIGURE 10 Traffic extended over 20 years, Loop 2, Design 2-3-4, 6 kips.

TABLE 2 Design 6-9-8, 30 kips

	Mean life years	Standard deviation	Light cracking %
AASHO traffic	3.58	0.58	53
½ damping	3.13	0.70	41
Constant load	3.83	0.79	44
Single wheel	2.02	0.37	44
Mixed traffic	2.48	0.42	61

of cracking increased to 4.2 percent per 100,000 standard loads (from 1.4 percent for the standard wheel) and for the 6-9-8 design to 12.8 percent (from 7.4 percent).

The results of the simulations are summarized in Tables 1 and 2.

CONCLUSION

The main conclusion is that the deterioration of pavements is a very complex process. It involves an interaction of pavement parameters, climatic effects, vehicle characteristics, and time. Any attempt at isolating the effects of a few parameters will fail if it does not consider the influence of all other parameters.

Sometimes the effects of dynamic loading are considered by adding the dynamic and the static load and calculating the equivalent number of standard axles using a fourth-power law. The results presented indicate that this would be completely erroneous. The effects of dynamic loading may be quite different on different types of distress such as roughness and rutting and cracking, and they will depend on a number of other parameters such as the type of pavement structure.

In the AASHO Road Test some of the important parameters were studied, and the SHRP Long-Term Pavement Performance Program (LTPP) will provide additional information. Even with this information, gaps will still exist. On the basis of the AASHO Road Test and the LTPP data it will not, for example, be possible to evaluate the effects of an improved suspension system or other aspects of vehicle-pavement interaction.

To try to fill some of the gaps in existing knowledge, it is recommended that computer simulation be used, as it is in many other fields of engineering. If a computer model can be developed to fit a number of experimental results, the model may with some confidence be used to extrapolate to other conditions. This may save some costly experiments and may even be used where experiments are not possible.

REFERENCES

1. P. Ullidtz. *Computer Simulation of Pavement Performance.* Report 18, Institute of Roads, Transport, and Town Planning, Technical University of Denmark, Lyngby, Denmark, 1978.
2. P. Ullidtz. A Fundamental Method for Prediction of Roughness, Rutting and Cracking of Pavements. *Proc., Association of Asphalt Paving Technologists,* Vol. 48, 1979.
3. P. Ullidtz. Pavement Analysis. *Developments in Civil Engineering,* Elsevier, 1987.
4. W. R. Bellini and E. N. Thrower. *A Digital Computer Program to Simulate the Passage of a Vehicle over a Road Surface.* RRL Report LR 181. Road Research Laboratory, Ministry of Transport, 1968.
5. J. Page. *A Review of Dynamic Loading Caused by Vehicle Suspensions.* TRRL Supplementary Report 82 UC. Transport and Road Research Laboratory, Department of the Environment, 1974.
6. L. M. Kachanov. Introduction to Continuum Damage Mechanics. *Mechanics of Elastic Stability.* Martinus Nijhoff Publishers, 1986.